Simulation and Analysis of Maximum-Power-Point-Tracker for Photovoltaic Arrays

Manju khare, Yogendra kumar, Ganga Agnihotri and V.K. Sethi

Abstract: **This paper presents an efficient way to search for the photovoltaic array's (PA's) maximum power point (MPP). The incremental conductance is used as the basis for the search process. The algorithm consists of two stages. First, it tries to reach the nearby MPP determined by the operating voltage based on the empirical formula. A modified incremental conductance algorithm is then utilized to reach the real MPP. Finally, a digitized high-performance solar photovoltaic power conversion system is developed and verified. The design method based on the adaptive MPPT algorithm is proposed to generate the optimal power output. A DSP-based control system for synchronization of plural AC power sources has also been implemented**.

Keywords-*Maximum Power Point Tracking, Photovoltaic Array, Conductance Inverter, Voltage Synchronization*

I. Introduction

In the study of photovoltaic arrays (PAs), most of the literature focused on the analysis of the PA's characteristics, illustrated as in Fig. 1. This figure clearly shows the maximum power point (MPP) and the nonlinear current-voltage relationship. Since the array efficiency is highly affected by the irradiance and temperature, it has been a popular research issue on how to determine the current and voltage which makes the PA operate at the MPP to maximize the power output. In practice, the PA's MPP tracking (MPPT) control methods usually adopt a power converter which can vary the load voltage or load current to attain this aim.

In [1], the authors presented an extensive discussion of various methods for determining the MPP. The hill-climbing and the incremental conductance (IncCond) methods are two of the major approaches. The hill-climbing method applies a small perturbation to systems to vary the operating voltage of the PA and hence achieves the MPP. It is simple enough to achieve the goal, but only applicable to environment that doesn't vary quickly. Moreover, its tracking speed is relatively slow. The IncCond method uses the measured changes of the PA's voltage and current to track the MPP [2]. The MPP is effectively tracked by comparing the instantaneous conductance to the incremental conductance. This has been shown to be a more effective approach than the hill-climbing method.

Manju khare is working as a Research Scholar, RGPV Bhopal, **Yogendra kumar, Ganga Agnihotri are with** Faculty of Electrical Engg. Deptt., MANIT Bhopal and **V.K. Sethi with** Faculty of Energy center UIT RGPV Bhopal, M.P, Email: kharemanju@gmail.com

In this paper, a simple but efficient algorithm for adaptively identifying the MPP is proposed, which consists of two stages of operations. Firstly, it quickly accesses to the nearby region of the MPP utilizing an empirical formula. Then, modification of the IncCond method follows where the updating steps for the operating voltage vary.

A numerical verification has been conducted to demonstrate the proposed approach. The results show that its search efficiency is faster than that of the IncCond method up to 5-20 times while remaining search accuracy.

Develop a digitized high-performance solar photovoltaic power conversion system, solar cells here capture sunlight and convert it into the DC power in an efficient and adaptive way. The novel design method based on the adaptive maximum power point tracking (AMPPT) algorithm is realized to generate the optimal power output. The sinusoidal pulse width modulation strategy is adopted to control the full bridge inverter advancing grid-connected system. Since plural AC power sources to be jointed in a parallel manner should be with consistent voltage amplitude and phase, an AC voltage synchronizer is implemented for controlling the current phase of the inverted voltage generated by the PAs and hence to track the commercial power supply.

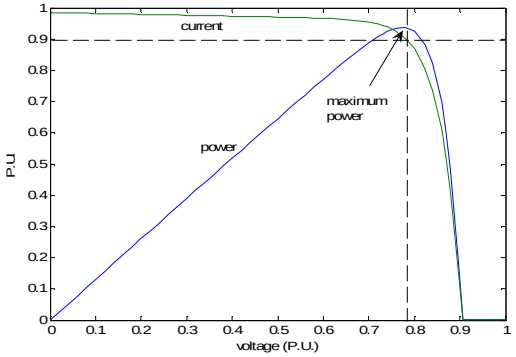

Fig. 1 P-V and I-V curves of the typical PAs

II. Battery dominated MPPT bus topology

PAs usually work with a power converter. The simplest configuration is illustrated as in Fig. 2. The PA supplies energy to the system bus through a DC-DC converter. A battery is in parallel with the system bus. It either acts as a power absorber or as a power supply depending on the supplying status of the PA. The DC-DC converter is controlled by the MPP tracker. It is usually a variable voltage gain to force the PA to work at the MPP.

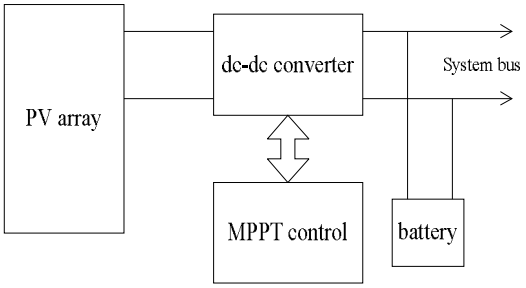

Fig. 2 Battery dominated MPPT bus topology

III. PA model

Figure 3 illustrates the equivalent circuit of a typical PA which consists of current source I_{ph}, parallel diode D, shunt resistance R_{sh}, series resistance R_s. The current source is proportional to the irradiance and temperature. The relationship can be written as

$$I_{ph} = [I_s + K_i(T - T_r)]\frac{S_i}{100} \quad (1)$$

where I_s is the PA operating current under the reference irradiance and temperature, T is the environmental temperature (K), T_r is the reference temperature, K_i is the temperature coefficient of short-circuit current and S_i is the solar radiation in mW/cm^2. The parallel diode determines the I-V characteristics of the PA. Neglecting the shunt resistance, it can be written as [3]:

$$I = I_{ph} - I_{sat}\left[\exp\left(\frac{q}{AKT}(V + IR_s)\right) - 1\right] \quad (2)$$

where I and V are, respectively, the output current and voltage, I_{sat} is the reverse saturation current, q is the charge of an electron, K is the Boltzmann's constant, and A is the diode quality factor. I_{sat} can be described as

$$I_{sat} = I_{rr}\left[\frac{T}{T_r}\right]^3 \exp\left[\frac{qE_{gap}}{KA}\left(\frac{1}{T_r} - \frac{1}{T}\right)\right] \quad (3)$$

where I_{rr} is the saturation current at T_r, E_{gap} is the band-gap energy of the semiconductor. The physical property of the PA has been shown in Fig. 1.

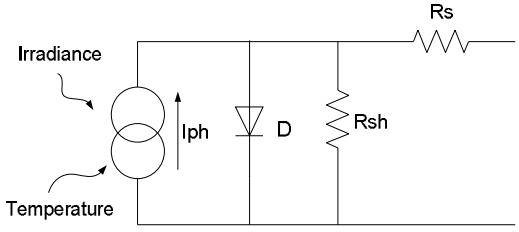

Fig. 3 Equivalent circuit of PAs

IV. Improved MPPT Method

IncCond Method

The general idea of the IncCond method comes from the observation of slope changes of dP/dV, or equivalently,

$$\begin{cases} dI/dV = -I/V, & \text{at MPP} \\ dI/dV > -I/V, & \text{at the left of MPP} \\ dI/dV < -I/V, & \text{at the right of MPP} \end{cases} \quad (4)$$

According to the above condition, the following equation is applied to reach the MPP:

$$V_{ref}(k+1) = V_{ref}(k) \pm V_{step} \quad (5)$$

where $V_{ref}(0)$ is the PA's initial voltage, V_{step} is a constant. In [2], a modified IncCond algorithm was proposed, in which V_{step} became a variable that was related to the incremental conductance to accelerate the search efficiency. The modified voltage adjustment is expressed as

$$V_{ref}(k+1) = V_{ref}(k) \pm (V_{step} + \alpha|G + \Delta G|) \quad (6)$$

where $G = I/V$, $\Delta G = \Delta I/\Delta V$ and α is a positive constant; $G + \Delta G$ serves as a voltage adjustment term, it changes with the twinkling current and voltage of the PA. When the PA works far away from the MPP, the magnitude of the voltage adjustment grows resulting an explicit update on V_{ref}. On the other hand, V_{ref} changes slightly and reaches to a constant when the correction ultimately decreases to zero. The major advantage of this modification is that it is able to respond to weather changes easily.

Approximate Power Search

The principles stated in [4,5,6] presented some quick ways to access an approximate MPP. In general, the voltage and current of the PA's MPP is roughly 70-90% to its open-circuit voltage V_{oc} and short-circuit current I_{sc}, i.e.

$$V_{MPP} \approx k_1 V_{oc} \quad (7)$$

$$I_{MPP} \approx k_2 I_{sc} \quad (8)$$

where $0.7 \le k_{1,2} \le 0.9$. On the basis of the relationship, one may simply allocate the approximate MPP. In [6], the author searched and collected the long-term optimum operating voltage, whose power loss was the smallest, to determine the near MPP operation (nMPPO). The above-mentioned methods could find the MPP very fast, but they all suffered from a disadvantage. That is, they weren't robust enough to against environmental changes and might cause prediction errors when weather is changeful.

Proposed Method

Figure 4 shows the P-V curves of a typical PA that works under the worst and best operating environments. The PA

has a MPP ($P_{mpp\min}$) and an open-circuit voltage $V_{o\min}$ under the worst operating environment. Also, it has a MPP ($P_{mpp\max}$) and an open-circuit voltage $V_{o\max}$ under the best operating environment. These values could be determined by experiments. Based on the information, one can conjecture that the MPP shall lie within the area between the two dotted lines in Fig. 4.

For the operation, we first determine the practically available operating voltage rang $[V_{o\min}, V_{o\max}]$ of PAs. A factor around 0.7-0.9 dependent on the PA is then multiplied to the open-circuit voltage as the near MPP.

Figure 5 illustrates the process of the proposed approach for adaptively identifying the MPP. Firstly, it checks if $V(k)$ of PA is already within the near MPP region. If not, it will be directed to the following process:

$$V_{ref}(k+1) = V_{ref}(k) \pm \alpha(V_{MPP} - V(k)) \qquad (9)$$

where the update gain α is a positive constant. If the operating voltage of PA is already within the near MPP region then go through the second process described by Fig. 6.

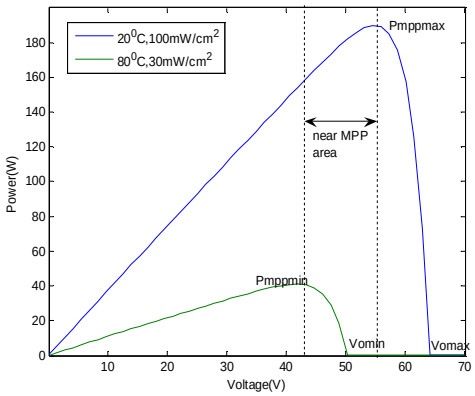

Fig. 4 P-V curves of the PA under the worst and best environments

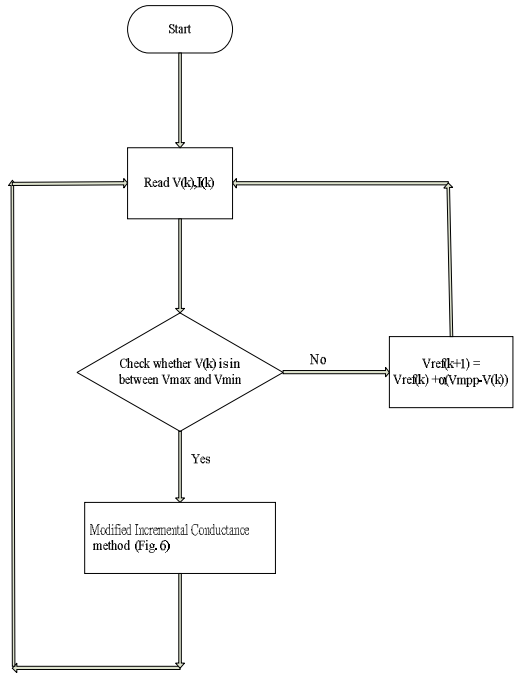

Fig. 5 Flowchart for searching the MPP

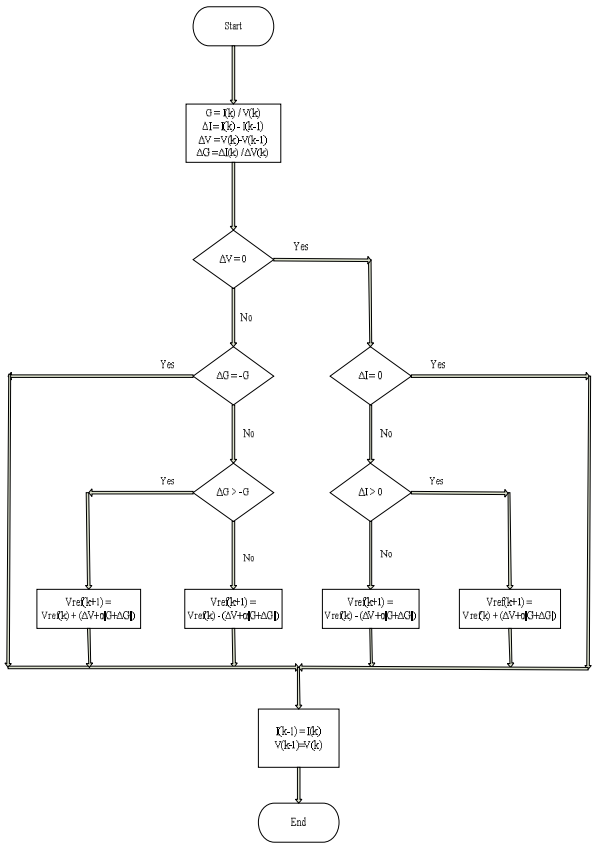

Fig. 6 Flowchart of the modified IncCond method

V. Grid-connected system

AC voltage power supplies should possess consistent voltage amplitude and phase in all available power inputs. To this aim, a synchronizer realized in a digital signal processing unit accompanied with related peripherals is developed. In which, the utility voltage (from the commercial power supply), after reduction, enters the signal processing unit or processing. Control commands are then calculated and output to the full-bridge inverter, see Fig. 7. Sinusoidal pulse modulation (Fig. 8) is adopted to control the full-bridge inverter. The modulated commands drive the inverter output voltage to track the utility voltage. In addition, the current control strategy realized as in Fig. 9 is implemented to achieve the utility power factor. Furthermore, a zero crossing detecting circuit is designed, which is built for detecting the zero crossing point of the utility network. The detected point is used as the phase reference for the digital signal processing unit when the system works under the on-grid mode.

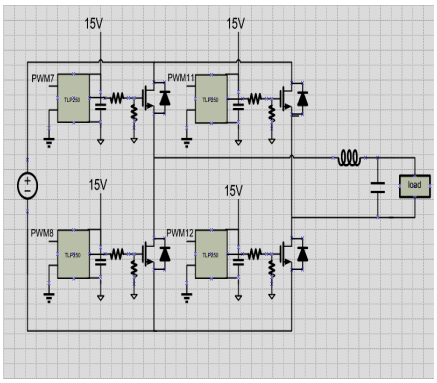

Fig. 7 Full-bridge inverter

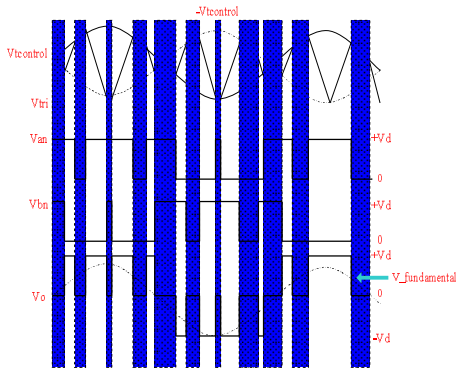

Fig. 8 Sinusoidal pulse modulation (SPWM)

The working pattern changes with the load power consumed. The DSP-based control system keeps monitoring the power consumption of the load to activate an appropriate power supply source. If the consumed load power is less than the instantaneous power that PAs can offer then the inverter simply works in the off-grid mode. On the contrary, the inverter works with the on-grid mode which AC voltage inverted from the DC voltage generated by the PA's are combined with the utility voltage. Fig. 11 illustrates configuration of the whole system.

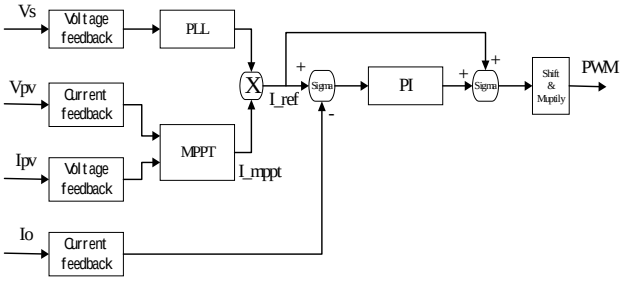

Fig 9 Current control circuit

VI. Simulated results

The proposed PA's MPPT system was first verified in Matlab-Simulink. The PA module was modeled by (1)-(2). We performed numerical simulations with the IncCond, the modified IncCond and the proposed methods. The characteristics of the PA under consideration are listed in Table 1.

The update gain α in (9) was set to be 1. Tracking rang of the operating voltages illustrated in Figs. 10-11 are from zero to V_{MPP}. From these figures, it can be observed that, among three methods, the proposed method is able to reach the MPP with the shortest time.

The PV-based power supply system was designed to jointly supply AC power with the commercial power supply. An AC voltage synchronizer has been implemented for controlling the current phase of the inverted voltage generated by the PA's to track the commercial power supply. A digital signal processing unit is designed to fulfill the function. An electromagnetic interference (EMI) filter and an isolation transformer were adopted to filter the noise.

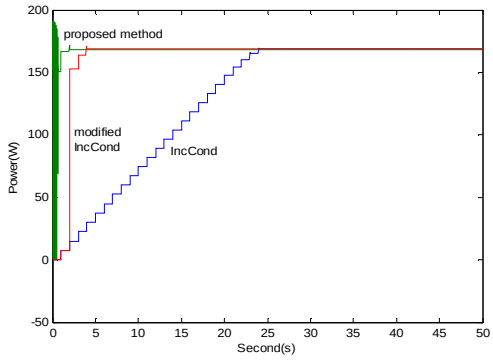

Fig. 10 Tracking power curve for comparison of the proposed method with the IncCond and modified IncCond methods

Figure 15 illustrates the result of zero crossing detection. When the power supply inverted from the PAs is higher than the instantaneous power consumption of the load power, the system works in off-grid mode.

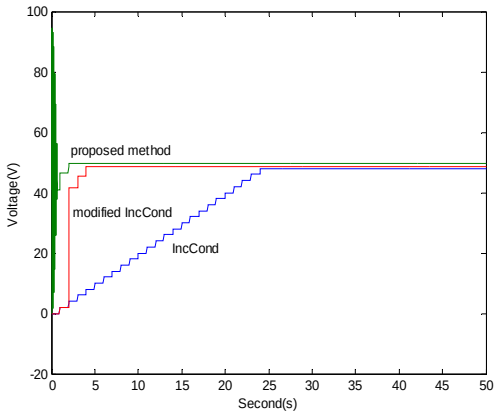

Fig. 11 Tracking voltage curve for comparison of the proposed method with the IncCond and modified IncCond method.

Fig. 12 Result of zero crossing detection

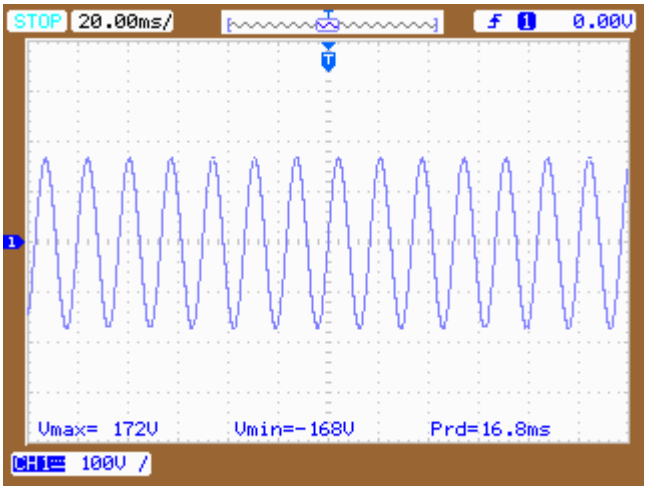

Fig. 13 Off-grid mode

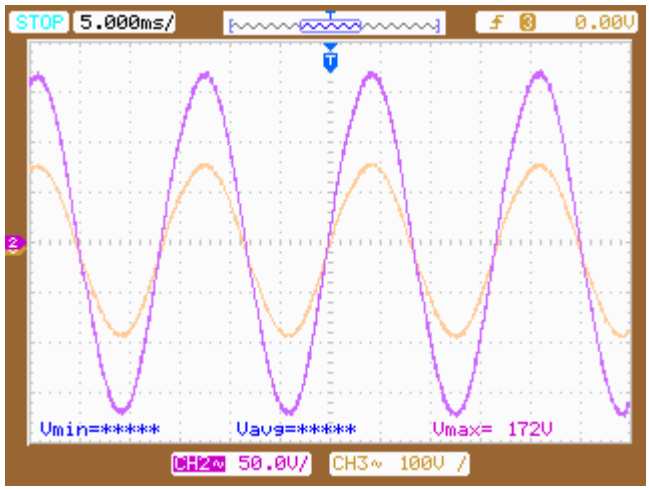

Fig. 14 On-grid mode (CH2 is inverter output and CH3 is utility voltage)

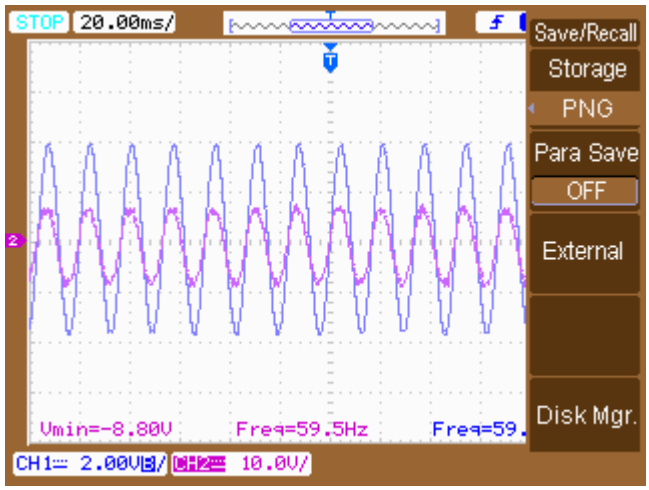

Fig. 15 Consistency of voltage and current

VII. Conclusions

This paper proposes an efficient and easily implementable approach for tracking the MPP of PV power systems. The approach simultaneously combines the advantage of the IncCond method and the approximate power searching principle for fast reaching the MPP. The approximate power searching principle provides the fastest way to reach the near MPP. The IncCond method proceeds next to access the real MPP. An AC voltage synchronizer has been implemented for controlling the current phase of the inverted voltage generated by the PAs and hence to track the commercial power supply.

.Table 1 Characteristics of the PA

Irradiance	100 mW/cm^2
Peak power	175W
Current at peak power	34.6A
Voltage at peak power	50.5V
Short-circuit current	3.75A
Open-circuit voltage	59.5V
Temperature coefficient of open-circuit voltage	$-164mV/^0C$
Temperature coefficient of short-circuit current	$0.86mA/^0C$
Nominal operating temperature	25^0C

REFERENCES

[1] T. Esram, P. L. Chapman, 'Comparison of Array Maximum Power Point Tracking Techniques', *IEEE Trans. Ind. Electron.*, 2007, vol. 22, pp 439-449.

[2] T. Y. Kim, H. G. Ahn, S. K. Park, and Y. K. Lee, 'A Novel Maximum Power Point Tracking Control for Power System under Rapidly Changing Solar Radiation', in *Proc. IEEE Int. Symp. Ind. Electron.*, 2001, pp. 1011-1014.

[3] C. Hua, J. Lin, and C. Shen, 'Implementation of a DSP-Controlled Photovoltaic System with Peak Power Tracking', *IEEE Trans. Ind. Electron.*, 1998, vol. 45, pp 99-107.

[4] K. Kobayashi, H. Matsuo, and Y. Sekine,'A Novel Optimum Operating Point Tracker of The Solar Cell Power Supply System', in *Proc. IEEE Power Electron. Specialists Conf.*, 2004, pp. 2147-2151.

[5] S. Yuvarajan and S. Xu,: 'Photo-voltaic Power Converter with a Simple Maximum-Power-Point-Tracker', in *Proc. Int. Symp. Circuits Syst.*, 2003, pp. 399-402.

[6] F. S. Sun, *Study of High Performance PV System*, Doctoral Dissertation, Department of Mechanical Engineering, National Taiwan University, 2005.

Manju Khare was born in 1971 in India. She received BE degree in Electrical engineering (1992) from GEC Sagar. M.E. degree (1997) in Control System Engineering from GEC Jabalpur India. Now she is perusing her Ph.D degree in the field of renewable energy. She is working with Laxmi Narayan Collage of Technology Bhopal, since 2001.

Yogendra Kumar born in 1965 in India. He received the M. Tech. degree in Heavy Electrical Equipment from Maulana Azad College of Technology Bhopal, India in 1998. He received his Ph.D degree from Indian Institute of Technology, Roorkee in 2006. Presently he is working as Professor in Maulana Azad National Institute of Technology, Bhopal, India. His research interests are in the area of Distribution Automation, Economic Load Dispatch and Optimization Techniques.

Dr. Ganga Agnihotri received BE degree in Electrical engineering from MACT, Bhopal (1972), the ME degree (1974) and PhD degree (1989) from University of Roorkee, India. Since 1976 she is with Maulana Azad College of Technology, Bhopal in various positions. Currently she is professor and Dean. Her research interest includes Power System Analysis, Power System Optimization and Distribution Operation.

Prof. V.K.Sethi M.Tech (Mech), Ph.D., is Rector of Rajiv Gandhi Technological University Bhopal (India) He is the recipient of Mother Teresa award for application of renewable energy in remote areas of Andhra Pradesh (India) he has published so many papers in International journals He is a member of board of studies of mechanical engineering of Rajiv Gandhi technological university Bhopal (India). He is a member of governing body as an AICTE nominee of engineering Institutions of M.P. (India). His research interests are in the field of renewable energy, Nano technology, distribution automation, and optimization techniques.

Application of ANN for Induction Motor Fault Classification Using Hilbert Transform

Mrs. Anjali.U.Jawadekar, Dr.G.M.Dhole, SRParaskar S.S .Jadhao and M.A.Beg

Abstract: ***This*** **paper addresses the development of new signal processing approach based on Hilbert transform to extract the fault features in number of induction motor conditions. The motor conditions considered are normal condition and motors with bearing defects like inner race, outer race, stator interturn faults and rotor bar crack. Present approach is based on extraction of envelopes of the stator currents by Hilbert Transform. Representative features like maximum and minimum value, mean, standard deviation and norm are obtained from current envelopes. These features are then used as input to Artificial Neural Network. Experimental results obtained show that diagnostic system using MLP neural network along with Hilbert Transform is capable of classifying multiple faults in induction motor with high accuracy recognition rate**

Keywords: **: Hilbert Transform, Induction motor, current envelope, artificial neural network, Multilayer perceptron.**

I. INTRODUCTION

Induction motors are widely used in industry due to their reliability, low cost and robustness and hence treated as workhouses of industry. But the possibility of faults is unavoidable .Fault identification and diagnosis schemes are intended to provide advanced warnings of incipient faults so that appropriate maintenance actions can be taken at an early stage. [1][2].This helps to reduce the maintenance cost and prevent unscheduled maintenance of these machines. Failures surveys [3] reported that forty percent of motor failures are caused by bearing related failures, thirty eight percent by stator interturn, ten percent by rotor related failures and twelve percent by mixed failures which affect other parts of the machine. Condition monitoring of the induction motor received considerable attention in recent year's .Many condition monitoring methods has been proposed for different types of induction motor fault detection and localization. Martelo [4] and Schoen et al [5] study bearing failures based on FFT analysis. Using same tool Benbouzid et al [6] and Cameron [7] analyze other types of failures such as rotor slot effect, saturation and static and dynamic eccentricities.

Stator interturn fault estimation using particle swarm optimization method is discussed in [8] and by current Concordia pattern based fuzzy decision system is given in [9]. An induction motor fault diagnosis using stator current envelopes for broken rotor bars and inter turn short circuit in stator winding have been proposed in [10].Time frequency domain techniques have been also used for fault diagnosis of induction motors which includes STFT,FFT ,bispectrum, high resolution spectral analysis and wavelet analysis.[11]-[14]. Another technique used for induction motor fault detection uses AI techniques such as expert systems ,fuzzy inference system ,neural network , SVM, genetic algorithm and adoptive neural fuzzy inference system[15]-[17].

Present work proposes a method that is capable to detect multiple faults in induction motor such as bearing faults like inner race and outer race defects, stator interturn short circuit and rotor bar crack by analyzing stator currents. The approach is based on extraction of the envelope of the signal to be analyzed using Hilbert Transform. Fault features are extracted from current envelopes which are further used as input to ANN which acts as a fault classifier and classifies multiple faults in induction motor with 100 percent accuracy.

II. HILBERT TRANSFORM:

Hilbert transform is a signal analysis method that is frequently used in different scientific fields. Mathematically Hilbert transform of a real signal $x(t)$ is defined as time domain convolution of $x(t)$ with 1/t and is defined for all t by equation 1.

$$y(t) = H(x(t)) = \frac{1}{\pi t} * x(t) = \frac{1}{\pi} \int_{-\infty}^{\infty} \frac{x(\tau)}{t-\tau} d\tau \qquad (1)$$

Following are the properties of Hilbert Transform

A real signal $x(t)$ and its Hilbert Transform $y(t)$ are mutually orthogonal

Mathematically $\int_{-\infty}^{\infty} x(t)y(t)dt = 0$ (2)

Mrs. Anjali.U.Jawadekar, Dr.G.M.Dhole, SRParaskar S.S .Jadhao and M.A.Beg are working in ***1-5 Department of Electrical Engineering, S.S.G.M.College of Engineering Shegaon. (M.S.),444203,India,*** ***anjali.jawadekar@gmail.com***

If $y(t)$ is Hilbert Transform of $x(t)$ then Hilbert Transform of $y(t)$ is $-x(t)$ (3)

$\pm\frac{\pi}{2}$ Phase shift is another basic property of Hilbert transform. Phase of positive frequency components is shifted by $-\frac{\pi}{2}$ and phase of negative frequency components is shifted by $+\frac{\pi}{2}$

$$\theta(\omega)=\frac{\pi}{2} \qquad \text{For} \quad \omega<0$$

$$\theta(\omega)=-\frac{\pi}{2} \qquad \text{For} \quad \omega>0 \tag{4}$$

A real function $x(t)$ and its Hilbert Transform $y(t)$ are such that they together create an analytic signal $z(t)$.

$$z(t)=x(t)+jy(t) \tag{5}$$

Signal $z(t)$ has the property that all negative frequencies of $x(t)$ has been filtered.

Envelope E(t) of a signal is defined as

$$E(t)=\left|z(t)\right|=\left|x(t)+jy(t)\right| \tag{6}$$

And instantaneous phase is defined as

$$\theta(t)=\arctan(\frac{y(t)}{x(t)}) \tag{7}$$

III. ARTIFICIAL NEURAL NETWORK

The application of artificial neural network to various decision making, forecasting and classification problems has gained a lot of attention recently. ANN s are able to learn the relationship among past, present and future variables. An ANN is an information processing paradigm, inspired by biological nervous systems. The basic processing element of neural network is called artificial neuron or simply neuron. The key element of it is the novel structure of the information processing system. It is composed of large number of highly interconnected processing elements working in union to solve specific problem.

Artificial neural system functions as distributed computing networks .Their most basic characteristics is their architecture. Only some networks provide instantaneous responses, other networks need time to respond and are characterized by their time domain behaviour, which often referred to as dynamics. Neural networks also differ from each other in their learning modes. There are varieties of learning rules that establish when and how the connecting weights changes. Networks exhibit different speeds and efficiency of learning. An ANN is configured for a specific application, such as pattern recognition or data classification, through a learning process. Learning in biological system involves adjustments to the synaptic connections that exist between the neurons.

Neural networks are typically organized in layers. Layers are made up of number of interconnected nodes which contain an 'Activation Function'. Patterns are presented to the network via a system of 'Weighted Connections'. The hidden layer then links to an output layer where the answer is output as shown in Figure 1

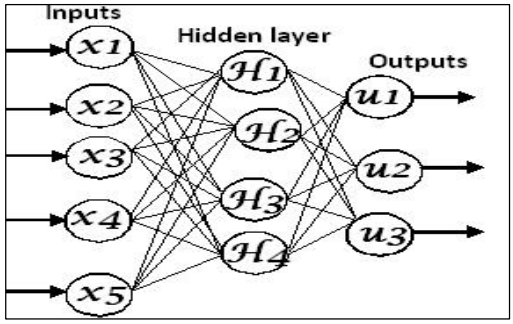

Figure 1.Architecture of Artificial Neural Network

Common type of artificial neural network consists of three layers of units; a layer of 'input' unit is connected to a layer of 'hidden' unit, which is then connected to a layer of 'output' units. The activity of input unit represents the raw information that is fed into the network. The activity of each hidden unit is determined by the activities of the input units and the weights on the connection between the input and hidden units. The behavior of the output unit depends on the activity of hidden units and the weights between the hidden and output units. Feed forward ANN allow signal to travel from input to output only. There is no feedback i.e. the output of any layer does not affect the same layer. Feed forward ANN tends to be straight forward networks that associate inputs with outputs.

Prediction with NNs involves two steps: training and learning. Training of FFNNs is normally performed in a supervised manner. The success of training is greatly affected by proper selection of inputs. In the learning process, a neural network constructs an input–output mapping, adjusting the weights and biases at each iteration based on the minimization or optimization of some error measure between the output produced and the desired output. This process is repeated until an acceptable criterion for convergence is reached. The most common learning algorithm is the back propagation (BP) algorithm, in which the input is passed layer through layer until the final output is calculated, and it

is compared to the real output to find the error. The error is then propagated back to the input adjusting the weights and biases in each layer. The standard BP learning algorithm is a steepest descent algorithm that minimizes the sum of square errors. In order to accelerate the learning process, two parameters of the BP algorithm can be adjusted: the learning rate and the momentum. The learning rate is the proportion of error gradient by which the weights should be adjusted. Larger values can give a faster convergence to the minimum. The momentum determines the proportion of the change of past weights that should be used in the calculation of the new weights.

IV. Experimental Setup:

Experimental studies have been performed on 2 H.P. three phase, four pole, 415 volts; 50 Hz squirrel cage induction motor .Experimental setup for the same is shown in figure 2. Motor used for experiment has 24 coils, 36 slots in all. Each phase comprising of 8 coils carries 300 turns. A phase has been tapped where each tapping is made after 10 turns, near to star point (neutral). Tapings are drawn from coils where each group comprises of approximately 70 to 80 turns. Spring and belt arrangement is used for mechanical loading of motor. Motor was loaded at 75 % of full load to full load conditions. To acquire the data the Tektronix DSO, TPS 2014 B, with 100 MHz bandwidth and adjustable sampling rate of 1GHz is used to capture the current and voltage signal. The Tektronix current probes of rating 100 mV/A, input range of 0 to 70 Amps AC RMS, 100A peak and frequency range DC to 100KHz are used to acquire the stator current signals. Approximately, 500 sets of signals were captured on different load conditions and at different mains supply conditions for following case of studies.

1. Healthy: 2 H.P motor is fed by three phase balanced supply Load on the motor is varied from 75 % of full load to full load with spring and belt arrangement .Stator current signals and phase voltages are captured for no load ,75 % of full load and at full load conditions.

2: Bearing Defects (Inner and Outer Race): Motor under test comprises of two bearings number 6204 and 6205. Bearings having natural defects caused by regular operation of motor are used in experimental study. Motor is fitted with different combinations of bearings having inner race or outer race defects. Stator currents and voltages for each combination of bearings are captured to compare it with healthy bearing condition. Different experiments were conducted with different combinations of rear side and load side bearings to access the performance of bearings and to study its effect on performance of motor.

3: Stator Interturn Short Circuit: For this case of study, stator windings of induction motor were modified to have several accessible tapings that can be used to introduce short circuits. For this experimentation phase A is tapped, where each tapping is made after 10 turns. Different experimentations were conducted with 10 turns, 20 turns and 30 turns short circuited respectively in phase A of motor and for different loading conditions phase voltage and stator current signals are captured.

4: Broken Rotor bars

Induction motor under test has 32 rotor bars, to carry out rotor broken bar test, two rotor bars are broken at both sides of end rings and stator current signals are captured at different loading conditions.

Figure2: Experimental Setup

Stator current signals recorded for normal and various abnormal conditions are shown in figure 3

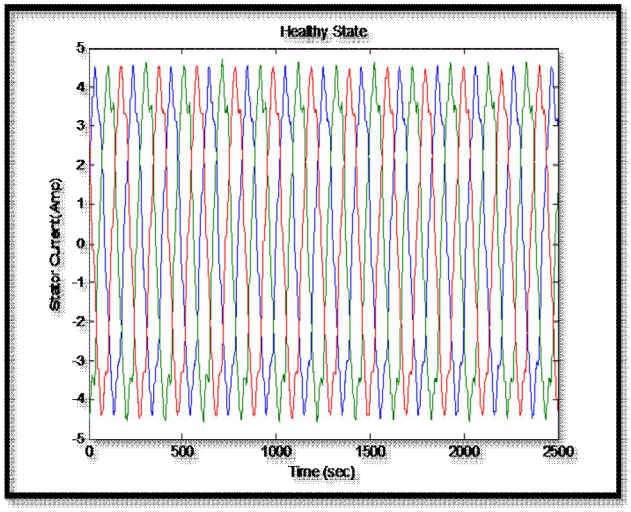

Figure 3.a Healthy condition

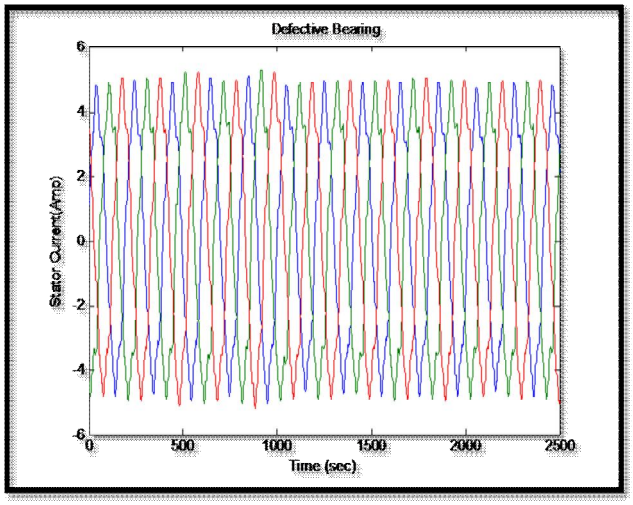

Figure 3.b Defective Bearing

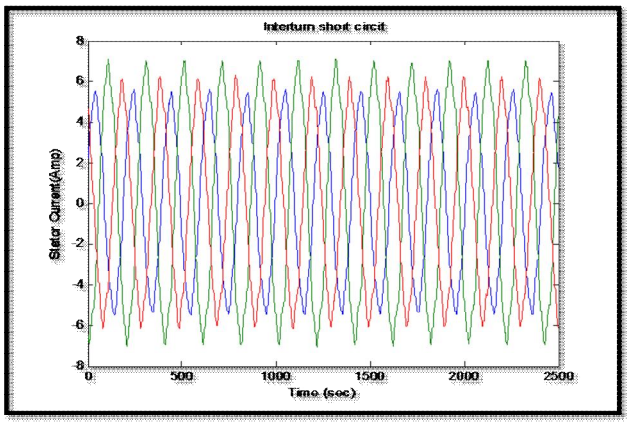

Figure 3 c Interturn short circuit

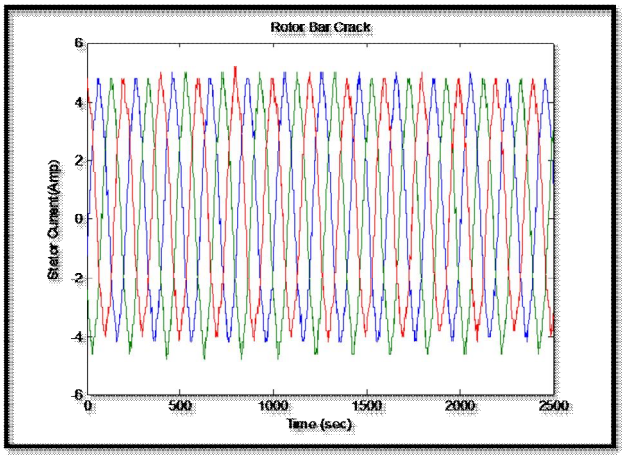

Figure 3 d. Rotor bar crack

V .FEATURE EXTRACTION

From time waveforms as shown in figure 3, no conspicuous differences exists among different conditions, so there is a need to come up with feature extraction method for fault classification. Present approach is based on extraction of envelopes from the stator current signals by Hilbert Transform using equation 1. Envelopes obtained for different conditions of motor are as shown in figure 4.

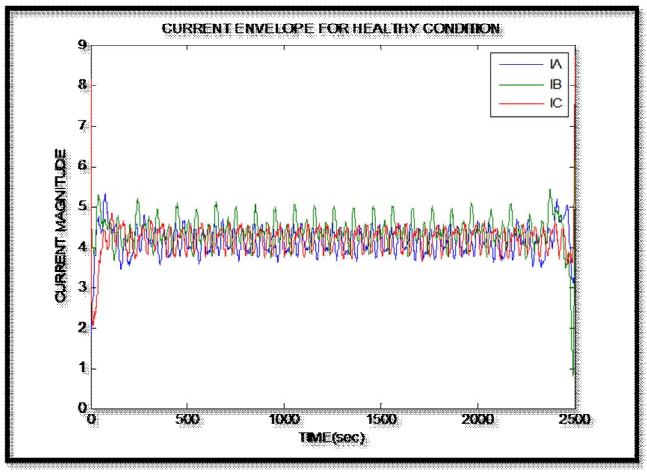

4a: Envelopes of the stator current for Normal condition

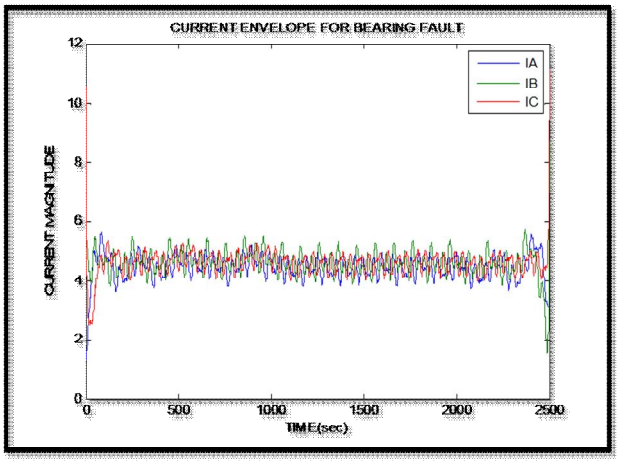

Figure 4b: Envelopes of the stator current for Bearing Fault

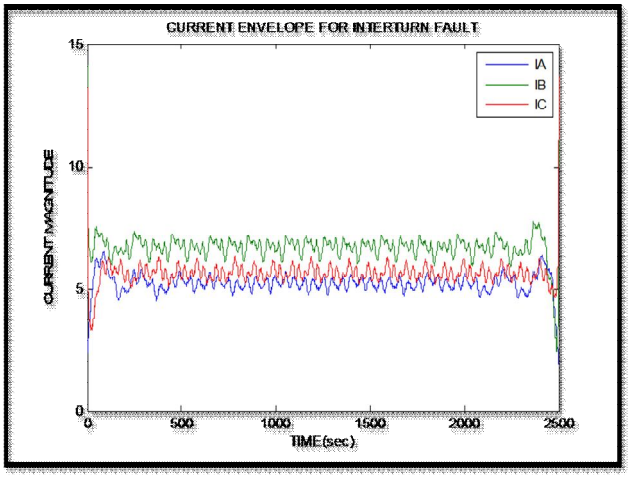

Figure 4c: Envelopes of the stator current for Interturn Fault

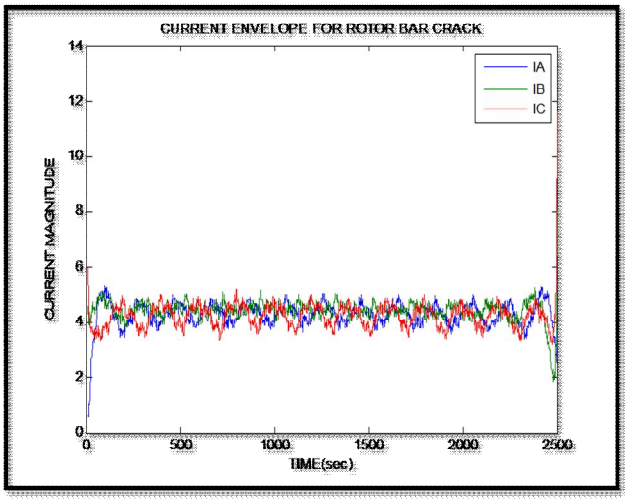

Figure 4d: Envelopes of the stator current for Rotor bar crack

The main problem facing the use of ANN are the selection of best inputs and how to choose the ANN parameters making the structure compact and creating highly accurate networks. For the proposed system to create training pattern statistical parameters like maximum, minimum, standard deviation, mean and norm are obtained from the current envelopes extracted from stator currents for different fault conditions.

VI. Results and Discussion:

Application of ANN to various decision making, forecasting and classification problem has gained lot of attention. An ANN with its excellent pattern recognition capabilities can be effectively employed for fault classification of three phase induction motor. In present study three layer fully connected feedforward artificial neural network is used and trained with supervised learning algorithm back propagation. FFANN consists of one input layer, one hidden layer and one output layer. Input layer consists of fifteen neurons, the inputs to these neurons are the statistical parameters computed from envelopes of stator currents. Output layer consists of four neurons representing healthy, bearing fault, interturn fault and rotor bar crack condition respectively.

Selected parameters for FFANN are as follows

Number of epochs=1000, Training data=60% , Testing data= 40%,

Number of hidden layers=01, Transfer function = TanhAxon, Learning Rule= Momentum

Step size =0.1, Momentum=0.7

With these assumptions variation of percentage accuracy of classification for induction motor under healthy and different fault conditions with respect to number of processing elements in hidden layer is obtained. Figure 5 shows the graph for the same.

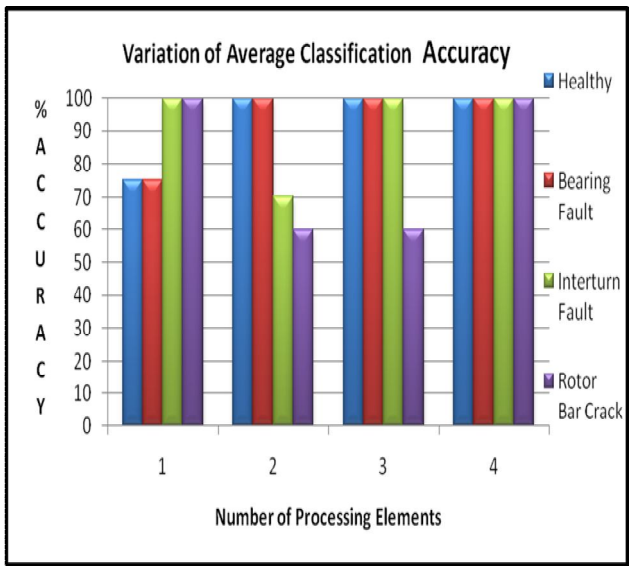

Figure 5 Variation of Average Classification Accuracy

VII .Conclusion

This work proposes Hilbert Transform based approach for fault classification of induction motor validating its effectiveness through different cases of study that considered the motor under diverse fault conditions like bearing fault, stator interturn fault and rotor bar crack. Line current signals recorded under healthy and different fault conditions are passed through signal processing procedures involving Hilbert transform. This methodology based on envelope concept derives rich information about the fault from stator current signals. Statistical parameters computed from fault features are further used as training and testing data for FFANN.

Envelope analysis with Hilbert Transform approach and FFANN with momentum learning rule and TanhAxon transfer function and with four processing elements in hidden layer produced best results for classifying multiple faults in induction motor.

REFERENCES

[1] F Boldea & A.Nasar Induction machine handbook CRC press 2002

[2] P Tavner, L.Ram,J Penman & H Sedding ,"Condition Monitoring of Rotating electrical machines" The Institution of Engineering & technology 2008

[3] W.T.Thomson & M Fenger " Current Signature Analysis to detect Induction motor faults" IEEE industry Applications Magazine vol 7, No 4, pp 26-34 July/August 2001

[4] Martelo A ," Fault detection of ball bearings in electrical motors by means of vibrations ,noise, and stator current spectral analysis Msc Thesis ,Dept of Mechanical Engineering University of Los Andes,Bogota Colombia 2000.

[5] Schoem R, Habetler T, Kamran F, Bartheld R ,"Motor bearing damage detection using stator current monitoring " IEEE Transaction Industrial Application pp 1274-1279 ,1995

[6] benbouzid M,Beguenane R, Viera M ,"Induction motor asymmetrical fault detection using advanced signal processing techniques "IEEE Transaction Energy Conversion 14(2) pp146-152, 1999

[7]Cameron JR, Thomson WT ,Dow A "Vibration and current monitoring for detecting air gap eccentricity in large induction machine IEEE Proceedings 133B(3) pp155-163,1986

[8] J.Penman , H.G.Seding , B.A.Lioyd & W.T.Fink,"Detection and location of interturn short circuits in stator winding of operating motor , IEEE Transaction Energy Conversion vol 9 , No4 December 1994, pp652-658

[9] J.Sottile & J.L Kohler ,"An online method to detect incipient failures of turn insulation in random wound motors IEEE transactions energy Conversion vol 8, No4, December 1993, pp 762-768.

[10] Aderiano M,da Silva ,Richard J Povinelli & Nabeel , A.O. Demerdash, "Induction Machines broken bar and stator short circuit fault diagnosis based on three phase stator current envelopes. " IEEE transaction Ind Electron vol 55, No 3, pp1310-1318 March 2008

[11] H.Douglas,P Pillay& A.K.Ziarani," A New algorithm for transient motor current signature analysis using wavelets , IEEE Transactions Industrial Application vol 40, pp1361-1368 September/ October 2004.

[12] M.E.H.Benbouzid ,Michella Vieira & Celine Theys ,"Induction motor fault detection and localization using stator current advanced signal processing techniques" IEEE Transaction Power Electrons vol 14, pp14-22 January1999.

[13]T.W.S. Chow & S Hai ,"Induction machine fault diagnostic analysis with wavelet technique ,IEEE Transaction Industrial Electron vol 51, No 3, pp558-565 January 2004

[14] W.Thomson & M .Fenger,"Current signature analysis to detect induction motor faults " IEEE Industrial Application magazine vol 7, No 4, pp26-34 July/August 2001

[15] Jover Rodrgez ,P Arkkio.A ," detection of stator winding fault in induction machine using fuzzy logic " Applied soft computing vol 8,No 2 pp1112-1120,2008

[16] F.Felippetti, G .Franceschini & C Tassoni ,"A survey of AI techniques approach for induction machine online diagnostic in proceeding PEMC 96 vol 2, pp314-318 1996

[17] M.Awadallah & M.Marcos ,"Application of AI tools in fault diagnosis of electrical machines and drives – An overview "IEEE transaction Energy Conversion vol 18, No 2 pp245-251 , June 2003.

Mrs.ANJALI U. JAWADEKAR received her B.E. and M.E. from the S.G.B.University of Amravati, India in 1994 and 2001 respectively in Electrical Power system Engineering and pursuing her Ph.D. from the S.G.B. University of Amravati in Induction Motorr protection. She is IEEE, IACSIT and ISTE member. In 2000, she joined S.S.G.M.College of Engg. Shegaon, where she is a faculty in Electrical Engg. Department. Her present research interest includes Digital protection of Induction motor & Signal Processing technique.

S.R.PARASKAR received his B.E. and M.E. from the S.G.B.University of Amravati, India in 1992 and 2001 respectively in Electrical Power system Engineering and pursuing his Ph.D. from the S.G.B. University of Amravati in Transformer protection. He is IEEE, IACSIT and ISTE member. In 1995, he joined S.S.G.M.College of Engg. Shegaon, where he Assistant Professor in Electrical Engg. Department. His present research interest includes Digital protection of Transformer, FACTS and Power Quality.

S.S.JADHAO received his B.E. and M.E. from the S.G.B.Amravati University of Amravati, India in 2009 and 2012 respectively in Electrical Power system Engineering and pursuing his Ph.D. from the S.G.B.University of Amravati, in Power Quality Enhancement. In 2011, he joined S.S.G.M.College of Engg. Shegaon, where he is a faculty in Electrical Engg. Department. His present research interest includes power quality monitoring and signal processing technique

MIRZA ANSAR BEG received his B.E. and M.E. from the S.G.B.Amravati University of Amravati, India in 1992 and 1998 respectively in Electrical Power system Engineering and Ph.D. from the S.G.B.University of Amravati, in Power Quality. He is IACSIT and ISTE member. In 1990, he joined S.S.G.M.College of Engg. Shegaon, where he is a faculty in Electrical Engg. Department. His present research interest includes power quality monitoring and signal processing technique applications in power systems applications in power syste

Congestion Mitigation based on Generator Sensitivities in Deregulation

T. Nireekshana, Dr.G.Kesava Rao and Dr.S.Siva Naga Raju

***Abstract*-Power system congestion is a main problem that the independent system operator (ISO) would face in the post-deregulated era. One of the most practiced and an obvious technique of congestion management is rescheduling the generators output power in the system. However, all generators in the system will not participate in congestion. Development of sound formulation and appropriate solution technique for this problem is aimed in this paper. Contributions made in the present paper are twofold. Firstly a technique for optimum selection of participating generators has been introduced using generator sensitivities to the power flow on congested lines. Secondly this paper proposes an algorithm based on arbitrary method which minimizes the deviations of rescheduled values of generator power outputs from scheduled levels.The suggested methodology is tested on few test cases like 6-bus system, IEEE 14-bus system, and also on IEEE 30-bus system which gives the best results in all the cases.**

Index Terms—Independent System Operator (ISO), Deregulation, Generator Sensitivity, Power world Simulator, Rescheduling.

I. INTRODUCTION

Deregulated power system means Transmission companies (TRANSCO's), Generation companies (GENCO's) and Distribution Companies (DISCO's) are under different organizations. Organizations can fix their own prices. To maintain coordination between them there will be independent system operator(ISO) in all types of deregulated power system models [1-4]. In this market GENCO's and DISCO's submit the sell and purchase decisions in the form of bids to the market operator in hourly price manner. Finally 24 hour energy prices to be paid by consumers and to be charged by producers.

T.Nireekshana is working as Asst. Prof., Dept. of EE Engineering, VNR VJIET, Hyderabad, India.nirixana@yahoo.co.in, Dr.G.Kesava Rao is working as Sr. Prof., Dept. of EE Engg., Vasireddy Venkatadri Institute of Tech., Nambur, A.P., India. deanvoice@yahoo.co.in, and Dr.S.Siva Naga Raju is working as Assoc. Prof., Dept. of Electrical Engineering, J.N.T.U College of Engg., Kakinada,A.P., India. sirigiri70@yahoo.co.in

NEED FOR AN INDEPENDENT SYSTEM OPERATOR (ISO)

With unbundling of generation from transmission sector in a competitive market, generation sector will be become fully competitive with many market participants whereas the transmission system remains regulated monopoly and it will be necessary to provide non-discriminatory and open access to all the market participants through planning and operation of power transmission system. It is also important to ensure reliability of the network in its region of operation. This function can be implemented by entity called Independent System Operator (ISO).

In deregulated power systems, ISO dispatches the generators so that to meet the demand of loads at the minimum cost while maintaining security and service quality of power system.ISO compute LMPs by running optimal power flow.

Bidding process for a specified period, e.g. next two hours, is as below.

• Every producer submits the following values to ISO:

Minimum and maximum power which can deliver to the network

Bid price for selling 1 MW electric power

• Every consumer submits the following values to ISO:

Minimum and maximum load demand

Load bid for load curtailment in emergency condition (if LMP of a load exceeds its bid then the load is curtailed till its LMP reduces to its bid)

• ISO run the optimal power flow and computes the following values:

MW dispatch of each generator

MW dispatch of each load

LMP of each bus

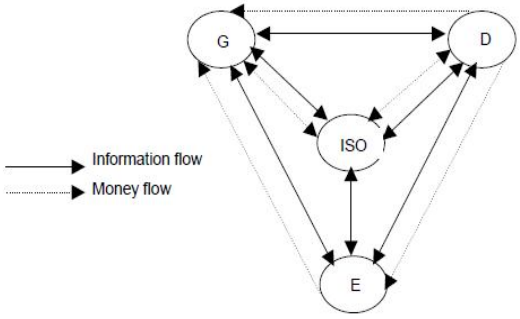

Figure1: ISO importance

With increasing demand for electric power all around the globe, electric utilities have been forced to meet the increasing demand by increasing their generation. However, the electric power that can be transmitted between two locations on a transmission network is limited by several transfer limits such as thermal limits, voltage limits and stability limits with the most restrictive applying at a given time. If the transmission line overcomes these limits, then the line is said to be "congested". Transmission networks are the main source of difficulty in deregulation [5,8]. We ensure that the power system operates within its limits is vital to maintain power system security, failing which can result in widespread blackouts with potentially severe social and economic consequences. Congestion management controlling the transmission system power transfer capability is the fundamental transmission management problem.

Congestion or overload in one or more transmission lines of the system may occur as a result of unexpected outages of generation, sudden increase of demand, tripping of transmission lines, or failures of other equipment [12,13,16]. In deregulated power Systems, congestion, which can also occur due to commercial reasons, has become a major concern. Fast, transparent, and effective tools are necessary for congestion management. Power system congestion management is a major problem in deregulated markets because of all the above reasons.

II. CONGESTION MANAGEMENT METHODS

There are two broad paradigms that may be employed for congestion management. These are the cost-free means and the not-cost-free means. The previous include actions like out aging of congested lines or operation of transformer taps, phase shifters, or FACTS devices. These means are termed as cost-free only because the marginal costs (and not the capital costs) involved in their usage are nominal [14].

The not-cost-free means include:

(1) Rescheduling generation. This leads to generation operation at an equilibrium point away from the one determined by equal incremental costs. Mathematical models of pricing tools may be incorporated in the dispatch framework and the corresponding cost signals obtained. These cost signals may be used for congestion pricing and as indicators to the market participants to rearrange their power injections/extractions such that congestion is avoided.

(2) Prioritization and curtailment of loads/transactions. A parameter termed as willingness-to-pay-to-avoid-curtailment was introduced in. This can be an effective instrument insetting the transaction restriction strategies which may then be incorporated in the optimal power flow framework.

In a congested power line, the incremental or decremented change in power outputs of all the generators do not affect the power transmitted on the congested line to the same extent. Due to this, there is no need to reschedule the outputs of generators whose generations do not affect the congested line flow. We should select the generators whose generation affects the congested line flow. To optimally select the generators participating in congestion management, the sensitivities of the generators to the congested line are used [6, 7]. The generators actually participating in congestion alleviation are chosen based on a criterion which reduces the number of participating generators.

III. PROBLEM FORMULATION

Based on the bids received from the participant generators, the amount of rescheduling required is computed by solving the following optimization problem:

$$\text{Minimize} \sum_{g}^{Ng} C_g(\Delta P_g)\Delta P_g$$

subject to

$$\sum_{g=1}^{Ng}((\mathrm{GS}_g)\Delta P_g) + F_k^0 \le F_k^{\max}$$

$$\mathrm{k} = 1, 2 \ldots \mathrm{n_l}$$

$$P_g - P_g^{\min} = \Delta P_g^{\min} \le \Delta P_g \le \Delta P_g^{\max} = P_g^{\max} - P_g$$

$$\mathrm{g} = 1, 2, \ldots \mathrm{N_g}$$

$$\sum_{g=1}^{N_g} \Delta P_g = 0$$

Where ΔP_g is the real power adjustment at bus-g and C_g are the incremental and decremented price bids submitted by generators? These are the prices at which the generators are willing to adjust their real power outputs. F_k^0 is the power flow caused by all contracts requesting the transmission service. $F_k^{\max}$ is the line flow limit of the line connecting bus-i and bus-j.

$\mathrm{N_g}$ is the number of participating generators, n_l is the number of transmission lines in the system, $P_g^{\min}$ and $P_g^{\max}$ denote respectively the minimum and maximum limits of generator outputs. It can be seen that the power flow solutions are not required during the process of optimization. .

IV. CALCULATION OF GENERATOR SENSITIVITY

The generators in the system have different sensitivities to the power flow on the congested line.

GENERATOR SENSITIVITY:

A change in real power flow in a transmission line k connected between bus i and bus j due to change in power generation by generator g can be termed as generator sensitivity to congested

line (GS).

$$\mathrm{GS}_g = \frac{\Delta P_{ij}}{\Delta P_{G_g}}$$

Where P_{ij} is the real power flow on congested line-k;P_{Gg} is the real power generated by the g^{th} generator. Basic power flow equation on congested line can be written as

$$P_{ij} = -V_i^2 G_{ij} + V_i V_j G_{ij} \cos(\theta_i - \theta_j) + V_i V_j B_{ij} \sin(\theta_i - \theta_j)$$

Where V_i andθ_i are the voltage magnitude and phase angle respectively at the ith bus; Gij and B_{ij} represent, respectively, the conductance and susceptance of the line connected between buses i and j.

$$\mathrm{GS}_g = \frac{\partial P_{ij}}{\partial \theta_i}.\frac{\partial \theta_i}{\partial P_{G_g}} + \frac{\partial P_{ij}}{\partial \theta_j}.\frac{\partial \theta_j}{\partial P_{G_g}}$$

$$\frac{\partial P_{ij}}{\partial \theta_i} = -V_i V_j G_{ij} \sin(\theta_i - \theta_j) + V_i V_j B_{ij} \cos(\theta_i - \theta_j)$$

$$\frac{\partial P_{ij}}{\partial \theta_j} = +V_i V_j G_{ij} \sin(\theta_i - \theta_j) - V_i V_j B_{ij} \cos(\theta_i - \theta_j) = -\frac{\partial P_{ij}}{\partial \theta_i}.$$

The active power injected at a bus-s can be represented as

$$P_s = P_{G_s} - P_{D_s}$$

Where P_{Ds} is the active load at bus-s .P_s can be expressed as

$$P_s = |V_s| \sum_{t=1}^{n} ((G_{st} \cos(\theta_s - \theta_t) + B_{st} \sin(\theta_s - \theta_t))|V_t|) = |V_s|^2 G_{ss} + |V_s| \sum_{\substack{t=1 \\ t \neq s}}^{n} \{(G_{st} \cos(\theta_s - \theta_t) + B_{st} \sin(\theta_s - \theta_t))|V_t|\}$$

Where n is the number of buses in the system. Differentiating above equation w.r.t.θ_t and ,θ_s the following relations can be obtained

$$\frac{\partial P_s}{\partial \theta_t} = |V_s||V_t|\{G_{st} \sin(\theta_s - \theta_t) - B_{st} \cos(\theta_s - \theta_t)\}$$

$$\frac{\partial P_s}{\partial \theta_s} = |V_s| \sum_{\substack{t=1 \\ t \neq s}}^{n} \{(-G_{st} \sin(\theta_s - \theta_t) + B_{st} \cos(\theta_s - \theta_t))|V_t|\}.$$

Neglecting P-V coupling, the relation between incremental change in active power at system buses and the phase angles of voltages can be written in matrix form as

$$\underset{n\times 1}{[\Delta P]} = \underset{\mathrm{n}\times\mathrm{n}}{[H]}\ \underset{n\times 1}{[\Delta\theta]}$$

$$\underset{\mathrm{n}\times\mathrm{n}}{[H]} = \begin{bmatrix} \frac{\partial P_1}{\partial \theta_1} & \frac{\partial P_1}{\partial \theta_2} & \cdots & \frac{\partial P_1}{\partial \theta_n} \\ \frac{\partial P_2}{\partial \theta_1} & \frac{\partial P_2}{\partial \theta_2} & & \frac{\partial P_2}{\partial \theta_n} \\ \vdots & & & \vdots \\ \frac{\partial P_n}{\partial \theta_1} & \frac{\partial P_n}{\partial \theta_2} & \cdots & \frac{\partial P_n}{\partial \theta_n} \end{bmatrix}_{\mathrm{n}\times\mathrm{n}}$$

$$[\Delta\theta] = [H]^{-1}[\Delta P] = [M][\Delta P]$$

$$[M] = [H]^{-1}.$$

To find the values of $(\partial\theta_i)/(\partial P_{G_g})and(\partial\theta_j)/(\partial P_{G_g})$in (5), $[M]$needs to be found out. However,$[H]$ is a singular matrix of rank one deficiency? So it is not directly invertible. The slack bus in the present work has been considered as the reference node and assigned as bus number 1. The elements of first row and first column of$[H]$ can be eliminated to obtain a matrix$[H_{-1}]$ which can be inverted to obtain matrix$[M_{-1}]$, where $(.)_{-1}$represents a matrix with its first row and column deleted or a vector with the first element deleted. Using these relations the following equation can be obtained.

$$[\Delta\theta_{-1}] = [M_{-1}][\Delta P_{-1}].$$

The actual vector $[\Delta\theta]$ can be found by simply adding the element $\Delta\theta_1$ to the above equation as shown by the following relation.

$$\underset{n\times 1}{[\Delta\theta]} = \begin{bmatrix} 0 & 0 \\ 0 & \underset{n\times n}{[M_{-1}]} \end{bmatrix} \underset{n\times 1}{[\Delta P]} + \Delta\theta_1 \underset{n\times 1}{\begin{bmatrix} 1 \\ 1 \\ \vdots \\ 1 \end{bmatrix}}.$$

The second term of the above equation vanishes as change in phase angle of slack bus is zero. Accordingly it reduces to

$$[\Delta\theta]_{n\times 1} = \begin{bmatrix} 0 & 0 \\ 0 & [M_{-1}] \end{bmatrix}_{n\times n} [\Delta P]_{n\times 1}.$$

Thus required elements of $(\partial\theta_i)/(\partial P_{G_g})$ and $(\partial\theta_j)/(\partial P_{G_g})$ are found out from above equation.

It is to be noted that the generator sensitivity values thus obtained are with respect to the slack bus as the reference. So the sensitivity of the slack bus generator to any congested line in the system is always zero.

GS_g denotes how much active power flow over a transmission line connecting bus-i and bus-j would change due to active power injection by generator g. The system operator selects the generators having non uniform and large magnitudes of sensitivity values as the ones most sensitive to the power flow on the congested line and to participate in congestion management by rescheduling their power outputs [9-11].

Based on the bids received from the participant generators, the amount of rescheduling required is computed by solving the following optimization problem.

V. TEST CASES & RESULTS

The proposed method is done by using power world simulator 8.0 [17] for the best results as follows.

6- BUS SYSTEM

Case 1: WHEN CONGESTION IN LINE (4-6)

Line 4-6 is congested by 101% as shown in figure 2 and it is relieved by rescheduling the generation of participating generators in congestion as follows.

SENSITIVITIES OF GENERATORS FOR CONGESTED LINE (4-6):

Table1: Sensitivities of generators to congested line (4-6)

Gen. No.	*1*	*2*	*3*	*4*
Sensitivity	*0*	*0.0647*	*-0.342*	*0.13*

Based on sensitivities of generators, the generators G1, G2, G3, and G4 are the participating generators for congestion in line 4-6 as shown in table1.

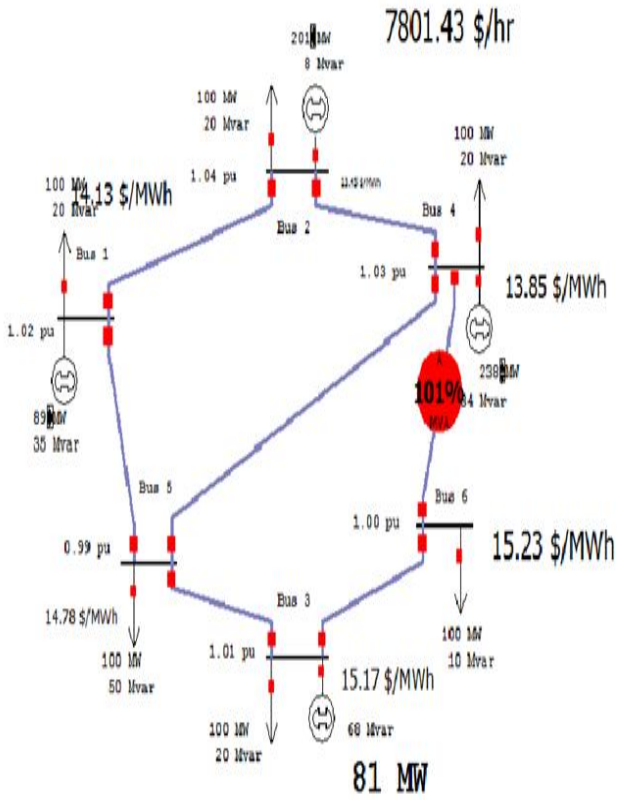

Figure 2: single line diagram of 6-Bus system (congestion case)

RESCHEDULE OF GENERATION 6-BUS SYSTEM:

Table 2: Reschedule of Generation in 6-Bus system

S N O	*GEN 1(M W)*	*GEN2 (MW)*	*GEN 3(M W)*	*GEN4 (MW)*	*TOTAL COST($/ MW)*	*% LOADI NG IN 4-6 LINE*
1	*88.9*	*201.2*	*81*	*238*	*7801.43*	*101*
2	*88.9*	*202*	*89*	*230*	*7801.34*	*99*
3	*92*	*204*	*84*	*230*	*7798.93*	*99*
4	*96*	*205*	*88*	*220*	*7804*	*96*
5	*101*	*205*	*84*	*220*	*7806.03*	*98*
6	*106*	*200*	*84*	*220*	*7807.70*	*97*
7	*106*	*200*	*94*	*210*	*7815.53*	*93*
8	*87*	*203*	*89*	*230*	*7801.5*	*97*
9	*77*	*204*	*89*	*239*	*7803.02*	*99*

Based on sensitivity of generators four generators are rescheduled their generation which should satisfy the objective function as minimization of cost and minimization

of congestion. The optimal rescheduling for this case is G1 92MW, G2 204MW, G3 84MW, G4 230MW and then the cost is 7798.93 $/MW and P_{4-6} is 99% as shown in table 2. The congestion in line 4-6 is relieved from 101% to 99% as shown in figure 3.

Case 2: WHEN CONGESTION RELIEVED IN LINE (4-6):

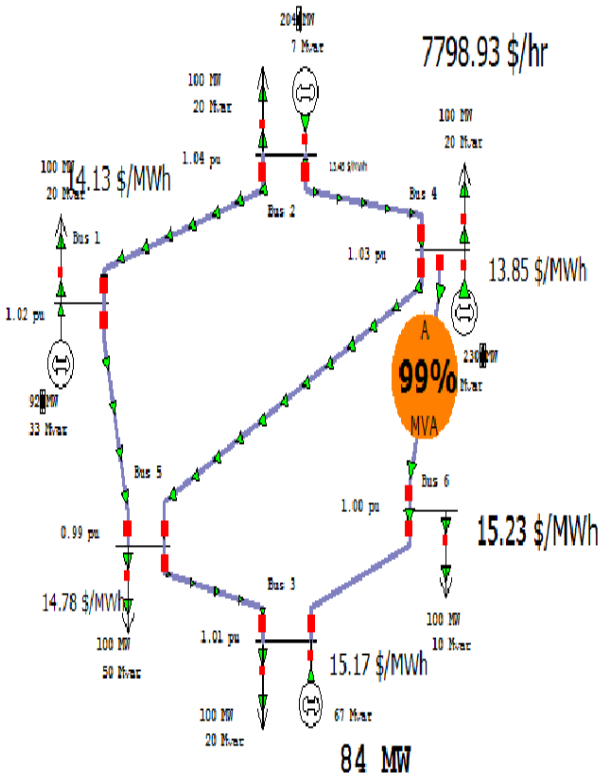

Figure 3: single line diagram of 6-Bus system (congestion relief case)

14- BUS SYSTEM

Case 1: When Congested line is 7-9:

Line 7-9 is congested by 104% as shown in figure 4 and it is relieved by rescheduling the generation of participating generators in congestion as follows.

SENSITIVITIES OF GENERATORs TO CONGESTED LINE (7-9):

Table 3: Sensitivities of generators to congested line (7-9)

Gen. No.	***1***	***2***	***3***	***6***	***8***
Sensitivity	***0***	***-0.0018***	***0.0036***	***-0.21***	***0.3281***

Based on sensitivities of generators, the generators G1, G2, G3, G6 and G8 are the participating generators for congestion in line 7-9 as shown in table 3.

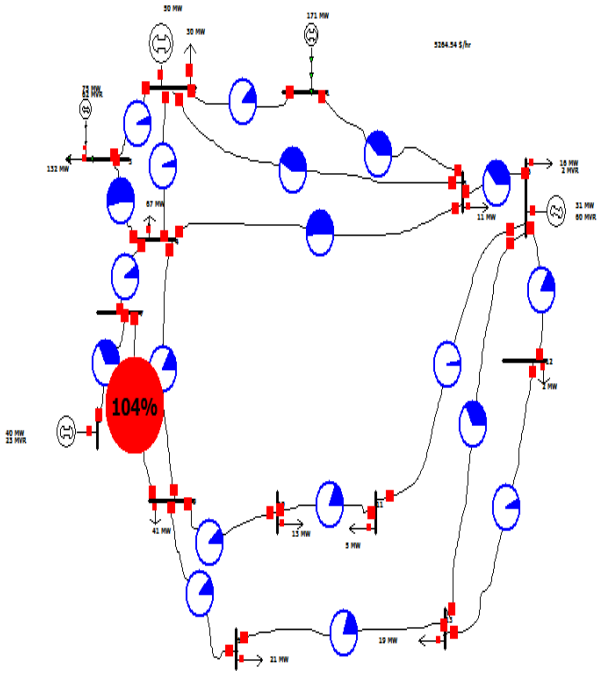

Figure 4: single line diagram of 14-Bus system (congested case)

RESCHEDULING OF GENERATORS TO CONGESTED LINE (7-9):

Table 4: Rescheduling of generators for congested line 7-9

S NO	***GEN1 (MW)***	***GEN2 (MW)***	***GEN3 (MW)***	***GEN6 (MW)***	***GEN8 (MW)***	***TOTAL COST***	***%LOADING ON 7-9 LINE***
1	***171***	***50***	***75***	***31***	***40***	***5264.54***	***104***
2	***171***	***50***	***75***	***51***	***20***	***5263.20***	***87***
3	***161***	***50***	***75***	***61***	***20***	***5257.18***	***84***
4	***151***	***60***	***75***	***61***	***20***	***5370.07***	***85***
5	***161***	***60***	***65***	***61***	***20***	***5256.93***	***86***
6	***151***	***50***	***75***	***61***	***30***	***5232.41***	***90***
7	***151***	***40***	***75***	***71***	***30***	***5146.41***	***90***
8	***151***	***30***	***75***	***81***	***30***	***5111.10***	***85***
9	***141***	***40***	***75***	***81***	***30***	***5189.36***	***90***
10	***145***	***51***	***83***	***45***	***40***	***5347.55***	***100***

Based on sensitivity of generators four generators are rescheduled their generation which should satisfy the objective function as minimization of cost and minimization of congestion. The optimal rescheduling for this case is G1

151MW, G2 30MW, G3 75MW, G6 81MW, G8 30MW and then the cost is 5111.10 $/MW and $P_{7\text{-}9}$ is 85% as shown in table 2.4. The congestion in line 7-9 is relieved from 104% to 85% as shown in figure 5.

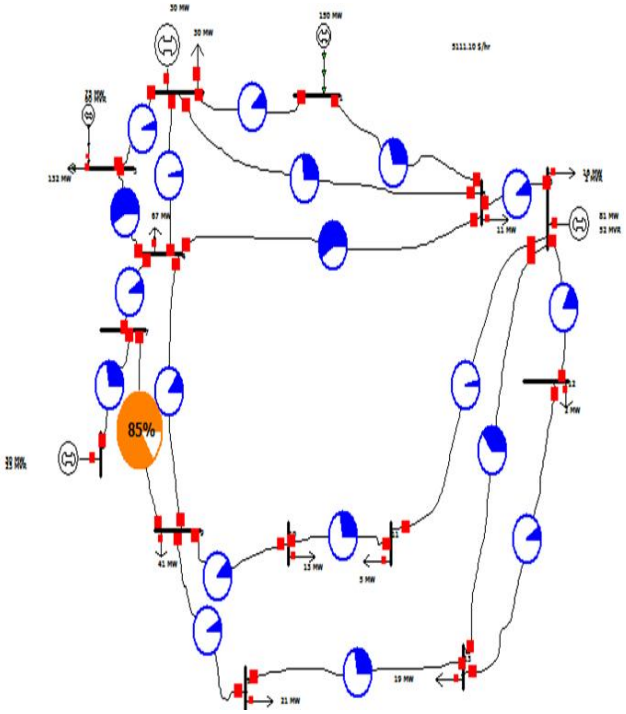

Figure 5: Single line diagram of 14- bus system (congestion relief case)

30-BUS SYSTEM

Case 1: When congested line is 12-13

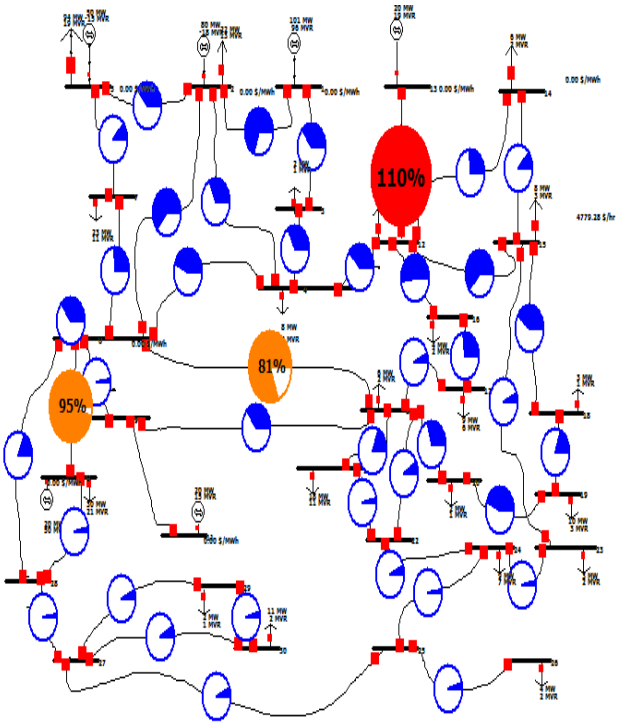

Figure 6: Single line diagram of 30-Bus system

Line 12-13 is congested by 110% as shown in figure 6 and it is relieved by rescheduling the generation of participating generators in congestion as follows.

SENSITIVITY OF GENERATORS TO CONGESTED LINE 12-13:

Table 5: Sensitivities of generators to congested line 12-13

Gen. No.	***1***	***2***	***5***	***8***	***11***	***13***
Sensitivity	***0***	***0***	***0***	***0***	***1.01***	***-1.09***

Based on sensitivities of generators, the generators G1, G2, G5, G8 and G13 are the participating generators for congestion in line 12-13 as shown in table 5.

RESCHEDULING OF GENERATORS:

Table 6: Rescheduling of 30- Bus system for line 12-13

SNO	***GEN 1***	***GEN 2***	***GEN 5***	***GEN 8***	***GEN 11***	***GEN 13***	***TOTAL COST($/MW)***
1	***101***	***80***	***50***	***20***	***20***	***20***	***4779.28***
2	***110***	***80***	***50***	***20***	***20***	***11***	***4749.58***
3	***120***	***70***	***50***	***20***	***20***	***11***	***4801.97***
4	***120***	***80***	***40***	***20***	***20***	***11***	***4208.97***
5	***120***	***90***	***30***	***20***	***20***	***21***	***3937.79***
6	***120***	***90***	***30***	***24***	***20***	***17***	***3923.59***
7	***120***	***90***	***30***	***26***	***20***	***15***	***3924.7***
8	***122***	***90***	***20***	***26***	***30***	***15***	***3740.07***
9	***111***	***81***	***20***	***35***	***30***	***15***	***3764.83***
10	***112***	***80***	***20***	***35***	***30***	***15***	***3769.48***
11	***82***	***80***	***50***	***15***	***35***	***30***	***4782.52***

Based on sensitivity of generators four generators are rescheduled their generation which should satisfy the objective function as minimization of cost and minimization of congestion. The optimal rescheduling for this case is G1 122MW, G2 90MW, G5 20MW, G8 26MW, G11 30MW, G13 15MW and then the cost is 3740.07 $/MW and $P_{7\text{-}9}$ is 96% as shown in table 6. The congestion in line 12-13 is relieved from 110% to 96%.

VI. CONCLUSION

This paper gives a method for congestion management in transmission grids using cost-efficient generation rescheduling to minimize the congestion. A realistic

frequency and voltage dependent modified fast decoupled load flow method is used with multi objective as minimization of cost and minimization of congestion to solve this complex problem. This method also provides a set of Pareto optimal solutions for any congestion problem, giving the system operator options for judicious decision in solving the congestion.

This paper focuses on demonstrating a technique for optimum selection of generators for congestion management and additionally the application of rescheduling in the solution of the congestion management problem. Generators from the system are selected for congestion management based on their sensitivities to the power flow of the congested line followed by corrective rescheduling. The problem of congestion is modelled as an optimization problem.

REFERENCES

[1] R. D. Christie, B. Wollenberg, and I. Wangensteen, "Transmission management in the deregulated environment," Proc. IEEE, vol. 88, no. 2, pp. 170–195, Feb. 2000.

[2] A. Kumar, S. C. Srivastava, and S. N. Singh, "Congestion management in competitive power market: A bibliographical survey," Elect. Power Syst. Res., vol. 76, pp. 153–164, 2005.

[3] Y. H. Song and I.-F. Wang, Operation of Market Oriented Power Systems. New York: Springer, 2003, ch. 6.

[4] K. L. Lo, Y. S. Yuen, and L. A. Snider, "Congestion management in deregulated electricity markets," in Proc. Int. Conf. Electric Utility Deregulation and Restructuring and Power Technologies, London, U.K., 2000, pp. 47–52.

[5] R. S. Fang and A. K. David, "Transmission congestion management in an electricity market,," IEEE Trans. Power Syst., vol. 14, no. 3, pp. 877–883, Aug. 1999.

[6] A. J. Conejo, F. Milano, and R. G. Bertrand, "Congestion management ensuring voltage stability," IEEE Trans. Power Syst., vol. 21, no. 1, pp. 357–364, Feb. 2006.

[7] G. Granelli, M. Montagna, F. Zanellini, P. Bresesti, R. Vailati, and M. Innorta, "Optimal network reconfiguration for congestion management by deterministic and genetic algorithms," Elect. Power Syst. Res., vol. 76, pp. 549–556, 2006.

[8] F. Jian and J. W. Lamont, "A combined framework for service identification and congestion management,," IEEE Trans. Power Syst., vol. 16, no. 1, pp. 56–61, Feb. 2001.

[9] H. Y. Yamina and S. M. Shahidehpour, "Congestion management coordinationin the deregulated power market," Elect. Power Syst. Res., vol. 65, no. 2, pp. 119–127, May 2003.

[10] F. Capitanescu and T. V. Cutsem, "A unified management of congestions due to voltage instability and thermal overload,," Elect. Power Syst. Res., vol. 77, no. 10, pp. 1274–1283, Aug. 2007.

[11] C. N. Yu and M. Ilic, "Congestion clusters based markets for transmission management," in Proc. IEEE Power Eng. Soc. Winter Meeting, New York, Jan. 1999, pp. 1–11.

[12] A. Kumar, S. C. Srivastava, and S. N. Singh, "A zonal congestion management approach using ac transmission congestion distribution factors,," Elect. Power Syst. Res., vol. 72, pp. 85–93, 2004.

[13] A. Kumar, S. C. Srivastava, and S. N. Singh, "A zonal congestion management approach using real and reactive power rescheduling,," IEEE Trans. Power Syst., vol. 19, no. 1, pp. 554–562, Feb. 2004.

[14] A. S. Nayak and M. A. Pai, "Congestion management in restructured power systems using an optimal power flow framework," M.S. thesis, Univ. Illinois, Urbana-Champaign, 2002, pp. 12–17.

[15] B. K. Talukdar, A. K. Sinha, S. Mukhopadhyay, and A. Bose, "A computationally simple method for cost-efficient generation rescheduling and load shedding for congestion management," Int. J. Elect. Power Energy Syst., vol. 27, no. 5, pp. 379–388, Jun.–Jul. 2005.

[16] G. Yesuratnam and D. Thukaram, "Congestion management in open access based on relative electrical distances using voltage stability criteria," Elect. Power Syst. Res., vol. 77, pp. 1608–1618, 2007.

[17] Power World Simulator 8.0 software.

Biography of Authors

T. Nireekshana obtained her B.Tech and M.Tech from JNT University in 2002 and 2005 respectively. She is Assistant professor in EEE, VNR VJIET Engineering College, Hyderabad. She has been pursuing Ph.D work, part-time with JNTU.

G. Kesava Rao obtained his PhD from Moscow Power Engineering Inst. Moscow, U.S.S.R. He worked in Institute of Technology at Banaras Hindu University, Varanasi, India in various administrative and academic positions. Currently, he is working at Vasireddy Venkatadri Institute of Technology Nambur, A.P., India. His fields of interest are power system deregulation and renewable energy sources.

Dr.S.Siva Nagaraju, is graduated in 1998, Masters in 2000 from IIT, Kharagpur and did his Ph.D from J.N.T.University in 2004. Working as Associate Professor in the Department of Electrical Engineering, J.N.T.U College of Engg. (Autonomous), Anantapur, Andhra Pradesh since November 2006. He has received two National awards (Pandit Madan Mohan Malaviya memorial prize award and Best Paper Prize award) from the Institute of Engineers (India) for the year 2003-2004. He is Referee for IEE Proceedings- Generation Transmission and Distribution and International Journal of Emerging Electric Power System. About 40 publications in National and International Journals and Conferences to his credit. His areas of interest are in Power Systems, Distribution Automation, Genetic Algorithm applications to distribution systems and power system.

Power Factor Improvement Using PQ Theory Based Hybrid Controller for Three Phase Converter

M.Abitha Thangam and Dr.V.Gopalakrishnan

***Abstract*—Three-phase controlled rectifiers have a wide range of applications, from small rectifiers to large High Voltage Direct Current (HVDC) transmission systems. It can handle reasonably high power and has acceptable input and output harmonic distortion. Harmonics present in the three phase converter is the major issue while it is been connected to the electric power distribution system. As the conventional model uses real time switching control, this paper deals with discrete event switching control based on hybrid system theory considering Lyapunov stability. Use of hybrid Controller is new to power electronic applications and hence the converters can provide input currents without distortion and with the unity power factor.**

***Keywords*— Harmonics, Discrete Event Switching Control, Hybrid controller, Lyapunov Stability**

I. INTRODUCTION

Diode rectifiers are widely employed in industrial fields and consumer products thanks to advantages of low cost, simple structure, robustness and absence of control. However, this type of converters results in only unidirectional power flow, low input power factor, high level of harmonic input currents, malfunction of sensitive electronic equipment, increased losses and also contributing to inefficient use of electric energy. Recently, many promising power factor correction (PFC) techniques have been proposed for rectifiers. Apart from application of active and passive filters, the best solution is in using pulse width modulated (PWM) rectifiers. Research interest in three-phase PWM rectifiers has grown rapidly over the last few years due to some of their important advantages, such as power regeneration capabilities, control of dc-bus voltage over a wide range, and low harmonic distortion of input currents.

Since the converter has abilities to control the input currents in sinusoidal waveforms, unity power factor [1]operation can be easily performed by regulating the currents in phase with the power-source voltages. From the control point of view, power electronic circuits and system constitute excellent examples of hybrid systems, since the discrete switch positions are associated with different modes of continuous time dynamics

Lyapunov theory has for long time been an important tool in linear as well as nonlinear control. However, its use within the nonlinear control has been changed by the difficulties to find the Lyapunov function for a given system. If one can be found, the system is known to be stable, but the task of finding such function has often been left to the imagination and experience of the designer [6].

M.Abitha Thangam and Dr.V.Gopalakrishnan are working in Department of ECE, Coimbatore Institute of Technology, Coimbatore, Email: abithathangam@yahoo.co.in

A. Aims and Objectives

The aims of this paper includes the design of the control law of the boost rectifier to determine the occurrence of control input function in both ac current and dc voltage control of the converter, to achieve the control of power and grid current in steady state and transient operating conditions and to implement Discrete event based switching control strategy with respect to lyapunov stability theorem for the switching action of three phase converter

The objectives are to limit the Total Harmonic Distortion (THD) of the input ac voltage and current and to control and to improve the Power Factor

II. ANALYSIS OF THREE PHASE CONVERTER

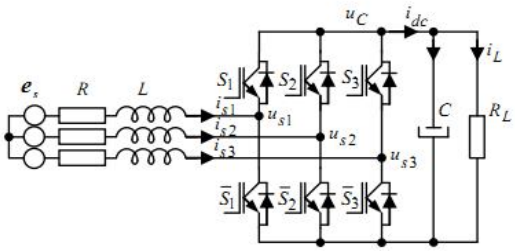

Fig. 1 Three Phase Converter

The circuit diagram of three phase converter is shown in Fig 1.The main circuit consists of a bridge rectifier made up of six power transistors with antiparallel diodes, which is connected to the three-phase supply, through an inductor *L*. A load and a capacitor *C* are connected to the dc side of the converter. The inductor *L* performs the voltage boost operation in combination with the capacitor *C* and at the same time acts as a low pass filter for the ac line current.

The dynamics of a three-phase boost rectifier in the three-phase reference frame for ac current control system is described as:

$$L\frac{di_j}{dt} + Ri_j = e_{sj} - u_{sj}$$

$$u_{sj} = \left\{ d_j - \left\{ \frac{(d_1 + d_2 + d_3)}{3} \right\} u_c \right\}, j = 1,2,3... \quad (1)$$

and for output voltage control system as:

$$C\frac{du_c}{dt} = i_{dc} - i_L = i_1 d_1 + i_2 d_2 + i_3 d_3 - \frac{u_c}{R_L} \quad (2)$$

where d_j is the duty ratio

From the point of view of the commutation process, converters can be classified in two important categories:

- Line Commutated Controlled Rectifiers (Thyristor Rectifiers)
- Force Commutated PWM Rectifiers.

Force-commutated rectifiers are built with semiconductors with gate-turn-off capability and it allows the commutation of the valves hundreds of times in one period, which is not possible with line commutated rectifiers, where thyristors are switched ON and OFF only once a cycle. This feature has the following advantages: a) the current or voltage can be modulated (Pulse Width Modulation or PWM), generating less harmonic contamination;b) power factor can be controlled, and even it can be made leading.

There are two ways to implement force-commutated three-phase rectifiers: a) as a current source rectifier, where power reversal is by dc voltage reversal; and b) as a voltage source rectifier, where power reversal is by current reversal at the dc link. The PWM pattern controls the rectifier in two different ways: 1) as a voltage source current controlled PWM rectifier, or 2) as a voltage source voltage controlled PWM rectifier. The first method controls the input current, and the second controls the magnitude and phase of the voltage. The current controlled method[2] is simpler and more stable than the voltage-controlled method. The current control is achieved by measuring the instantaneous phase currents and forcing them to follow a sinusoidal current reference. Input voltages and currents should be sinusoidal shaped without a phase delay between the voltage and the current and output dc voltage should be a constant value by change of voltage dependent current and parameters of the converter [4]

III. SVPWM BASED SWITCHING CONTROL

Space-vector pulse width modulation (SVPWM) technique has become a popular PWM technique for three-phase voltage-source converters. The structure of a typical three-phase converter is shown in Fig 1. The u_{s1}, u_{s2}, u_{s3} are the output voltages of the converter.

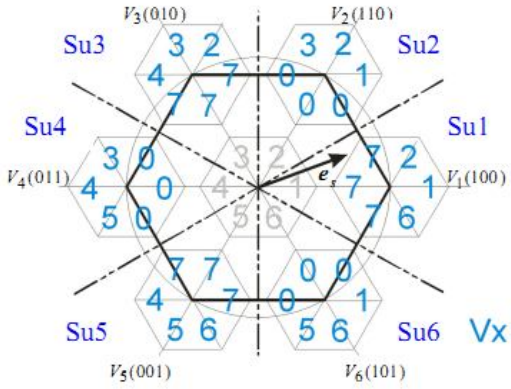

Fig. 2 The Basic Space Vectors (Normalized w.r.t. e_s) and Switching States

The six power transistors that shape the output are controlled by S_1, $\sim S_1$, S_2 , $\sim S_2$, S_3 and $\sim S_3$. [5]When an upper transistor is switched on (i.e., when S_1, S_2 or S_3 is 1), the corresponding lower transistor is switched off (i.e., the corresponding $\sim S_1$, $\sim S_2$ or $\sim S_3$ is 0). The on and off states of the upper transistors, or equivalently, the state of S_1, S_2 and S_3 , are sufficient to evaluate the output voltage for the purpose of this discussion. As shown in Fig 2, there are eight possible combinations of on and off states for the three upper power transistors

TABLE I. SIGN E_S VS SIGN D_J

Sign E_s		Su1	Su2	Su3	Su4	Su5	Su6
Sign D_j		100	110	010	011	001	101
Sdi0	000	V7	V0	V7	V0	V7	V0
Sdi1	100	V1	V1	V7	V0	V7	V1
Sdi2	110	V2	V2	V2	V0	V7	V0
Sdi3	010	V7	V3	V3	V4	V7	V0
Sdi4	011	V7	V0	V4	V5	V4	V0
Sdi5	001	V7	V0	V7	V6	V5	V5
Sdi6	101	V6	V0	V7	V0	V6	V6
Sdi7	111	V7	V0	V7	V0	V7	V0

The proposed logical event-driven grid current control[3] can be realized in the form described in Table I, where states of grid current control error are presented by *sign(Dj)* (*Dj* $=S_1$, $S_2.S_3$) and currently active voltage sector is presented by *sign Es* (e_{S1}, e_{S2}, e_{S3}). The transition between converter switch states is performed by switching only one converter leg, converter switching frequency grid current chattering are reduced.

IV. PROPOSED CONTROL SCHEME

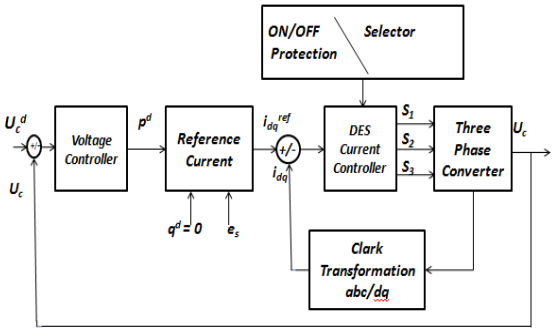

Fig. 3 Block Diagram of Proposed method

Fig. 3 shows the block diagram of proposed method. The description about the control method is discussed in the following sections.

A. Output Voltage Control

The unity power factor of ac/dc boost rectifier will be achieved for $u_C = u_d$, $u_q = 0$ in d-q output reference frame.

The output voltage control error

$$\sigma_u = u_c^d - u_c \tag{3}$$

determines the input dc current i_{dc} which also plays the role of the rectifier output current.

With $\frac{d}{dt}(\sigma_u) = -d_u \sigma_u$ we get a robust PI-control algorithm [8]:

$$i_{dc}(k) = i_{dc}(k-1) + \left(\frac{G_u C}{T}\right) * \left((1 + T d_u)\sigma_u(k) - \sigma_u(k-1)\right) \tag{4}$$

In the proposed algorithm the output load resistance R_L does not appear, therefore the control is independent of its value. The resistive load can change its value in transient states, i.e. which includes step change of its value. The rectifier dc current i_{dc} ,which forms an input for dc boost rectifier part is influenced by a dc output voltage error $\sigma_u(k)$, dc bus capacitor C, used sampling time T and feedback gain G_u. The asymptotical stability of algorithm is guaranteed with the proper choice of parameter du.

B. Reference Input Power

The reference input active power would be determined with dc current i_{dc} and bus voltage u_{dc}:

$$p^d = u_{dc} i_{dc} \tag{5}$$

C. Unity Power Factor Control

The calculation of active and reactive components of modulating currents is produced by the method of instantaneous power, known as the "Akagi-Nabae theory" [8]. This theory, also known as pq-theory, is based on Clark transformation. Thus, the reference current signals i_{sd}^{ref} , i_{sq}^{ref} can be received as:

$$\begin{bmatrix} i_{sd}^{ref} \\ i_{sq}^{ref} \end{bmatrix} = \frac{1}{e_{sd}^2 + e_{sq}^2} \begin{bmatrix} e_{sd} & e_{sq} \\ e_{sq} & -e_{sd} \end{bmatrix} \begin{bmatrix} p^d \\ q^d \end{bmatrix} \tag{6}$$

where p^d and q^d are reference active and reactive power signals.

Reference current signals in three-phase system are calculated by reverse Clark transformation. For unity power factor $q^d = 0$ and the reference grid current will

$$i_{sd}^{ref} = \left(\frac{e_{sd}}{\left(e_{sd}^2 + e_{sq}^2\right)}\right) * p^d \tag{7}$$

$$i_{sq}^{ref} = \left(\frac{e_{sq}}{\left(e_{sd}^2 + e_{sq}^2\right)}\right) * p^d \tag{8}$$

One of the main advantages of pq-theory is that there is no need for phase synchronization with system voltages. Also, average components p and q can be easily detected (filtered) by means of low-order low-pass filters. The latter makes positive impact on system dynamic and stability.

D. Lyapunov Theorem Based Control Method

1) Lyapunov's second method for stability

Lyapunov, proposed two methods for demonstrating stability. The first method developed the solution in a series which was then proved convergent within limits. The second method, which is almost universally used nowadays, makes use of a *Lyapunov function V(x)* which has an analogy to the potential function of classical dynamics. It is introduced as follows. Consider a function $V(x) : Rn \rightarrow R$ such that

- $V(x) \geq 0$ with equality if and only if $x = 0$ (positive definite)
- $\frac{d}{dt} V(x) \leq 0$ with equality if and only if $x = 0$ (negative definite).

Then V(x) is called a Lyapunov Function candidate and the system is asymptotically stable in the sense of Lyapunov .

2) Design of Control Law For Three Phase Converter

The aim of this project is the design of a control law for a boost rectifier in order to achieve a output voltage and grid current control in a steady state and transient operation conditions. The feedback system is globally asymptotically stable in the sense of Lyapunov stability theory. Therefore, we are interested in the aim extension of the Lyapunov function concepts.

On the basis of Lyapunov stability theory, a positive definite scalar function V, as a candidate for the Lyapunov function, is to be found, such that the total energy of the system is continuously dissipated. In such a case, any nonlinear system must eventually settle down to an equilibrium point. For the Lyapunov function candidate

$$V = \frac{1}{2} \Delta i_s^T \Delta i_s = \frac{1}{2} \left(i_s - i_s^d\right)^T \left(i_s - i_s^d\right) \tag{9}$$

the stability requirement will be fulfilled if control can be selected as such, that the derivative of the Lyapunov function candidate is negative.

Derivatives of the current control error (9) may be expressed with the voltage equation

$$\frac{d}{dt}\left(i_s - i_s^d\right) = \frac{1}{L}\left(e_s - R i_s - u_s\left(V_i\right)\right) - \frac{d}{dt} i_s^d \tag{10}$$

where i_s^d , i_s are desired and actual grid current,

$u_s(V_i)$ is voltage control input,

Ri_s is resistive voltage drop and

e_s is ac input voltage.

For $d(\Delta i_s)/dt = 0$ the equivalent control voltage [7] can be expressed as:

$$u_{equ} = e_s - R i_s - L \frac{d}{dt} i_s^d \tag{11}$$

and derivative of Lyapunov function is

$$\frac{d}{dt}V(x)=\left(i_s-i_s^d\right)\frac{\left(u_{equ}-u_s\left(V_i\right)\right)}{L}<0 \qquad (12)$$

The conditions for the sequential switching of the power converter are selected as:

$S_1 = \frac{1}{2}$ (1-sign(A))

$S_2 = \frac{1}{2}$ (1-sign(B))

$S_3 = \frac{1}{2}$ (1-sign(C))

where

$$A=\left(i_{sd}-i_{sd}^{ref}\right)$$

$$B=-\frac{1}{2}\left(i_{sd}-i_{sd}^{ref}\right)-\frac{\sqrt{3}}{2}\left(i_{sq}-i_{sq}^{ref}\right)$$

$$C=-\frac{1}{2}\left(i_{sd}-i_{sd}^{ref}\right)+\frac{\sqrt{3}}{2}\left(i_{sq}-i_{sq}^{ref}\right) \qquad (13)$$

which is evolved from the Lyapunov function derivative. When U_{dc} has enough magnitude that V<=0 , than $V \rightarrow 0$ and $i_s \rightarrow i_s^d$.

V. IMPLEMENTATION

A. Steps To Implement Discrete Event Model

- Obtaining feedback signals such as input ac current, input ac voltage, output dc current, output dc voltage to generate current error signals
- Generating input voltage sector states
- Implementing the table obtained for current error signals and voltage sector states using Hybrid controller

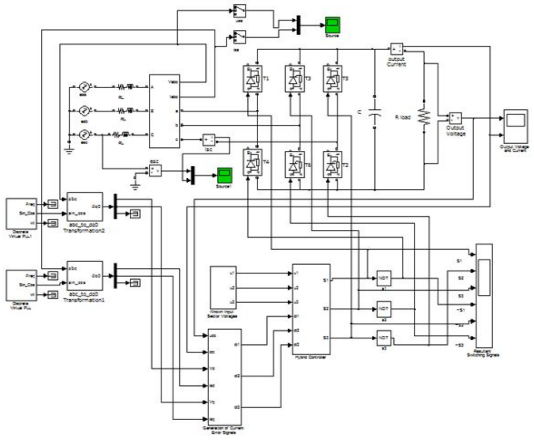

Fig .4 Simulink model of proposed method

The simulink model shown in Fig 4 has three voltage sources phase shifted by 120˚ in order to obtain the three phase voltage input to the converter. The resistance and inductance are connected serially to the three phases of the voltage source.Three phase voltage and current in abc axis is transformed to dqo axis using abc to dqo transformation block in simulink. The o axis signal is blocked using the terminator. The available voltage and current signals in dq axis is given as the feedback signals to generate current error.

Three phase converter is composed of six thyristor switches, where three switches are connected to the top of the three phase leg and other three to the bottom of the leg. The gate pulses to the switches are given from the output of the hybrid controller. As no two switches in the same leg can be switched on at the same instant, the switching pulses to the upper and lower switches in a leg are inverted. The resistive load is connected at the output side of the three phase converter. The filter capacitor is connected in parallel to the resistive load to remove the noise in the circuit. The harmonics is analysed for three phase input current and voltage after developing the discrete event model using FFT analysis.

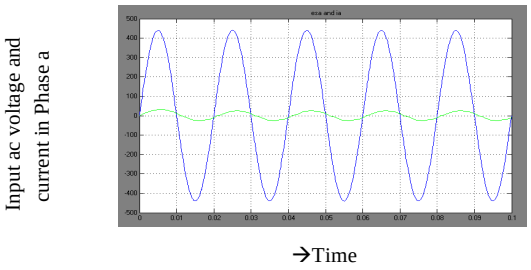

Figure 5(a) Input ac voltage and current in Phase a Vs Time

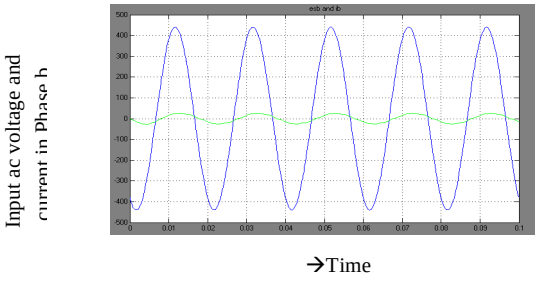

Figure 5(b) Input ac voltage and current in Phase b Vs Time

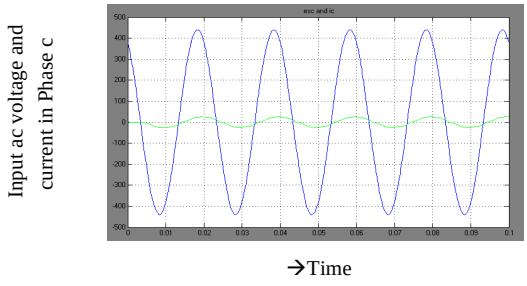

Figure (c) Input ac voltage and current in Phase c Vs Time

The ac current in the three phases of the converter after implementing the discrete event model is analyzed and shown in Fig 5(a),(b),(c).The input ac voltage and current are in phase in all the three phases a,b,c. Thus the unity power factor is achieved in the three phase converter using discrete event model. The FFT analysis for harmonics is shown in Fig 6.

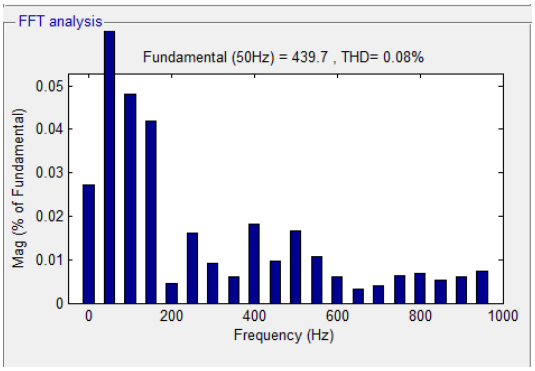

Fig 6 FFT Analysis for three phase input current using Discrete event model

VI. CONCLUSION

The hybrid based discrete event model is designed for auxiliary steering and protection functions for a three phase rectifier. The proposed discrete event model generates switching signals and controls the switches of the three phase converter. The power factor is improved by neglecting the reactive power and controlling only the active power. The stability is taken into account for analyzing the voltage and current using Lyapunov method. The feedback system is globally asymptotically stable in the sense of Lyapunov.

REFERENCES

[1] H.M. Suryawanshi, M.R. Ramteke, K.L. Thakre and V.B. Borghate, "Unity-Power-Factor Operation of Three-Phase AC-DC Soft Switched Converter based on Boost Active Clamp Topoly in Modular Approach," *IEEE Tran. Power Electronics*, vol. 23, no. 1, pp. 229-236, 2008.

[2] J. Dannehl and F.W. Fuchs, "Discrete Sliding Mode Current Control of Three-phase Grid-Connected PWM Converters," in *Proc. 13th European Conference on Power Electronics and Applications*, EPE'09, pages 1-10, 2009.

[3] A. Polic and K. Jezernik, "Closed-loop matrix based model of discrete event systems for machine logic control design," *IEEE Trans. Industrial Informatics*, vol. 1, no. 1, pp. 39-46, 2005.

[4] P. Antoniewicz and M.P.Kazmierkowski, "Virtual-Flux-Based Predictive Direct Power Control of AC/DC Converters with Online Inductance Estimation," *IEEE Tran. Ind. Electronics*, vol. 55, no. 12, pp. 4381 - 4390, 2008.

[5] A. Sabanovic, K. Jezernik and N. Sabanovic, "Sliding Modes Applications in Power Electronics and Electrical Drives," in *Lecture notes in control and information sciences*, 1st ed., Y.U. Xinghuo, X.U. Jian-Xin, (Ed.). Berlin: Springer, pp. 223–251, 2002.

[6] M.S. Branicky, V.S. Borkar and S.K. Mitter, "A unified framework for hybrid control: model and optimal control theory," IEEE Trans. Autom. Control., vol. 43, no. 1, pp. 31-45, Jan. 1998.

[7] V.I. Utkin, Sliding Modes in Control and Optimization. Berlin: Springer Verlag, 11992.

[8] H. Akagi, Y. Kanazava and A. Nabae, "Generalized Theory of the Instantenous reactive Power in Three-phase Circuits". In Proc. of the 1983 Int. Power Electronics Conference, Tokyo, Japan, 1983.

Artificial Neural Network Based Control of Doubly Fed Induction Generator

G. Venu Madhav and Y. P. Obulesu

Abstract : **In this paper, Artificial Neural Network (ANN) control technique has been developed for Doubly Fed Induction Generator (DFIG) based wind energy generation system. With the increasing use of wind power generation, it is required to instigate the dynamic performance analysis of Doubly Fed Induction Generator under various operating conditions. In this paper, two control techniques have been proposed, the first one is using PI controller and the second one is based on ANN. The performance of the proposed control techniques is demonstrated through the results. From the results it is observed that the dynamic performance of the DFIG is improved with the ANN control technique.**

Index Terms — **Wind power generation, Simulation, Control, Neural networks, Doubly fed induction generator.**

I. INTRODUCTION

The impact of wind farms on the power systems has mainly been on the voltage of the local feeder and the local substation. As the size of the wind farms increases on as well as the level of penetration into power system, the impact on the power system is not only local but has influence on a much larger part of the system including the unit commitment and dispatch.

Present growth and related installed power level make necessary to develop wind farm control capabilities and strategies that had features equivalent to conventional power plants. These features include capabilities to control the output power of the total wind farm, control of the reactive power and robustness to faults in the grid. This will enable wind power plants to be included as active components of the power supply system, [2]-[3].

The purpose of the control system is to manage the safe, automatic operation of the turbine, within a framework of optimizing generated power. This reduces operating costs, provides consistent dynamic response and improved product quality, and helps to ensure safety by maximizing the capture of the wind energy due to minimization of turbine loads.

G. Venu Madhav is with Padmasri Dr. B. V. Raju Institute of Technology, Narsapur, Medak Dist., AP, India (phone: 9848749953 fax: 08458-222002; e-mail: venumadhav.gopala@ gmail.com) and Y. P. Obulesu is with LakiReddy BaliReddy College of Engineering, Mylavaram, Krishna Dist., AP, India. He is now with the Department of Electrical and Electronics Engineering as Professor (e-mail: ypobulesh@gmail.com).

Many wind power turbines with related control strategies were developed by so many authors. These strategies include fixed and variable wind turbines with the same purpose of extracting the maximum wind power with the best quality service.

This paper describes wind generation models for operation within power system in order to perform stability analysis and turbine control to maximize the power generated with the lowest impact on the grid voltage and frequency during normal operation and under several disturbances, such as a transmission line earth fault. The discussed methods considers wind turbines based on induction generator and a grid-connected converter with constant or variable blade angle applied to variable speed wind turbines. The study is performed within the multiple technologies design tool MATLab/Simulink, [4].

In this paper, two power control techniques are investigated and they are: PI controller based technique and ANN based technique for better dynamic control of DFIG. To ensure better stability and power regulation generated by the wind turbine the ANN technique will allow the increase of robustness, performance, and flexibility.

II. MODELING OF DFIG

The overall structure of the model that is being used in this work includes aerodynamic, mechanical and electric system components, with an overall control system model. The electric model interfaces with the grid model, whereas the aerodynamic model interfaces to the wind model, [2]-[3].

A. Doubly Fed Induction Generator

The induction generator model adopted in this work is the qd0 stationary rotating reference frame model because it is more appropriate to simulate induction machine transients. The mathematical transformation abc to qd0 facilitates the computation of the transient solution of the induction generator model by transforming the differential equations with time-varying inductances to differential equations with constant inductances, [5]-[8].

$$v_{qs} = R_s i_{qs} + \omega \Psi_{ds} + \frac{d\Psi_{qs}}{dt} \quad (1)$$

$$v_{ds} = R_s i_{ds} - \omega \Psi_{qs} + \frac{d\Psi_{ds}}{dt} \quad (2)$$

$$v'_{qr} = R'_r i'_{qr} + (\omega - \omega_r)\Psi'_{dr} + \frac{d\Psi'_{qr}}{dt} \quad (3)$$

$$v'_{dr} = R'_r i'_{dr} - (\omega - \omega_r)\Psi'_{qr} + \frac{d\Psi'_{dr}}{dt} \quad (4)$$

$$T_{em} \approx \frac{3}{2}\frac{p}{2} L_m (i'_{dr} i_{qs} - i'_{qr} i_{ds}) \quad (5)$$

The study of the induction generator reveals the stability and performance in transient condition of the induction generator to mechanical input torque when connecting the doubly fed induction generator to the power system.

B. Power Electronics Converters

Using a PWM back-to-back converter the voltage fluctuations, frequency, and output power from the wind turbine can be controlled. The converter takes control on the fluctuating non-grid frequency output power of the induction generator to a DC voltage level that will be injected through a PWM-converter into a three-phase grid frequency power, [9]-[10].

The electronic power converter used was a back-to-back converter which allows to inject and get current from the rotor with current flowing both sides, [5], [7].

III. PI CONTROLLER BASED DFIG

It is intended to control the power delivered by each generator in a way to optimize the operation of the wind park with propose to deliver the maximum active power to the grid in conditions of quality of service an d safety. Also it intends to control the reactive power flow according to specified needs and dispatch. Thus, an adequate control strategy cans [9]:

1) Control the active power supplied by the turbine in order to optimize the operating point;
2) Limit the active power in the case of high wind speed;
3) Control the interchange of the reactive power between the generator and the grid, especially in the case of weak grids, where voltage fluctuations can occur;
4) Guarantee the quality of service of the wind park, namely the grid voltage;
5) Minimize the exploration and maintenance costs of the wind park.

A typical configuration of PI control based DFIG is illustrated in Figure 1.

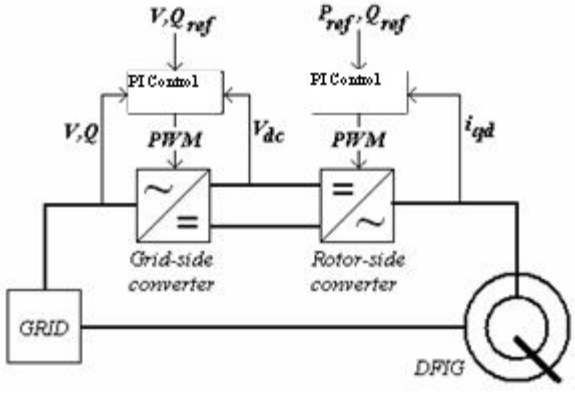

Fig. 1. General DFIG PI control structure.

The aim of the rotor- side converter is the independent control of the active power and reactive power which are controlled, not directly, but by the control of the rotor current. The aim of the grid-side converter is to keep constant the DC voltage in the intermediate capacitor in order to guarantee an operation of the converter with power factor equal to one guaranteeing only the exchange of reactive power through the stator, [10].

In Figure 1, P_{ref} is the optimal value for the active power and is gotten from the characteristic of the turbine for the speed of rotation of the rotor and the pitch angle. The value of Q_{ref} is defined in a way to keep the voltage stable at the grid connection point.

Several strategies of control have been vastly argued in literature. The use of vector control allows the decoupling of rotor current components q and d in order to control the flow of the active and reactive energies, [5], [10].

A. Grid-Side Converter Control

The main objective of the grid-side converter is to keep a constant DC link voltage independent of the value and direction of the rotor power flow. For this, a vector control strategy is used considering a referential oriented with the position of the voltages of the stator or grid. This allows independent control of the active and the reactive power between the converter and the grid.

For the internal control loop it is necessary to design the PI controllers' functions, which are obtained by application of the Laplace transform of (5) that represents the grid-side converter voltages in its dq components, [9].

$$v_q = R\ i_q + L\frac{di_q}{dt} + \omega_e L i_d + v_{q1} \quad (6)$$

$$v_d = R\ i_d + L\frac{di_d}{dt} - \omega_e L i_q + v_{d1} \quad (7)$$

Using the Laplace transformation

$$v_q = (R + sL) i_q + \omega_e L i_d + v_{q1} \quad (8)$$

$$v_d = (R + sL) i_d - \omega_e L i_q + v_{d1} \quad (9)$$

Assigning in the previous equations:

$$v'_q = (R + sL) i_q \quad (10)$$

$$v'_d = (R + sL) i_d \quad (11)$$

the following equations can be used to design the current control loops, [9]:

$$F(s) = \frac{i_q}{v'_q} = \frac{i_d}{v'_d} = \frac{1}{R+sL} \quad (12)$$

Replacing (7) in (6), respectively, and being $v_q(s) = 0$ the reference for the voltages values v_{q_ref} and v_{d_ref} can be obtained by:

$$v_{q\_ref} = -v'_q - \omega_e L i_d + v_q \quad (13)$$

$$v_{d\_ref} = -v'_d - \omega_e L i_q + v_d \quad (14)$$

These reference values are the inputs used in the PWM converter in order to guarantee the DC voltage level and required power factor.

The grid-side converter control diagram is shown in Figure 2, for which normalized design techniques can be applied.

B. Rotor-Side Converter Control

The control of the induction generator rotor is carried through in a synchronous rotating dq referential, with the d-axis aligned with the stator flux position. In this way decoupling between the electromagnetic torque and rotor the magnetizing current can be obtained. The PWM converter acts on the generator rotor and the control is done by means of the signals of the rotor and the stator currents, the stator voltage and the rotor position.

Figure 3 presents the controller of the rotor-side converter control diagram. The control design of the rotor-side converter can be made in a similar way as the one considered for the grid-side converter. The rotor voltage in the dq referential can be obtained from (10).

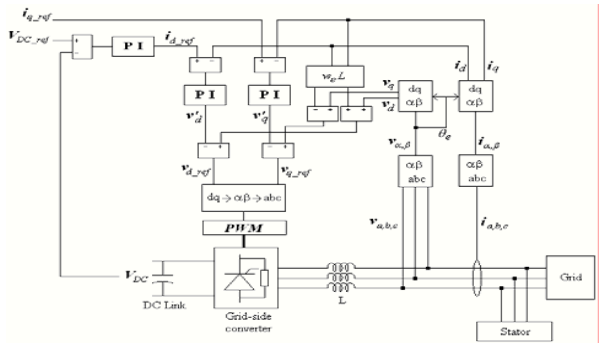

Fig. 2. Grid-side converter controller diagram.

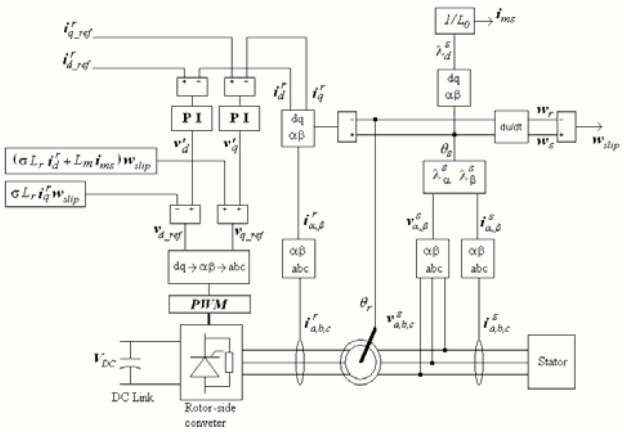

Fig. 3. Rotor-side converter controller diagram.

$$v_d^{'r} = R_r i_d^r + \sigma L_r \frac{di_d^{'r}}{dt} \quad (15)$$

$$v_d^{'r} = R_r i_q^r + \sigma L_r \frac{di_q^{'r}}{dt} \quad (16)$$

The error signals i^r_d and i^r_q are applied to the PI controller to obtain the voltages v^r_d and v^r_q respectively. To compensate the control are added the decoupling terms to the previous equations in order to get the reference voltages $v^r_{d\_ref}$ and $v^r_{q\_ref}$, [10], in accordance with:

$$v_{d\_ref}^r = v_d^{'} - \sigma L_r i_q^r \omega_{slip} \quad (17)$$

$$v_{q\_ref}^r = v_q^{'r} + (L_m i_{ms} + \sigma L_r i_d^r)\omega_{slip} \quad (18)$$

IV. ANN CONTROLLER BASED DFIG

The new control system will use a NN to substitute some blocks of the traditional system of vector control, [11] - [12].

Thus, it is intended to present a control system based on neural networks to be used in the control system alternatively to the one based on PI controllers, with the intention of efficiently extract the wind energy, i.e. to be able to extract the maximum power of the turbine during some situations of functioning through the estimation of the control parameters for the grid-side and rotor-side converters. The proposed control configuration of ANN control based DFIG is shown in Figure 4.

A. NN Controllers Architecture

The learning algorithm updates the values of the weights and bias values according to the descendent gradient with momentum factor and adaptive learning ratio, also indicated in Table I, as well as the activation functions used in each layer and respective parameter.

The sampling frequency is 20 kHz. The numbers of time delays used in each layer of the neural network had been adjusted as resulted of several simulations.

The used learning input-output pairs were generated by several system simulations and contemplate operation points with the machine operating in a zone below the synchronism speed, where active power is supplied to the rotor of the machine; in a zone near the synchronism speed, where the active power flow in the rotor of the machine is practically null; and a zone above the synchronism speed, where the machine supplies active power to the grid through the stator and the rotor.

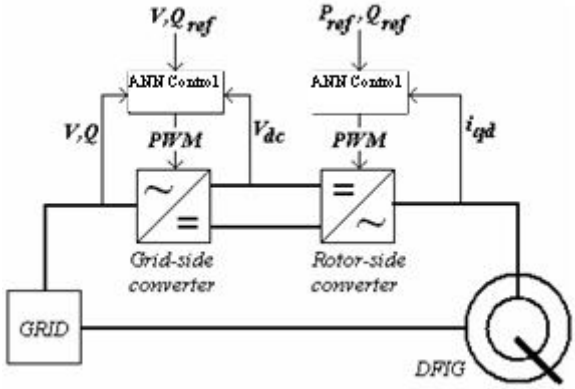

Fig. 4. Proposed DFIG ANN control structure.

TABLE I. - NN layers parameters.

	1st Hidden Layer	2nd Hidden Layer	Output Layer
Activation function - φ	Symmetric sigmoidal	Symmetric sigmoidal	Linear
Parameter – γ	2,0	2,0	-
Parameter - a	2,0	2,0	-
Parameter - c	-1,0	-1,0	-
Learning coefficient – η	0,05		
Momentum - α	0,9		

For the rotor-side controller was used a 7-15-10-2 neural network configuration as is shown in Table II, where the inputs are the stator and rotor currents, the rotor-side reference currents and the rotor angular speed, and the outputs are the reference voltages to control the rotor-side converter.

For the grid-side controller was used a 7-18-8-2 neural network configuration as is shown in Table III, where the inputs are the stator voltages and currents, the grid-side reference currents, and the angular frequency ω_s, and the outputs are the reference voltages to control the rotor-side converter.

TABLE II. - NN architecture and training parameters of the rotor-side controller.

	1st Hidden Layer	2nd Hidden Layer	Output Layer
No of inputs	7 inputs		
No of neurons	15	10	2
No input-output training pair	80.000		
No of iterations	1633		
Error	<9,98E-6		

TABLE III. - NN architecture and training parameters of the grid-side controller.

	1st Hidden Layer	2nd Hidden Layer	Output Layer
No of inputs	7 inputs		
No of neurons	18	8	2
No input-output training pair	80.000		
No of iterations	1313		
Error	<9,99E-6		

V. RESULTS AND DISCUSSION

A. Reactive Power Control

The proposed control strategies have been implemented using MATLab/Simulink and results are presented. It is intended to vary the reference value of the reactive power in two steps, a first positive of 0.2 p.u., and the other equal to -0,4 p.u. Figures 5 and 6 show the signals of the reference voltages generated by the current regulators for the controllers of the grid-side and the rotor-side converters with NN (in the blue colour) and PIs (in the green colour).

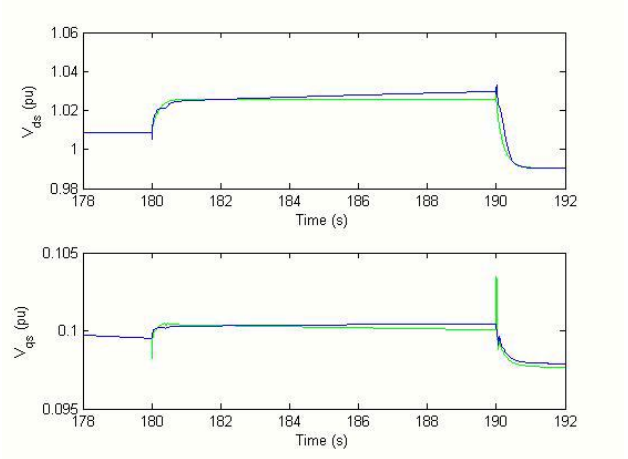

Fig. 5. Reference grid-side voltage v_{dq}, due to reactive power control.

It can be verified that the behavior of the system with the NN is identical to the system with PI controllers. The response of the NN, face to the PI controllers' response presents, generally, lesser transient amplitudes and faster response.

As expected, the quadrature component of the reference voltage has a significant level to the control of the reactive

power. The following figure represents the active power and reactive power delivered to the grid.

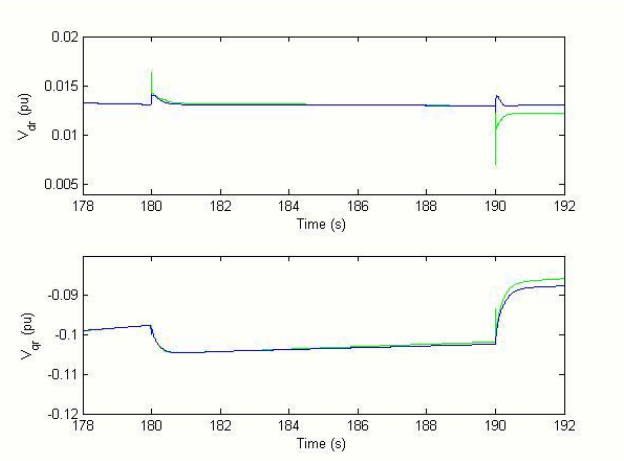

Fig. 6. Reference rotor-side voltage v_{dq}, due to reactive power control.

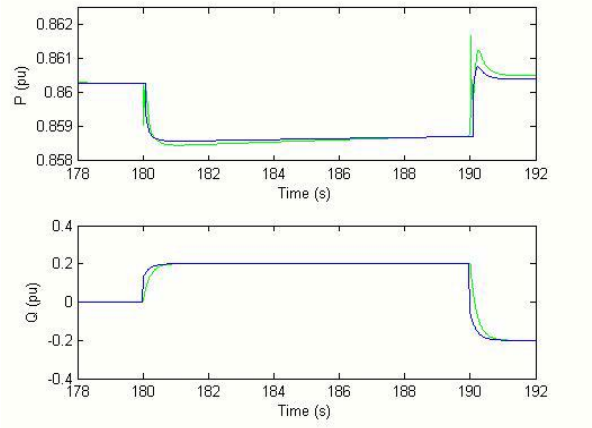

Fig. 7. Active power and reactive power, due to reactive power control.

It can be verified that the NN response is more desirable; it has a faster response to reach the stationary regimen, namely the value of the active power after 190 seconds. Power flows is shown in Figure 7 due to reactive power control.

B. Active Power Control

In a second simulation it is intended to verify the system response due to a variation of the active power flow, obtained through a variation in the quadrature component of the rotor current. This variation consisted in applying a negative pulse of amplitude equal to 0,2 p.u. The reference voltage signals for the controllers of the grid- side and rotor-side converters have been registered in Figures 8 and 9, and the power flows in Figure 10.

Also in this situation, the maximum difference verified between the two control types is less than 0.5%, as in the previous case. The NNs present, generally, transients of lesser amplitude and greater speed to reach the steady- state condition. This behavior is also verified in the main electric and mechanical variables.

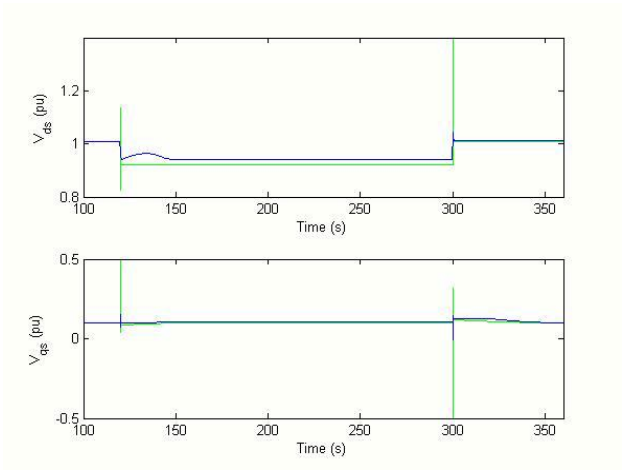

Fig. 8. Reference grid-side voltage v_{dq} due active power control.

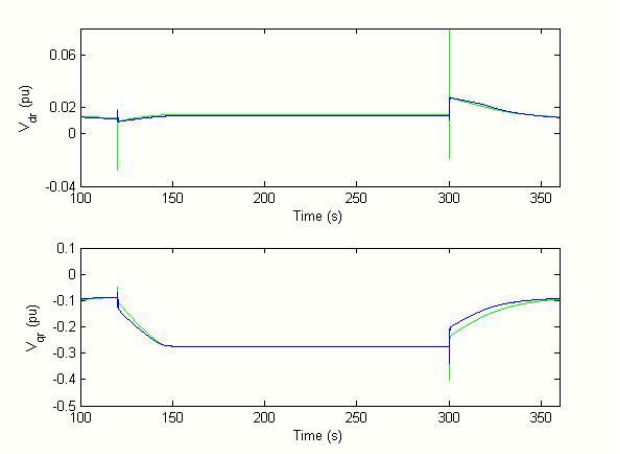

Fig. 9. Reference rotor-side voltage v_{dq}, due to active power control.

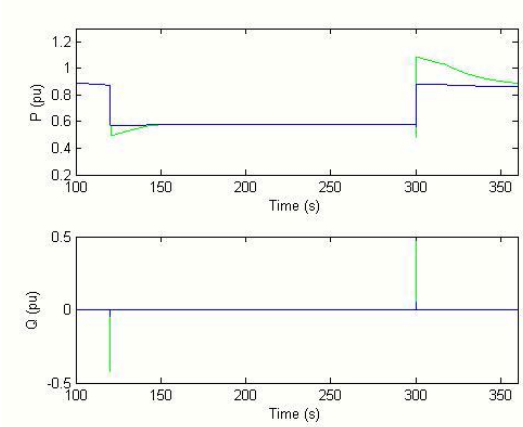

Fig. 10. Active power and reactive power, due to active power

C. Phase-to-Earth Fault

A phase-to-earth fault in a line of the electrical network located near the wind park occurred at t =180 s with a duration of 180 ms. The fault impedance was 1 m.

Figures 11 and 12 show again the signals of the reference voltages used to control the stator-side and rotor-side converters, respectively, with NNs (in the blue color) and PIs

(in the green color).

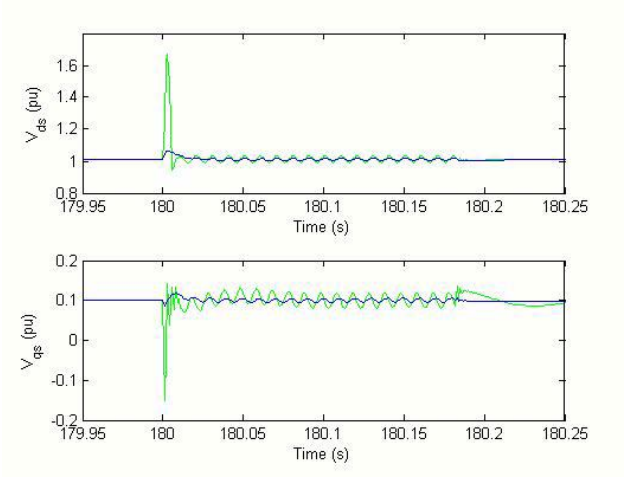

Fig. 11. Reference grid-side voltage v_{dq}, due to a phase-to-earth fault.

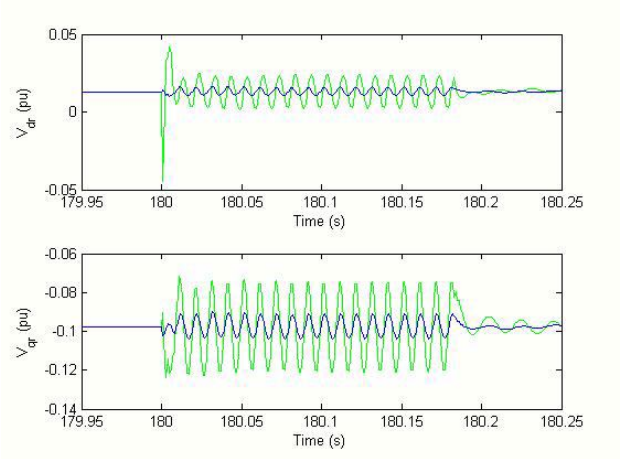

Fig. 12. Reference rotor-side voltage v_{dq}, due to a phase-to-earth fault.

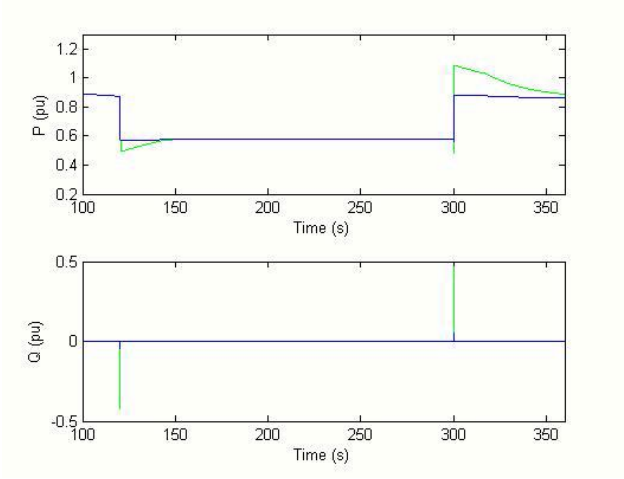

Fig. 13. Active power and reactive power, due to a phase-to- earth fault.

During the fault period, it was verified that the NNs response presents better results than the system using PI controllers; beside the peak s already related previously in the transitions, they present a lesser ripple. It is important to relate that in the direct component of the stator voltage with PI controllers the peaks can reach about 1,7 p.u. and that can cause some unwanted effects in the electronic devices used in the converters.

In Figure 13 it can be verified that the disturbances caused in the active power and reactive power delivered to the grid are smoother with the use of the NNs.

VI. CONCLUSION

There are certain advantages of using artificial neural network control when comparing with PI control of DFIG. There are smaller overshoots, or absence of them in some cases, which gives a faster response, i.e. the system retakes the permanent regimen in lesser time; and smaller oscillatory behavior. The ANN-based system that estimates the control parameters of the generator shown satisfactory characteristics as was verified in the presented results. It was demonstrated that the reference signals for the grid-side and rotor-side converters of the DFIG can be obtained using control systems based on ANNs. These can show the superiority of the proposed ANN control of DFIG with the referred advantages.

REFERENCES

[1] Orlando Manuel Soares and et al *"Analysis and NN-Based Control of Doubly Fed Induction Generator in Wind Power Generation"* International Conference on Renewable Energies and Power Quality (ICREPQ'09) Valencia (Spain), 15th to 17th April, 2009

[2] J. F. Walker, N. Jenkins, "*Wind Energy Technology* John Wiley & Sons, Ltd, 1997.

[3] T. Ackermann, "*Wind Power in Power Systems*", John Wiley & Sons, Ltd, England, 2005.

[4] C. Ong, "*Dynamic Simulation of Electric Machinery*", Prentice Hall, 1998.

[5] A. Tapia, G. Tapia, J. X. Ostolaza, J. R. Saenz, R. Criado, J. L. Berasategui, "Reactive power control of a wind farm made up with doubly fed induction generators", (I) and (II), *IEEE PortoPower Tech Conference*, 2001.

[6] J. G. Slootweg, H. Polinder, W. L. Kling, "Initialization of wind turbine models in power system dynamics simulations", *IEEE Porto Power Tech Conference*, 2001.

[7] A. Tapia, G. Tapia, X. Ostolaza, E. Fernández, J. R. Saenz, "Modeling and dynamic regulation of a wind farm", *VII IEEE International Power Electronics Congress*, CIEP 2000, pp. 293-297, Acapulco, Mexico, 2000.

[8] J. L. Rodríguez-Amenedo, S. Arnalte, J. C. Burgos, "Automatic generation control of a wind farm with variable speed wind turbines", *IEEE Transactions on Energy Conversion*, vol. 17, no 2, pp. 279-284, 2002.

[9] J. G. Slootweg, H. Polinder, W.L. Kling, "Dynamic modeling of a wind turbine with direct drive synchronous generator and back to back voltage source converter and its controls", *European Wind Energy Conference and Exhibition*, Copenhagen, Denmark, July , 2001.

[10] R. Pena, J. C. Clare, G. M. Asher, "Doubly fed induction generator using back-to-back PWM converters and its

application to variable-speed wind-energy generation", *IEE Proc.-Elect. Power Appl.*, vol. 143, no 3, May 1996.

[11] S. Haykin, "*Neural Networks. A Comprehensive Foundation*", 2nd Edition, Prentice Hall, 1999.

[12] M. G. Simões, B. K. Bose, "Neural network based estimation of feedback signals for vector controlled induction motor drives", *IEEE Transactions on Industry Applications*, vol. 31, no 3, pp. 620-629, May-June 1995.

A Review Paper of Automatic Canal Gate Control of 3-ø Induction Motor with PLC and VFD, Powered by Solar System and Monitoring by SCADA

Mahesh Nandaniya

Abstract: **This paper intended as an overview of canal automation. The purpose is to introduce in a concise manner the fundamental theory, main results, and practical applications of canal automation. The paper is focused on the gate control of canal. The paper is purposefully written without "state-of-the-art" terminology for the benefit of practicing engineers in facilities today who may not be familiar with automation and its application in canal gate control. Water is basic need of human and animal. In day to day life many requirement of water and government has most problem distribution of water in all places. Government has also got more priority funding and to distributed water in all places. So that save water is main purpose of project. With respect to irrigation canal modelling, a detailed procedure to obtain data-driven linear Irrigation canal models is successfully developed Control the level of water is the main aim of project. In Gujarat, Narmada is one of the biggest river and Sardar Sarovar dam one of the biggest dam. So we would control gate of Narmada Canal in Sardar Sarovar Dam. These system of canal automation and water transport systems are difficult to manage and present low efficiencies in practice. As a result, an important percentage of water is lost; maintenance costs increase and water users follow a rigid irrigation schedule. All problems can be reduced by automating the operation of irrigation canals. In my project I am develop a system of automatic control gate of Narmada Canal or any canal. Various types of devices are use in my project to control of canal gate. When command given to PLC to open gate of canal at that time motor will rotate forward direction and when command given to PLC to close the gate of canal at that time motor will rotate reverse direction, in these procedure automation is not much required, But Canal gate open or close to percentagewise achieved by motor control is must required in these project. This Motor speed (rpm) is controlled by Variable Frequency Drive. Gate will open or close as per command and after that procedure completed then system will automatically stop. This project automatically operated by Programmable Logic Controller. After completed this wiring and programming of VFD and PLC then we connect Solar panel with this project to operate this project by solar system.**

Technically Abstract: One of the difficulties with the application of canal automation is that individual components are available from different sources and frequently are not compatible. All check structures on the main canals are fitted with motorized gates and are controlled, using SCADA, from a computer. Because of the incompatibility of components, this system was not functional properly.

The district modified the hardware and developed a supervisory control system, but only for canal. However, motorized gates on canals, while not actively used by the district, provide an excellent site for studying both the hardware and software aspects of canal automation. The U.S. Water Conservation Laboratory (USWCL) and Automata, Inc., entered into an agreement to develop a canal automation system. This system includes sensors, gate control hardware, remote terminal units (RTUs), radio communication, a base station, a commercial supervisory control and data acquisition (SCADA) package, and newly developed USWCL canal control logic. This system has been implemented for testing and demonstration on the WM lateral canal of MSIDD. This paper describes the system and its application to the WM canal.

Index Terms: Automatic Canal Gate Control, Variable Frequency Drive, PLC and SCADA programming, Solar System

1. Introduction

While beginning from concepts by discussing introductory details of various types of devices of automation from industrial point of view, slowly this paper converges to its focused area. This paper mainly covers of various device of automation to gate control of canal like PLC, Variable Frequency Drive, Relay, Rectifier, Power supply, MCB, Contactor and also Gear Box(Constant and Variable rpm) , Induction Motor, Electromagnetic Clutch and etc. devices are study deeply with its future. After complete this system we connect inverter to give 3 phase power supply with the use of Solar panel.

2.History of Canal Automation

Early canal automation (pre-1950's) was characterized by the use of hydraulic gates. Flap gates were investigated in The Netherlands by Vlugter (1940). Cal Poly ITRC has recently reported the history of these gates and a new design procedure for them (Burt, 2001). Danaidean gates have been used in California since the 1930's and are still used in many irrigation districts for both automatic upstream control and downstream control. The Nerytec Company from France

Mahesh N. is s Student of M.Tech. Instrumentation and Control Engineering Department,Dharmsinh Desai University, Nadiad, Gujarat, Email: mahesh04_nandaniya@yahoo.in,
Internal Guide: Sanjay S. Bhavsar, *Asst. Professor@ IC Dept., FoT, DD University, Nadiad, Gujarat, India, External Guide: Er. Jayanta Sikdar, Technical Executive, EQDC, Sector-25, Gandhinagar, Gujarat, India*

became famous in the 1950's and 1960's for its hydraulic gates, such as the AVIS, A VIO, and AMIL models. These robust gates have been used around the world for upstream control and level top downstream control (Goussard, 1987). [3] [4].

In the 1960's and 1970's, canal automation in the U.S.A. proceeded in 4 aspects:

1. Electro-mechanical controllers (commonly called "Littlemen") were developed and installed on projects throughout the western U.S. The legacy of these controllers continues, as many new automated sites with PLCs retain the old Littlemen logic - with its inherent simplicity and limitations.

2. A few large water conveyance canals were installed with remote monitoring and remote manual control. Most notable is the California Aqueduct, which has been mistakenly identified as an automated facility for decades.

3. With the advent of computers, a few researchers were able to develop unsteady open channel flow simulation models - which began to open up possibilities for studying new methods of canal automation.

4. A few engineers and researchers began to try to apply control theory to the actual automation of canals. Perhaps most notable are the early attempts by staff from the US Bureau of Reclamation to install HY-FLO and ELFLO on several canals for downstream control.

The California Polytechnic State University Irrigation Training and Research Centre (ITRC) have been involved in canal automation training, technical assistance, and research since the 1980's. ITRC believes in the "Keep It Simple" rule, and continues to recommend simple solutions such as hydraulic gates, long crested weirs, regulating reservoirs, and remote monitoring where appropriate. But there is an increased need for tighter and more flexible control that often cannot be accomplished with those simple techniques. Therefore, ITRC has actively participated in PLC-based irrigation district automation implementation since the mid-1990 [5].

There are so many challenges to successful implementation of PLC-based control that it would be fool-hardy for ITRC to work with anything but the best in co-operators, hardware, and software. In general, ITRC's role is to:

1. Select the control logic to be used for a particular project.

2. Select, develop and tune the control algorithm that dictates the gate movement.

3. Assist the irrigation district in specifying the SCADA system characteristics.

4. Work with the district in locating a good SCADA integrator.

Our ultimate objective is to make the technology much more user-friendly, easily operates, simple to implement and robust, so that commercial companies can implement it rapidly and effectively in canal automation and irrigation of distribution water.

In the remainder of this paper, we will share some of what we have recently learned for each of these PLC-based components:

I. Simulation models

2. Simulation procedures

4. Tuning of algorithms

5. PLC and sensor constraints

6. PLC programming by integrators

Introduction of this project is very complex to other types of project, Because of various types of automation devices are used in this project. The main purpose of this project is to control gate of Canal to use of irrigation canals, is to optimize the water supply in order to match the expected water demands at the off takes level, because they are rugged, reliable.

In past of years for reliable closure during a rain event canal operators would like to be able to operate the gate controls remotely via telephone or Internet and other sources. The operators should receive messages by the same communication method that the gate closed successfully, or a warning message of failure to close due to a jammed gate, or something else that requires their attention. A power backup system or manual operation of the gates is required in case of a power outage.

There are mainly five methods which control Canal Gate

1. Local Manually Control to use of push button by any person
2. Local Automatic control by the use of level sensor
3. SCADA based Monitoring by use of computer and SCADA software
4. Automatic control by use of PLC and VFD
5. GSM based control by use of sending message

Local manual control has been the conventional method of canal operation by the use of SCADA. Local automatic control allows for control of each check structure without human intervention. Local automatic systems consist of sensors connected to control devices; the sensors detect changes in the canal water level, and then through the logic programmed into the PLC the check position of gate and adjust it. Weighted gates are a strictly mechanical application of local automatic control.

The components of automation system include

- Sensors for sensing the input parameters
- Transmitters for transmitting the raw signal in electrical form
- Control system which includes PLC, DCS & PID controllers

- Output devices such as actuators, drives, control valves, solenoid valves, coils, indicating lamps.

Supervisory control is the operation of the canal by the water master from a central location. Information such as water level and gate location are sent to a PLC and SCADA by the use of level sensor which located in the canal are sensed signal and get output to the PLC. Combinations of all five control methods are often employed.

Upper and Lower level control are the important concepts in fully automatic canal gate control.

A. Operational Improvement by using this project

Flow through the main gate is a function of the level of the water, so it is critical to maintain the desired position of the gates because of changing water level is easily. [2]

Gate of canal is very weighted to operate it. So we have used 3 phase induction motor and two various types of Gear box (which one of fixed Gear Ratio used for increased Torque and other one is variable Gear Ratio for change speed of motor and Torque of output). We also used Programmable Logic controller to Control RPM of induction motor and control of various devices, relay which connect with output of PLC, sensor which used for Level of water, Gate position etc. Programmable Logic Controller (PLC) and Variable frequency Drive (VFD) are used for control and monitor Gate of canal at field. 3-ø induction motor is used for control of this gate of canal.

Fig.1 Local manually control of canal gate (Now a days)

Various part of automation devices are used to control three phase induction motor in this project. The project must achieve the ability on controlling the following aspect.

- START/ STOP Motor
- Forward/Reverse Position Control of motor
- Speed Control of motor

The start and stop actions can be control directly through the status change of the PLC output. Meanwhile the speed and forward/reverse position control can be controlled by the PLC through the Variable Frequency Drive (VFD). VFD is used for percentagewise open and close gate of canal.

In this project canal gate is joined with Gearbox (Constant rpm and variable rpm). Gearbox is connected with 3-phase Induction motor. This motor controlled by VFD and VFD operated through PLC.

Block diagram shown below.

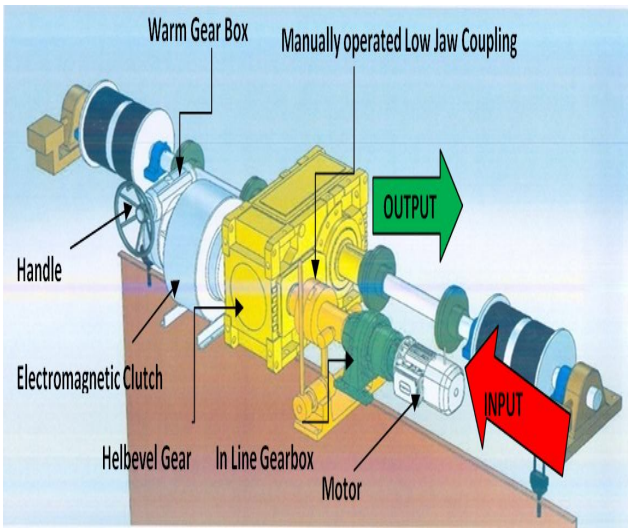

Fig. 2 Mechanical Structure of Gate control project

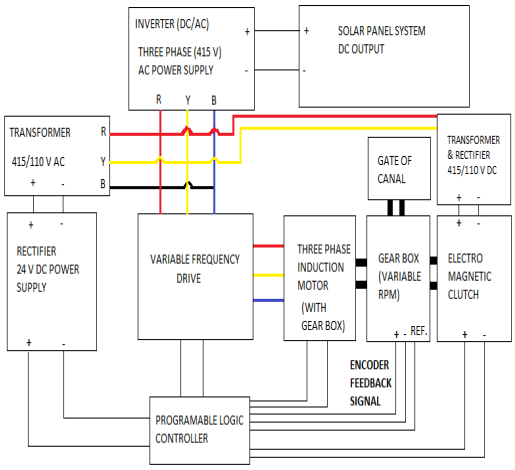

Fig. 3 Electrical connection of canal gate control

3. Devices Using in Project

1. PLC (Control of VFD and Other I/O)
2. Variable Frequency Drive (to control rpm of Induction Motor)
3. 3 Phase induction motor (Moving Gear Box)
4. Gearbox (Change Torque and Speed of Gate)
5. Electromagnetic clutch (to engagement and disengagement of Shaft)
6. SCADA Software (Monitoring and simulation of real process)

7. Switched Mode Power Supply (Give 24 V DC Power of PLC and other Devices)
8. Power supply of 110V DC (Give 110 V DC power to the Electromagnetic Clutch)
9. Relay and connector (Using control of PLC output and other devices)
10. Miniature circuit breaker (For Security purpose)

1. PLC (Control of VFD and Other I/O)

PLC-based canal automation is relatively newer technology. A PLC (Programmable Logic Controllers) is an industrial computer used to monitor inputs, and depending upon their state make decisions based on its program or logic, to control (turn on/off) its outputs to automate a machine or a process. PLC can control digital data as well as analog signal also. PLC is a digital computer used for automation of electromechanical processes, such as control of machinery on factory assembly lines. PLCs are used in many industries and machines.

The CPU used in PLC system is a standard CPU present in many other microprocessor controlled systems.

The RAM is essential for the operation of the program and the temporary storage of input and output data. Typical memory sizes of PLC systems are about 1 kb for small PLCs, few kb for medium sizes and more than 10-20 kb for larger PLC depending on the conditions.

Many PLC would support easy memory upgrades. Input/output modules are the boundary between the internal PLC systems and the external processes to be monitored and controlled.

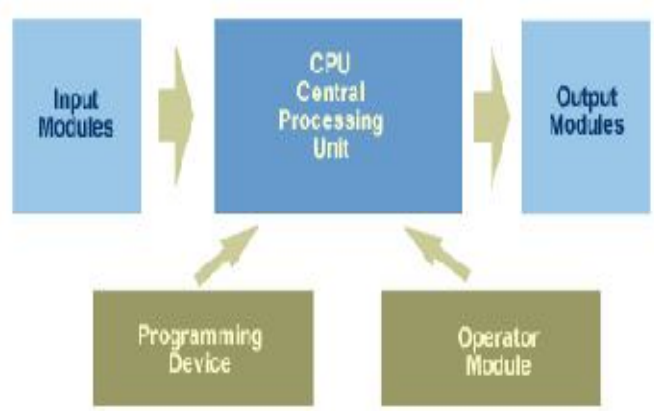

Fig. 4 working operation of PLC

Programming devices are essential components of the PLC systems. The program in a ladder diagram or other form can be designed and usually tested before downloading to the PLC.

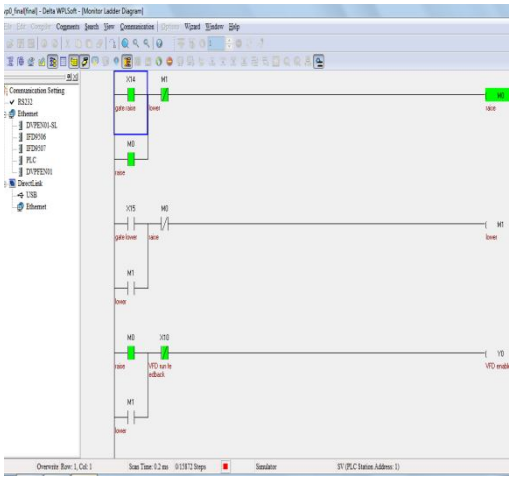

Fig. 5 Programming of PLC in Ladder Diagram

2. Variable Frequency Drive (to control rpm of Induction Motor)

VFD is a type of adjustable-speed drive used in electro-mechanical drive systems to control AC motor speed and torque by varying motor input frequency and voltage. However, about a third of the world's electrical energy is consumed by electric motors in fixed-speed centrifugal pump, fan and compressor applications and VFDs' global market penetration for all applications is still relatively small. This highlights especially significant energy efficiency improvement opportunities for retrofitted and new VFD installations. Over the last four decades, power electronics technology has reduced VFD cost and size and improved performance through advances in semiconductor switching devices, drive topologies, simulation and control techniques, and control hardware and software. The AC electric motor used in a VFD system is usually a three-phase induction motor. Some types of single-phase motors can be used, but three-phase motors are usually preferred. Various types of synchronous motors offer advantages in some situations, but three phase induction motors are suitable for most purposes and generally the most economical choice are designed for fixed-speed operation are often used. So we have used VFD in our project to control rpm of motor. [9]

A. Requirement of VFD

When an induction motor starts, it will draw very high inrush current due to the absence of the back EMF at start. This results in higher power loss in the transmission line and also in the rotor, which will eventually heat up and may fail due to insulation failure. The high inrush current may cause the voltage to dip in the supply line, which may affect the performance of other utility equipment connected on the same supply line. When the motor is operated at a minimum load (i.e., open shaft), the current drawn by the motor is primarily the magnetizing current and is almost purely inductive. As a result, the PF is very low, typically as low as 0.1.When the load is increased, the working current begins to rise. The magnetizing current remains almost constant over

the entire operating range, from no load to full load. Hence, with the increase in the load, the PF will improve. When the motor operates at a PF less than unity, the current drawn by the motor is not sinusoidal in nature. This condition degrades the power quality of the supply line and may affect performances of other utility equipment connected on the same line.

The PF is very important as many distribution companies have started imposing penalties on the customer drawing power at a value less than the set limit of the PF. This means the customer is forced to maintain the full-load condition for the entire operating time or else pay penalties for the light load condition. In many applications, the input power is a function of the speed like fan, blower, pump and so on. In these types of loads, the torque is proportional to the square of the speed and the power is proportional to the cube of speed. Variable speed, depending upon the load requirement, provides significant energy saving.

The basic function of the VFD is to act as a variable frequency generator in order to vary speed of the motor as per the user setting. The rectifier and the filter convert the AC input to DC with negligible ripple. The inverter, under the control of the PIC microcontroller, synthesizes the DC into three-phase variable voltage, variable frequency AC. Additional features can be provided, like the DC bus voltage sensing, OV and UV trip, over current protection, accurate speed/position control temperature control, easy control setting, display, PC connectivity for real-time monitoring, Power Factor Correction (PFC) and so on.

With the rich feature set of the PIC microcontroller, it is possible to integrate all the features necessary into a single chip solution so as to get advantages, such as reliability, accurate control, space saving, cost saving and so on. The base speed of the motor is proportional to supply frequency and is inversely proportional to the number of stator poles. The number of poles cannot be changed once the motor is constructed.

B. **Internal Block Diagram of VFD**

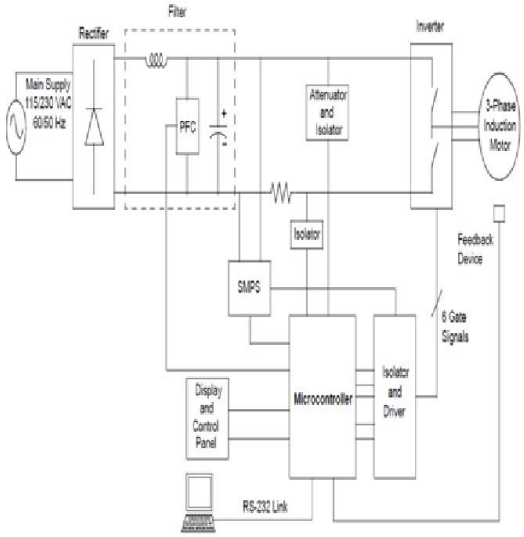

Fig. 6 Internal Block Diagram of VFD

Table 1 Comparison between various types of VFD

Drive type	**DC**	VFD	VFD	VFD
Criteria	Brush Type DC	AC V/Hz Control	AC Open-Loop Vector	AC Closed-Loop Flux Vector
Typical speed regulation (%)	0.01	1	0.5	0.01
Typical speed range at constant torque (%)	0-100	10-100	3-100	0-100
Min. speed at 100% torque (% of base)	Standstill	8	2	Standstill
Multiple-motor operation recommender	NO	YES	NO	NO
Fault protection (Fused only or inherent to drive)	Fused only	Inherent	Inherent	Inherent
Maintenance	Brushes	Low	Low	Low
Feedback device	Tachometer or encoder	NO	NO	Encoder

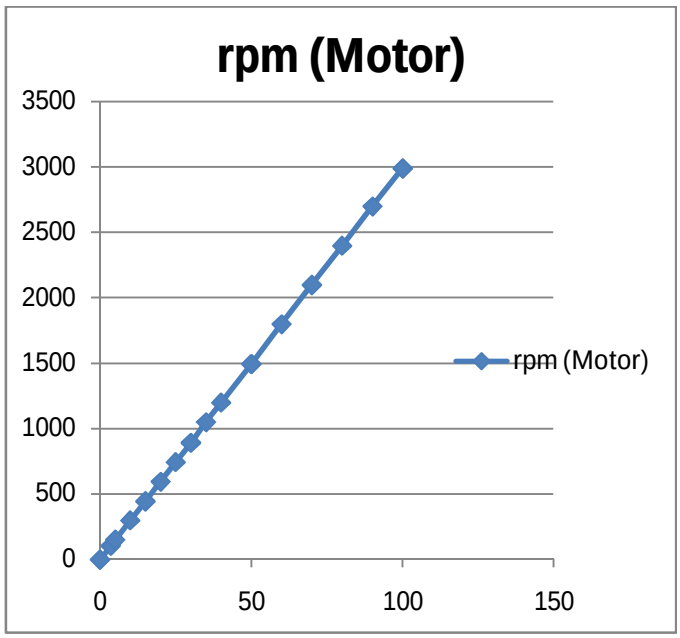

Fig. 7 Frequency of VFD (Hz) Vs Motor Speed (rpm)

6. *SCADA Software (Monitoring and simulation of real process)* [7]

Many irrigation districts use SCADA software to manage their canal systems. Whether home grown or commercial, these programs require a significant amount of training for new operators. While some SCADA operators are hired with extensive field experience, others are hired with no field experience at all and require extended training to gain an understanding of the behaviour of open channel systems.

SCADA software itself needs to be tested for proper response to various alarm conditions. Currently, there are no practical methods to simulate emergency conditions for SCADA systems. The U.S. Water Conservation Laboratory (USWCL) has created a method for replacing the real canal with a simulation model without making any changes to the SCADA software. The connection from the SCADA computer to the radio is replaced with a connection to another computer that performs the canal simulation.

If the simulation model were a good representation of the canal, gates, etc., the SCADA operators would not be able to tell the difference. This additional computer also runs software modelling the telemetry system, including communications, sensors and remote terminal units (RTU's) or programmable logic controllers (PLC's), as well as the physical components of the canal sites such as gate positions and battery voltages.

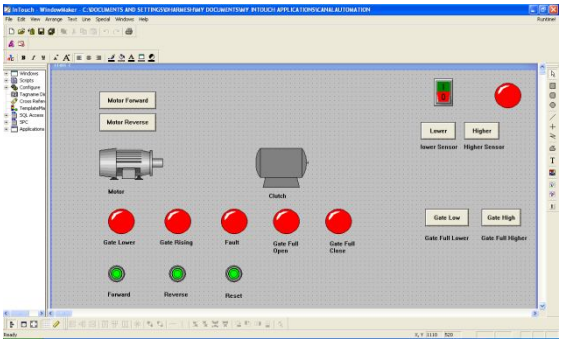

Fig. 8 SCADA Programming Display

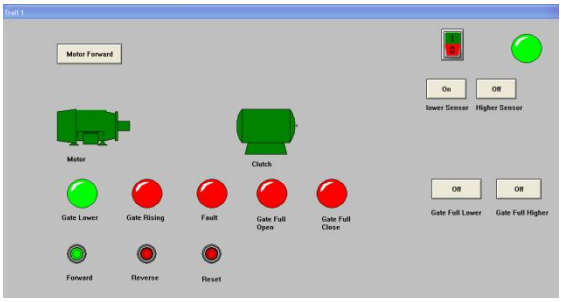

Fig. 9 SCADA at Runtime Application [Forward]

Through the simulation system, situations such as a noisy transducer, a stuck gate, an electrical failure, or an unexpected supply or demand change can be simulated. If needed, these situations can be easily repeated. This paper describes this prototype system and potential uses for training and for validation of SCADA and automatic control functions.

3. *Three phase Induction Motor*

An induction or asynchronous motor is a type of AC motor where power is supplied to the rotor by means of electromagnetic induction. The induction motor is an alternating (AC) rotating machine. In an AC induction motor, one set of electromagnets is formed in the stator because of the AC supply connected to the stator windings. The alternating nature of the supply voltage induces an Electromagnetic Force (EMF) in the rotor as per Lenz's law, thus generating another set of electromagnets.

A. Speed of an Induction Motor

Synchronous speed (*NS*) of Induction Motor

$$Ns = \frac{120f}{P} \quad (1)$$

Where

Ns = the synchronous speed of the stator magnetic field in RPM

P = the number of poles on the stator

f = the supply frequency in Hertz

B. Motor Sizing

To lift a head gate, the gate operator must lift the weight of the gate, and overcome the friction resistance between the gate frame and gate leaf (Appendix 1). The amount of friction is proportional to the hydrostatic force on the gate leaf, Eq. 1 was use to calculate the load on the gate operator.

$$L = W + \mu \frac{1}{2} \acute{y} h W$$

Where

L is the load on the operator (lbs);

W is the weight of the gate;

μ is a coefficient of friction;

ý is the specific weight, which was taken to be 62.4 lb/ft3;

h is the height of water against the closed leaf measured from the bottom of the channel;

W is the width of the gate.

The USBR recommends using a μ value of 0.35 (U.S. Bureau of Reclamation, 1991).

The load L was calculated for two upper water levels h, the First is the high water mark in the canal from years of operation at some level. The other level is a worst-case scenario with the water over topping the canal gates, at the full gate height. The load on the operator when the canal is at normal operating level.

Once the load on the lift is found the required motor torque to lift the load is calculated. The torque required is found using Eq. 2

$$M = L * r * tan(\theta + \phi)$$

Where

M is the torque (ft lbs);

L is the load on the operator;

r is the radius of the rising stem;

θ is the lead angle of the rising stem;

φ is the friction angle between the rising stem and the brass nut.

The friction angle, φ, is equal to the arctangent of the coefficient of friction. Tabulated values for friction between brass and steel vary from 0.44 to 0.51 (Bhushan & Gupta, 1991). [2]

C. Power Requirement

The electrical system of this project has enough capacity of power required to operate canal gate. I have used 1 HP 3 phase induction motor, variable frequency Drive, electromagnetic clutch, rectifier circuit, 24 V DC power supply, MCB, Contactor, Relay and other component. All the components have 3150 Watt power required. So this power is give by the solar panel via inverter.

4. Application of this Project

- Canal gate control and supervise level of water and gate location
- System Monitoring and Control and water level indication
- Cost Analysis for maintenance water distribution
- Security of water control and distribution
- Easily programming and editing to changed level of water and gate
- SCADA operator implements the gate movement through the SCADA interface

Conclusion of Project paper

Water is becoming a scarce resource and water districts are under pressure to use water more judiciously. Improved operation of water resources facilities, such as canals and reservoirs, has been touted as necessary for making proper use of these limited water supplies. Operation of irrigation-water delivery systems can be improved by providing canal operators with better tools for determining control actions. One such tool is computerizing automatic control of canal gates.

While canal automation may appear simple in concept, it is actually a complex technical problem. This complexity has led to a large gap between theory and practice. Because this concept is easily operate in theoretical, but when we installation this problem there are many problem faced like, jammed gate, power supply failure, virus affection in SCADA, etc. Existing hardware components for automatic control are often incompatible.

This paper describes a new canal automation system that has an integrated hardware and software system--from gate control to a commercially available supervisory control system. These results should be of use to irrigation districts, consultants, and the Bureau of Reclamation. In summary, what we started out thinking was a simple algorithm challenge is in fact quite complex. As a profession, we underestimated the complexity of automating canals with PLCs - even with simple upstream control. We now understand that there are challenges in equipment, simulation models, tuning procedures, and field programming.

Having identified the weaknesses, we are systematically solving each one. Based on the criteria of reliability, operational improvement, cost and safety, it is recommended to install a multi-turn gate actuator on each head gate, along with replacing one section of the spillway stop logs with a sliding gate. To power the gate actuators, the available single-phase, 240-volt utility would be the most economical. And, to make the implementation of the improvements to the Crockett canal head gates less cost prohibitive, the installation could be done in phases.

REFERENCES

1. http://www.ars.usda.gov/research/publications/publications.htm?seq_no_115=104928
2. Remote Control and Automation of the Crockett Canal Head Gates
3. Chainnan, Irrigation Training and Research Center (ITRC); and Professor, Bio Resource and Agricultural Engineering Dept. California Polytechnic State University. San Luis Obispo, CA 93407 web link: cburt@calooly.edu
4. Visiting Scholar. Cal Poly ITRC. Jilin University, Agricultural Engineering Department. Nanling Campus, Changchun City, China
5. http://www.loganutah.org/public_works/Engineering/pdf/StormWaterDesignCriteria2010.pdf
6. A. J. Clemmens, M.ASCE; E. Bautista, A.M.ASCE; B. T. Wahlin, A.M.ASCE; and R. J. Strand, Simulation of Automatic Canal Control Systems.
7. R.J. Strand1, A.J. Clemmens2, N.T. Denny, Training SCADA Operators with Real-Time Simulation.
8. Campbell, Sylvester J. (1987). *Solid-State AC Motor Controls.* New York: Marcel Dekker, Inc.. pp. 79–189. ISBN 0-8247-7728-X.
9. Jaeschke, Ralph L. (1978). *Controlling Power Transmission Systems.* Cleveland, OH: Penton/IPC. pp. 210–215

Bibliography: *Student of M.Tech. in Instrumentation and Control Department, FoT, Dharmsinh Desai University,Nadiad, Gujarat.*

Studied Bachelor of Engineering in Instrumentation and Control Department Government Engineering College, Gandhinagar, Gujarat, India.

Algorithm for Removal of DC Offset in Current and Voltage Signals

Shilpi Nayak, Shraddha Kaushik and Ishawari Prasad Sahu

Abstract: Protecting transmission lines frequently involves adopting distance relays. Protecting relays must filter their inputs to reject unwanted quantities and retain signal quantities of interest. This paper presents a new algorithm suitable for calculating impedances from digitized voltages and currents sampled at a relay location. Each input is assumed to be composed of a decaying d. c. component and components of the fundamental and harmonic frequencies. Parameters of a digital filter determined by using the least error squares approach are then used to compute the real and imaginary components of the voltage and current phasors. Impedances as seen from a relay location are then calculated.

***Keywordss*— Digital filtering, distance relay, decaying DC component, discrete fourier transform.**

I. INTRODUCTION

Transmission lines form a major part of a power system. Different types of relays are used to protect these lines. The most commonly used relays are from the family of distance relays. One of these relays, the impedance relay is used on its own or in conjunction with communication facilities for communicating with the relays at the remote terminal of the line. These relays basically evaluate the impedance looking into the transmission line from the voltages and currents at the relay location. The impedance is assumed to be proportional to the distance from the relay to the fault and, this determines if the fault is in the relay's protective zone.

The conventional impedance relays are of either electromechanical or solid state (electronic) type. Some relays which use a digital processor for computing the impedance and making decisions have been developed in the last few years. The algorithms used to calculate the apparent impedance used in these relays can be categorized into four groups. The first group is developed assuming that the waveforms presented to the relay are pure sinusoids. The second group of algorithms use Fourier analysis and the third group use digital filters to extract the fundamental frequency information from the inputs. The last group of algorithms numerically solve a differential equation which describes the behaviour of the transmission line.

Shilpi Nayak and Ishawari Prasad Sahu are working as Assistant Professors in Electrical and Electronics Engineering Department at Chhatrapati Shivaji Institute of Technology, Durg, Chhattisgarh and Shraddha Kaushik is current working an Assistant Professor in Electrical and Electronics Engineering Department at Rungta college of Engineering and Technology, Bhilai, (INDIA). Emails: shilpi.nayak88@gmail.com ,shraddha.kaushik01@gmail.com,ishawarisahu@csitdurg.in

Mann and Morrison proposed an algorithm which uses the fact that the amplitude of a sinusoid can be determined from its value and its rate of change at any instant and the rate of change of a function can be calculated by using difference equations. Gilcrest, Rockefeller and Udren used the first and second derivatives to calculate the peak values of the sinusoids. Miki and Makino expressed the peak squared values of the voltage and current in terms of two sampled values, each of the voltage and current. The calculated peak values were then used to compute the real and reactive components (R and X) of the apparent impedance. Gilbert and Shovlin calculated R and X directly from the sampled values except that three sets of samples were used instead of two sets used in reference 3. The second group of algorithms use some form of Fourier analysis to extract the fundamental frequency information. Ramamoorty suggested an algorithm which samples the signals over one cycle of the fundamental frequency and determines the real and imaginary parts of the fundamental frequency component. Using sampling intervals of ninety degrees at the fundamental frequency in the algorithm provides the Carr and Jackson algorithm. Phadke, Hlibka and Ibrahim used this approach and one half cycle data window in their algorithm. The third type of algorithms use digital filters to extract information concerning the fundamental frequency components; Hope and Umamaheswaran used finite impulse response filters. The last group of algorithms have been proposed and used by McInnes and Morrison, Ranjbar and Cory1o and Breingan. These algorithms numerically solve the differential equation representing the transmission line by a series R-L model.

This paper presents a new algorithm which is based on the least error squares curve fitting technique. The algorithm assumes that the input is composed of a fundamental frequency component, a decaying d. c. and harmonics of specified order. The decay rate of the d. c. component is not assumed in advance because it is affected both by the resistance of the arc at the fault and the effective resistance of the system. Mathematical background necessary for developing this algorithm is first presented. Effects of sampling frequency, data window, time reference and changing the model of the decaying d. c. component are then examined. The selected parameters are then used in the impedance calculating algorithm. Impedances calculated from the data of a single phase to ground fault remote from the relay and a close-in three phase fault on 138 kV lines over approximately three cycles after the inception of the faults are reported. The fault data which was recorded at the Regina South switching station of the Saskatchewan Power Corporation was used for these tests.

II. MATHEMATICAL ALGORITHM

In all previously designed digital relays, voltage and current outputs of the transducers are preprocessed and converted to millivolts level. The function of the preprocessors is two fold; one is to suppress surges travelling from the power system to the relay and the other is to block high frequencies from reaching the relays. Preprocessed signals of the millivolt level are converted to numerical values by analog to digital converters. The digital information Is then provided to a processor which analyzes the information and makes appropriate decisions. The mathematics of the proposed least error squares filter is presented in this section. The outputs of this filter are the real and imaginary components of the fundamental frequency phasor. These components are then used to calculate the impedance as seen from the relay location.

Calculating the Real and Imaginary Components of Voltages and Currents-

The output of a CCVT or voltage transformer during a fault is a waveform composed of a decaying d. c. component and many harmonic components. At time $t=t_1$, this waveform can be mathematically expressed as:

$$f(x) = A e^{-t/\tau} + \sum_{n=1}^{M} \left(A_n \sin(n \omega t + \phi_n)\right) \quad \textbf{(1)}$$

A= magnitude of the decaying dc offset;

τ =time constant of the decaying dc offset;

A_n= amplitude of the nth harmonics; $\omega = 2\pi f$;

The time constant τ depends on the X/R ratio of the system; but is also affected by the arc resistance which varies from fault to fault. In practice, even harmonics are not present in the fault voltages and currents. Also, higher order harmonics are blocked from reaching the relay by the signal conditioning equipment which usually includes analog filters. The cut-off frequency of these filters is determined by the overall design considerations for the relay.

So, equation (1) becomes;

$$f(x) = Ae^{-t/\tau} + A_1 \sin(\omega t+\phi_1)+A_3 \sin(3\omega t+\phi_3) \quad \textbf{(2)}$$

The exponential term $e^{-t/\tau}$ of equation (2) can be expanded using Taylors's series, such that

$$e^{-t/\tau} = 1 - \frac{t}{\tau} + \frac{t^2}{2!\tau^2} - \frac{t^3}{3!\tau^3} + \quad \textbf{(3)}$$

Using the first three terms of this series and assuming that

(i) the signal conditioning equipment has effectively blocked the fifth and higher order harmonics and (ii) no even harmonics are present in the input.

By considering only the first terms of this expression, equation (2) can be expressed as

$$f(x)= A - A\frac{t}{\tau} + A\frac{t^2}{2!\tau^2} + A_1 \sin(\omega t+\phi_1) + A_3 \sin(3\omega t+\phi_3) \quad \textbf{(4)}$$

Equation (5) is obtained from expanding sine terms.

$$f(x) = A - A\frac{t}{\tau} + A\frac{t^2}{2\tau^2} + A_1 cos\phi_1 \sin(\omega t) + A_1 sin\phi_1 \cos(\omega t) + A_3 cos\phi_3 \sin(3\omega t) + A_3 sin\phi_3 cos(3\omega t) \quad \textbf{(5)}$$

This equation may be written in the more convenient form:

$$S_1 = f(x) = a_{11}x_1+a_{12}x_2+a_{13}x_3+a_{14}x_4+a_{15}x_5+a_{16}x_6+a_{17}x_7 \quad \textbf{(6)}$$

Where S_1 is sample measured at time t_1. The coefficient in equation (6) is related only on the time at which the samples are taken, and they form:

$a_{11}=1$; $a_{14}=\sin(3\omega t_1)$; $a_{12}=\sin(\omega t_1)$; $a_{15}=\cos(3\omega t_1)$;

$a_{13}=\cos(\omega t_1)$; $a_{16}=t_1$; $a_{17}=t_1^2$;

The x values are functions of the unknown, and are given by:

$x_1 = A$; $x_2 = A_1\cos\phi_1$; $x_3 = A_1\sin\phi_1$; $x_4 = A_3\cos\phi_3$;

$x_5 = A_3 sin\phi_3$; $x_6 = -A/\tau$; $x_7 = A/\tau^2$;

The samples measured at time $t = t_2$ can likewise be expressed as:

$$S_2 = f(x) = a_{21}x_1+a_{22}x_2+a_{23}x_3+a_{24}x_4+a_{25}x_5+a_{26}x_6+a_{27}x_7 \quad \textbf{(7)}$$

As mentioned previously, the a-coefficients are functions of time. Therefore if t_1 is taken as a time references and the current is sampled at preselected times, then the values of the sampled t coefficient of equations (7) and (8) can be specified. So equations can be written in matrix form:

$$[A]\ [X] = [S] \quad \textbf{(8)}$$

From equation (8) we can find the value of matrix [X]

$$[X] = [A]'\ [S] \quad \textbf{(9)}$$

$$[A]' = [A^T A]^{-1}\ [A^T] \quad \textbf{(10)}$$

Then we can find fundamental phasor from [X]

$$A_1 = \sqrt{x_2^{\,2} + x_3^{\,2}} \quad \textbf{(11)}$$

$$A = x_1 \quad \textbf{(12)}$$

III. Result and Discussion

Fundamental Component	100.0000
DC Component	100.2782
Error DC Percentage	0.2782

From the above results we can say that least square technique is very effective method for computing fundamental and harmonics component and DC offset. It requires 0.205093 sec to execute full program in MATLAB.

This algorithm requires that digitized values of voltages and currents be multiplied by the elements of the second and third rows of an $[A]^{I}$. Two approaches can be used for this purpose. One mould be to use a hardware multiplier. The strength of the proposed algorithm lies in two areas; the freedom in choosing the equation of condition and some flexibility In selecting the size of the data window. The freedom of choosing the equation of condition allows prespecified harmonics to be included in the equation. This enables the harmonic components to be determined for applications such as, transformer differential protection.

This algorithm explicitly takes account of the decaying d.c. component by including it in the equation of condition.

IV. Conclusion

This paper describes the least error squares approach for developing a digital filter which explicitly takes account of the decaying d. c. components in the system voltages and currents. The concept of pseudo inverse which has been used in developing the algorithm is also presented. It is shown that the proposed approach can effectively calculate the impedance from the fault data obtained from a power system.

The technique presented in this paper is general enough to be extended and applied in situations, such as, transformer differential faults. If the harmonics observed in transformer in-rush currents are included in the equation of conditions, the resulting algorithm can provide information concerning the harmonic components for use in transformer differential relays.

References

[1] M. S. Sachdev and M. M. Giray, "A least error squares technique for determining power system frequency," *IEEE Trans. Pow. App. Syst.*, vol. PAS-104, no. 2, pp. 437–444, Feb. 1985.

[2] V. V. Terzija, M. B. Djuric, and B. D. Kovacevic, "Voltage phasor and local frequency estimation using Newton type algorithm," *IEEE Trans. Pow. Del.*, vol. 9, no. 3, pp. 1368–1374, Jul. 1994.

[3] H. J. Altuve F., I. Diaz V., and E. Vazquez M., "Fourier andWalsh digital filtering algorithms for distance protection," *IEEE Trans. Power System*, vol. 11, no. 1, pp. 457–462, Feb. 1996.

[4] Y. Guo, M. Kezunovic, and D. Chen, "Simplified algorithms for removal of the effect of exponentially decaying DC-offset on Fourier algorithm," *IEEE Trans. on Power Delivery*, vol. 18, no. 3, pp. 711-717, July 2003.

[5] Y. Cho, C. Lee, G. Jang, and H. Lee, "An innovative decaying DC component estimation algorithm for digital relaying," *IEEE Trans. On Power Delivery*, vol. 24, no. 1, pp. 73-78, Jan. 2009.

[6] S. Kang, D. Lee, S. Nam, P. Crossley, and Y. Kang, "Fourier transform-based modified phasor estimation method immune to the effect of DC offsets", *IEEE Trans. on Power Delivery*, vol. 24, no. 3, pp. 1104-1111, July 2009.

[7] P. Jiuping, K. Yu, and Y. Hu, "An efficient compensation algorithm for current transformer saturation effects," *IEEE Trans. Power Del.*, vol. 19, no. 4, pp. 1623–1628, Oct. 2004.

[8] A. Isaksson, "Digital protective relaying through recursive leastsquares identification," *Proc. Inst. Elect. Eng., Gen., Transm. Distrib.*, vol. 135, no. 5, pp. 441–449, Sept. 1988.

Shilpi Nayak received her Bachelor degree in Electrical and Electronics Engineering from Chhatrapati Shivaji Institute Of Technology, Durg,Chhattisgarh (INDIA) in 2010. She is pursuing her Master of Engineering in Power Electronics (Electrical) from Rungta College of Engineering & Technology, Bhilai, ,Chhattisgarh (INDIA). She is currently working as an Assistant Professor in Electrical and Electronics Engineering Department at Chhatrapati Shivaji Institute Of Technology, Durg, Chhattisgarh, (INDIA). Her research interests includes Power Generation, Transmission, Distribution, and Power Electronics.

Shraddha Kaushik received her Bachelor degree in Electrical and Electronics Engineering from Government Engineering College, Raipur (INDIA) in 2009 and M.Tech in Power Systems and Automation from GITAM Institute of Technology, GITAM University Visakhapatnam, (INDIA) in 2012. She is currently working as an Assistant Professor in Electrical and Electronics Engineering Department at Rungta college of Engineering and Technology, Bhilai, (INDIA). Her research interests includes Distribution Generation, Smart Grids and Machine Designing.

Ishawari Prasad Sahu received his bachelor degree in Electrical and Electronics Engineering from Chhatrapati Shivaji Institute Of Technology, Durg, Chhattisgarh (INDIA) in 2010 and M.Tech in Integrated Power Systems from Visvesvaraya National Institute of Technology,Nagpur (INDIA) in 2012. He is currently working as an Assistant Professor in Electrical and Electronics Engineering Department at Chhatrapati Shivaji Institute Of Technology, Durg, Chhattisgarh (INDIA). His research interests include Power Transmission, Distribution, protection and FACTS.

Hybrid Solar and Wind Power Conversion Using DFIG with Grid Power Leveling

Mrs. S. Sathana and Ms. Bindukala M.P.

Abstract: **Renewable energy systems are being used more prominently nowadays because they are environment friendly. Also, the lack of availability of fossil fuels leads to the use of solar and wind energy. This paper makes use of a hybrid solar-wind energy system. Doubly fed induction generator (DFIG) based Wind Energy Conversion System (WECS) is used. The rotor side converter and grid side converter along with Battery Energy Storage System (BESS) are used since the BESS reduces the power fluctuation on grid due to unpredictability of wind. The grid power leveling concepts are considered .Maximum Power Point Tracking (MPPT) concepts are used to extract maximum power from wind and sun when available. Perturb and Observe algorithm is used for PV array. The proposed system is simulated using MATLAB-SIMULINK.**

***Keywords*—Battery energy storage system (BESS), doubly fed induction generator (DFIG), maximum power point tracking (MPPT), wind energy conversion system (WECS), grid power leveling.**

I. INTRODUCTION

With the depletion of fossil fuel reserves, increase in the pollution and global warming, many are looking at sustainable energy solutions to preserve the earth for the future generations. Wind energy is capable of supplying large amounts of power but its presence is highly unpredictable as it can be here one moment and gone in another. Similarly, solar irradiation levels vary due to sun intensity and unpredictable shadows due to clouds, birds, trees, etc. The common drawback of wind and photovoltaic systems is that they are intermittent in nature and thus unreliable. These two intermittent sources are combined together and maximum power point tracking (MPPT) concepts are applied to make system more efficient and reliable.

The doubly fed induction generator (DFIG) is used for wind energy conversion systems because of its advantages like reduced converter ratings for power conversion, efficient power capture due to the variable speed operation, improved efficiency, reduced cost and losses, easy implementation of power factor correction and variable speed operation. The total energy output is 20%–30% higher because of variable speed operation. It ensures improved capacity utilization factor and reduced cost per kWh energy generation [2].

Mrs. S. Sathana and Ms. Bindukala M.P. are with Department of Electronics and Communication,Adithya Institute of Technology,Coimbatore- 641 107. Email: saisathana@yahoo.co.in, ambikanair.m.p@gmail.com

The block diagram of the proposed system is shown in figure1.

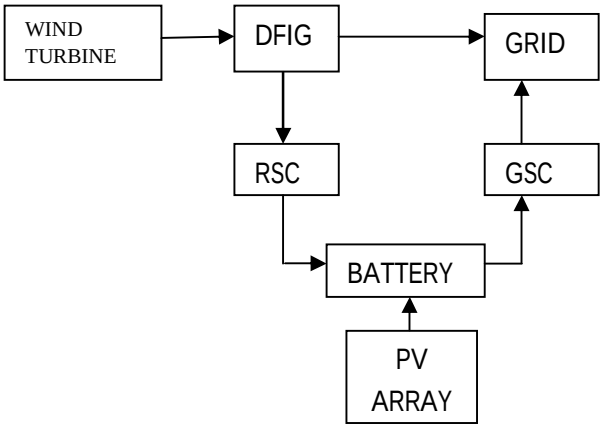

Fig 1: Block diagram of proposed system

In case of WECS, the stator windings of the DFIG are directly connected to the grid and the rotor windings are fed through bidirectional converters to control the rotor and stator output power fed to the grid for variable speed operation. The rotor current injection is controlled using fully controlled electronic converters to ensure effective operation in sub-synchronous and super-synchronous speed modes. The converter handles only around 25% of the machine rated power while the range of the speed variation is 33% around the synchronous speed.

The grid connectivity is a serious issue because of the varying nature and unpredictability of wind speeds. An effective control strategy is used to maintain the output power constant. A battery storage device is used for temporary storage of energy during the period of high wind speeds. The grid is always supplied with constant power irrespective of varying wind speed. This is called as grid power leveling.

II. MAXIMUM POWER EXTRACTION FROM PROPOSED CIRCUIT

Renewable energy resources like wind and solar energy are intermittent in nature. It is important to incorporate maximum power point tracking (MPPT) schemes to make the system efficient and reliable. The mechanical power generated by the wind is given by;

$$P_m = 0.5 \times C_p(\lambda, \beta) \times \rho \times A \times V^3 \qquad (1)$$

where;

C_p - power coefficient
ρ - air density
A - swept area of rotor blades
λ - tip speed ratio
β - pitch angle
V - wind velocity

The power coefficient (Cp) represents the efficiency of the wind turbine to convert wind energy into mechanical energy. It depends on two variables, the tip speed ratio (TSR) and the pitch angle. The TSR, λ, is the ratio of the turbine angular speed to the wind speed [3]. The pitch angle, β, is the angle in which the turbine blades are aligned with respect to its longitudinal axis.

$$\lambda = \frac{\omega R}{V} \qquad (2)$$

where ;

ω - rotational speed of generator

R - radius of rotor blades

V - wind velocity

Figure 2 and 3 are illustrations of a power coefficient curve and power curve for a typical fixed pitch (β =0) horizontal axis wind turbine. It is clear from figure 2 and 3 that the power curves have a shape similar to that of the power coefficient curve for wind turbines. Since TSR is a ratio between the turbine rotational speed and the wind speed, it follows that each wind speed would have a different corresponding optimal rotational speed that gives the optimal TSR. For each turbine, there is an optimal TSR value that corresponds to a maximum value of the power coefficient (Cp,max) and therefore the maximum power. Therefore, maximum power can be obtained for different wind speeds by controlling the rotational speed of generator.

PV arrays are constructed by connecting numerous solar cells in series and in parallel. A solar cell produces currents based on photovoltaic effect. A PV cell is a diode of a large-area forward bias and the equivalent circuit is shown by Figure 4. The current-voltage characteristic of a solar cell is as shown in figure 5. The equations are given by

$$I = I_{PH} - I_D \qquad (3)$$

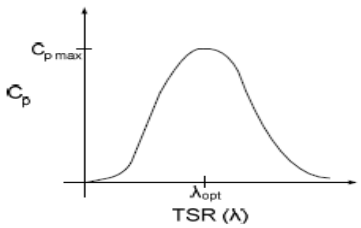

Fig 2: Power Coefficient Curve For a Typical Wind Turbine

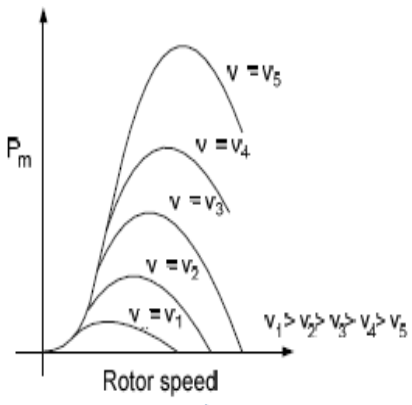

Fig 3: Power Coefficient Curve For a Typical Wind Turbine

$$I = I_{PH} - I_0\left[exp\left(\frac{q(v + R_S I)}{AK_B T}\right) - 1\right] - \frac{V + R_S I}{R_{sh}} \quad (4)$$

Where

I_{PH} = photocurrent
I_D = diode current
I_0 = saturation current
A = ideality factor
q = electronic charge
K_B =Boltzmann's Constant
R_S = series resistance
R_{sh} = shunt resistance
I = cell current
V = cell voltage

It is common to neglect the shunt and series resistances as they are large and small respectively. This simplifies the solar cell model. The resultant ideal V-I characteristic of a photovoltaic cell is given by the equation below and is illustrated in figure5.

$$I = I_{PH} - I_0\left[exp\left(\frac{qv}{kT}\right) - 1\right] \qquad (5)$$

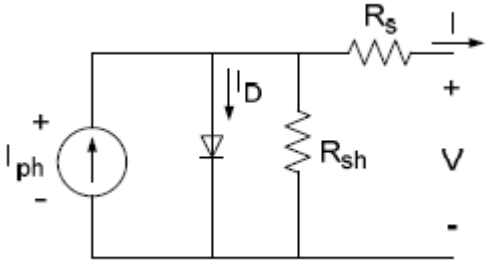

Fig 4. PV cell equivalent circuit

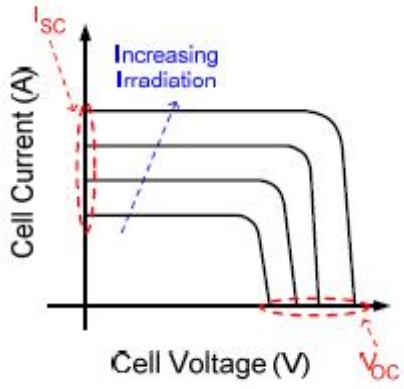

Fig 5. PV cell voltage current characteristics

Figure 6 shows the typical output power characteristics of a PV array under various degrees of irradiation. It is clear from Figure 6 that there is a particular optimal voltage for each irradiation level that corresponds to maximum output power. Thus, the output current (or voltage) of the PV array is adjusted to extract maximum power from the array.

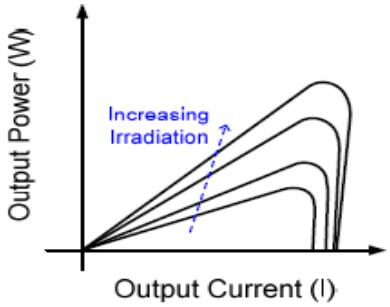

Fig 6.PV cell power characteristics

The Perturb and observe algorithm involves the perturbation of the operating voltage of the DC link between PV array and the power converter. In this method, the next perturbation is decided by the sign of last perturbation and sign of last increment in power. The P and O algorithm is shown in figure 7.

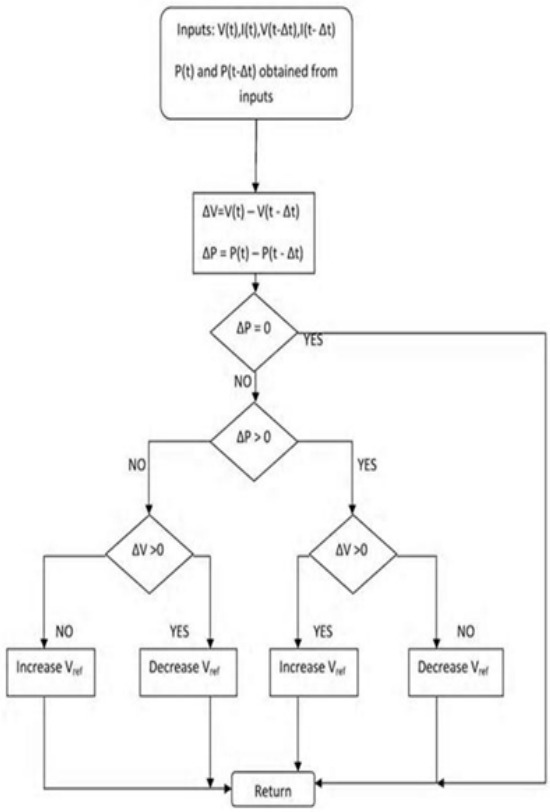

Fig 7.Perturb and observe algorithm

III. DESIGN AND CONTROL OF PROPOSED SYSTEM

Because of unpredictability of wind, the design of BESS is very important. This section deals with design of wind turbine, BESS and control strategy to obtain grid power levelling [2].

A. Design of wind turbine

The output power of the turbine is given by

$$P_m = 0.5 \times C_p(\lambda, \beta) \times \rho \times A \times V^3 \qquad (6)$$

Where C_p is power coefficient, ρ is air density, A swept area of rotor blades, V is the wind- velocity, λ is the tip speed ratio and β is the pitch angle.

The power coefficient is defined as the power output of the wind turbine to the available power in the wind regime. This coefficient determines the "maximum power" the wind turbine can absorb from the available wind power at a given wind speed. It is a function of the tip-speed ratio and the blade pitch angle. The blade pitch angle can be controlled by using a "pitch-controller" and the tip-speed ratio (TSR) is given as

$$\lambda = \frac{\omega R}{V} \qquad (7)$$

where ω is the rotational speed of the generator and R is radius of the rotor blades

Thus, the TSR can be controlled by controlling the rotational speed of the generator. For a given wind speed,

there is only one rotational speed of the generator which gives a maximum value of Cp, at a given β . This is the principle behind "maximum-power point tracking" (MPPT) for a wind turbine.

B. Design of BESS

The design of BESS should be proper necessary for satisfactory operation of WECS. The rating of the BESS is decided by the total energy stored into it and this energy is stored for only those periods in which power generated by the machine is more than the average value that is to be fed to the grid. Knowing the value of the average power to be fed to the grid, the required rating of the battery bank (E_b) is calculated as

$$E_b = \sum_{i=1}^{n} P_{mi} \times t_i \qquad (8)$$

where P_{mi} is the excess power at any instant than the average value of the power fed to the grid and t_i is the time period for which the excess power is produced. At any instant the value of P_{mi} can be calculated as

$$P_{mi} = \left(P_{inst} - P_{avg}\right) \qquad (9)$$

where P_{inst} is the instantaneous power of the wind turbine and P_{avg} is the average active power to be fed to the grid.

C. Control of GSC

The grid power should be maintained at a fixed value and this is given as the reference active power. This is then compared with the actual grid power at any instant. Proportional-integral (PI) controller is used to generate the q-axis component of the reference grid current. The expression for the reference q -axis grid current is as

$$i_{gqref} = \left(k_{pp} + \frac{k_{ip}}{s}\right)\left(P_{gref} - P_{grid}\right) \qquad (10)$$

Where k_{pp} and k_{ip} are the proportional and integral constants respectively. The reference d -axis grid current is chosen according to the reactive power sharing between the stator and the GSC. These reference currents are then compared with the actual grid side currents and the error signal is processed with a PI controller to generate the control voltages for the PWM generator on the grid side. The expressions for the control are given as

$$v_{dgsc} = \left(K_{pgsc} + \frac{K_{igsc}}{s}\right)\left(i_{gdref} - i_{gd}\right) \qquad (11)$$

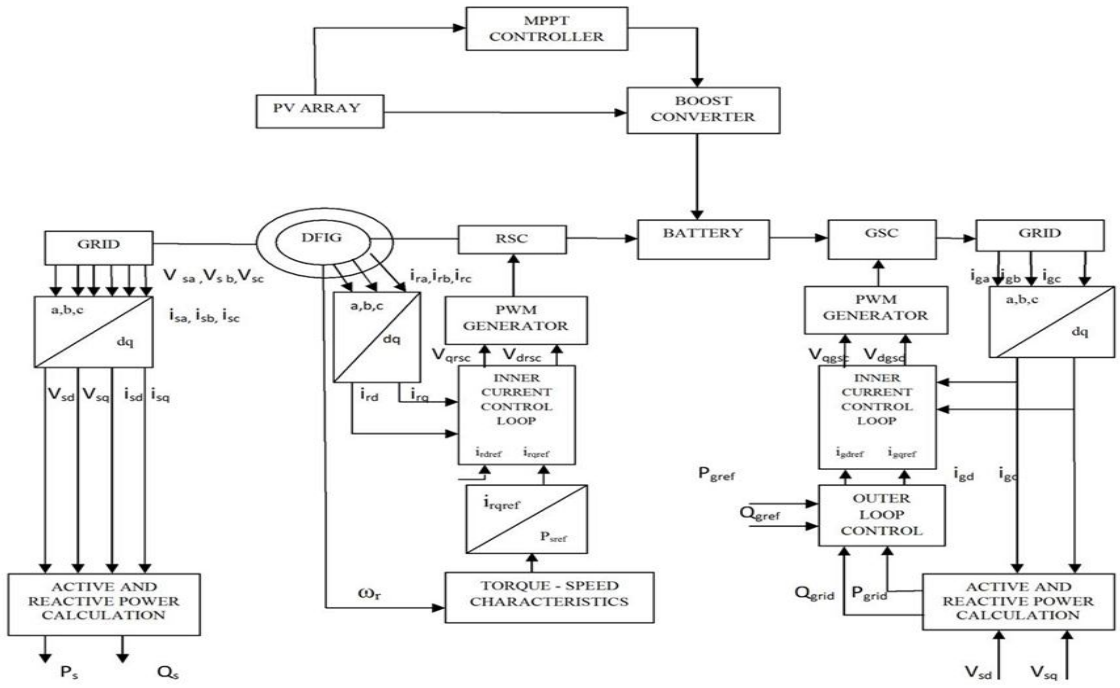

Fig 8. Detailed block diagram of proposed system including control strategy

$$v_{qgsc} = \left(K_{pgsc} + \frac{K_{gisc}}{s}\right)\left(i_{gqref} - i_{gq}\right) \qquad (12)$$

Where i_{gd} and i_{gq} are the sensed $d-q$ components of the grid currents and K_{pgsc} and K_{gisc} are the proportional and integral constants respectively.

D. Control of GSC

The control of RSC is to extract the maximum power from the wind. The active power set point is obtained from the instantaneous value of the rotor speed and the rotor current is controlled in the stator flux-oriented reference frame to obtain the desired active power according to the optimum torque speed characteristics.

The reference rotor currents are given by:

$$i_{rqref} = -\frac{L_s}{v_s L_m} P_{sref}$$

$$i_{rdref} = \frac{\phi_s}{L_m} - \frac{L_s}{v_s L_m} Q_{sref}$$

These reference values of rotor currents are compared with the actual values of rotor currents and the obtained error signal is processed with a PI controller to generate the control voltages for the PWM generator on the rotor side.

$$v_{drsc} = \left(k_{prsc} + \frac{k_{irsc}}{s}\right)\left(i_{rdref} - i_{rd}\right)$$

$$v_{qrsc} = \left(k_{prsc} + \frac{k_{irsc}}{s}\right)\left(i_{rqref} - i_{rq}\right)$$

where i_{rd} and i_{rq} are the d-q sensed components of the rotor currents k_{prsc} and k_{irsc} are the proportional and integral constants respectively. These control voltages are fed for PWM generation of the RSC.

E. PV array and MPPT

P and O algorithm is used for MPPT in PV array. PV array can be connected to BESS using boost converter which in turn is controlled by MPPT controller. Boost converter steps up the input voltage to desired level of the battery. The main components of the boost converter; the inductor, the diode and the switch works in coordinated manner to make the output voltage high. The switch is controlled by MPPT controller based on the solar irradiation levels. Thus, maximum power is utilized from the PV array. In case of sufficient irradiation levels, PV array may be used to feed grid directly.

V. SIMULATION RESULTS

A portion of the proposed system has been simulated using MATLAB-SIMULINK. The matlab model of the WECS is shown in figure 9.The analysis including the PV array is under progress. The results without including the PV array for wind speeds 10m/s,13m/s and 7m/s are given in Figs. 10, 11and 12 respectively. The waveforms for stator voltage (Vabc), grid current (Iabc), rotor speed (wr), reactive power (Q), grid power (P) and battery power (Vdc) are presented for different wind speeds. In all cases, the value of the grid power is maintained to be constant at 5 MW by the modified grid power control strategy. However, this is maintained by either charging or discharging the battery in the corresponding region of operation. The analysis has been performed at variable wind speeds and the grid power is maintained to be constant at the reference value. Hence, the grid power reference is chosen to be 5 MW. The system can be made more reliable and efficient by making it a hybrid system. Photovoltaic array can be used for charging the battery energy storage system (BESS). Also, it can used to meet other local loads. If the solar insolation level is high enough in the place,it can directly feed the grid.

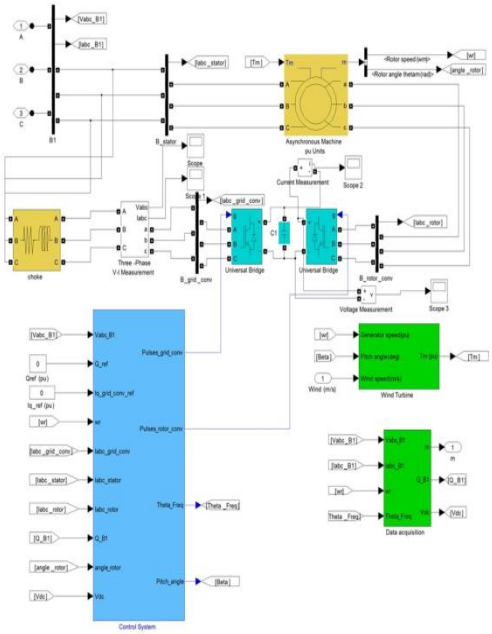

Fig 9: Matlab model of WECS

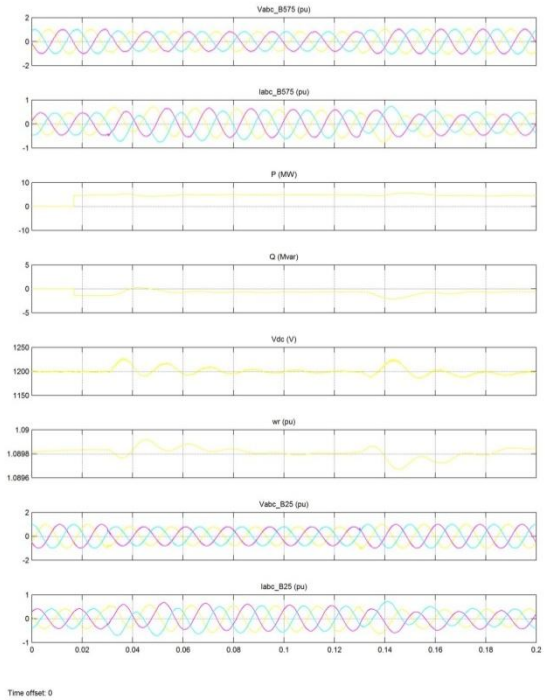

Fig 10: Waveforms for wind speed 10m/s

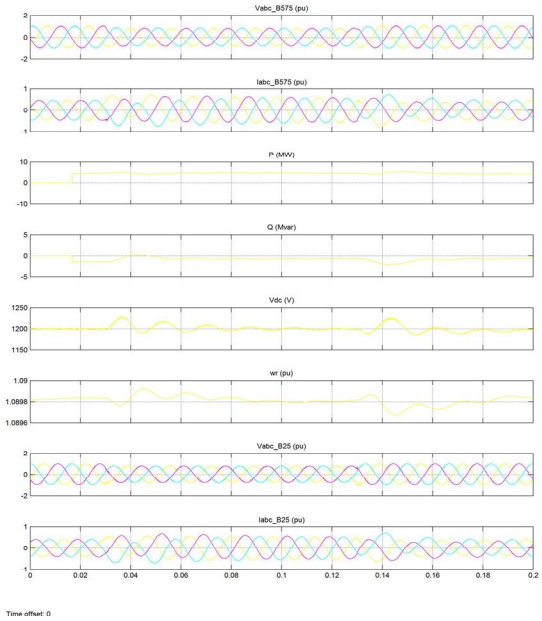

Fig 11: Waveforms for wind speed 13m/s

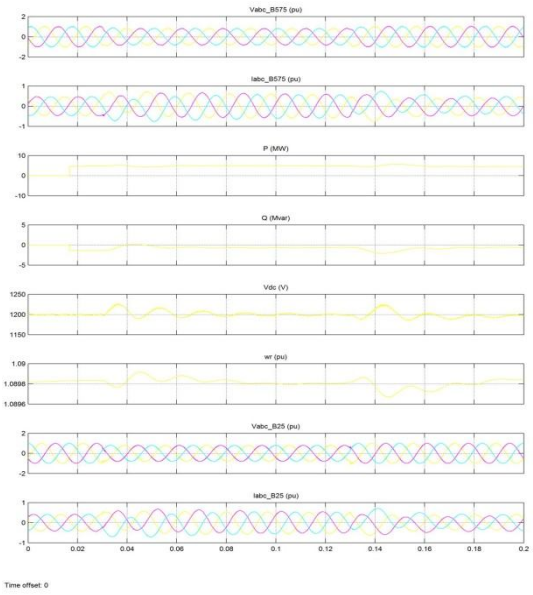

Fig 12: Waveforms for wind speed 7m/s

VI. CONCLUSION

A hybrid solar-wind energy system has been proposed. A DFIG-based WECS with a BESS has been simulated with a control strategy to maintain the grid power constant. Performance of a DFIG-based WECS with a BESS was studied at different wind speeds. It has been observed that the grid power leveling is obtained with help of BESS. During the periods of over generation, the excess power produced is stored in BESS. When the wind speeds goes low, the stored energy is utilized to maintain grid power constant. The system can be made more efficient and reliable by inclusion of photovoltaic array to obtain a hybrid system. If wind speed goes low for prolonged period, PV array can be used for charging BESS. If sufficient solar energy is available, it can directly feed the grid also.

REFERENCES

[1] Kui-Jun Lee and Rae-Young Kim, "An Adaptive Maximum Power Point Tracking Scheme Based on a Variable Scaling Factor for Photovoltaic Systems", IEEE Trans. Energy conversion,vol.27, no.4, December 2012

[2] Vijay Chand Ganti, Bhim Singh, Shiv Kumar Aggarwal and Tara Chandra Kandpal, "DFIG-Based Wind Power Conversion With Grid Power Leveling for Reduced Gusts" ,IEEE Trans.on sustainable energy, vol.3, no.1, January 2012

[3] Joanne Hui, Alireza Bakhshai and Praveen K. Jain, "Hybrid Wind-Solar Energy System: A New Rectifier A Stage Topology ", Queen's Center for Energy and Power Electronics Research (ePOWER), Queen's University Kingston, Ontario, Canada,2011.

[4] N. Femina, D. Granozio,G. Petrone,G. SPagnuolo, M. Vitelli," Predictive Adaptive MPPT Perturb and Observe Method", IEEE Trans .on aerospace and electronic systems., vol. 43, no.3 , pp. 934–950, July 2007.

[5] L. Xu and Y. Wang, "Dynamic modeling and control of DFIG-basedwind turbines under unbalanced network conditions," IEEE Trans. Power Syst., vol. 22, no. 1, pp. 314–323, Feb. 2007

[6] A.Tapia, G. Tapia, J. X. Ostolaza, and J. R. Saenz, "Modeling and control of a wind turbine driven doubly fed induction generator," IEEE Trans. Energy Convers., vol. 18, no. 2, pp. 194–204, Jun. 2003.

[7] M. Black, V. Silva, and G. Strbac, "The role of storage in integrating wind energy," in Proc. Int. Conf. Future Power Systems, Nov. 16–18,2005, pp. 1–6.

[8] A. Nourai, "Large-scale electricity storage technologies for energymanagement," in Proc. IEEE Power Eng. Soc. Summer Meeting, 2002,vol. 1, pp. 310–315.

[9] J. Eto, "Research, development and demonstration needs for largescalereliability enhancing integration of distributed energy resources,"in Proc. 33rd Annu. Hawaii Int. Conf. Syst. Sci., Jan. 4–7, 2000, p. 2.

[10] R. Pena, J. C. Clare, and G. M. Asher, "A doubly fed induction generatorusing back to back PWM converters supplying an isolated loadfrom a variable speed wind turbine," in *Proc. Inst. Elect. Eng., Electr.Power Appl.*, May 1996, vol. 143, no. 3, pp. 231–241.

[11] L. Xu and W. Cheng, "Torque and reactive power control of a doublyfed induction machine by position sensorless scheme," IEEE Trans. Ind. Appl., vol. 31, no. 3, pp. 636–642, May/Jun. 1995.

[12] L. H. Walker, "10-MW GTO converter for battery peaking service,"IEEE Trans. Ind. Appl., vol. 26, no. 1, pt. 1, pp. 63–72, Jan./Feb. 1990.

Mrs. S. Sathana was born in Erode, India, in 1985. She received her B. E. degree from K .S. R college of Engineering under Anna University, Chennai and M.E. from K . S. R. College of Technology under Anna University, Coimbatore. Presently she is working as Assistant Professor in Aditya Institute of Technology, Coimbatore.

Bindukala M.P. was born in Palakkad, India India, in 1989. She received her B.Tech (Electrical and Electronics Engineering) from Nehru College of Engineering and Research Centre, Trissur, Kerala under University of Calicut. Presently she is doing M .E (Applied Electronics) in Adithya Institute of Technology under Anna University, Chennai.

Optimal Reactive Power Flow using Fuzzy logic Controller Technique

T.Hariharan and Dr.M.GopalaKrishnan

Abstract: **Optimal reactive power flow is an optimization problem with one or more objective of minimizing the real power losses. The ancillary service for a generator has two components that have been recently recognized, i.e., one for sustaining its own real power communication and the other for providing reactive demand, enhancing system security, and scheming system voltage; and that only the next part should get financial compensation in aggressive power markets. In this paper planned incorporated technique will be united with fuzzy logic controller. This paper discusses the estimation of post-outage reactive power generation and flows using Linear estimation method for deregulated power system. One of the knowledge base intelligence techniques which will be utilized for verifying the generator reactive power operating limits and the power loss was the fuzzy logic. Representative results are presented using the IEEE 14 bus system by using MATLAB working platform and the ORPF presentation will be estimated.**

Keywords: **Optimum Reactive Power Flow (ORPF), Linear Estimates, Fuzzy Logic Controller (FLC)**

I. INTRODUCTION

Traditional power system security analysis includes the simulation of static as well as dynamic performance of a power system in response to a list of possible disturbances. In fact, in the vertically integrated utility structure and the competitive environment, the distribution entities have the obligation to serve all consumers at all times, i.e., provide a reliable service to all the loads. Operational reliability is normally checked using contingency analysis. Contingencies include the outage of system components and abrupt changes in loads.

The use full Newton power flow [1] for contingency analysis is Computationally expensive. To speed up the computations, fast approximate power flow methods were proposed, such as the decoupled power flow [2,3] and the iterative linear AC power flow [4].

In the estimation of reactive power outputs and flows, the explicit consideration of reactive power limits is very important [5]. The estimation methods based on distribution factors and optimization discussed in the literature ignore equipment limits, thus increasing the estimation error [6]. An innovative, optimization-based method for post-line outage reactive flow and voltage computation is presented in [7].In this paper, the use of sensitivities for the estimation of post-contingency reactive generation and flows is discussed. No decoupling assumption is made in the derivation of the sensitivities. However, the method is flexible and the incorporation of decoupling is straightforward. Multiple outage contingencies and the redistribution of generation after a generation outage are easily handled. Employing linear estimates, the effect of devices' limits on the estimates is effectively captured. Representative results are presented on the IEEE 14 -bus test system. The numerical results show that by taking into account equipment limits, the estimation errors are significantly reduced.

II. POWER FLOW BACKGROUND

Consider an **N**-bus power system characterized by the admittance matrix **Y**. The *i, j* element Y_{ij} of **Y** is given by

$$Y_{ij} = -yij, i \neq j \quad (1)$$

$$Yii = \sum_{j} y_{ij} + y_{ig} \quad (2)$$

Where y_{ij} is the admittance of the line between buses *i* and *j*, and is the ground admittance of bus *i*. We denote the total active power generation and the total active load at bus *i* by P_i^g and P_i^l ,respectively, and their reactive power counterparts by Q_i^g and Q_i^l .The load terms P_i^l and Q_i^l are assumed to be fixed. The net power injections at bus i in terms of the load and generation are

$$P_i = P_i^g - P_i^l \quad (3)$$

$$Q_i = Q_i^g - Q_i^l \quad (4)$$

The net power injections at bus i satisfy [1]

$$P_i = \sum_{j=1}^{N} V_i V_j [G_{ij} \cos(\theta_i - \theta_j) + B_{ij} \sin(\theta_i - \theta_j)] \quad (5)$$

$$Q_i = \sum_{j=1}^{N} V_i V_j [G_{ij} \cos(\theta_i - \theta_j) - B_{ij} \sin(\theta_i - \theta_j)] \quad (6)$$

T.Hariharan is working as assistant professor in Sree Sastha Institute of Engineering and Technology, Chennai, Email: thariharanme@gmail.com and **Dr.M.GopalaKrishnan** is a Professor, Sri Venkateshwara College of Engineering, Sriperumpudhur Email: [2]gopala@svce.ac.in.

Where θ_i and V_i are the bus *i*'s voltage phase angle and magnitude, respectively.

The reactive power produced or consumed by a generator is limited, and depends on the active power being produced [5]. Assuming there is one generator at bus, and denoting the upper and lower limits for the reactive power generation by $\overline{Q_i^g}(P_i^g)$ and $\underline{Q_i^g}(P_i^g)$, respectively, the reactive power output is constrained by

$$\underline{Q_i^g}(P_i^g) \le Q_i^g \le \overline{Q_i^g}(P_i^g). \quad (7)$$

Let V_i^{sp} be the specified at the PV bus i. If $Q_i^g = \overline{Q_i^g}(P_i^g)$ then $V_i \le V_i^{sp}$, and we call the bus *max VAr constrained*. If $Q_i^g = \underline{Q_i^g}(P_i^g)$, then $V_i \ge V_i^{sp}$ and we call the bus *min VAr constrained*.

The vector **x** is constructed with the voltage angles of the PV and PQ buses, and the voltage magnitudes of the PQ buses, and the vector $\tilde{x}$ is constructed with the voltage angles and magnitudes of all buses. Let $f(\tilde{x})$ be the vector of the PQ and PV buses' active power injections, and the PQ buses' reactive power injections, both as explicit functions of $\tilde{x}$. Let f^{sp} be the vector with the specified values for $f(\tilde{x})$. The power flow problem is to obtain $\tilde{x}$ such that

$$f(\tilde{x}) = f^{sp} \quad (8)$$

In the solution of the power flow problem, the Jacobian

$$J := \frac{\partial f(\tilde{x})}{\partial x} \quad (9)$$

is used.

The *full Jacobian J* is defined as

$$\tilde{J} := \frac{\partial f(\tilde{x})}{\partial \tilde{x}} \quad (10)$$

The power $S_{ij}=P_{ij}+jQ_{ij}$ flowing from *i* bus on the line that connects buses *i* and *j* is given by

$$P_{ij} = \sum_{j=1}^{N} V_i V_j [G_{ij}\cos(\theta_i-\theta_j) + B_{ij}\sin(\theta_i-\theta_j)] - V_i^2 (G_{ij} - g_{ijg/2}) \quad (11)$$

$$Q_{ij} = \sum_{j=1}^{N} V_i V_j [G_{ij}\sin(\theta_i-\theta_j) - B_{ij}\cos(\theta_i-\theta_j)] - V_i^2 (B_{ij} - b_{ijg/2}) \quad (12)$$

The focus of this paper is the estimation of post-contingency reactive power outputs Q_i^{gc} and flows Q_{ij}^c. The computation of these quantities under different contingencies requires the solution of (8) under each contingency.

III. LINEAR ESTIMATES

We linearly parameterize the occurrence of a contingency using the parameter K. Hence, we let all the quantities defined the previous Section be functions of K. Since the parameterization is linear, the specified quantity changes are proportional to changes in K. Consider, for example, the outage of the load and generation at bus *j*, and let K change from K^O to K^C. Then $P_j(K^O)$ and $Q_j(K^O)$ take their pre-contingency values P_j^O and Q_j^O, and the post-contingency values are $P_j(K^c)=0$ and $Q_j(K^c)=0$. For $K^O<K<K^c$

$$P_j(K) = (K^C-K)P_j^O$$

and

$$Qj(K) = (K^C-K)\, Q_j^O.$$

The net active power injections at PV and PQ buses do not change with the contingency, and so $P_i(K) = P_i^O$ Also, the net reactive power injections PV at PQ buses do not change with the contingency, and so $Q_i(K) = Q_i^O$. we can obtain Q_i^g and Q_{ij} as functions of K for $K^O< K <K^c$ .We use the Taylor series of these functions to express the post-contingency reactive power output Q_i^{gc} and the flow Q_{ij}^c as

$$Q_{ij}^c = Q_{ij}^o + \frac{dQ_{ij}}{dK}\Delta K + h.o.t \quad (13)$$

$$Q_i^{gc} = Q_i^{go} + \frac{dQ_i^g}{dK}\Delta K = h.o.t \quad (14)$$

Where we denote pre-contingency quantities with a superscript o. Whenever ΔK is sufficiently small, the h.o.t. can be neglected to obtain approximate values of Q_i^{gc} and Q_{ij}^c. To give K a physical interpretation, in the remainder of the paper we set K before the contingency equal to 0 and after the contingency equal to 1, so that ΔK=1 for the occurrence of the contingency.

A. Load and Generation Contingencies

Consider contingencies where a change in K implies a change in the active and or reactive power injections/withdrawals, including generator and load outages. Using (4), the derivatives in (13)–(14) are

$$\frac{dQ_{ij}}{dK} = \nabla_X Q_{ij} . \frac{dx}{dK} \quad (15)$$

$$\frac{dQ_i^g}{dK} = \nabla_X Q_i^g . \frac{dx}{dK} + \frac{\partial Q_i^g}{\partial K} = \nabla_X Q_i . \frac{dx}{dK} + \frac{\partial Q_i}{\partial K} + \frac{\partial Q_i^l}{\partial K}. \quad (16)$$

The elements of $\nabla_X Q_{ij}$ are computed using (12). The gradient $\nabla_X Q_i$ is obtained from the full Jacobian.

The differential change in K leads to a differential change in the system state x. Changes in the system state are subject to (5) and (6), which in a differential sense are reduced to

$$df = Jdx \quad (17)$$

Thus

$$\frac{dx}{dK} = J^{-1}\frac{df}{dK} \quad (18)$$

In practice, for computational efficiency reasons (dx/dK) is obtained directly using factorization methods. Note that when the contingency involves the outage of generator *p*, there is a change in the reactive generation at bus. For this change to be enforced, bus *p* needs to be modeled as a PQ bus for the purpose of the computation of (dx/dK). Under these circumstances, the term $(\partial Q_p/\partial K)$ of (16) takes into account the reduction of reactive power generation at bus *p*. The term $(\partial f/\partial K)$ is the rate of change of real and reactive power injections with respect to a change in K, and is known for a specified contingency. For example, if after the contingency

- real load increased an amount k_i at bus *i*;
- reactive generation remained constant at bus j;
- active generation at bus *h* decreased by k_h; then

$(\partial P_i/\partial K)=-k_i$, $(\partial Q_j/\partial K)=-k_i$, and $(\partial P_h/\partial K)=-k_h$. Thus, the sensitivities in (16)–(18) can be computed for any change in load and corresponding generation response. Replacing (15)–(16) and (18) in (13)–(14), and neglecting the *h.o.t.*, we obtain

$$Q_{ij}^{c} \cong Q_{ij}^{o} + \nabla_X Q_{ij}.J^{-1}\frac{df}{dK} \qquad (19)$$

$$Q_i^{gc} \cong Q_i^{go} + \nabla_X Q_i.J^{-1}\frac{df}{dK} + \frac{\partial Q_i}{\partial K} + \frac{\partial Q_i^{l}}{\partial K}. \qquad (20)$$

Note that the linear estimation of all the desired quantities requires the solution of only one linear system of equations, (20). If the decoupling *P-V* and *Q-θ* of and holds, this linear system of equations can be decoupled into two subsystems, improving the solution speed. The linear estimates (19)–(20) have been applied to a variety of power systems problems.

IV. FUZZY LOGIC CONTROLLER

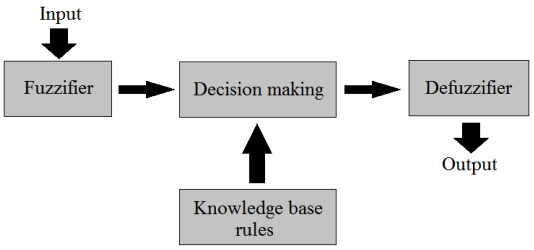

Figure.1. Structure of the proposed FLC

Fig 1 shows the structure of fuzzy logic controller. In this proposed system, the real power is the physical input of the fuzzy logic and the rules are generated depending on the real power input. The fuzzy rules has been generated by the three categories i.e., low, medium and high. These rules are used to assign the generator reactive power generation. In this generation limit is given to the optimization algorithm, it can be provide the minimized power loss of the system.

V. RESULTS AND DISCUSSION

The schemes presented have been applied to the estimation of post-contingency reactive power outputs and flows in various test systems. In this paper, representative results on the IEEE 14 -bus test system shown in fig.2 are presented to illustrate the capabilities of the proposed methods. The results for two contingencies for each test system are presented in detail. These contingencies have been chosen to allow the quick comparison of the results with other estimation methods in the literature. All generation limits are explicitly considered. Matlab and Power System Toolbox 2.0 were used in the implementation of the estimation methods.

For the IEEE 14-bus test system, the outages of line 2–4 and transformer 5–6 are presented in detail. The estimations were done using (19)-(20). The post-outage reactive power Outputs and flows are in Tables I and II, respectively. The outage of line 2–6 does not result in any generator becoming constrained.

TABLE I. POST-OUTAGE MVAR GENERATION FOR IEEE 14-BUS TEST SYSTEM

Line and Direction	Outage of Line 2-6		Outage of Transformer 4-7	
	Exact	Linear	Exact	Linear
1-2	-16.95	-16.83	-21.46	-20.93
1-5	6.18	5.54	1.30	-0.82
2-3	2.18	1.93	3.30	3.37
2-4	0.00	0.00	-1.48	-5.07
2-5	-0.36	-1.32	-1.22	-3.86
3-4	2.30	1.70	3.77	0.17
4-5	23.10	22.67	8.42	12.07
4-7	-12.13	-11.95	-4.83	-10.38
4-9	-1.37	1.30	3.22	-1.80
5-6	9.24	9.58	0.00	0.00
6-11	4.03	3.96	5.39	10.71
6-12	2.53	2.52	3.26	3.95
6-13	7.48	7.44	7.85	10.58
7-8	-19.87	-19.67	-21.52	-12.29
7-9	6.08	6.08	10.26	-2.80
9-10	3.82	3.88	4.90	-3.68
9-14	3.36	3.40	3.88	-1.69
10-11	-2.00	-1.94	-1.76	-9.67
12-13	0.78	0.77	1.59	2.29
13-14	1.99	1.94	3.53	7.17

TABLE II. POST OUTAGE MVAR FLOWS

Bus	Outage Of Line 2-6		Outage Of Transformer 4-7	
	Exact	Linear	Exact	Linear
1	-10.77	-11.29	-20.16	-21.75
2	36.38	34.83	42.82	35.72
3	29.28	28.30	25.37	21.48
6	17.15	16.64	24.00	32.73
8	20.49	20.27	22.25	12.48

The estimates are extremely accurate in this case. The average reactive generation absolute errors are reduced by 97% and 93%, respectively, compared to other technique. The reasons for the accuracy improvement is that we use exact sensitivities, while in there are approximations involved in the computation of the sensitivities. Generator 6 becomes max VAr constrained with the outage of transformer 4-7. Fig.3.shows that at K=0.51, i.e., the flows on transformer 4-7 are reduced by 51%, generator 6 becomes constrained. This is indicated with a O. Thus, for K > 0.51 the reactive output at bus 6 is fixed and the voltage magnitude at bus 6 decreases. The estimated K -distance to the change in status, indicated by *, is K=0.57.In any case, the average reactive flows absolute errors with the linear estimates are reduced by 37% and 85% respectively.

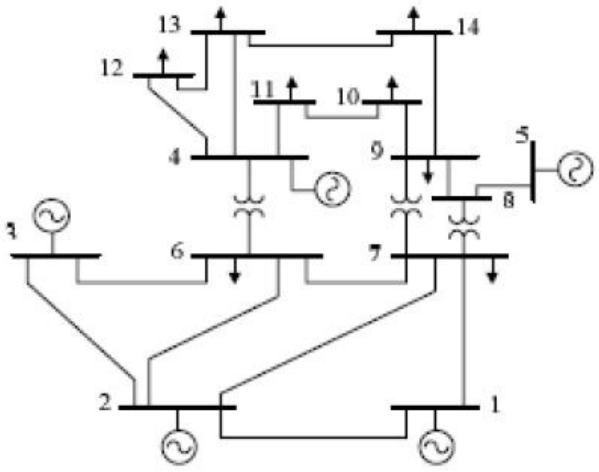

Figure.2. IEEE 14 bus system structure

In the IEEE 14-bus test systems, 23 contingencies were simulated. These consisted of all line and generation outages except for those resulting in load shedding. A summary of the estimation errors is presented in Table III, with the errors defined as the absolute value of the difference between the exact value and the estimated one. Note that the linear estimates are significantly more accurate for all three estimated quantities for IEEE 14-bus test system. For the linear estimation methods, the mean errors obtained are extremely small compared to the results presented in the literature.

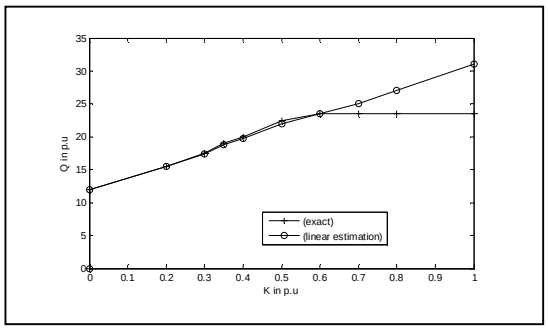

Figure. 3: Reactive power generation at bus 6 as a function of the per unit reduction in power flow.

The high maximum errors occur in few contingencies which lead to significant changes in the system, and in devices very close to those outaged. In these cases, V_i , Q_i^g and Q_{ij} are highly nonlinear functions of K, and so first-order estimates are not very accurate. For example, the maximum reactive power output error of 21.54 MVAr in the 14-bus test system occurs on generator 2 in the estimation of the effect of the outage of the slack generator 1. Generator 2 is the new slack generator for that contingency, and its post-contingency active power generation is 220MW higher than its pre-contingency active power output, a 570% increase. For the 14-bus test system, the total computation time was 43% of that taken by running power flows for the linear estimation method.

TABLE III. SUMMARY OF ESTIMATION ERRORS FOR IEEE 14-BUS TEST SYSTEM

Method	Linear Estimation		
Error	Mean	St Dev	Max
Gen[Mvar]	1.64	3.75	21.54
Flow[Mvar]	0.88	3.10	61.58

VI. CONCLUSION

The estimation of post-contingency reactive power generation and flows using sensitivities has been discussed. A linear estimation method and fuzzy logic controller has been proposed to capture the effect of equipment limit activation/deactivation on the estimates. The method is flexible and allows the representation of all type of contingencies. Representative results on the IEEE 14 bus test systems show that the estimation errors are significantly reduced with the proposed method, compared to the methods in the literature.

The estimation method proposed is useful in system reliability planning and operations, where contingency studies are intensively done.

Other direction for future work in the area is the comparison of the estimation accuracy using sensitivities with respect to flows and with respect to network admittances, for branch outage studies.

REFERENCES

[1] B. Wollenberg and A. Wood, Power Generation, Operation and Control,
2nd ed. New York: Wiley, 1996.

[2] B. Stott and O. Alsaç, "Fast decoupled load flow," *IEEE Trans* Power App. Syst., vol. PAS-93, pp. 859–869, May/Jun. 1974.

[3] A. Monticelli, A. Garcia, and O. R. Saavedra, "Fast decoupled load flow: Hypothesis, derivations, and testing," IEEE Trans. Power Syst., vol. 5, pp. 1425–1431, Nov. 1990.

[4] N. Peterson, W. F. Tinney, and D. Bree, "Iterative linear ac power flow
solution for fast approximate outage studies," IEEE Trans. Power App. *Syst.*, vol. PAS-91, pp. 2048–2058, Sep./Oct. 1972.

[5] M. A. Pai, Computer Techniques in Power *System Analysis*, 2nd ed. New Delhi, India: Tata McGraw-Hill, 2006.

[6] C. Lee and N. Chen, "Distribution factors of reactive power flow in transmission line and transformer outage studies," *IEEE Trans. Power Syst.*, vol. 7, pp. 194–200, Feb. 1992.

[7] ——, "Post-outage reactive power flow calculations by genetic algorithms: Constrained optimization approach," *IEEE Trans. Power Syst.*, vol. 20, pp. 1622–1272, Aug. 2005.

Review of Renewable Energy Resources in Clean Green Environment

K. K. Saravanan, Dr. N. Stalin and S. T. Jayasuthahar

Abstract--The potential of renewable energy sources is enormous as they can in principle meet many times the world's energy demand. Renewable energy sources such as biomass, wind, solar, hydropower, and geothermal can provide sustainable energy services, based on the use of routinely available, indigenous resources. A transition to renewable-based energy systems is looking increasingly likely as their costs decline while the price of oil and gas continue to fluctuate. In the past 30 years solar and wind power systems have experienced rapid sales growth, declining capital costs and costs of electricity generated, and have continued to improve their performance characteristics. In fact, fossil fuel and renewable energy prices, and social and environmental costs are heading in opposite directions and the economic and policy mechanisms needed to support the widespread dissemination and sustainable markets for renewable energy systems are rapidly evolving. It is becoming clear that future growth in the energy sector will be primarily in the new regime of renewable energy, and to some extent natural gas-based systems, not in conventional oil and coal sources. Because of these developments market opportunity now exists to both innovate and to take advantage of emerging markets to promote renewable energy technologies, with the additional assistance of governmental and popular sentiment. The development and use of renewable energy sources can enhance diversity in energy supply markets, contribute to securing long term sustainable energy supplies, help reduce local and global atmospheric emissions, and provide commercially attractive options to meet specific energy service needs, particularly in developing countries and rural areas helping to create new employment opportunities there.

***Keywords*—**Renewables, Sequestration efforts, Municipal solid waste, Photovoltaics, Hybridization

INTRODUCTION

Conventional energy sources based on oil, coal, and natural gas have proven to be highly effective drivers of economic progress, but at the same time damaging to the environment and to human health. Furthermore, they tend to be cyclical in nature, due to the effects of oligopoly in production and distribution. These traditional fossil fuel-based energy sources are facing increasing pressure on a host of environmental fronts, with perhaps the most serious challenge confronting the future use of coal being the Kyoto Protocol greenhouse gas (GHG) reduction targets. It is now clear that any effort to maintain atmospheric levels of CO2 below even 550 ppm cannot be based fundamentally on an oil and coal-powered global economy, barring radical carbon sequestration efforts.

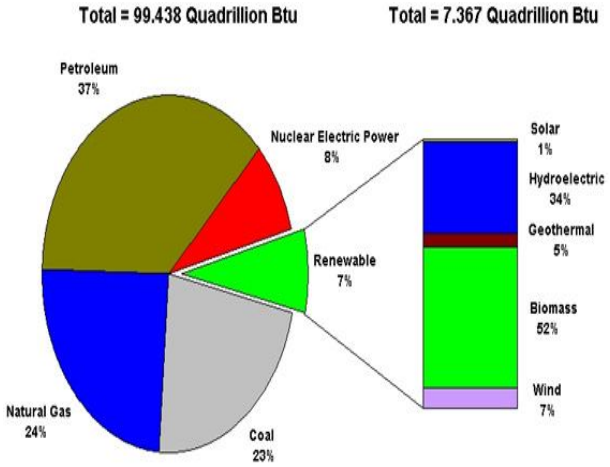

Figure (1): Renewable energy consumption in the nation's energy supply

Renewable energy sources currently supply somewhere between 15 percent and 20 percent of world's total energy demand. The supply is dominated by traditional biomass, mostly fuel wood used for cooking and heating, especially in developing countries in Africa, Asia and Latin America. A major contribution is also obtained from the use of large hydropower; with nearly 20 percent of the global electricity supply being provided by this source. New renewable energy sources (solar energy, wind energy, modern bio-energy, geothermal energy, and small hydropower) are currently contributing about two percent. A number of scenario studies have investigated the potential contribution of renewable to global energy supplies, indicating that in the second half of the 21st century their contribution might range from the present figure of nearly 20 percent to more than 50 percent with the right policies in place.

Biomass Energy

Biomass is the term used for all organic material originating from plants (including algae), trees and crops and is essentially the collection and storage of the sun's energy through photosynthesis. Biomass energy, or bio energy, is the conversion of biomass into useful forms of energy such as heat, electricity and liquid fuels. Biomass for bio energy comes either directly from the land, as dedicated energy crops, or from residues generated in the processing of crops for food or other products such as pulp and paper from the wood industry. Another important contribution is from post

K. K. Saravanan and S. T. Jayasuthahar are working in University College of Engineering, Thirukkuvalai, Email: kksaravanan_vpm@yahoo.co.in and ***Dr. N. Stalin*** is Assistant Professor, University College of Engineering, Trichy.

consumer residue streams such as construction and demolition wood, pallets used in transportation, and the clean fraction of municipal solid waste (MSW). The biomass to bio energy system can be considered as the management of flow of solar generated materials, food, and fiber in our society. These interrelationships which presents the various resource types and applications, showing the flow of their harvest and residues to bio energy applications. Not all biomass is directly used to produce energy but rather it can be converted into intermediate energy carriers called bio fuels. This includes charcoal, ethanol (liquid fuel), or producer-gas. Biomass and bio energy flow chart (Source: R.P. Over end, NREL, 2000)

Biomass was the first energy source harnessed by humans and for nearly all of human history, wood has been our dominant energy source. Only during the last century, with the development of efficient techniques to extract and burn fossil fuels, have coal, oil, and natural gas, replaced wood as the industrialized world's primary fuel. Today some 40 to 55 exajoules (EJ = 1018joules) per year of biomass is used for energy, out of about 450 EJ per year of total energy use, or an estimated 10-14 percent, making it the fourth largest source of energy behind oil (33 percent), coal (21 percent), and natural gas (19 percent). The precise amount is uncertain because the majority is used non-commercially in developing countries.

Biomass is usually not considered a modern energy source, given the role that it has played, and continues to play, in most developing countries. In developing countries it still accounts for an estimated one third of primary energy use while in the poorest up to 90% of all energy is supplied by biomass. Biomass energy has the potential to be "modernized" worldwide, that is produced and converted efficiently and cost-competitively into more convenient forms such as gases, liquids, or electricity. A variety of technologies can convert solid biomass into clean, convenient energy carriers over a range of scales from household/village to large industrial. Some of these technologies are commercially available today while others are still in the development and demonstration stages. If widely implemented, such technologies could enable biomass energy to play a much more significant role in the future than it does today, especially in developing countries.

The Future Role of Biomass

Modernized biomass energy is projected to play a major role in the future global energy supply. This is being driven not so much by the depletion of fossil fuels, which has ceased to be a defining issue with the discovery of new oil and gas reserves and the large existing coal resources, but rather by the recognized threat of global climate change, caused largely by the burning of fossil fuels. Its carbon neutrality (when produced sustainably) and its relatively even geographical distribution coupled with the expected growth in energy demand in developing countries, where affordable alternatives are not often available, make it a promising energy source in many regions of the world for the 21st century. Most households in developing countries that use biomass fuels today do so either because it is available at low (or zero) financial cost or because they lack access to or cannot afford higher quality fuels. As incomes rise, preferences tend to shift away from biomass.

Implementation of Biomass Energy Systems

Raw biomass has several disadvantages as an energy source. It is bulky with a low energy density and direct combustion is generally highly inefficient (other than advanced domestic heaters) producing high levels of indoor and outdoor air pollution. The goal of modernized biomass energy is to increase the fuel's energy density while decreasing its emissions during production and use. Modernizing biomass energy production however faces a variety of challenges that must be adequately addressed and dealt with before the widespread implementation of bio energy systems can occur. These issues include technical problems (just discussed), resource availability, environmental impacts, and economic feasibility.

Wind Energy

Wind has considerable potential as a global clean energy source, being both widely available, though diffuse, and producing no pollution during power generation. Wind energy has been one of humanity's primary energy sources for transporting goods, milling grain, and pumping water for several millennia. From windmills used in China, India and Persia over 2000 years ago to the generation of electricity in the early 20th century in Europe and North America wind energy has played an important part in our recorded history. As industrialization took place in Europe and then in America, wind power generation declined, first gradually as the use of petroleum and coal, both cheaper and more reliable energy sources, became widespread, and then more sharply as power transmission lines were extended into most rural areas of industrialized countries. The oil crises of the 70's, however, triggered renewed interest in wind energy technology for grid connected electricity production, water pumping, and power supply in remote areas, promoting the industry's rebirth.

This impetus prompted countries; notably Denmark and the United States, to establish government research and development (R&D) programs to improve wind turbine technology. In conjunction with private industry research this lead to a reemergence in the 1980's of wind energy in

the United States and Europe, when the first modern grid-connected wind turbines were installed. In the 1990's this development accelerated, with wind becoming the fastest growing energy technology in the world developing into a commercially competitive global power generation industry. While in 1990 only about 2000 MW of grid-connected wind power was in operation worldwide by 1999 this figure had surpassed 10,000 MW, not including the over one million water-pumping wind turbines located in remote areas. Since 1990 the average annual growth rate in world wind generating capacity has been 24 percent, with rates of over 30 percent in the last two years. Today there is more than 13,000 MW of installed wind power, double the capacity that was in place just three years earlier. This dramatic growth rate in wind power has created one of the most rapidly expanding industries in the world, with sales of roughly $2 billion in 1998, and predictions of tenfold growth over the next decade. Most 2000 forecasts for installed capacity are being quickly eclipsed with wind power having already passed the 10,000 MW mark in early 1999.

Solar Photovoltaic and Solar Thermal Technologies

There are two basic categories of technologies that convert sunlight into useful forms of energy, aside from biomass-based systems that do this in a broader sense by using photosynthesis from plants as an intermediate step. First, solar photovoltaic (PV) modules convert sunlight directly into electricity. Second, solar thermal power systems use focused solar radiation to produce steam, which is then used to turn a turbine producing electricity. The following provides a brief overview of these technologies, along with their current commercial status.

Solar Photo voltaics

Solar PV modules are solid-state semiconductor devices with no moving parts that convert sunlight into direct-current electricity. The basic principle underlying the operation of PV modules dates back more than 150 years, but significant development really began following Bell Labs' invention of the silicon solar cell in 1954. The first major application of PV technology was to power satellites in the late 1950s, and this was an application where simplicity and reliability were paramount and cost was a secondary concern.

Since that time, enormous progress has been made in PV performance and cost reduction, driven at first by the U.S. space.

Solar Thermal Systems

Solar thermal power systems use various techniques to focus sunlight to heat an intermediary fluid, known as heat transfer fluid that then is used to generate steam. The steam is then used in a conventional steam turbine to generate electricity. At present, there are three solar thermal power systems currently being developed: parabolic troughs, power towers, and dish/engine systems. Because these technologies involve a thermal intermediary, they can be readily hybridized with fossil fuels and in some cases adapted to utilize thermal storage. The primary advantage of hybridization and thermal storage is that the technologies can provide dispatchable power and operate during periods when solar energy is not available. Hybridization and thermal storage can enhance the economic value of the electricity produced, and reduce its average cost. Parabolic trough solar thermal systems are commercially available. These systems use parabolic trough-shaped mirrors to focus sunlight on thermally efficient receiver tubes that contain a heat transfer fluid. This fluid is heated to about 390° C. (734° F) and pumped through a series of heat exchangers to produce superheated steam that powers a conventional turbine generator to produce electricity. Nine of these parabolic trough systems, built in 1980s, are currently generating 354 MW in Southern California. These systems, sized between 14 and 80 MW, are hybridized with up to 25 percent natural gas in order to provide dispatchable power when solar energy is not available. Power tower solar thermal systems are in the demonstration and scale-up phase. They use a circular array of heliostats (large individually-tracking mirrors) to focus sunlight onto a central receiver mounted on top of a tower. The first power tower, Solar One, was built in Southern California and operated in the mid-1980s. This initial plant used a water/steam system to generate 10 MW of power. In 1992, a consortium of U.S. utilities joined together to retrofit Solar One to demonstrate a molten-salt receiver and thermal storage system. The addition of this thermal storage capability makes power towers unique among solar technologies by allowing dispatchable power to be provided at load factors of up to 65 percent. In this system, molten-salt is pumped from a "cold" tank at 288° C. (550° F) and then cycled through the receiver where it is heated to 565° C. (1,049° F) and finally returned to a "hot" tank. The hot salt can then be used to generate electricity when needed. Current designs allow storage ranging from 3 to 13 hours. Dish/engine solar thermal systems, currently in the prototype phase, use an array of parabolic dish-shaped mirrors to focus solar energy onto a receiver located at the focal point of the dish. Fluid in the receiver is heated to 750° C (1,382° F) and used to generate electricity in a small engine attached to the receiver. Engines currently under consideration include Stirling and Brayton-cycle engines. Several prototype dish/engine systems, ranging in size from 7 to 25 kW, have been deployed in various locations in the U.S. and elsewhere. High optical efficiency and low startup losses make dish/engine systems the most efficient of all solar technologies, with electrical conversion efficiencies of up to 29.4 percent. In addition, the modular design of dish/engine

systems make them a good match for both remote power needs, in the kilowatt range, as well as grid-connected utility applications in the megawatt range.System capital costs for these systems are presently about $4-5 per watt for parabolic trough and power tower systems, and about $12-13 per watt for dish/engine systems. However, future cost projections for trough technology are higher than those for power towers and dish/engine systems due in large part to their lower solar concentration and hence lower operating temperature and efficiency. By 2030, the U.S. Department of Energy forecasts costs of $2.70 per watt, $2.50 per watt, and $1.30 per watt, respectively, for parabolic trough, power tower, and dish engine systems.

Hydropower

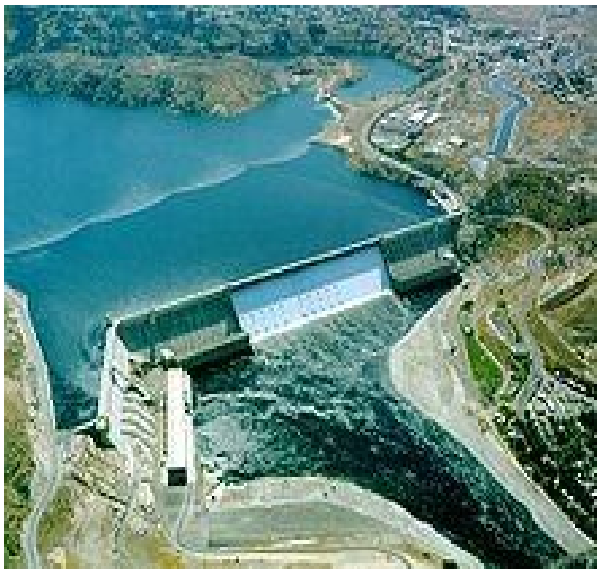

Hydropower is the largest renewable resource used for electricity. It plays an essential role in many regions of the world with more than 150 countries generating hydroelectric power. A survey in 1997 by The International Journal on Hydropower & Dams found that hydro supplies at least 50 percent of national electricity production in 63 countries and at least 90 percent in 23 countries. About 10 countries obtain essentially all their commercial electricity from hydro, including Norway, several African nations, Bhutan and Paraguay. There is about 700 GW of hydro capacity in operation worldwide, generating 2600 TWh/year (about 19 percent of the world's electricity production). About half of this capacity and generation is in Europe and North America with Europe the largest at 32 percent of total hydro use and North America at 23 percent of the total. However, this proportion is declining as Asia and Latin America commission large amounts of new hydro capacity. Small, mini and micro hydro plants (usually defined as plants less than 10 MW, 2 MW and 100kW, respectively) also play a key role in many countries for rural electrification. An estimated 300 million people in China, for example, depend on small hydro.

Geothermal Energy

Geothermal energy, the natural heat within the earth, arises from the ancient heat remaining in the Earth's core, from friction where continental plates slide beneath each other, and from the decay of radioactive elements that occur naturally in small amounts in all rocks. For thousands of years, people have benefited from hot springs and steam vents, using them for bathing, cooking, and heating. During this century, technological advances have made it possible and economic to locate and drill into hydrothermal reservoirs, pipe the steam or hot water to the surface, and use the heat directly (for space heating, aquaculture, and industrial processes) or to convert the heat into electricity.

Environmental Impacts

Geothermal fluids contain variable concentrations of gases, largely nitrogen and carbon dioxide with some hydrogen sulphide and smaller proportions of ammonia, mercury, radon and boron.Most of these chemicals are concentrated in the disposal water which is usually reinjected back into the drill holes so that there is minimal release into the environment. The concentrations of the gases are usually low enough not to be harmful or else the abatement of toxic gases can be managed with current technology.Carbon dioxide is the major component of the noncondensible gases in the steam, but its emission into the atmosphere per kWh is well below the figures for natural gas, oil, or coal-fired power plants. Hydrogen sulphide is the pollutant of most major concern in geothermal plants yet even the sulfur emitted with no controls is only half what is emitted from a coal-fired plant. Overall, with present technology able to control the environmental impact of geothermal energy development, it is considered to be a relatively benign source of energy.

Conclusions

Hydropower is a significant source of electricity worldwide and will likely continue to grow especially in the developing countries. While large dams have become much riskier investment there still remains much unexploited potential for small hydro projects around the world. It is expected that growth of hydroelectricity will continue but at a slower rate than that of the 70's and 80's. Thus, the fraction of hydroelectricity in the portfolio of primary sources of energy, which is today at 19 percent, is expected to decrease in the future. Improvements and efficiency

measures are needed in dam structures, turbines, generators, substations, transmission lines, and environmental mitigation technology if hydropower's role as a clean renewable energy source is to continue to be supported.

Geothermal as noted is not available everywhere especially with the resources required for the production of electrical energy on an industrial scale. Nonetheless, geothermal energy is generally cost competitive with conventional energy sources and is produced by well proven conventional technology. It is reliable and has been used for the more than half of the last century to heat large municipal districts, as well as to feed power plants generating hundreds of megawatts of electricity. It has strong potential to continue to expand, especially in the developing countries and is a clean energy source which can help contribute to reducing our greenhouse gas emissions. It is felt that in the near-term the future development of geothermal could help fulfill a bridging function during the next few decades as other more modern clean fuel technologies and renewable mature enough to provide a meaningful share of the world energy supply. In conclusion, we believe that the promise of renewable energy has now become a reality. Both solar photovoltaics and wind energy are experiencing rapid sales growth, declining capital costs and costs of electricity generated, and continued performance increases. Because of these developments, market opportunity exists now to both innovate and to take advantage of emerging markets, with the additional assistance of governmental and popular sentiment. The development and use of these sources can enhance diversity in energy supply markets, contribute to securing long term sustainable energy supplies make a contribution to the reduction of local and global atmospheric emissions provide commercially attractive options to meet specific needs for energy services particularly in developing countries and rural areas, and create new employment opportunities.

REFERENCES

[1]. Zinyowera, Moss (eds), Chapter 19, Cambridge University Press, Cambridge, 1996.

[2]. Johansson, T.B., Kelly, H., Reddy, A.K.N., and Williams, R.H. (editors) (1993) *Renewable Energy: Sources for Fuels and Electricity*

[3]. Kartha, Sivan and Eric D. Larson, Bioenergy Primer: Modernised Biomass Energy for sustainable development, United Nations Development Programme, Energy and Atmosphere Programme, New York, 2000

[4]. Margolis, R. and Kammen, D. M. (1999) "Underinvestment: The energy technology and R&D policy challenge", *Science*

[5]. U.S. Department of Energy (1997) *Renewable Energy Technology Characterizations*, Topical Report Prepared by U.S. DOE Office of Utility Technologies and EPRI, TR-109496, December

[6]. Maycock, P. (2000) "The World PV Market 2000: Shifting from Subsidy to 'Fully Economic'?" Renewable Energy World.

[7]. World Energy Assessment (WEA) (2000), *Energy and the Challenge of Sustainability*, Report Prepared by United Nations Development Programme, Chapter 5 and 7,United Nations Department of Economic and Social Affairs and World Energy Council, September

[8]. Worldwatch Institute (1999) *Vital Signs 1999: The Environmental Trends that are Shaping our Future*, (W.W. Norton & Co., London).

[9]. uke, R. D., and Kammen, D. M. (1999) "The Economics of Energy Market Transformation Initiatives", *The Energy Journal*.

[10]. Hall, D.O. and Scrase, J.I. (1998) "Will Biomass be the Environmentally Friendly Fuel of the Future?", *Biomass and Bioenergy*

Reliability Assessment of Power Generation System Using Seeker Optimization Algorithm

M.Lavanya and J.Krithika Jothi

Abstract: **Reliability evaluation of power system is essential in system planning and efficient operation. System states at various uncertainties such as equipment failures and variations of generation and load are determined to find the reliability indices. Power-generating system involves large number of system states and hence it is normally not feasible to enumerate all possible failure states to calculate the reliability indices. The most probable failure states contribute significantly to the adequacy indices. Existing sampling method called as Monte Carlo simulation is less efficient in selecting system failure states. Hence, some metaheuristics-based search algorithms, through their inherent convergence mechanisms, appear promising to find out the meaningful system states in a reasonable time. In this paper an attempt is made to evaluate system reliability indices using an advanced optimization technique called Seeker optimization algorithm.**

Keywords: **Reliability Assessment, Reliability Indices, Seeker Optimization Algorithm (SOA).**

I. INTRODUCTION

Reliability is a measure of the ability of a system to perform its designated functions under the conditions within which it was designed to operate. Power system reliability is a measure of the ability to deliver electricity to all points of utilization at acceptable standards and in the amount desired. Various adequacy indices are defined to evaluate the existence of sufficient facilities within the system to satisfy load demand as well as system operational constraints[1]. Adequacy assessment is an important component to ensure the proper operations of power systems. Power generation adequacy relates to the facilities necessary to generate sufficient energy in the presence of different system uncertainties. For most combinatorial optimization problems, as their dimension increases, the computational time needed by exact methods grows exponentially [2].

M.Lavanya is with [1]Department of Electrical and Electronics Engineering KPR Institute of Engineering and Technology Coimbatore, India, Email: lavanyaeee.31@gmail.com and J.Krithika Jothi is with Department of Electrical and Electronics Engineering Coimbatore Institute of Technology Coimbatore, India, Email: jkrithikajothi@gmail.com.

Metaheuristics are approximate methods for resolving these challenging problems, and they can be applied to derive an adequate solution in a reasonable amount of time[3]. In today's power-generating systems, the number of generating units has become very large. Inevitably, adequacy assessment of power systems becomes more challenging due to their larger scale and increasing complexity. Thus, in adequacy assessment, exhaustive enumeration is usually impractical due to an innumerable number of system states incurred.

To solve the problem, in this study Seeker Optimization Algorithm (SOA) is used to find out a set of probable failure states, which contribute most significantly to the entire system adequacy indices. SOA is based on the guided stochastic search inspired by human behaviour. Like genetic algorithm (GA).SOA is also a population based stochastic search algorithm. In this study, based on its optimization mechanism.SOA is used to scan and find out a set of most probable failure states which contribute considerably to system reliability indices.

Section 2 of the paper elucidates the adopted optimization algorithm. Section 3 provides the steps to find the system failure states using Seeker Optimization Algorithm.

II. SEEKER OPTIMIZATION ALGORITHM

Seeker Optimization algorithm is a human search capability and understandability based algorithm with greater convergence speed and search criteria. The number of control parameters to search global optima is decreased with SOA. The algorithm works on a population set where each member in the population is called as Seeker. Total population set is divided into K sub populations with equal number of seekers [4] to [6]. Seekers in the subpopulation search in different domains of search space to attain optimal solution.

SOA involves
(i) Computing Search Direction for each seeker.
(ii) Calculating Step Length for each seeker.

A. Computation of Search Direction

Search direction for each seeker is based on two main behaviors, Self and cognitive learning. Every seeker believes that he should achieve his best position from his experience. This is called as Egotistic behavior. Also every seeker in the subpopulation acts as neighbor for every other seeker and communicates with each other within neighborhood and neighbor subpopulation to attain global best position. (1-3).

Directions are computed as below.

$$d_i e(t) = \text{sign}(p_{ibest}(t) - x_i(t)) \quad (1)$$

$$d_i a1(t) = \text{sign}(g_{best}(t) - x_i(t)) \quad (2)$$

$$d_i a2(t) = \text{sign}(n_{best}(t) - x_i(t)) \quad (3)$$

In addition to above behaviors, each seeker acts in response to its past position. This is given by (4).

$$d_i p(t) = \text{sign}(x_i(t1) - x_i(t2)) \quad (4)$$

p_{ibest} is seekers personal best position, g_{best} is neighborhood best position of each seeker and n_{best} is neighbors best position in the subpopulation. Thus each seeker has its own four directions. Sign function gives a combination 1, 0,-1 set of directions for each seeker. The final search direction is computed based on the following rule.

Let

n_z = number of zeros for a seeker

n_p = number of positive ones for a seeker

n_n = number of negative ones for a seeker

with a randomly selected number (r),the search direction is computed as per the selection rule.

$$\text{search direction } d_{ij} = \begin{cases} 0 & \text{if } r_j \le p_j^{(0)} \\ +1 & \text{if } p_j^{(0)} \le r_j \le p_j^{(0)} + p_j^{(+1)} \\ -1 & \text{if } p_j^{(0)} + p_j^{(+1)} < r_j \le 1 \end{cases} \quad (5)$$

B. Computation of Step Length

One of the differentiating features of SOA from that of other algorithms is that fuzzy reasoning is applied to compute the step length. Step length decides how far a seeker has to move its position for the computed direction. Fuzzy system replicates the human reasoning for any specified applications. Sequence numbers are allotted for fitness values sorted in descending order to calculate μ_i value (equation 6).

$$\mu_i = \mu_{max} - \left(\frac{s - I_i}{s-1}\right)(\mu_{max} - \mu_{min}) \quad (6)$$

I_i is the sequence number representing the i_{th} seeker, S is the subpopulation number and μ_{max}, μ_{min} can take values of 0.95 and 0.0111 respectively.

Step length for each seeker is computed as per (7).

$$\text{step length, } \alpha_{ij} = \delta * \sqrt{-\ln(\mu_{ij})} \quad (7)$$

with

$\delta = \omega * \text{abs}(g_{best} - x_i)$, ω ranging from 0.9 to 0.1.

$\mu_{ij} = \text{rand}(\mu_i, 1)$.

Each seeker is updated to a new value based on search direction and step length as in (8).

$$x_{update} = x_i(t) + \alpha_{ij} * d_i \quad (8)$$

To avoid subpopulations trapping local optimal solution, the worst seeker from each subpopulation is replaced with the best from other to subpopulation. Binomial crossover method [7] is applied for avoiding the worst seeker to take part in consequent steps.

III. RELIABILITY EVALUATION OF GENERATION SYSTEM USING SOA

Adequacy analysis of power systems essentially consists of identification and evaluation of failure states, states in which the power system cannot satisfy customer demand and load shedding action is needed to maintain the system integrity. These most probable failure states contribute most significantly to the adequacy indices including loss of load expectation (LOLE), loss of load frequency (LOLF), and expected energy not supplied (EENS).

Monte Carlo simulation is currently the most common method used in states sampling, yet it suffers from three major drawbacks. The first one is the excessive simulation time. The second one is the lack of information about outage scenarios that can happen and the contribution of different system components to these outages. The third one is the difficulty to sample failure states when system reliability is very high which the case is in most practical systems.

The developed technique uses SOA as a search tool to find the most probable system failure states. These states are

stored in an array during the search operation, and then this array is convoluted discretely with hourly load values to find all the indices [8]. Every generation unit is assumed to have two states, up and down. It has its own forced outage rate (FOR), failure rate λ and repair rate μ. The probability of any unit down is equal to it's FOR. Each state i have its own probability PGi, contribution to system failure frequency FG_i, generation capacity Cap_i and total number of equivalent permutations $copy_i$.

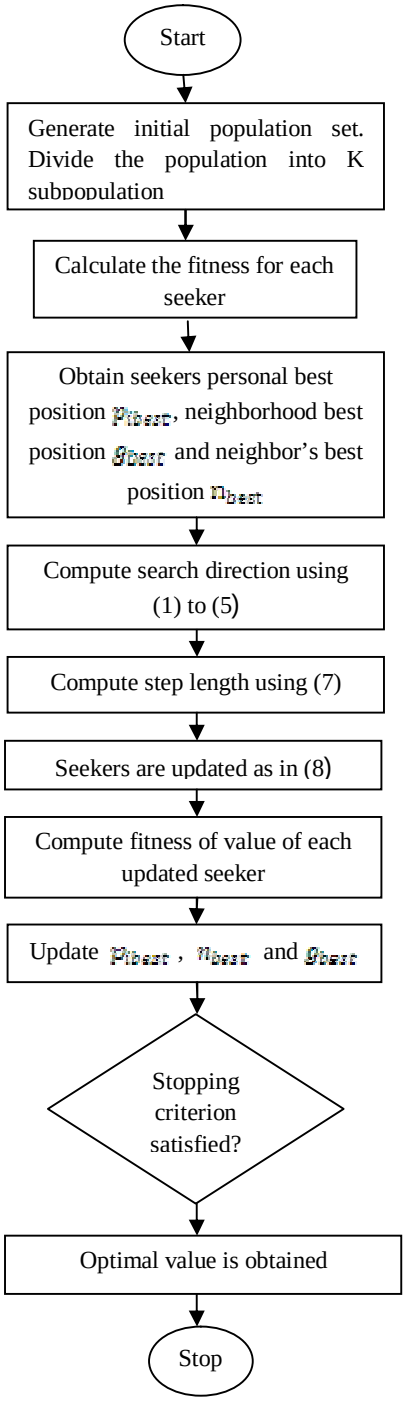

Figure 3.1 Flowchart for SOA implementation for reliability assessment

A. SOA algorithm structure for state array construction

Power generation system state array can be constructed as follows.

1. Generate a population of individuals randomly. The states of generators are initialized by binary numbers.
2. Evaluate each individual based on the defined objective function. If its value is less than the specified threshold (a small value below which the corresponding states are filtered out), it is assigned a very small fitness value in order to reduce its chance of participating in subsequent SOA operations.
3. Based on the attained state array, the overall system probability of load loss against the maximum load demand is calculated. The objective value of state is calculated as follows.

$$Cap_i = \sum_{j=1}^{n} b_j \, g_j \qquad (9)$$

where b_j is the value of the binary number representing generating unit j, and g_j is its generating capacity

1. (a) For failure state Calculate chromosome probability

$$P_i = \prod_{j=1}^{m} gp_j \qquad (10)$$

gp_j is generating unit state probability which can take one of the following values:

gp_j = 1-FORj if $b_j = 1$ or $gp_j = FOR_j$ if $b_j = 0$

(b) Calculate the number of all possible permutations $Copy_i$ of the evaluated state.

(c) The fitness of the chromosome can be calculated as

$$Fit_i = Copy_i * P_i \qquad (11)$$

(d) Update the probability of loss of load for max load

$$lolp(maxlaod)_{new} = lolp(maxload)_{old} + Fit_i$$

The steps are repeated for all units in the population.

a. Calculating Reliability Indices

The obtained state array is used to find the various reliability indices of the system. Consider the load value at hour j is LHj. Loss-of-load probability (LOLP) for this load value is calculated as follows.

$$LOLP = \sum_{i=1}^{n} S_i P_i copy_i \qquad (13)$$

After calculating LOLP for all load values, LOLE in hours per year is calculated

$$LOLE = \sum_{j=1}^{8760} LOLP \qquad (14)$$

Power not supplied (PNS) in megawatts is calculated for each hourly load value LH*i*, and consequently, expected energy not supplied in megawatts hour is calculated.

$$PNS = \sum_{j=1}^{n} S_j P_j copy_j \left(LH_j - Cap_i\right) \qquad (15)$$

$$EENS = \sum_{j=1}^{8760} PNS(LH_j) \qquad (16)$$

IV. RESULT

The proposed method has been tested on the IEEE RTS-79 [9]. The RTS-79 consists of 32 generating units with the smallest unit capacity of 12MW and the largest unit capacity of 400MW. The total installed capacity is 3405MW. Results obtained in comparison with those obtained by the other algorithms are given in Table I. The number of yearly hours used is 8736 and not 8760 as indicated in previous equations since the load data are given for only 364 days in the IEEE-RTS.

Table I: Comparison of reliability indices from various optimization algorithms

Adequacy indices	Monte Carlo simulation	Genetic Algorithm	SOA
EENS	1168	1163	1159
LOLE	9.355	9.324	9.299

The best values obtained from 100 trials with different population are tabulated in table II.

Table II: Best values of reliability indices obtained from 100 trials

No of seekers	LOLP (hrs/year)	EENS (MWh)
30	9.299	1159
60	9.294	1159
90	9.194	1158
120	9.194	1158

The iteration versus reliability indices graph is shown in figure 4.1 and figure 4.2

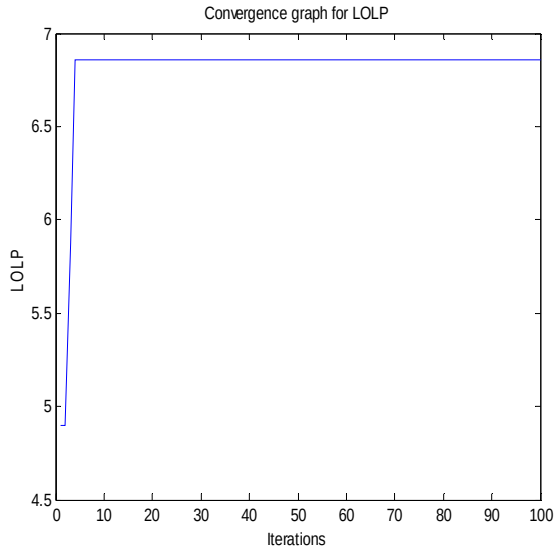

Figure 4.1 LOLP convergence for RTS with iteration count 100(60 seekers)

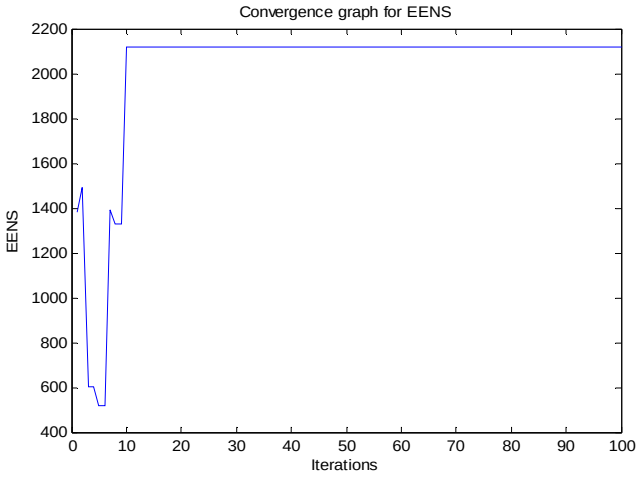

Figure 4.1 EENS convergence for RTS with iteration count 100(60 seekers)

Simulation result shows that the adopted SOA proves to be more efficient in finding the failure states than other propose algorithms.

V. CONCLUSION

The work presented illustrates a new method to calculate generation system adequacy indices. The proposed method is based on Seeker Optimization Algorithm that searches the state space to scan most probable failure states and stores them in a state array. The search process is guided through its fitness function. State array is also used to obtain useful information about the contribution of different states and generation unit combinations to the probability of system failure. SOA has shown to be effective in searching out eligible system states within a reasonable time. The

advantages of the proposed method are also evaluated with respect to other existing methods including the analytical method and Monte Carlo simulation.

REFERENCES

[1] R. Billinton and R. N. Allan. (1988) 'Reliability Assessment of Large Electric Power System', Kluwer Academic Publishers.

[2] R. Billinton and W. Li. (1994), 'Reliability Assessment of Electric Power Systems Using Monte Carlo Methods', New York: Plenum Press.

[3] N. Samaan and C. Singh. (Nov. 2002), 'Adequacy assessment of power system generation using a modified simple genetic algorithm', IEEE Trans. Power Syst,Vol. 17, pp. 974-981.

[4] B. Shaw, V.Mukherjee, S.P.Ghoshal.(2011) 'Seeker optimisation algorithm: application to the solution of economic load dispatch problems', IET Gener. Transm. Distrib, Vol. 5(1), pp. 81–91

[5] Chaohua Dai, Weirong Chen, Yunfang Zhu, and Xuexia Zhang.(August 2009), 'Seeker optimization algorithm for optimal Reactive Power Dispatch', IEEE Transactions on Power Systems, Vol. 24, No. 3.

[6] Chaohua Daia,,Weirong Chena, Yunfang Zhub, Xuexia Zhanga. (2009),' Reactive power dispatch considering voltage stability with seeker optimization algorithm', Elsevier.

[7] Daniela Zaharie, 'A Comparative Analysis of Crossover Variants in Differential Evolution' Proceedings of the International Multiconference on Computer Science and Information Technology , pp. 171–181

[8] Lingfeng Wang and Chanan Singh,(August 2008),'Population-Based Intelligent Search in Reliability Evaluation of Generation Systems With Wind Power Penetration', IEEE Transactions on Power systems, Vol. 23, No. 3..

[9] "IEEE committee report. IEEE reliability test system 1979, 'IEEE Trans Power App. Syst', Vol. PAS-98, No. 6, pp. 2047–2054.

Sensorless Approach for Speed Control of Induction Motor using MRAS

Shrinivas P. Ganjewar and Chandulal guguloth

ABSTRACT: This paper presents a model reference adaptive system-based sensorless induction motor drive. In this scheme, an adaptive pseudoreduced-order flux observer is used instead of the adaptive full-order flux observer. Simulation results show that proposed scheme can estimate the motor speed under various adaptive PI gains and estimated speed can replace to measured speed in sensorless induction motor drives.

Index Terms—adaptive speed estimation, Induction motor, Model reference adaptive control.

I. INTRODUCTION

Indirect field-oriented control (IFOC) method is widely used for IM drives. By providing decoupling of torque and flux control demands, the vector control can navigate an AC motor drive similar to a separately excited DC motor drive without sacrificing the quality of the dynamic performance. Within this scheme, a rotational transducer such as a tachogenerator, an encoder or a resolver, was often mounted on the IM shaft. However, a speed sensor cannot be mounted in some cases, such as motor drives in a hostile environment or high-speed motor drives. Also such sensors lower the system reliability and require special attention to noise. Therefore, sensorless induction motor (IM) drives are widely used in industry for their reliability and flexibility, particularly in hostile environment.

Various sensorless field-oriented control (FOC) methods for induction motor (IM) drives have been proposed using software instead of hardware speed sensor. Adaptive full-order flux observers (AFFO) for estimating the speed of IM were developed using Popov's and Lyapunov's stability criteria. While these schemes are not computationally intensive, an AFFO with a non-zero gain matrix may become unstable. The proportionality constant in the adaptive algorithm has to be adapted for different speeds. If the gain matrix of the AFFO is set to Zero, no adaptation is required. However, large speed errors may occur under heavy loads and steady-state disturbances affecting light loads. An adaptive pseudoreduced- order flux observer (APFO) for sensorless FOC was proposed in using the Lyapunov's method. The performance of the estimator using APFO was shown to be superior compared to that using AFFO scheme only at medium speed. Further, accuracy of speed estimation over the entire operating speed range strongly depends on this mechanical model and the IM torque estimation.

Shrinivas P. Ganjewar and Chandulal guguloth *are working in Electrical Engineering Dept. SKN Sinhgad College of Engineering Koti, Pandharpur, and Maharastra, Email:* chandu05210@gmail.com

In the MRAS-based technique for sensorless induction motor drives the rotor speed is estimated with an APFO and is used as the feedback signal for the FOC. The rotor flux is estimated through a closed-loop observer, thus eliminating the need for auxiliary variables related to the flux and need for the pure integration for flux calculations. As a result, the drive has a wider adjustable speed range and can be operated at zero and very low speeds.

II. MODEL REFERENCE ADAPTIVE SYSTEM (MRAS):

The model reference adaptive system (MRAS) is one of the major approaches for adaptive control and is one of many promising techniques employed in adaptive control. Among various types of adaptive system configuration, MRAS is important since it leads to relatively easy to- implement systems with high speed of adaptation for a wide range of applications. The basic scheme of the MRAS given in Fig. 1 is called a parallel configuration (output error method) MRAS in order to differentiate it from other MRAS configurations where the relative placement of the reference model and of the adjustable system is not the same. The MRAS scheme presented above are characterized by the fact that the reference model was disposed in parallel with the adjustable system. The series–parallel configuration (equation error method) is used in general for parameter identification. In this configuration, the reference model is partitioned into two parts: one in series with the adjustable system and one in parallel with the adjustable model. The series configuration is also used for identification and is often called the input error method. In this scheme the reference and adjustable models are located in series.

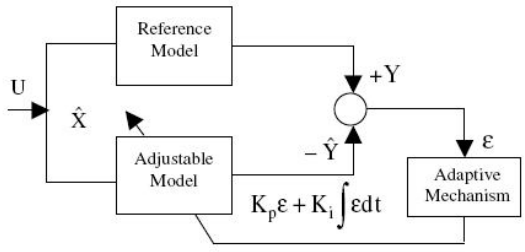

Fig. 1. Basic configuration of a parallel model reference adaptive system.

The use of parallel MRAS is determined by its excellent noise-rejection properties that allow obtaining unbiased parameter estimates, and in this scheme an error vector is derived using the difference between the outputs of two dynamic models, i.e. the reference and adjustable models, where only one of the models includes the estimated parameter as a system parameter, i.e. speed/resistance, and the inputs of two models are the same. The error vector, e, is

driven to zero through an adaptive law. As a result, the estimated parameter, X1 , will converge to its true value X. One of the most noted advantages of this type of adaptive system is its high speed of adaptation. This is due to the fact that a measurement of the difference between the outputs of the reference model and adjustable model is obtained directly by the comparison of the states (or outputs) of the reference model with those of the adjustable system. The block ''reference model'' represents demanded dynamics of actual control loop. The block ''adjustable model'' has the same structure as the reference one, but with adjustable parameters instead of the unknown ones.

The main drawbacks of this algorithm are its sensitivity to inaccuracies in the reference model, and difficulties of designing the adaptation mechanism block in MRAS. Selection of adaptive mechanism gains is a compromise between achieving a high speed of response and high robustness to noise and disturbances affecting the system. With the large PI gains for rotor speed identification in adaptive mechanism, K_p and K_i, the convergence speed for speed estimation is fast; however, high order harmonic components and noises are present in the estimated speed.

III. ADAPTIVE FLUX OBSERVER:

For an induction motor, if the stator current i_s and rotor flux Φ_r are selected as the state variables, the state equations can be expressed as (1) in the stationary reference Frame.

$$\frac{\mathrm{d}}{\mathrm{d}t}\begin{bmatrix} \boldsymbol{i}_s \\ \boldsymbol{\phi}_r \end{bmatrix} = \begin{bmatrix} \boldsymbol{A}_{11} & \boldsymbol{A}_{12} \\ \boldsymbol{A}_{21} & \boldsymbol{A}_{22} \end{bmatrix}\begin{bmatrix} \boldsymbol{i}_s \\ \boldsymbol{\phi}_r \end{bmatrix} + \begin{bmatrix} \boldsymbol{B}_1 \\ 0 \end{bmatrix}\boldsymbol{v}_s = \boldsymbol{A}\boldsymbol{x} + \boldsymbol{B}\boldsymbol{v}_s \quad (1)$$

$$\boldsymbol{i}_s = \boldsymbol{C}\boldsymbol{x} \quad (2)$$

where

$\boldsymbol{i}_s = [i_{ds}\ i_{qs}]^T$ is stator current

$\boldsymbol{\phi}_r = [\phi_{dr}\ \phi_{qr}]^T$ is rotor flux

$\boldsymbol{v}_s = [v_{ds}\ v_{qs}]^T$ is stator voltage

$\boldsymbol{x} = [\boldsymbol{i}_s\ \boldsymbol{\phi}_r]^T$

$\boldsymbol{A}_{11} = -\{R_1/(\sigma L_1) + (1-\sigma)/(\sigma\tau_r)\}\boldsymbol{I} = a_{r11}\boldsymbol{I}$

$\boldsymbol{A}_{12} = L_m/(\sigma L_1 L_2)\{(1/\tau_r)\boldsymbol{I} - \omega_r\boldsymbol{J}\} = a_{r12}\boldsymbol{I} + a_{i12}\boldsymbol{J}$

$\boldsymbol{A}_{21} = (L_m/\tau_r)\boldsymbol{I} = a_{r21}\boldsymbol{I}$

$\boldsymbol{A}_{22} = -(1/\tau_r)\boldsymbol{I} + \omega_r\boldsymbol{J}$

$\boldsymbol{B}_1 = 1/(\sigma L_1)\boldsymbol{I}, \boldsymbol{C} = [\boldsymbol{I}\ 0]$

$\sigma = 1 - L_m^2/L_1L_2$ is the inductance leakage coefficient,

$$\boldsymbol{I} = \begin{bmatrix} 1 & 0 \\ 0 & 1 \end{bmatrix} \text{ and } \boldsymbol{J} = \begin{bmatrix} 0 & -1 \\ 1 & 0 \end{bmatrix}$$

Where R_1, R_2 and L_1, L_2 are stator and rotor resistances and self-inductances, respectively, Lm is mutual inductance, T_r is the rotor time constant L_2/R_2 and ω_r is electrical motor angular speed.

The APFO flux observer can be written as follows

$$\frac{\mathrm{d}\hat{\boldsymbol{i}}_s}{\mathrm{d}t} = \hat{\boldsymbol{A}}_{11}\hat{\boldsymbol{i}}_s + \hat{\boldsymbol{A}}_{12}\hat{\boldsymbol{\phi}}_r + \boldsymbol{B}_1\boldsymbol{v}_s + \boldsymbol{G}(\hat{\boldsymbol{i}}_s - \boldsymbol{i}_s) \quad (3)$$

$$\frac{\mathrm{d}\hat{\boldsymbol{\phi}}_r}{\mathrm{d}t} = \hat{\boldsymbol{A}}_{22}\hat{\boldsymbol{\phi}}_r + \boldsymbol{A}_{21}\hat{\boldsymbol{i}}_s \quad (4)$$

here I_s and V_s are measured values of stator current vector and stator voltage vector, respectively, G is the reduced-order observer gain matrix which is also determined to make (3) stable and ^ denotes the estimated values. The observer is a closed-loop system, which is obtained by driving the estimated model of the induction motor by the residual of the current measurement, e_{is}.

$$\boldsymbol{e}_{is} = \boldsymbol{i}_s - \hat{\boldsymbol{i}}_s$$

The estimation of stator currents is conducted by a closed-loop observer with a[2 × 2] feedback gain matrix G, as in (3), whereas the estimation of rotor fluxes is carried out by an open-loop observer of (4) without the flux error. Therefore, the real and estimated rotor fluxes are assumed the same.

$$\boldsymbol{\phi}_r = \hat{\boldsymbol{\phi}}_r$$

The observer gain matrix is chosen as:

$$\boldsymbol{G} = \begin{bmatrix} g_1 & g_2 \\ -g_2 & g_1 \end{bmatrix}^T \quad (5)$$

Where the observer gain matrix G is calculated based on the pole placement technique. The selection of the observer poles is a compromise between the rapidity of error responses and the sensitivity to disturbances and measurement noises. In practice, the eigenvalues of the observer are selected to be negative, so that the state of The observer will converge to the state of the observed system, and they are chosen to be somewhat more negative than the eigenvalues of the observed system so that convergence is faster than other system effects. Based on the above mentioned criteria

Let we chose,

$$\begin{aligned} g_1 &= (k-1)a_{r11} \\ g_2 &= k_p,\ k_p \geq 1 \end{aligned} \quad (6)$$

Where g_1 is proportional to the IM parameters, g_2 is an arbitrary gain, k is an arbitrary positive constant value, and k_p is an arbitrary value ($k_p \geq -1$).

IV. Adaptive scheme for speed estimation:

The error equation of state variables can be driven from (1) and (3) as follows:

$$\frac{\mathrm{d}\boldsymbol{e}_{is}}{\mathrm{d}t} = (\boldsymbol{A}_{11} + \boldsymbol{G})\boldsymbol{e}_{is} + \Delta\boldsymbol{A}_1\hat{\boldsymbol{i}}_s + \Delta\boldsymbol{A}_2\hat{\boldsymbol{\phi}}_r = (\boldsymbol{A}_{11} + \boldsymbol{G})\boldsymbol{e}_{is} - \boldsymbol{W} \quad (7)$$

$$\boldsymbol{W} = -\Delta\boldsymbol{A}_1\hat{\boldsymbol{i}}_s - \Delta\boldsymbol{A}_2\hat{\boldsymbol{\phi}}_r \quad (8)$$

Where W is the nonlinear block and is defined as:

W

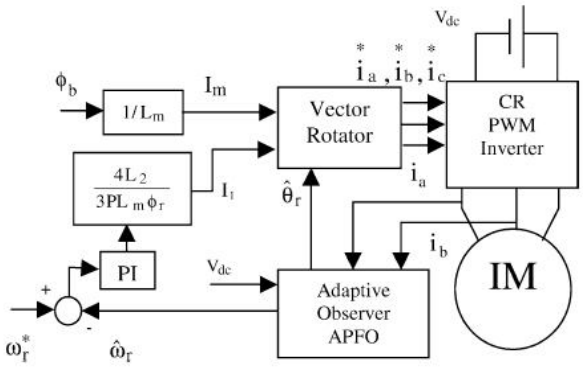

Fig. 3. Block diagram of sensorless IM drive.

The error matrices ΔA_1, and ΔA_2 are represented by:

Where $\Delta\omega_r$ is the estimated speed error, and ΔR_1 is the estimated error of stator resistance. Using (7), a MRAS representation of the system is shown in Fig. 2, which is constructed from a linear time-variant forward path transfer

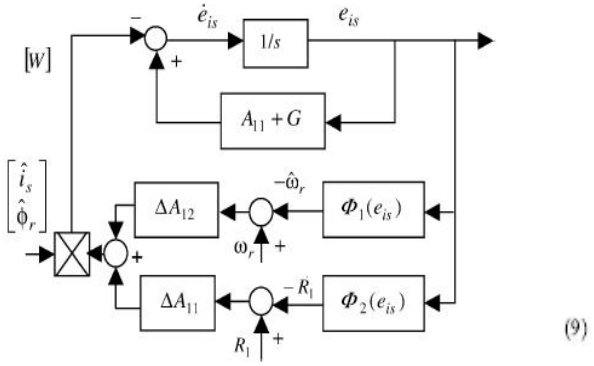

(9)

Fig. 2. MRAS representation for identifying the speed and stator resistance.

matrix and a nonlinear feedback block. $\Phi_1(e_{is})$ And $\Phi_2(e_{is})$ are the identifying mechanisms for the motor speed and stator resistance estimators, respectively. The system is hyper stable, if the forward path transfer matrix is strictly positive real and the input and output of the nonlinear feedback block satisfies Popov's integral inequality of (9).

In this section we discuss the case where the primary resistance and rotor speed are set incorrectly. In such a case, the Popov's integral inequality as follows:

Where $\rho = L_m/\sigma L_1 L_2$ and γ^2 is a finite positive constant, which is independent of t_0.

It is verified that the Popov's inequality of (9) is satisfied if the estimate of the resistance is chosen to be a linear function of an inner product of the current estimate and the estimation error and the estimate of the rotor speed is chosen to be a linear function of an inner product of the flux estimate and the stator current estimation error. Stating in the form of a theorem we get:

V. SIMULATION RESULTS:

The basic configuration of speed estimation of sensorless induction motor drive is shown in Fig. 3. This configuration will be used for both simulation and experimentation. All reference or command preset values are superscripted with a ''*'' in the diagram. IM speed will be estimated by (11) and will be compared with the set point in order to create speed error. The error between the estimated and command values of speed drives the speed PI controller

$$\Delta A_1 = A_{11} - \hat{A}_{11} = -\Delta A_{11}\Delta R_1 = \frac{\Delta R_1}{\sigma L_1} I$$

$$\Delta A_2 = A_{12} - \hat{A}_{12} = \Delta A_{12}\Delta\omega_r = -\frac{L_m}{\sigma L_1 L_2} J\Delta\omega_r$$

which in turn generates the required command value for the torque current component (I_t).

The current controlled voltage source inverter with field orientation control provides a fast time response and a smoother inverter current output. Although many current control algorithms have been proposed in recent years, hysteresis band current control is still a preferred method. It presents a simple and fast control as well as flexibility in maintaining the stator current in a predetermined specified. This algorithm is especially suitable for implementing the field orientation control. Hysteresis band current control can rapidly follow any dynamical current demand change in a shorter time span than any other control method. As a result, this control algorithm offers a higher quality dynamical torque control. Estimated rotor speed $\hat{\omega}_r$ and estimated rotor flux angle $\hat{\theta}_r$ are achieved by the MRAS-based pseudoreduced- order flux observer. I_m And I_t are the magnetizing and torque components of the stator current, respectively. These components are the equivalent dc values in the synchronously rotating reference frame. By the application of inverse Clarke and Park transformations in ''Vector Rotator'' block, the command values i^*_a, i^*_b, and i^*_c can be obtained. These real time values will be compared with the measured or sensed currents i_a, i_b, and i_c to generate proper pulsing sequence in order to fire the IGBT switching devices of the inverter.

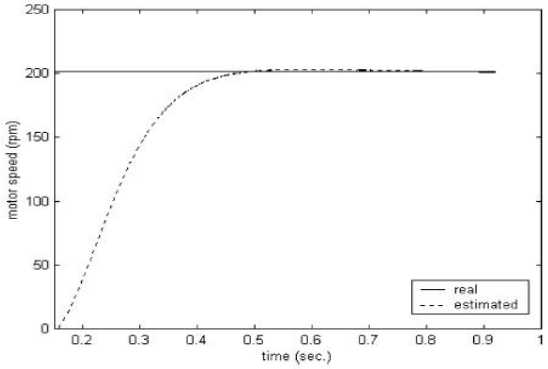

Fig. 4. Behaviour of speed estimation at $K_{p3} = 4$, $K_{i3} = 150$.

Figs. 4and 5 show the behavior of IM speed estimation under various values of adaptive scheme PI gains. These figures show that with the large PI gains for the adaptive scheme, Kp3 and Ki3, the convergence for the speed estimation is fast, however, a lot of high order harmonics are present in the estimated speed. In Fig. 4 where the IM rotates at a constant speed (200 rpm) under no load condition and initial value of the estimated speed is zero, the estimated

speed reaches the real one in less than 0.35 s. With larger PI gains the convergence time reduces to 0.25 s as in Fig. 5.

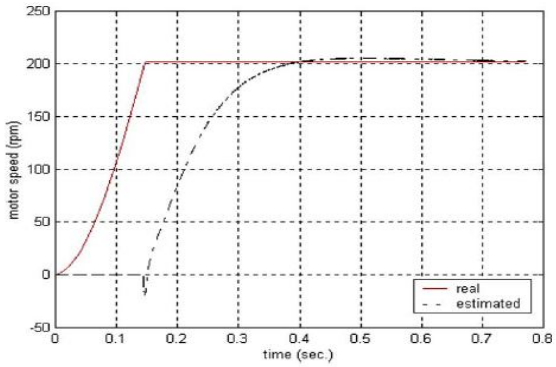

Fig. 5. Behaviour of speed estimation at $K_{p3} = 5$, $K_{i3} = 250$.

VI. CONCLUSION:

This paper presents a MRAS-based APFO sensorless induction motor drive. This method has been applied to a direct field-oriented induction motor control with and without speed sensors. The simulation results demonstrated that with larger PI gains for the adaptive PI regulators, the convergence for the speed estimation is fast, however, higher order harmonics and noises are included in the estimated speed. The validity of the MRAS-based pseudoreduced-order flux observer has been verified by simulation.

REFERENCES:

[1]. G. Yang, T.H. Chin, "*Adaptive-speed identification scheme for a vector-controlled Speed Sensorless inverter-induction motor drive*", IEEE Trans. Ind. Appl. 29 (4) (1993) 820–825. Fig. 12. Sensorless IM drive, (a) measured speed, (b) estimated Speed. H.M. Kojabadi / Simulation Modelling Practice and Theory 13 (2005) 451–464 463

[2]. H. Madadi Kojabadi, "*Simulation and Experimental studies of model reference Adaptive system for sensorless induction motor drive*", Simulation modeling practice And Theory 13 (2005) 451- 464.

[3]. C. Schauder, "*Adaptive speed identification for vector control of induction motors Without rotational transducers*", IEEE Trans. Ind. Appl. 28 (5) (1992) 1054–1061.

[4]. I.D. Landau, "*Elimination of the real positivity condition in the design of parallel MRAS*", IEEE Trans. Automat. Contr. 23 (6) (1978) 1015–1020.

[5]. H.M. Kojabadi, L. Chang, "*Model reference adaptive system pseudoreduced-order Flux observer for very low speed and zero speed estimation in sensorless induction Motor drives*", in: IEEE Annual Power Electronics Specialists Conference, Australia, vol. 1, 2002, pp. 301–308.

[6]. J. Maes, J.A. Melkebeek, "*Speed—sensorless direct torque control of induction motor Using an adaptive flux observer*", IEEE Trans. Ind. Appl. 36 (3) (2000) 778–785.

[7]. Y.N. Lin, C.L. Chen, "*Adaptive pseudoreduced-order flux observer for speed Sensorless field oriented control of IM*", IEEE Trans. Ind. Electron. 46 (5) (1999) 1042–1045.

Auther's Profile

Mr. Shrinivas P Ganjewar received his M.E degree from Govt.College of Engg. Aurangabad, Maharastra. Presently he is working as an Asst.Prof & Head in Electrical Engineering Dept. SKN Sinhgad College of Engineering Koti, Pandharpur, and Maharastra.

Mr.Chandulal Guguloth received his M.Tech degree from National Institute of Technology Karnataka (NITK). Presently he is working as an Asst.Prof in Electrical Engineering Dept. SKN Sinhgad College of Engineering Koti, Pandharpur, and Maharastra.

Simulation of New Multilevel Inverter Topology

A Mallikarjuna Prasad, S Thirumalaiah, U chaithanya and P Nagarjuna

Abstract:-**Multilevel inverters have been widely accepted for high-power high-voltage applications. In this paper, a new topology with a reversing-voltage component is proposed to improve the multilevel performance by compensating the disadvantages of increased number of components, complex pulse width modulation control method, and voltage-balancing problem. This topology requires fewer components compared to existing inverters (particularly in higher levels) and requires fewer carrier signals and gate drives. There-fore, the overall cost and complexity are greatly reduced particularly for higher output voltage levels. Finally, a simulation result of the seven-level proposed topology is observed.**

Keywords: **Multilevel inverter, power electronics, SPWM, topology.**

I. INTRODUCTION

Multilevel power conversion was first introduced more than two decades ago. The general concept involves utilizing a higher number of active semiconductor switches to perform the power conversion in small voltage steps. There are several advantages to this approach when compared with the conventional power conversion approach. The smaller voltage steps lead to the production of higher power quality waveforms and also reduce voltage (dv/dt) stress on the load and the electromagnetic compatibility concerns. Another important feature of multilevel converters is that the semiconductors are wired in a series-type connection, which allows operation at higher voltages. One clear disadvantage of multilevel power conversion is the higher number of semiconductor switches required. It should be pointed out that lower voltage rated switches can be used in the multilevel converter and, therefore, the active semiconductor cost is not appreciably increased when compared with the two - level cases. Another disadvantage of multi-level power converters is that the small voltage steps are typically produced by isolated voltage sources or a bank of series capacitors. To some extent, the voltage balancing can be addressed by using redundant switching states, which exist due to the high number of semiconductor devices. However, for a complete solution to the voltage-balancing problem, another multilevel converter may be required In recent years, there has been a substantial increase in interest to multilevel power conversion.

A Mallikarjuna Prasad and S Thirumalaiah are working as Associate Professor, SJCET, Yemmiganur, Kurnool, India, **U chaithanya** is working as [3]Assistant Professor, SJCET, Yemmiganur, Kurnool, India and **P. Nagarjuna** is a PG scholar, SJCET, Yemmiganur, Kurnool, India, Email: Mallikarjunaprasad0307@gmail.com

Recent research has involved the introduction of novel converter topologies and unique modulation strategies. However, the most recently used inverter topologies, which are mainly addressed as applicable multilevel inverters, are cascade converter, neutral-point-clamped (NPC) inverter, and flying capacitor inverter. There are also some combinations of the mentioned topologies as series combination of a two-level converter with a three-level NPC converter which is named cascade 3/2 multilevel inverter. There is also a series combination of a three-level cascade converter with a five-level NPC converter which is named cascade 5/3 multilevel inverter Some new approaches have been recently suggested such as the topology utilizing low-switching-frequency high-power devices Although the topology has some modification to reduce output voltage distortion, the general disadvantage of this method is that it has significant low-order current harmonics. It is also unable to exactly manipulate the magnitude of output voltage due to an adopted pulse-width modulation (PWM) method

In multilevel output is generated with a multi-winding transformer. However, the design and manufacturing of a multi-winding transformer are difficult and costly for high-power applications. A novel four-level inverter topology is also proposed, and it is valid for inverters with even number of voltage levels and not capable of outputting a zero-voltage state. As a result, the inverter output phase voltage for zero modulation indexes is a bipolar waveform taking two distinct values and exhibits high rms value and considerable harmonic energy concentrated at the switching frequency. This is a disadvantage of the proposed inverter, particularly when it should output low or zero voltage to a load. This paper presents an overview of a new multilevel inverter topology named reversing voltage (RV). This topology requires less number of components compared to conventional topologies. It is also more efficient since the inverter has a component which operates the switching power devices at line frequency. Therefore, there is no need for all switches to work in high frequency which leads to simpler and more reliable control of the inverter.

This paper describes the general multilevel inverter schematic. A general method of multilevel modulation phase disposition (PD) SPWM is utilized to drive the inverter and can be extended to any number of voltage levels. The simulation results of the proposed topology are also presented.

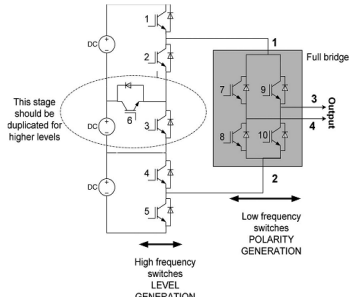

Fig.1. Schematic of a seven-level inverter in single phase.

II. NEW MULTILEVEL TOPOLOGY

A. *General Description*

In conventional multilevel inverters, the power semiconductor switches are combined to produce a high-frequency wave- form in positive and negative polarities. However, there is no need to utilize all the switches for generating bipolar levels. This topology is a hybrid multilevel topology which separates the output voltage into two parts. One part is named level generation part and is responsible for level generating in positive polarity. This part requires high-frequency switches to generate the required levels. The switches in this part should have high-switching-frequency capability. The other part is called polarity generation part and is responsible for generating the polarity of the output voltage, which is the low-frequency part operating at line frequency.

The topology combines the two parts (high frequency and low frequency) to generate the multilevel voltage output. In order to generate a complete multilevel output, the positive levels are generated by the high-frequency part (level generation), and then, this part is fed to a full-bridge inverter (polarity generation), which will generate the required polarity for the output. This will eliminate many of the semiconductor switches which were responsible to generate the output voltage levels in positive and negative polarities. The RV topology in seven levels is shown in Fig. 1. As can be seen, it requires ten switches and three isolated sources. The principal idea of this topology as a multilevel inverter is that the left stage in Fig. 1 generates the required output levels (without polarity) and the right circuit (full-bridge converter) decides about the polarity of the output voltage. This part, which is named polarity generation, transfers the required output level to the output with the same direction or opposite direction according to the required output polarity. It reverses the voltage direction when the voltage polarity requires to be changed for negative polarity.

This topology easily extends to higher voltage levels by duplicating the middle stage as shown in Fig. 1. Therefore, this topology is modular and can be easily increased to higher voltage levels by adding the middle stage in Fig 1. It can also be applied for three-phase applications with the same principle. This topology uses isolated dc supplies. Therefore, it does not face voltage-balancing problems due to fixed dc voltage values. In comparison with a cascade topology, it requires just one-third of isolated power supplies used in a cascade-type inverter.

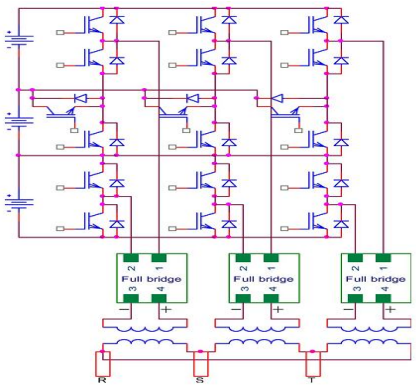

Fig. 2. Three-phase RV multilevel topology.

In Fig 2, the complete three-phase inverter for seven levels is shown with a three-phase delta-connected system. According to Fig. 2, the multilevel positive voltage is fed to the full-bridge converter to generate its polarity. Then, each full-bridge converter will drive the primary of a transformer. The secondary of the transformer is delta (Δ) connected and can be connected to a three-phase system. This topology requires fewer components in comparison to conventional inverters. Another advantage of the topology is that it just requires half of the conventional carriers for SPWM controller. SPWM for seven-level conventional converters consists of six carriers, but in this topology, three carriers are sufficient. The reason is that, according to Fig. 1, the multilevel converter works only in positive polarity and does not generate negative polarities. Therefore, it implements the multilevel inverter with a reduced number of carriers, which is a great achievement for inverter control. It is also comparable to single-carrier modulation while this topology requires the same number of signals for PWM. However, this topology needs one modulation signal which is easier to generate as opposed to the single-carrier modulation method which needs several modulation signals another disadvantage of this topology is that all switches should be selected from fast switches, while the proposed topology does not need fast switches for the polarity generation part.

TABLE I
SWITCHING SEQUENCE FOR EACH LEVEL

Level / Mode	0	1	2	3
1	2,3,4	2,3,5	1,4	1,5
2		2,4,6	2,6,5	

B. *Switching Sequences*

Switching sequences in this converter are easier than its counter parts. According to its inherent advantages, it does not need to generate negative pulses for negative cycle control. Thus, there is no need for extra conditions for controlling the negative voltage. Instead, the reversing full-bridge converter performs this task, and the required level is produced by the high-switching-frequency component of the inverter. Then, this level is translated to negative or positive according to output voltage requirements. This topology is redundant and flexible in the switching sequence. Different switching modes in generating the required levels for a seven-level RV inverter are shown in Table I. In Table I, the numbers show the switch according to Fig. 1 which should be turned on to generate the required voltage level. According to the table, there are six possible switching patterns to control the inverter. It shows the great redundancy of the topology. However, as the dc sources are externally adjustable sources (dc power supplies), there is no need for voltage balancing for this work.

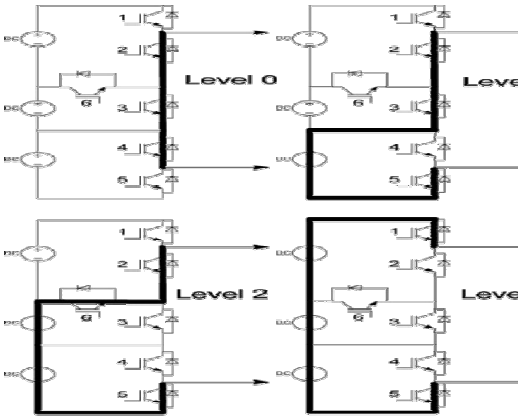

Fig.3.Switching sequences for different level generation.

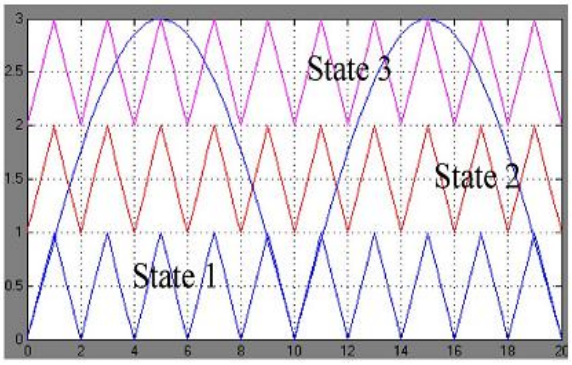

Fig. 4. SPWM carrier and modulator for RV topology

In order to avoid unwanted voltage levels during switching cycles, the switching modes should be selected so that the switching transitions become minimal during each mode transfer. This will also help to decrease switching power dissipation. According to the aforementioned suggestions, the sequences of switches (2–3-4), (2-3-5), (2-6-5), and (1, 5) are chosen for levels 0 up to 3, respectively. These sequences are shown in Fig. 3. As can be observed from Fig. 3, the output voltage levels are generated in this part by appropriate switching sequences. The ultimate output voltage level is the sum of voltage sources, which are included in the current path that is marked in bold. In order to produce seven levels by SPWM, three saw-tooth waveforms for carrier and a sinusoidal reference signal for modulator are required as shown in Fig. 4. In this paper, PD SPWM is adopted for their simplicity. Carriers in this method do not have any coincidence, and they have definite offset from each other. They are also in phase with each other. The modulator and three carriers for SPWM are shown in Fig.4.

TABLE II
SWITCHING CASES IN EACH STATE ACCORDING TO RELATED COMPARATOR OUTPUT

States	One		two		Three	
Compare	+	-	+	-	+	-
Mode	2-3-5	2-3-4	2-5-6	2-3-5	1-5	2-5-6

According to Fig. 4, three states are considered. The first state is when the modulator signal is within the lowest carrier. The second state is when it is within the middle carrier. Finally, the third one is when it is within the highest carrier. In each state, certain switching patterns are adopted to cover the voltage requirements. According to this definition, the switching states and switching modes are described in Table II.

Table II shows the relation between the right comparator output according to the current state and required states for switching to meet the voltage requirements. The right comparator here refers to the comparator output of the current state. As illustrated in Table II, the transition between modes in each state requires minimum commutation of switches to improve the efficiency of the inverter during switching states.

The number of switches in the path of conducting current also plays an important role in the efficiency of overall converter. For example, a seven-level cascade topology has 12 switches, and half of them, i.e., six switches, conduct the inverter current in each instance. However, the number of switches which conduct current in the proposed topology ranges from four switches (for generating level 3) to five switches conducting for other levels, while two of the switches are from the low-frequency (polarity generation) component of the inverter.

Therefore, the number of switches in the proposed topology that conduct the circuit current is lower than that of the cascade inverter, and hence, it has a better efficiency.

The same calculation is true in a topology mentioned in the least number of switches in the current path for a seven-level inverter according to its firing (for generating level 3), which requires one switch more in the current path compared to the proposed topology which requires only four conducting switches.

The signal stage should be isolated from the power stage by opto couplers for control circuit protection. The drive circuit is also responsible to generate the dead time between each successive switching cycle across the dc source.

The gating signal for the output stage, which changes the polarity of the voltage, is simple. Low-frequency output stage is an H-bridge inverter and works in two modes: forward and reverse modes. In the forward mode, switches 8 and 9 as in Fig. 1 conduct, and the output voltage polarity is positive.

However, switches 7 and 10 conduct in reverse mode, which will lead to negative voltage polarity in the output. Thus, the low-frequency polarity generation stage only determines the output polarity and is synchronous with the line frequency. The resulting PWM waveforms for driving the high-frequency switches in the level generation part are illustrated for one complete cycle in Fig. 5. According to Fig. 5, high- frequency switches can be adopted in this stage based on the required frequency and voltage level. However, low-frequency polarity generation part drive signals are generated with the line frequency (50 Hz), and they only change at zero-voltage crossings.

C. Number of Components

As mentioned earlier, one of the promising advantages of the topology is that it requires less high-switching-frequency components. High-frequency switches and diodes are expensive and are more prone to be damaged than low-frequency switches, the reliability of a system is indirectly proportional to the number of its components. Therefore, as the number of high-frequency switches is increased, the reliability of the converter is decreased.

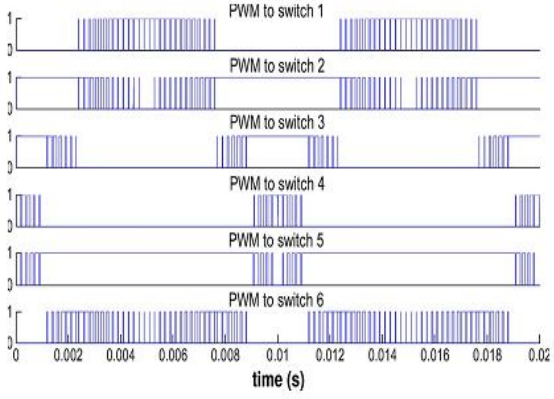

Fig. 5. Complete gate signals for level generation part.

TABLE III
NUMBER OF COMPONENTS FOR THREE-PHASE INVERTERS

Inverter type	NPC	Flying capacitor	Cascade	RV
Main switches	6(N-1)	6(N-1)	6(N-1)	3((N-1)+4)
main diodes	6(N-1)	6(N-1)	6(N-1)	3((N-1)+4)
Clamping diodes	3(N-1)(N-2)	0	0	0
DC bus capacitors/ Isolated supplies	(N-1)	(N-1)	3(N-1)/2	(N-1)/2
Flying capacitors	0	$\frac{3}{2}$(N-1)(N-2)	0	0
Total numbers	(N-1)(3N+7)	$\frac{1}{2}$(N-1)(3N+20)	$\frac{27}{2}$(N-1)	(13N+35)/2

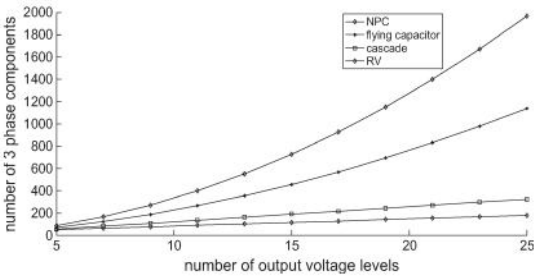

Fig. 6. Components for multilevel inverters.

The proposed converter, as can be seen, half of the switches in the full-bridge converter will not require to be switched on rapidly since they are only switched at zero crossings operating at line frequency (50 Hz). Thus, in this case, the reliability of the converter and also related expenses are highly improved. The number of required three-phase components according to output voltage levels (N) is illustrated in Table III

It can clearly be inferred that the number of components of the proposed topology is lower than that of other topologies even more so as the voltage levels increase and it will decrease tremendously with higher voltage levels. Fig. 6 shows the required components versus different volt- age levels as mentioned in Table III. As the most important part in multilevel inverters is the power semiconductor switches which define the reliability and control complexity, the number of required switches against the required voltage levels is shown in Fig. 7 for the new topology as well as other topologies.

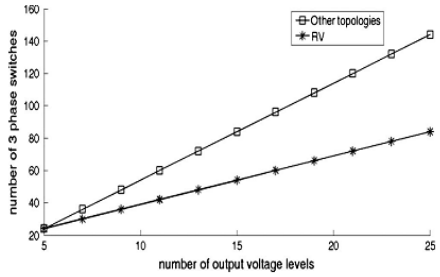

Fig.7. Required switches for multilevel inverter.

According to Figs. 6 and 7, the new topology requires fewer components and also fewer switches compared to others. Therefore, it should have the potential of finding widespread applications in high-voltage power devices and apparatus that includes FACTS and HVDC. It also requires less number of components as to conventional inverters that use phase shift transformers for increasing the output voltage levels. STATCOM, which is a type of FACTS apparatus and has been widely developed in recent years, can be a good candidate for applying the topology. In order to fulfill the stringent voltage harmonic standard such as IEEE519, a STATCOM of the conventional 48-pulse inverter is normally used .The topology requires eight three-phase transformers and eight full-bridge inverters requiring 48 switches. However, the proposed topology is superior compared to this conventional topology since it requires 84 switches for implementing similar output voltage waveform with the same quality while omitting eight bulky transformers.

III. SIMULATION RESULTS

The topology is used to generate seven voltage levels for a resistive and inductive load. The output voltage is 300 VP−P. The switching frequency is 4 kHz. According to the PD-SPWM method as mentioned. The control signals are unipolar. In the proposed multilevel inverter, and the unipolar modulation presents better results in terms of harmonics

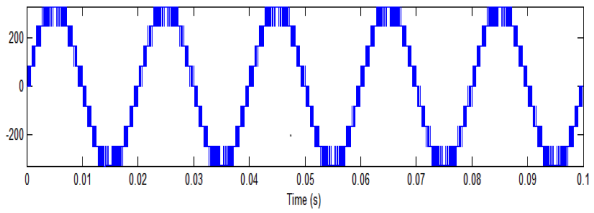

Fig. 9 shows how the ouptut voltage is made in the polarity generation part.

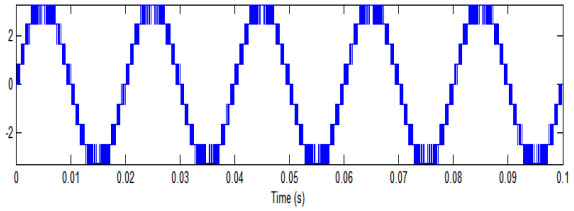

Fig. 10. Shows how the output current is made in the polarity generation part.

In Fig. 9, the voltage output of the level generating part and output of the polarity generation part are shown. According to Fig. 9, the voltage, which is generated by the high-frequency level generating component, is fed to the polarity generating component to define its polarity. The complete output waveform is then created, resulting in the production of the desired voltage waveform of the multilevel inverter as shown in Fig. 9. The waveform of the proposed multilevel inverter with an output filter and a resistive load of 124 Ω is shown in Fig. 10. The resulting current THD was 3.85%, which complies with the IEEE 519 harmonic standard. Figs. 9 and 10 clearly show the performance of the proposed inverter for resistive and inductive loads. Therefore, this pro-posed topology is proven to work with different kinds of loads as shown in Figs. 9and 10. The output waveform with an inductive load of 182 mH, which is equal to 115 Ω, is also shown in Fig. 10. The resulting THD for current was 2.3%, which is in compliance with the IEEE 519 harmonic standard.

IV. CONCLUSION

A new inverter topology has been proposed which has superior features over conventional topologies in terms of the required power switches and isolated dc supplies, control requirements, cost, and reliability. This topology can be a good candidate for converters used in power applications such as FACTS, HVDC, PV systems, UPS, etc., the switching operation is separated into high- and low-frequency parts. This will add up to the efficiency of the converter as well as reducing the size and cost. The PD-SPWM control method is used to drive the inverter. The PWM for this topology has fewer complexities since it only generates positive carriers for PWM control. The results clearly show that the proposed topology can effectively work as a multilevel inverter with a reduced number of carriers for PWM.

ACKNOWLEDGMENT

The authors would like to thank the **Mr.B.Gururaj**, Assistant professor for helping us to assist this paper successfully.

REFERENCES

[1]. K. Nakata, K. Nakamura, S. Ito, and K. Jinbo, “A three-level traction inverter with IGBTs for EMU,” in Conf. Rec. IEEE IAS Annu. Meeting, 1994, vol. 1, pp. 667–672.

[2]. N. Seki and H. Uchino, “Converter configurations and switching frequency for a GTO reactive power compensator,” IEEE Trans. Ind. Appl., vol. 33, no. 4, pp. 1011–1018, Jul./Aug. 1997

[3]. L. M. Tolbert, F. Z. Peng, and T. G. Habetler, “Multilevel converters for large electric drives,” IEEE Trans. Ind. Appl., vol. 35, no. 1, pp. 36–44, Jan./Feb. 1999. [4] R. H. Osman, “A medium-voltage drive utilizing series-cell multilevel topology for outstanding power quality,” in Conf. Rec. 34th IEEE IAS Annu. Meeting, 1999, vol. 4, pp. 2662–2669.

[4]. T. L. Skvarenina, The Power Electronics Handbook. Boca Raton, FL: CRC Press, 2002. [15] R. Teodorescu, F. Blaabjerg, J. K. Pedersen, E. Cengelci, and P. N. Enjeti, “Multilevel

inverter by cascading industrial VSI," IEEE Trans. Ind. Electron., vol. 49, no. 4, pp. 832–838, Aug. 2002.
[5]. P. Barbosa, P. Steimer, J. Steinke, L. Meysenc, M. Winkelnkemper, and N. Celanovic, "Active neutral-point-clamped multilevel converters," in Proc. IEEE 36th Power Electron Spec. Conf., 2005, pp. 2296–2301.
[6]. G. M. Martins, J. A. Pomilio, S. Buso, and G. Spiazzi, "Three-phase low- frequency commutation inverter for renewable energy systems," IEEE Trans. Ind. Electron., vol. 53, no. 5, pp. 1522–1528, Oct. 2006.
[7]. G. Ceglia, V. Guzman, C. Sanchez, F. Ibanez, J. Walter, and M. I. Gimenez, "A new simplified multilevel inverter topology for dc-ac conversion," IEEE Trans. Power Electron., vol. 21, no. 5, pp. 1311–1319, Sep. 2006.
[8]. D. A. B. Zambra, C. Rech, and J. R. Pinheiro, "A comparative analysis between the symmetric and the hybrid asymmetric nine-level series connected H-bridge cells inverter," in Proc. Eur. Conf. Power Electron. Appl., 2007, pp. 1–10.
[9]. G. S. Perantzakis, F. H. Xepapas, and S. N. Manias, "A novel four-level voltage source inverter-influence of switching strategies on the distribution of power losses," IEEE Trans. Power Electron., vol. 22, no. 1, pp. 149–159, Jan. 2007.
[10]. .G. Mondal, K. Gopakumar, P. N. Tekwani, and E. Levi, "A reduced switch-count five-level inverter with common-mode voltage elimination for an open-end winding induction motor drive," IEEE Trans. Ind. Electron., vol. 54, no. 4, pp. 2344–2351, Aug. 2007.
[11]. K. Jang-Hwan, S.-K. Sul, and P. N. Enjeti, "A carrier-based PWM method with optimal switching sequence for a multilevel four-leg voltagesource inverter," IEEE Trans. Ind. Appl., vol. 44, no. 4, pp. 1239–1248, Jul./Aug. 2008.
[12]. S. Daher, J. Schmid, and F. L.M. Antunes, "Multilevel inverter topologies for stand-alone PV systems," IEEE Trans. Ind. Electron., vol. 55, no. 7, pp. 2703–2712, Jul. 2008.
[13]. G. Shahgholiyan, E. Haghjou, and S. Abazari, "Improving the mitigation of voltage flicker by usage of fuzzy control in a distribution static synchronous compensator (DSTATCOM)," Majlesi J. Elect. Eng., vol. 3, no. 2, pp. 25–35, Jun. 2009.
[14]. J. Selvaraj and N. A. Rahim, "Multilevel inverter for grid-connected PV system employing digital PI controller," IEEE Trans. Ind. Electron., vol. 56, no. 1, pp. 149–158, Jan. 2009.
[15]. S. G. Song, F. S. Kang, and S.-J. Park, "Cascaded multilevel inverter employing three-phase transformers and single dc input," IEEE Trans. Ind. Electron., vol. 56, no. 6, pp. 2005–2014, Jun. 2009.
[16]. S. Srikanthan and M. K. Mishra, "DC capacitor voltage equalization in neutral clamped inverters for DSTATCOM application," IEEE Trans. Ind. Electron., vol. 57, no. 8, pp. 2768–2775, Aug. 2010.
[17]. K. Y. Lau, M. F. M. Yousof, S. N. M. Arshad, M. Anwari, and A. H. M. Yatim, "Performance analysis of hybrid photovoltaic/diesel energy system under Malaysian conditions," J. Energy, vol. 35, no. 8, pp. 3245–3255, Aug. 2010.
[18]. C. Govindaraju and K. Baskaran, "Analysis and implementation of multiphase multilevel hybrid single carrier sinusoidal modulation," J. Power Electron., vol. 10, no. 4, pp. 365–373, Jul. 2010.
[19]. E. Babaei, "Optimal topologies for cascaded sub-multilevel converters," J. Power Electron., vol. 10, no. 3, pp. 251–261, May 2010.
[20]. Y.-M. Park, H.-S. Ryu, H.-W. Lee, M.-G. Jung, and S.-H. Lee, "Design of a cascaded H-bridge multilevel inverter based on power electronics building blocks and control for high performance," J. Power Electron., vol. 10, no. 3, pp. 262–269, May 2010.
[21]. M. Malinowski, K. Gopakumar, J. Rodriguez, and M. A. Pe´rez, "A survey on cascaded multilevel inverters," IEEE Trans. Ind. Electron., vol. 57, no. 7, pp. 2197–2206, Jul. 2010.
[22]. C. Cecati, F. Ciancetta, and P. Siano, "A multilevel inverter for photovoltaic systems with fuzzy logic control," IEEE Trans. Ind. Electron., vol. 57, no. 12, pp. 4115–4125, Dec. 2010.

A.MALLIKARJUNA PRASAD has obtained his B.E from MADRAS University in the year 2001. He has obtained his M.E from Sathyabama University in the year 2004. He has 9 years of teaching experience. Presently he is a research scholar in JNTU, KAKINADA. He is working in the area of high power density dc-dc converters.

S.THIRUMALAIAH has obtained his B.TECH from S.K University in the year 2002. He has obtained his M.TECH from J.N.TU HYDERABAD in the year 2008. He has 6 years of teaching experience. Presently he is a research scholar inJNTU, ANATAPUR. He is working in the area of power system quality control with application of power electronics.

U.CHAITHANYA has obtained his B.Tech from JNTU Ananthapur in the year 2008. He has obtained his M.Tech from JNTUUniversity Ananthapur in the year 2010. He has 3 years of teaching experience.. He is working in the area of high power electronics and control applications.

Simulation of PQ Disturbances by MATLAB

Ms.Santoshi Gupta

Abstract: In recent years, PQ (power quality) problem makes quality of power supply drop, which even triggers power accident, so PQ has attracted widespread attention. To improve and increase PQ, it needs to analyze and research on PQ disturbance systematically. The paper establishes models of short-term voltage change and harmonic disturbance with the method of setting fault and changing load based on simulation platform of Matlab. The simulation of the model gets wavelet of short-term voltage change and harmonic disturbance, the waveform is analyzed through Flourier transform. The simulation results and the theoretical analysis show that the model in this paper could simulate the voltage change and harmonic disturbance well, which can provide data and basis for detection and identification of PQ and further control measures.

Keywords: Power quality, modelling, simulation, Matlab

I. Introduction

Electricity power quality has grown from obscurity to a major issue. Particularly ,the increasing penetration of power electronics based load (non linear loads) is creating a growing concern for problem of power quality in ac power system. Then electricity power quality is major issue for utilities and their customers and both are quickly adopting the philosophy and limlits proposed in the new international standards (IEC,EN,BS AND IEEE).The issue of power quality is very important to both the consumers and the distribution of electric power. There are many facts of power quality disturbances and each has its own source and mitigation technique. The first step towards any solution for a disturbance is to recognize the presence of particular type of disturbances and locate its source.

At the University of Tasmania, a project is under way to automotive this processs. The ultimate goal is to develop an Automatic Disturbances Recognition System(ADRS).In its current state, tests with simulated as well as real disturbance data yielded encouraging results, some of which are presented in this paper .In this paper ,the main power quality (PQ) problems are presented with their associated causes and consequences. The economic impacts associated with PQ are characterized .Finally ,some solution to mitigate the PQ problems are presented.

Ms. Santoshi Gupta is working as Assistant Professor, Department of Electrical Engineering, Bapurao Deshmukh College Of Engineering,Sewagram

Simulink is a visual simulation tool of Matlab, it can be used in the simulation of power system and power electronics device. This paper builds PQ disturbance model based on Simulink of Matlab, it gets disturbance waveform of voltage change and harmonic disturbance through simulation. The waveforms are analyzed in the paper also

II. Transient PQ Disturbance Modeling and Simulation

The PQ disturbance can be divided into transient and steady disturbance. Transient PQ problems include voltage change and various transient phenomenons. Voltage change is phenomenon that Root Mean Square (RMS) of node voltage changes in a short time. Because of system failure or large load transformation, the voltage changes with time, including voltage sag, voltage swell and voltage interruption. Transient phenomenon is normally mean transient overvoltage, which can be divided into transient pulse and transient oscillation [3]. Voltage change is the most serious transient PQ problem affecting many electronic equipment's normal run [4], so this paper considers voltage change mainly

1. Design of voltage change model and parameter setting

Short fault often occurs in power system. It contains three phase shorting, two phase shorting, two phase earthing and single phase earthing. Most fault of transmission and distribution system are single phase earthing fault, which is the main reason of voltage sag [5]. Single phase earthing fault may make the power system voltage fluctuation happen, causing voltage sag, interruption, swell and current swell. The schematic diagram of phase A earthing in power system is as following:

When the line occurs phase A earthing, the fault line voltage to earth are [6]:

$$U_{A\text{-}D} = 0 \quad (1)$$

$$U_{B\text{-}D} = U_B - U_A = \sqrt{3}U_A e^{-j150^\circ} \quad (2)$$

$$= \sqrt{3}U_A e^{j150^\circ} \quad (3)$$

$$U_{C\text{-}D} = U_C - U_A =$$

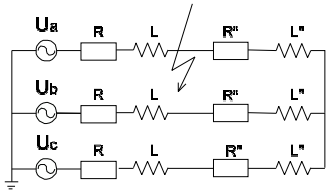

Fig. 1. Single phase earthing fault schematic diagram

Among them, the U_A, U_B, U_C are the voltage of phase A, B and C receptively. When phase A happens single

phase earthing fault, the voltage to earth of phase A is equal to 0, and the voltage of phase B,C of the fault spot raise up to $3^{1/2}$ of the original.

Build the voltage disturbance model in Matlab on the basis of Fig. 1. Use the three-phase voltage source as power supply, separate parameter line as transmission line, and series RLC branch as load. The fault breaker supplies fault for the system.

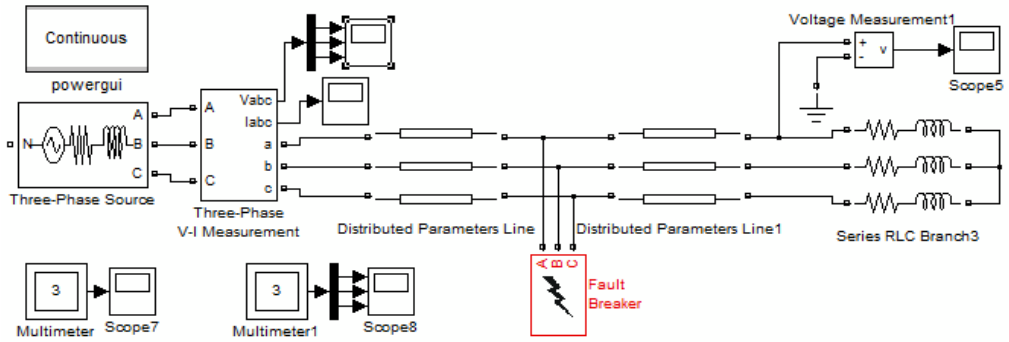

Fig. 2. Single phase earthing fault model

Choose the simulation time as 0.35s and set a single-phase earthing fault between 0.11s-0.15s. Parameters of the module in the model shown in Fig. 2 are set as following: Power module: set the voltage source as neutral grounding, the phase voltage of the three-phase voltage source as 380V and power grid frequency as 50 Hz; Transmission lines module: adopt the separate parameter line which is 40 km long; Failure module: three-phase fault breaker is located between line 1 and line 2, it's set as phase A single earthing fault. The fault takes place in 0.11 s and it's cut off in 0.15s .Fault point resistance and fault point grounding resistance are selected for 0.001 Ω; Load module: select RL load, R = 10 Ω, L =

0.005 H; Measurement modules: three-phase *V-I* measurements are put in the circuit to measure voltage and current wavelet of the power side and the load side, the multimeter is put in the fault point to measure the voltage and current of it.

2. Simulation result

Select ode23tb as simulation algorithm and 0.35s as simulation time in configuration parameter choice box. Then activate the simulation button, the voltages of phase A, B, C are shown in Fig. 3.

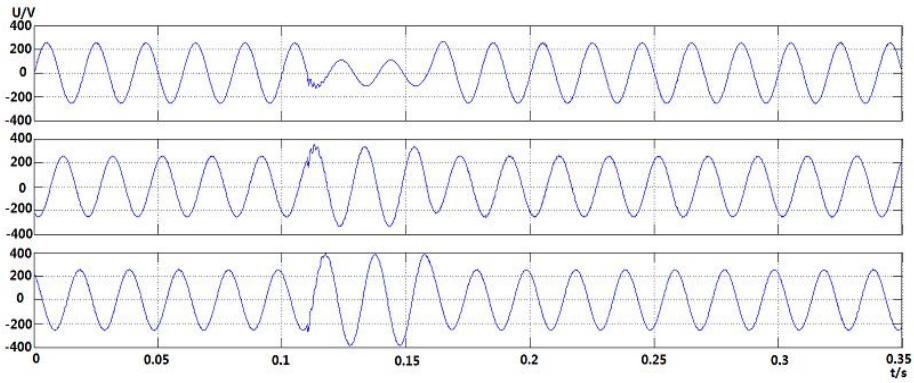

Fig. 3. Voltage of power side in single phase earthing fault

In Fig. 3, phase A voltage beside power drops with shake when single phase earthing happens in 0. 11s, voltage of phase B and C rise. When fault generator disconnects in 0.15 s, short-circuit fault is cut off. Because of the existence of dc (direct current) component in shorting current, the voltage of phase A is a little larger than normal voltage at this time. With the decline of dc component, voltage of phase A recovers to normal. When the fault is cut off, voltages of phase B, C drop to normal.

Using a multimeter to detect current waveform of phase A, B and C showing in Fig. 4 (the colours of phase A is blue and B, C are red). In Fig. 4, current of phase A, B, C are 0 before the single phase shorting fault. Current of phase A is no longer for 0 when phase A shorting happens, the current of phase A shakes greatly with the law of sine wave while current of phase B, C remain for 0. Current of phase A drops to 0 quickly when the fault is cut off.

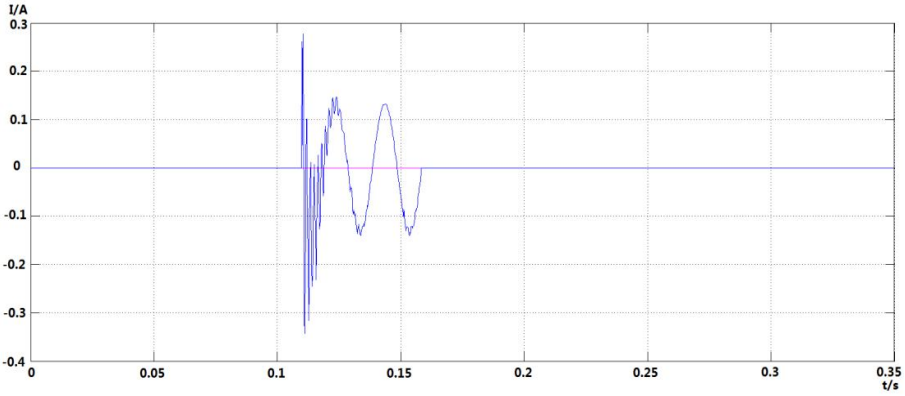

Fig. 4. Current waveform of fault point

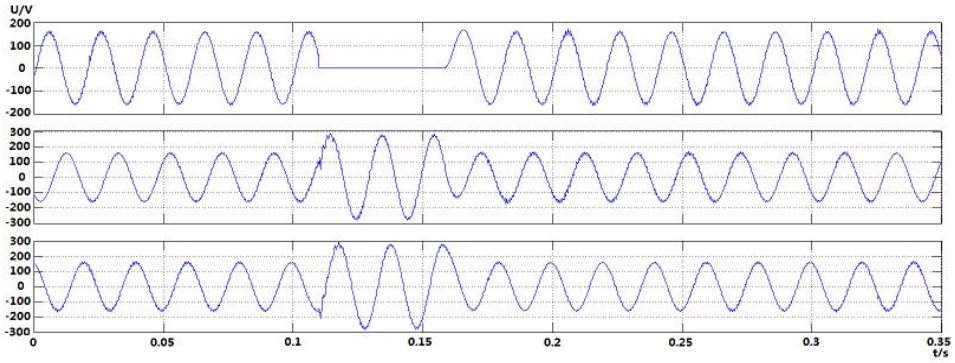

Fig. 5. The voltage waveform of fault point

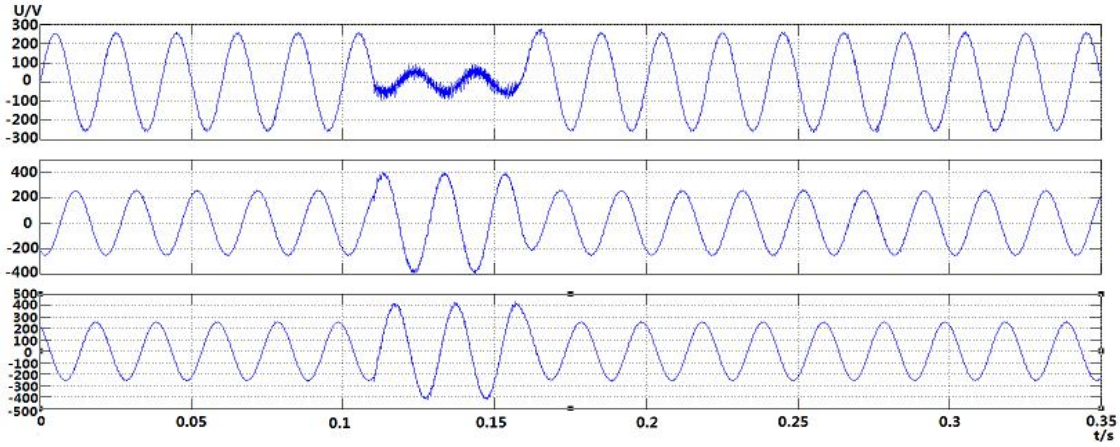

Fig. 6. The voltage waveform beside power after the fault

Similarly, the voltage of phase A, B, C of fault point can be detected by a multimeter, the voltage is showing in Fig. 5:

As the figure shows, the voltage of phase A is interrupted when the three fault generator is closed in 0.11s. The voltage of phase A is 0, while voltage of phase B and C rise. The voltage to earth of phase B, C before fault is 160V, while the voltage rise to 270V after fault, $270=160\times3^{1/2}$, which are fit to the formula (1), (2), (3). When the three phase fault generator is cut off in 0.15s, the voltages of phase A, B, C return to normal.

3. The factors influenced voltage change

The difference in the distance from fault to load and the type of shorting fault will lead into the different extent of voltage changing.

The fault location will influence the extent of voltage change. The fault of model in Fig. 2 is set between 40 m and 40 m, while move fault to the position between 20 m and 60 m, that means setting the discrete parameter line 1 as 20 m long and discrete parameter line 2 as 60 m long. Through re-simulation can get phase A, B, C voltage beside power respectively after the fault happening. The rise and drop scale of voltage are changed as Fig. 6.

In Fig. 3, single phase earthing leads voltage of A into dropping, the maximum voltage falls from 250 to 120, the drop scale is 0.48; The fault leads voltage of phase B, C into rising, the maximum voltage rises up from 250 to 340, the rise scale is 1.36. Fig. 6 shows the voltage of the power side after changing the fault position, voltage of phase A drops, the maximum voltage falls from 250 to 100, the drop scale is 0.4; voltage of phase B, C rise, the maximum voltage rise up from 250 to 400, the rise scale is 1.6. Comparing with the Fig. 3, it's found that the shorter the distance between the load and fault point is, the more the voltage drops and the less the voltage rises.

The difference in type of fault will also result in different extent of voltage change. Set the three phase fault generator in model 3 as three phase shorting. The voltage of power side will be obtained through simulation, the voltage is shown in Fig. 7.

The voltage of phase A,B,C all happen sag, the maximum voltage falls from 250 to 210, the drop scale is 0.807. Comparing with the Fig. 3, it's found that the scale of voltage drop in three phase shorting is smaller than scale of voltage drop in single phase earthing.

The analysis above showing that different fault type and the fault location parameters will cause different voltage disturbance to power system. Three phase shorting and single phase earthing cause different scale of voltage drop and rise. The scale of voltage drop and rise caused by two phase shorting are also different form them, while this situation is not analyzed in this paper. Even in the same type of shorting fault, the different fault position will cause different sag and swell of voltage.

A short time voltage change is the most common PQ distribution in power system, the simulation result of model in Fig. 2 is consistent with the theory, it can simulate the voltage change well. This model can help to set up intuitive understanding for all sorts of voltage change and provide the basis for the identification and further control measures of the voltage change disturbance.

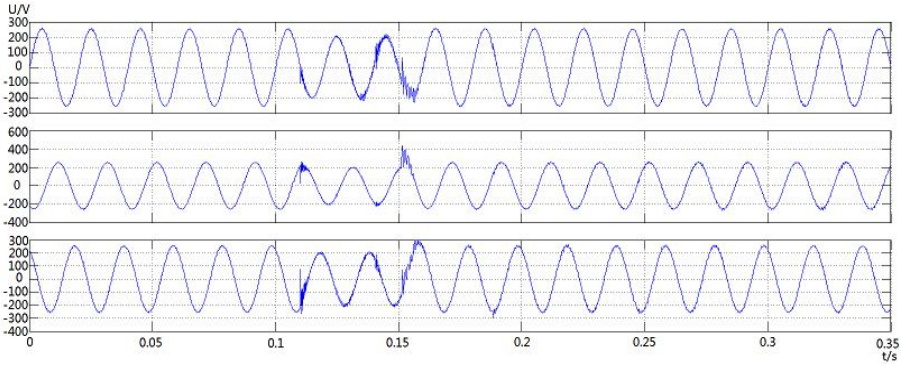

Fig. 7. Voltage waveform beside power in three phase shorting

III. Transient PQ Disturbance Modeling and Simulation

1. Design of voltage change model and parameter setting

Steady PQ disturbance mainly includes three phase voltage unbalance, voltage fluctuation and flicker, voltage offset, frequency offset, waveform in the characteristic of distortion, such as harmonics, inter- harmonic and notch, among these disturbances harmonic wave does the greatest harm to power system especially.

With the wide application of various power electronic devices, they bring harmonic and inter-harmonic pollution into power system. Harmonic and inter-harmonic pollution do harm to the safety, stability and economic run of power system [7]. Building harmonic simulation model can analyze the harmonic pollution brought by power electronic devices in power system. The analysis has important theoretical and practical significance, therefore this paper will model and simulate harmonic disturbance mainly.

Taking three-phase bridge controllable rectifier circuit as an example, this paper analyzes the influence of power electronic equipment to the grid harmonics. Its principle diagram is shown as shown in Fig. 8, which chooses diode rectifier bridge as rectifier bridge.

Decompose the current of three-phase diode bridge rectifier with resistance load into Flourier series, taking phase A for example: make the middle point of negative half wave and positive half wave as time horizon:

$$i_a = \sqrt{2}I_1 \sin wt + \sum_{\substack{n=6k\pm1 \\ k=1,2,3,\ldots}} (-1)^k \sqrt{2}I_n \sin nwt \quad (4)$$

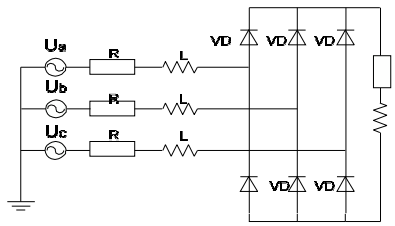

Fig. 8. Three-phase bridge controllable rectifier circuit schematic diagram

Among them, the I_1 is RMS of base frequency current, I_n is the RMS of the Nth times harmonic current. From the formula (4) can get base frequency current and the effective value of every harmonic are:

$$i_1 = \frac{\sqrt{6}}{\pi} I_d, \quad i_n = \frac{\sqrt{6}}{n\pi} I_d, n = 6k \pm 1, k = 1, 2, 3\ldots \quad (5)$$

Id is average value of output current. Visibly, the current contains only 6k±1st (k is a positive integer) times harmonic.

This paper aims to build a model applicable to analyze various disturbances. In the basis of the model of transient disturbance, taking off fault generator, changing the load to three-phase diode bridge rectifier according to Fig. 8, the harmonic disturbance model will be showed in Fig. 9. Three-phase diode bridge rectifier is a harmonic source.

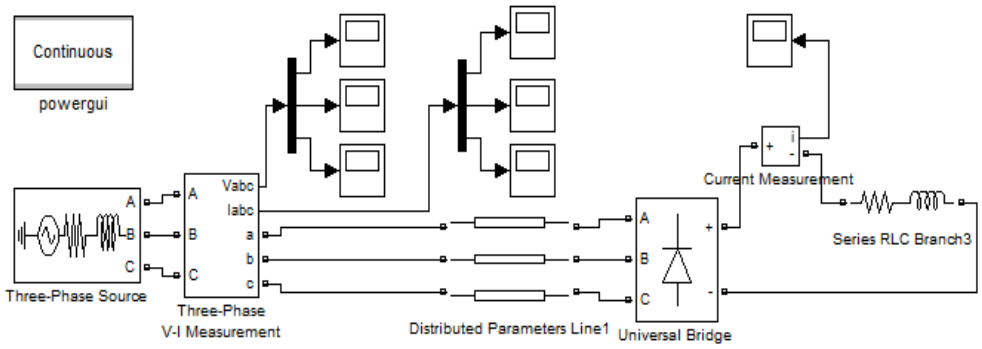

Fig. 9. Harmonic disturbance model

2. Simulation result

Similarly, select ode23tb as simulation algorithm in configuration parameter and 0.35s as simulation time. Then activate the simulation button, the voltage of phase A of power side and its Flourier analysis are shown in Fig. 10.

The basis frequency component of phase A voltage is 195.8, THD (total harmonic distortion) is 23.68%, harmonic numbers are 5, 7, 11, 13 etc, that is 6k±1st. It can be seen from the graph that harmonic RMS is inversely proportional to the number of the harmonic.

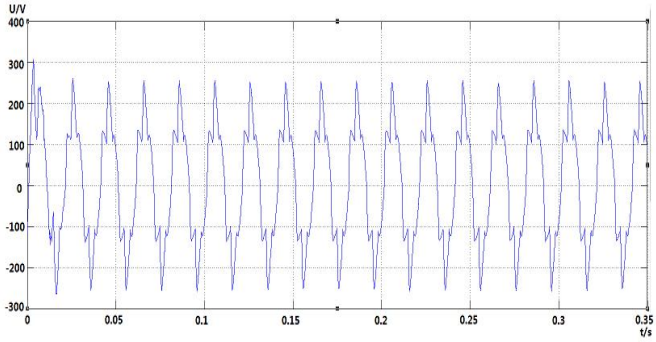

Fig. 10. (a) The voltage of phase A of power side

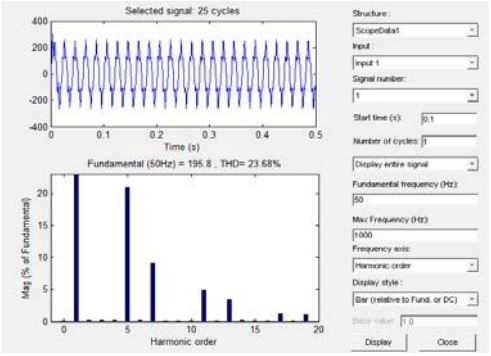

Fig. 10 (b) Flourier analysis of the voltage

Current waveform of the power supply side is shown in Fig. 11 (a), its Fourier analysis is shown in Fig. 11 (b).

The basis frequency component of phase A current is 27.33, THD (total harmonic distortion) is 6.00%, harmonic numbers are 5, 7, 11, 13 etc, that is 6k±1st. It can be seen from the graph that harmonic RMS is inversely proportional to the number of the harmonic.

From the Flourier analysis of voltage and current waveform of power side, it's found that rectifier equipments bring harmonic into power system, which makes voltage and current waveform occur distortion. The voltage and current beside the power side contains only 6k±1st (k is a positive integer) times harmonic, which is according with formula (5). It's demonstrated that this model can simulate harmonic disturbance well.

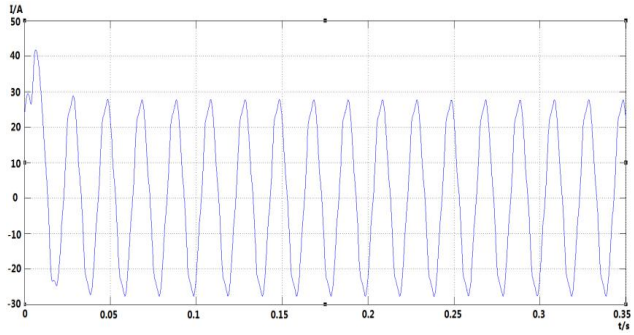

Fig. 11. (a) The current of phase A of power side

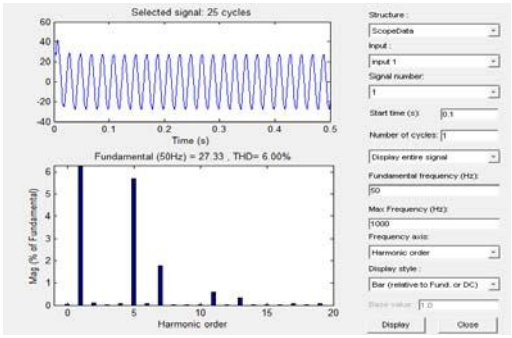

Fig. 11 (b) Flourier analysis of the current

IV. Conclusions

The model built based on Matlab simulation platform in this paper is applicable to analyze voltage change and harmonic disturbance. The model is simple, efficient and highly applicable. The wavelet of voltage sag, voltage swell, and voltage interruption are getting from the simulation. The paper also analyzes the voltage and current contained harmonic through Flourier transformation. The simulation results and the theoretical analysis show that the model in this paper can simulate the voltage change and harmonic disturbance well, which can provide data and basis for detection and identification of PQ and further control measures.

References

[1] Yuan B, Chen J, Zhang W. Power transmission lines shorting analysis based on Matlab. *Science Technology and Engineering*,2008; 8(15):4319-4320.

[2] He C. Powe quality disturbance classification based on the wavelet transform and the artificial neural network. Master thesis, Hunan University. Hunan, China; 2009.

[3] Hu M, Chen HG. Power quality and its analysis methods summarize. *Power grid technology*, 2000; 24(2):36-38.

[4] Shi J. Research on location of transient power quality disturbance. Master thesis, Hunan University. Hunan, China; 2008.

[5] A*nalysis and Control of Power Quality*. Beijing: China Electric Power Press; 2010.

[6 H.Van der Broeck, M. Miller, "Harmonics in DC to AC converters of Single Phase Uninterruptible Power Supplies," presented at IEEE INTELEC, 1995.

[7] J.F. Moynihan, M.G. Egan, J.M.D. Murphy, "Theoretical Spectra of Space-Vector Modulated Waveforms," *IEE Proc.-Electr. Power Application*, vol. 145, January 1998, pp. 17-24.

Study Analysis of Hybrid Power Plant (Wind-Solar) - Vertical Axis Wind Turbine-Giromill Darrieus Type with Evacuated Tube Collectors

C.Bhuvaneswari and R.Rajeswari

ABSTRACT: The vital input for the growth of any nation is energy. In India, so many types of energies playing a major role. It has become inevitable to seek nonpolluting renewable energy sources for the power generation. So Renewable energy technologies range from the well established, such as hydro power to the emergent. Each technology has its own individual measurement and requirements. A steps involved in hybrid system deserve extra attention because of its importance or uniqueness. Hybrid system is most often used for larger applications such as village power, residential systems where generators already exist and in applications like telecommunications where availability requirements are near 100 percent. Among this wind energy and solar energy plays a vital role in many countries. The growth of installations of Wind turbine and solar plate collector is increasing every year. In wind power plant, Giromill Darrieus type vertical axis wind turbine provides high good efficiency, small torque ripple and low stress on the tower which contributes to good reliability, self starting. In solar power plant , Evacuated tube solar collectors are well suited to commercial and industrial heating applications and can be effective alternative to flat plate collectors for domestic space heating in areas, especially where it is often cloudy and it is also more efficient. This paper presents the study analysis of wind –solar hybrid power plant by using vertical axis wind turbine-GiromillDarrieus type with evacuated tube solar collectors.

Key words: **Wind Turbine, Giromill Darrieus type, Solar collectors, Evacuated tube collectors.**

I. INTRODUCTION:

The oil crises in the early 70's and the steadily increasing environmental concern have initiated a major interest for the exploitation of renewable sources of energy for the generation of electric power. Most promising among them appear be the wind and at a second level, the solar energy.

Peoples are looking for ways that will enable them to curb and reduce the greenhouse gas emissions so that the planet can be saved from the harsh effects of global warming. The wind turbines have proven to be most effective way of dealing with these emissions. The first one to be designed was the horizontal axis wind turbine. Now there is some new and modern vertical axis wind turbine designed. The main advantage of a vertical wind axis turbine over a horizontal axis wind turbine is its insensitivity to wind direction and can be located near the ground. Among then vertical axis wind turbine Giromill Darrieus type is the advantage because it provides high good efficiency, small torque ripple and low stress on the tower which contributes to good reliability, self starting. Similarly in solar power plant the Heart of a solar thermal system is a solar collector. It absorbs solar radiation as heat and transfers useful heat to the solar system. There are different design concepts for collectors such as flat plate collectors, evacuated flat plate collector, evacuated tube collector and concentrating collectors.

Among this evacuated tube collector are the more efficient and can achieve very high temperature. In this paper the study of wind solar hybrid power plant with Giromill Darrieus type vertical axis wind turbine and evacuated tube collector has been presented.

II. WIND POWER GENERATION SYSTEM

Differential heating of the earth surface by the sun causes the movement of large air masses on the surface of the earth, ie, the wind. Wind power generation has been recognized has an environmentally friendly and economically competitive means of electric power generation.

In meteorology, winds are often referred to according to their strength and the direction from which the wind is blowing. Short bursts of high speed wind are termed as gusts. Strong winds of intermediate duration are termed squalls, long duration winds have various names associated with their average strength, such as breeze, gale, storm, hurricane and typhoon. Wind occurs on a range of scales from thunderstorm flows lasting lens of minutes, to local breezes generated by heating of land surfaces and lasting a few hours, to global winds resulting from the difference in adsorption of solar energy between the climate zones on earth. The two main causes of large scale atmosphere circulation are the differential heating between the equator and the poles, and the rotation of the planet.

C.Bhuvaneswari and R.Rajeswari are working in Department of electrical and electronics engg Priyadarshini engg college-vaniyssambadi, E-Mails: bhuvana_manoharsha@yahoo.co.in, gt_rajivarsha@yahoo.com,

Wind power can be computed by using the concept of kinetics. The wind mill works on the principle of converting kinetic energy of the wind to mechanical energy.

Power density in moving air is given by

$$P_w = KU_w^3 \ w/m^2 \quad (1)$$

Where U_w = Wind speed in km/hr and

$$K = 1.3687 * 10^{-2} \quad (2)$$

Theoretically a fraction 16/27 = 0.5926 of the power in the wind is recoverable. This is called Gilbert's limit or Betz co-efficient. Aerodynamically efficiency for converting wind energy to mechanical energy can be reasonably assumed to be 70%. So the mechanical energy available at the rotating shaft is limited to 40% or at the most 45%of wind energy.

III. WIND TURBINES:

Wind turbines are the machines that convert the kinetic energy into mechanical energy. When the mechanical energy is converted to electricity, then the machines is referred to as a wind turbine or a wind energy converter.

When such mechanical energy is used directly by machines such as pumps, then the machine is referred to as a wind mill.

HISTORY OF WIND TURBINES:

Wind machines have been used since 200BC in Persia for grinding grain. It was introduced in 250BC in the Roman Empire. Wind mills were used in the 14th century in Holland to drain the areas of the Rhine River Delta. In the 1900's wind mills were used in Denmark for pumps and mills. Wind mills were also used in USA and USSR to produce electricity on farms.

VERTICAL AXIS WIND TURBINE:

Wind turbines are of two types: Horizontal axis wind turbines and Vertical axis wind turbines. In a horizontal axis wind turbine, the main rotor shaft and electrical generator is placed at the top of the tower and it must be pointed into the direction of the wind. In a vertical wind turbine, the rotor shaft runs vertically.

The advantages of a Vertical axis wind turbine are that the rotor shaft is placed vertically and can be located near the ground. The generator and the gear box are placed near the ground. Thus the tower need not support it. Also the turbine need not be pointed into the wind. This makes the maintenance of the wind turbine quite easy. Also the Vertical axis wind turbine is quite cost effective. These can be placed on hilltops, on ridgelines and any areas where the force of the wind is more near the ground. Since they are placed lower, they can be used where the tall devices are not allowed by the law. The main advantage of Vertical axis wind turbine, however is that it turns in any direction with the wind.

DARRIEUS TYPE WIND TURBINE:

The Darrieus wind turbine is a type of vertical axis wind turbine used to generate electricity from the energy carried in the wind. The turbine consists of a number of aero foils usually- but not always vertically mounted on a rotating shaft or framework. This design of wind turbine was patented by Georges Jean Marie Darrieus, a French aeronautical engineer in 1931.

IV. METHOD OF OPERATION OF DARRIEUS WIND TURBINE

In the original versions of the Darrieus design, the aero foils are arranged so that they are symmetrical and have zero rigging angle, that is, the angle that the aero foils are set relative to the structure on which they are mounted. This arrangement is equally effective no matter which direction the wind is blowing in contrast to the conventional type, which must be rotated to face into the wind.

When the Darrieus rotor is spinning, the aero foils are moving forward through the air in a circular path. Relative to the blade, this oncoming airflow is added vectorially to the wind, so that the resultant airflow creates a varying small positive angle of attack to the blade. This generates a net force pointing obliquely forwards along a certain, "line of action'. This force can be projected inwards past the turbine axis at a certain distance giving a positive torque to the shaft, thus helping it to rotate in the direction it is already travelling in. The aero dynamic principles which rotates rotor are equivalent to that in autogiros and normal helicopters in autorotation.

As the aero foil moves around the back of the apparatus, the angle of attack changes to the opposite sign but the generated force is still obliquely in the direction of rotation, because the wings are symmetrical and the rigging angle is zero. The rotor spins at a rate unrelated to the wind speed and usually many times faster. The energy arising from the torque and speed may be extracted and converted into useful power by using an electrical generator.

GIROMILL TYPE:

Darrieus 1927 patent also covered practically any possible arrangement using vertical airfoils. One of the most common type is the giromill or H-bar design, in which the long 'egg beater' blades if the common Darrieus design are replaced with straight vertical blade sections attached to the central tower with horizontal supports. In low winds, the blades are pitched flat against the wind generating drag forces and starting the turbine turning cheaper and easier to build than a standard Darrieus turbine.

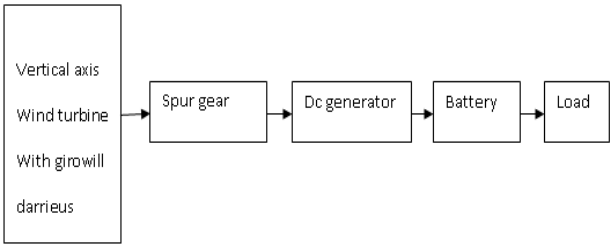

Figure.1-Wind power generation system.

V. SOLAR POWER GENERATION:

The most popular non conventional power resources are solar energy or solar heat to electricity. The sun is a continuous fusion reactor in which hydrogen combine to form helium and evolving huge amount of heat energy as per the following reaction.

$$4_1H^1 \longrightarrow {}_2He^4 + 26.7MeV \quad (3)$$

This heat energy from the sun is emitted in the universe and the earth by transmission of tiny bundles of energy particles called photons which move with finite speed (almost speed of light) and energy. When photons strike an atom, they interact with the electrons by transferring their energy and hence they are absorbed. The sun rays are composing if different wavelength spectrum from the low to the very high ranges, but UV (ultra violet) radiation, other low and very high range wavelength radiations are absorbed by ozone, oxygen, nitrogen, watervapour etc…lying above the earth's atmosphere. Thus the sun ray consists of wavelength radiations between 0.29μm to 2.3 μm (approximately).

The conversion of sunlight into electricity is done, either directly using photovoltaic (PV) or indirectly using concentrated solar power. Concentrated solar power system uses lens or mirrors and tracking system to focus a large area of sunlight into a small beam. Photovoltaic convert light into electric current using the photoelectric effect.

Concentrating solar power (CSP) uses lens or mirror or tracking system to focus a large area of sunlight into a small beam. The concentrated heat is then used as a source for a conventional power plant. Various techniques are used to track the sun and focus light. In all of these systems a working fluid is heated by the concentrated sunlight and is then used for power generation of energy.

SOLAR COLLECTORS:

The solar collectors concentrate sunlight to heat a heat transfer fluid to a high temperature. The hot heat transfer fluid is then used to generate system that drives the power conversion subsystem, producing electricity. The solar collector is the key element in a solar energy system. It is also the novel technology area that requires new understanding in order to make captured solar energy a viable energy source for the future. The function of solar collector is simple; it intercepts incoming isolation and changes into a usable form of energy that can be applied to meet a specific demand.

FLAT PLATE COLLECTORS:

Flat plate collector, developed by Hottel and Whillier in the 1950's is the most common type. They consists of i) a dark flat plate absorber of solar energy ii) a transparent cover that allows solar energy to pass through but reduces heat losses iii) a heat transport fluid to remove heat from the absorber and iv) a heat insulating backing.

EVACUATED TUBE SOLAR COLLECTOR:

Evacuated tube solar collector is very efficient and can achieve very high temperature. Evacuated tube solar collectors are well suited to commercial and industrial heating applications and can be an effective alternative to flat plate collectors for domestic space heating, especially in areas where it is cloudy.

A evacuated tube collectors contains several rows of glass tubes connected to a header pipe. Each of the air removed from it to eliminate heat loss through convection and radiation. Inside the glass tube, a flat or curved aluminium or copper fin is attached to a metal pipe. The fin is covered with a selective coating that transfers heat to the fluid that is circulating through the pipe.

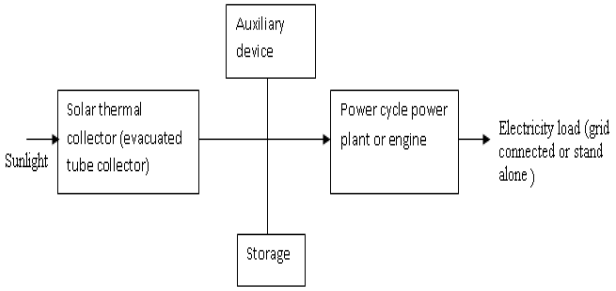

Figure.2-Solar power generation.

VI. COMBINED WIND AND SOLAR POWER PLANT :(GIROMILL DARRIEUS TYPE VERTICAL AXIS WIND TURBINE AND EVACUATED TUBE SOLAR COLLECTOR):

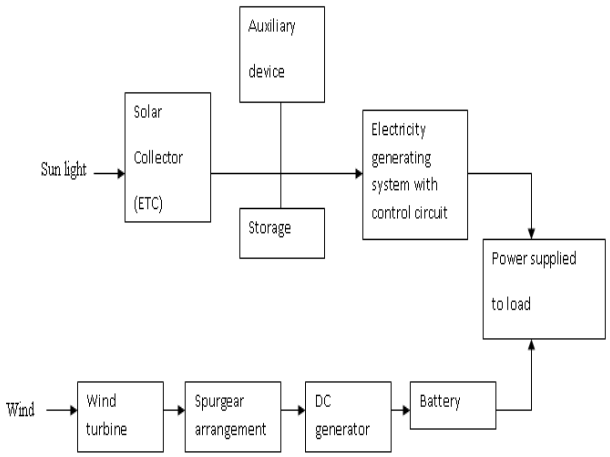

Figure.3-Combined power generation (wind and solar).

Evacuated tube solar collector can maintain their efficient over a wide range of ambient temperature and heating requirements. Evacuated tube collector works as a thermal one way valve due to their heat pipe. This also gives them an inherent maximum operating temperature which may be considered as a safety feature. They have less aerodynamic drag, which allow them to be laid onto the roof without being tied down. They can collect thermal radiation from the bottom in addition to the top. Tubes can be replaced individually without shutting down the entire system. There is no condensation or corrosion within the tubes. It captures sunlight better as they have a greater surface area exposed to the sun at any time. It is more efficient in transferring heat up to 163%.

By using Giromill darrieus type vertical axis wind turbine, in low winds the blades are pitched flat against the

wind generating drag forces and starting the turbine turning cheaper and easier to build than a standard Darrieus turbine.

VII. CONCLUSION AND FUTURE DIRECTIONS OF WORK

The paper presented here will be highly effective in all places, especially in rural areas and where the commercial electricity has not reached or undelivered. It causes no effect on nature i.e., pollution free, at the same time it won't cause any kind of accident due to lightning and highly suitable for domestic purposes. It is also useful to urban and city areas simultaneously with the commercial power supply to minimize power supply load i.e., cut short power charge. By using this system, people can save electricity charge and very less maintenance to this equipment is required.

In future we can replace the evacuated tube collector in solar power plant by a ring array concentrator. The ring array concentrator is an ultra powerful optical lens based on an array of nested ring design completely free from the light dispersion effects of conventional refractive lenses.

VIII.ACKNOWLEDGEMENT:

We wish to thank the authors P.K.Nag,Rajput and M.R.patel,US dept of energy,wind power today 2001 for the lot of information we got from their books about this paper, and also we thank all the members who helped us to finish this paper successfully.

References:

[1] Liuchen chang IEEE Canadian review spring/printemps 2002 University of Brunswick.

[2] US dept of energy, wind power today,2001.

[3] Pijush kanti bhattacharjee, member IACSIT.(solar-rain-wind-lightning energy source power generation systems).

[4] Bill Williams, 2002 solar & energy renewable energy technologies.

[5] GM Joselin Herberts, S.Iniyan, L.Suganthi&Ranko Goic - analysis of wind farm. International journal of green energy ,Energy and Environment.

[6] M.R.Patel,1999,wind and solar power systems, Florida.

[7] P.K.Nag,2005,power plant engineering,2nd edition,tata MC graw hill publishing company ltd, Newdelhi,

[8] Christophertrinkl,wilfried zerner,clausart, Christian stadler (June 21,2005) performance of flat plate collectors & evacuated tube collectors, centre of excellence for solar engineering at lngolstadi university of applied science.

[9] Pecen.r and Timmerman (1999 Nov).Anovel power quality scheme to improve a utility interface in a small sized hybrid solar /wind generation unit.10th international power quality conference.

Modeling and Power-Synchronization Control of Grid-Connected VSC- HVDC

Banothu Thavu, Thuraka Rajendra, Ravi Bukya and M. Maheswararao

Abstract- **In this project, a novel control method of grid-connected voltage-source converters (VSCs) is proposed. The method can be generally applied for all grid-connected VSCs but may be of most importance in high-voltage dc (HVDC) applications. Different from the previous control methods, the proposed method utilizes the internal synchronization mechanism in ac systems, in principle, similar to the operation of a synchronous machine. By using this type of power-synchronization control, the VSC avoids the instability caused by a standard phase-locked loop in a weak ac-system connection. Moreover, a VSC terminal can give the weak ac system strong voltage support, just like a normal synchronous machine does. The control method is verified by both analytical models and time simulations. The implementation of this work is carried out in MATLAB/SIMULINK.**

Index Terms—Control, converters, HVDC, phase-locked loops, power systems, stability.

I. INTRODUCTION

Pulse width-modulation (PWM)-based voltage source converter (VSC) techniques have been widely used in grid-connected applications, such as adjustable-speed drives (ASDS) with PWM rectifiers, power quality improvement, wind turbines, etc.. Thanks to the gradually increased rating and reduced costs, they have also been applied for high-voltage dc (HVDC) transmission in recent years. Compared to the conventional thyristor-based HVDC, VSC-HVDC has a number of technical merits: reactive-power support to the ac system, possibility to connect to very weak ac systems, black-start capability, and lower cable cost, just to name a few. Several control methods of grid-connected VSCs have been proposed. Among them, power-angle control and vector-current control are the two that have been mostly investigated. The principle of power-angle control is fairly simple and easily implemented. The active power is controlled by the phase-angle shift between the VSC and the ac system, while the reactive power is controlled by varying the VSC voltage magnitude. Power-angle control has been studied for HVDC, static-synchronous- compensator (STATCOM), and wind-turbine applications.

Banothu Thavu, Thuraka Rajendra, Ravi Bukya are working in department of EEE, Daripally Anantha Ramulu College of Engg & Tech, Kuravi Road, Khammam and **M. Maheswararao** is working in Swarna Bharathi Institute of Science and Technology, Khammam.

One disadvantage of power-angle control is that the control bandwidth is limited by a resonant peak at the grid frequency. Another disadvantage is that the control system does not have the capability to limit the current flowing into the converter. The latter is a serious problem, as VSCs usually do not have an over-current capability. In high-power applications, it is highly important for the control to limit the valve current to prevent the converter from being blocked (tripped) at disturbances.

Vector-current control is a current-control-based technology. Thus, it can naturally limit the current flowing into the converter during disturbances. The basic principle of vector-current control is to control the instantaneous active power and reactive power independently through a fast inner current control loop. By using a decomposition technique with the grid voltage as phase reference, the inner current control loop decouples the current into and components, where outer loops can use the component to control active power or direct voltage, and the component to control reactive power or alternating voltage. Due to its successful application in ASDs, doubly-fed induction-generator (DFIG) wind turbines, etc.

Interestingly, as one of the original purposes to use VSCs for HVDC applications was its possibility to connect to very weak ac systems, where the conventional thyristor-based HVDC is not applicable, some difficulties have been experienced by VSC-HVDC based on vector-current control in weak ac-system connections. One of the problems is the low-frequency resonance that is typically present. This can interfere with the fast inner current control loop, thereby limiting the VSC control performance. The other one has to do with the phase-locked loop (PLL). In almost all VSCs connected to ac systems, a PLL is used to obtain an accurate synchronization to the ac system. This has since long been believed to be a pre-condition for any grid-connected VSC. However, several investigations have shown that the PLL dynamics might have a negative impact on the performance of VSC-HVDC in weak ac-system connections.

II. HVDC TRANSMISSION

The first commercially used HVDC link in the world was built in 1954 between the mainland of Sweden and island of Gotland. Since the technique of power transmission by HVDC has been continuously developed. In India, the first HVDC line in Rihand-Delhi in 1991 i.e. I 500 KV, 800 Mkl, 1000 KM. In Maharashtra in between Chandrapur & Padaghe at 1500 KV & 1000 MV. Global HVDC transmission capacity has increase from 20 MW in 1954 to 17.9 GW in 1984. Now the growth of DC transmission capacity has reached an average of 2500 MW/year.

Advantages of HVDC System:

- The cost of D.C. transmission line is less than 3 - phase a.c. line because only two conductors are necessary for D.C. line.
- Tower designs are simple.
- The dielectric strength of cable is high.
- The dielectric loss is low.
- For D.C. overhead transmission lines length is unlimited.
- Power transmission capacity is higher than A.C.
- Corona & radio frequency interference losses are less.
- HVDC link has accurate & quick control of power in the required direction.

Limitation of HVDC Transmission:

1. Transformer for step up – step down voltages are not available in case of HVDC.
2. The terminal equipment is costly.
3. Reliable D.C. ckt. Breakers for higher ratings are not available.
4. Earth current may cause some side effects.
5. Reactive MVA cannot be transferred over a HVDC link.
6. Although inverters are used, the wave form of output A.C. is not exactly sinusoidal and it contains harmonic distortion.

HVDC Transmission System:

The standard voltages used are:-

100, 200, 300, 400, 600 & 800 KV.

The HVDC system is accepted for transmission of power for following reasons:

(i) For long distance high power transmission.

(ii) For interconnection between two A.C. systems having their own load frequency control.

(iii) For back-to-back a synchronous tie substations.

Principles Ac/Dc Conversion:

HVDC transmission consists of two converter stations which are connected to each other by a DC cable or DC line. A typical arrangement of main components of an HVDC transmission. Two series connected 6 pulse converters (12-pulse bridge) consisting of valves & converters transformer are used. The valves convert AC to DC, and the transformer provides a suitable voltage ratio to achieve the desired direct voltage and galvanic separation of the AC & DC systems. A smoothing reactor in the DC ckt reduces the harmonic currents in the DC line, & possible transient over currents. Filters are used to take care of harmonics generated at the conversion. By varying the firing angle & the DC output voltage can be controlled between two limits, +ve and negative. When a is varied, we get,

Maximum DC voltage when $\propto = 0^0$.

Rectifier operation when $0< \propto < 90^0$

Inverter operation When $90^0< \propto < 180^0$

Principles of HVDC Control:

One of the most important aspects or HVDC systems is its fast and stable controllability. In DC transmission, the transmitted power can be rapidly controlled by changing the DC voltages. The current in the system can only flow in one direction for a given setting power is transported from rectifies to inverter and by altering voltages, the power flow direction is reversed. It contains harmonic distortion.

.

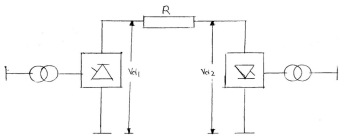

Fig.2.1 HVDC Transmission system

In HVDC transmission, one of the converter stations, generally the inverter station is so controlled that the direct voltage of the system is fixed & has rigid relation to the voltage on the AC side. Tap changers take care of the slow variations on the AC side the other terminal station (rectifier) adjust the direct voltage on its terminal so that the current is controlled to the desired transmitted power.

$$Id = \frac{Vd_1 - Vd_2}{R} \tag{2.1}$$

Where R is the Resistance of link & includes loop transmission resistance (if any), and resistance smoothing reactors and converter valves the power received is, therefore, given as

$$P = \left[\frac{Vd_1 - Vd_2}{R}\right] \mathrm{Vd}_2 = Id\ Vd_2 \tag{2.2}$$

The rectifier and inverter voltages are given by

$$\mathrm{Vd}_1 = \eta\left[\frac{3\sqrt{2}\ \mathrm{V}\pi}{\pi}\mathrm{COS}\alpha - \frac{3\mathrm{Xcr}}{\pi}\mathrm{Id}\right] \tag{2.3}$$

$$\mathrm{Vd}_2 = \eta\left[\frac{3\sqrt{2}\ \mathrm{V}\pi}{\pi}\mathrm{COS}\ \gamma - \frac{3\mathrm{Xci}}{\pi}\ \mathrm{Id}\right] \tag{2.4}$$

η : - number of series connected bridges.

$\mathrm{Vlr}, \mathrm{Vli}$: - line to line AC Voltages at the rectifier and inverter bridges, respectively.

$\mathrm{Xcr}, \mathrm{Xci}$:- Commutation reactance at the rectifier and inverter, respectively.

From equation (2). It is clear that the DC power per pole is controlled by relative control of DC terminal voltages; Vd_1 and Vd_2 control on DC voltage is exercised by the

converter control angles α & γ as given by Eqs. (3) and (6). Normal operating range of control angles is:

$$\alpha_{min} = 5^0,\ \alpha_{max} = (15 \pm 3)^0,\ \gamma_{min} = 15^0$$

The prime considerations in HVDC transmission are to minimize reactive power requirement at the terminals and to reduce the system losses. For this DC voltage should be as high as possible and α should be as low as possible.

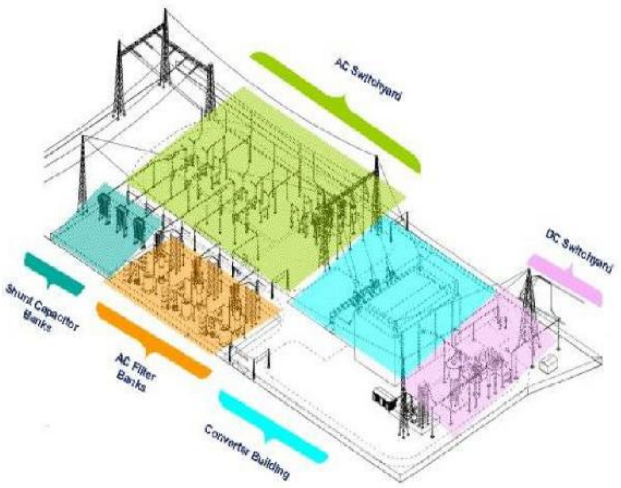

Fig: 2.2 Typical HVDC Station

HVDC Applications:

Transmission of power through underground or submarine cables.

A.C. & D.C. lines in parallel.

Connection of D.C. transmission to a.c.

Frequency conversion. Transmission of power over a long distance.

FUTURE TRENDS:

Considerable research and development work is under way to provide a better understanding of the performance of HVDC links to achieve more efficient and economic designs of thyristor valves and related equipment and to justify the use of Alternatives AC/DC system configurations. Future power systems would include a transmission mix of AC & DC. Future controllers would be more & more Microprocessor based which can be modified or upgraded without requiring Hardware changes. It is by now clear that HVDC transmission is already a reliable, efficient & cost effective alternative to HVAC for many applications.

III. HVDC with High-Impedance AC Systems

General aspects of high-impedance ac systems:

There is an inherent weakness with the conventional LCC-HVDC system, i.e., the commutations of the thyristor valves are dependent on the stiffness of the alternating voltage. The most outstanding contribution on this subject is according to, an ac system can be considered as weak from two aspects: 1. ac-system impedance is high. 2. ac-system inertia is low. Either of the two system conditions may become an obstacle for conventional LCC-HVDC applications.

The following is a definition of the strength of an ac system based on the classification of:

- Strong system, if the SCR of the ac system is greater than 3.0.
- Weak system, if the SCR of the ac system is between 2.0 and 3.0.
- Very weak system, if the SCR of the ac system is lower than 2.0.

One of the driving forces to develop the VSC-HVDC technology is to overcome the weak-ac-system connection problem of the conventional LCC-HVDC system. By applying VSC techniques, the two notorious weak-ac-system related problems for conventional LCC-HVDC systems. For VSC-HVDC systems, large ac capacitors are not needed for reactive-power compensation. However, weak-ac-system connections still represent more challenging operation conditions for VSC-HVDC systems due to the following reasons:

1. The filter-bus voltage is more sensitive to power variations of the VSC-HVDC link in weak ac systems. Thus, a weak-ac-system connection requires that the control system of the VSC-HVDC link must be less dependent on the stiffness of the filter bus voltage.

2. The SCR of the ac system imposes a theoretical limitation on the maximum power that the VSC-HVDC system is possible to transmit to or from the ac system. This limitation has traditionally been analyzed by the maximum power curve (MPC) for conventional LCC-HVDC systems. As it was discussed, such power limitations are basic characteristics of the ac system that are related to the operating-point-dependent zeros of the ac Jacobian transfer matrix. Moreover, for a VSC-HVDC link, the RHP zero of the ac Jacobian transfer matrix imposes a fundamental limitation on the achievable bandwidth of the control system.

3. The off-diagonal elements of the Jacobian transfer matrix are larger for weak-ac system connections, especially with high loadings. This problem is in common for vector current control and power-synchronization control, but it is more serious for vector current control. High off-diagonal elements imply more interactions between the active-power control and the alternating-voltage control.

Comparison of power-synchronization control and vector current control:

In this section, the dynamic performance of power-synchronization control and vector current control are compared for VSC-HVDC links connected to high-impedance weak ac systems. For simplicity, the impedance-

source system shown in Fig is assumed as the ac-network configuration.

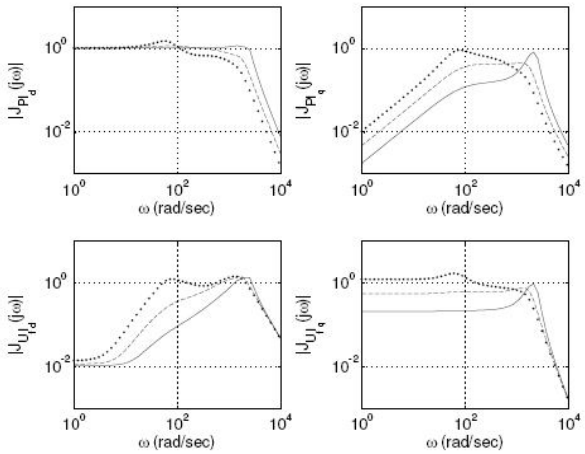

Fig. 3.1 Bode plots of the transfer functions of the Jacobian transfer matrix for vector current control with P = 0.0 p.u. (solid: SCR = 5.0, dashed: SCR = 2.0, dotted: SCR 1.0).

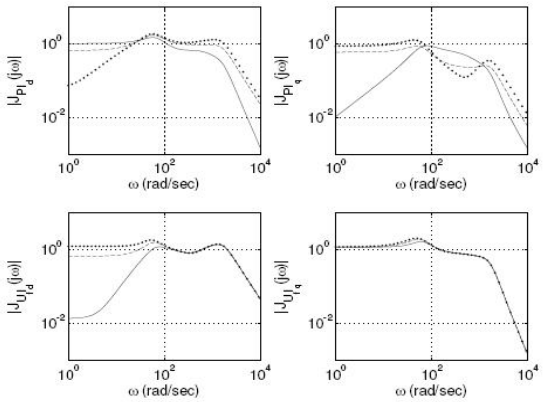

Fig. 3.2 Bode plots of the transfer functions of the Jacobian transfer matrix for vector current control with SCR = 1.0 (solid: P = 0.0 p.u., dashed: P = 0.5 p.u., dotted: P = 0.7 p.u.).

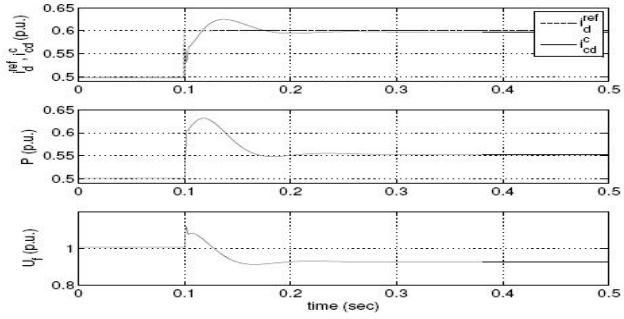

Fig. 3.3 Step response of id for vector current control at P = 0.0 p.u. with SCR = 1.0

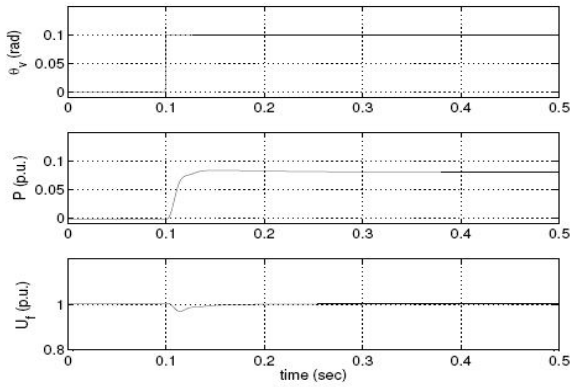

Fig. 3.4 Step response of id for vector current control at P = 0.5 p.u. with SCR = 1.0.

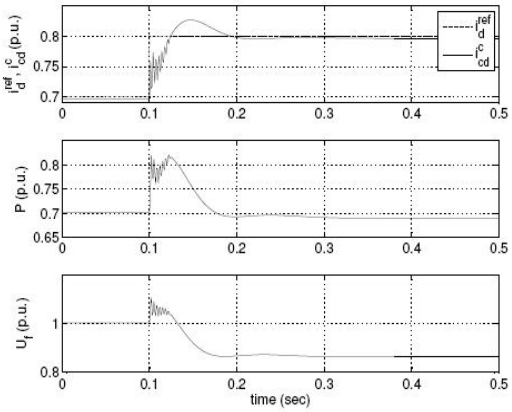

Fig. 3.5 Step response of id for vector current control at P = 0.7 p.u. with SCR = 1.0.

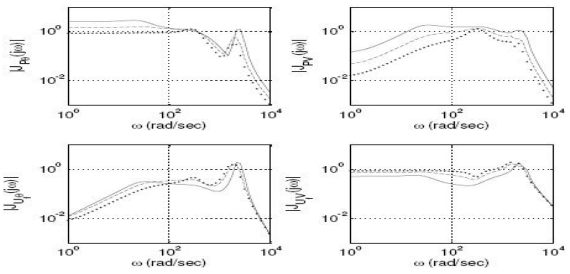

Fig. 3.6 Bode plots of the transfer functions of the Jacobian transfer matrix for power-synchronization control with P = 0.0 p.u. (solid: SCR = 5.0, dashed: SCR = 2.0, dotted: SCR 1.0).

Generally speaking, with power-synchronization control, the control system can maintain stable operation with load angle up to _u0 = 60◦, i.e., approximately 86% of the rated power, for VSC-HVDC links connected to ac systems with SCR = 1.0, whereas it is very difficult for vector current

control to operate even with 50% loading. However, if the connected ac system is strong, vector current control seems to be more advantageous than power-synchronization control.

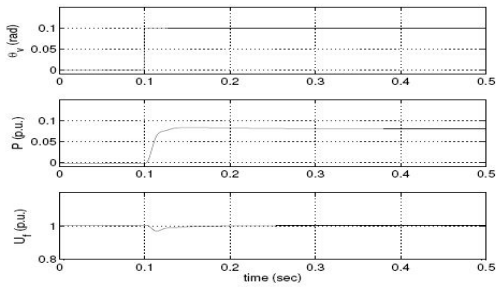

Fig. 3.7 Step response for power-synchronization control at P = 0.0 p.u. with SCR = 1.0.

IV. HVDC with low inertia AC Systems

General aspects of low-inertia ac systems:

In this chapter, various aspects of a VSC-HVDC link connected to another type of weak ac systems, i.e., low-inertia or island systems are investigated. Low-inertia systems are considered to have limited number of rotating machines in the system, or no rotating machine at all. It may also be the case when an HVDC link initially is connected to a large ac system, but comes into island operation due to tripping of critical ac lines to the large system, or black start after a blackout.

For the conventional LCC-HVDC system, the commutations of the converter valves depend on the ability of the ac system to maintain the required voltage and frequency. Therefore, the conventional LCC-HVDC system has a requirement on the minimum inertia of the connected ac system. Similar to the definition of SCR, which is defined as Where Hac (MW- s) is the total rotational inertia of the ac system and PdcN is the rated dc power. For a conventional LCC-HVDC link connected to an island system, an effective inertia constant, Hdc, of at least 2.0s to 3.0s is required for satisfactory operation. Synchronous condensers (SCs) have been the traditional means to increase the inertia of an island system. Since SCs also increase the short-circuit capacity of the ac system, the weak-ac-system problem of the conventional LCC-HVDC system, either low SCR or low inertia, can generally be solved by installation of SCs. However, SCs can substantially increase the investment and maintenance costs of an HVDC project.

In this respect, the VSC-HVDC technology has a clear advantage over the conventional LCC-HVDC technology. Different from the thyristor valves, where relatively stiff voltage and frequency of the ac system are pre-conditions for valve commutations, the VSC can produce its own alternating-voltage waveform independent of the ac system. Thus, a VSC-HVDC link can even be connected to a passive network with no other power source at all.

However, control of VSC-HVDC links connected to an island system is technically different from connected to a large ac system for the following reasons:

1. Due to the relatively limited number of power generating units in a typical island system, the VSC-HVDC link should participate in frequency control of the island system instead of applying constant power control.

2. An island system with low inertia is often of small geographic extent and the generators and loads are found electrically close to the converter station. More interactions are expected between the VSC-HVDC converter and other input devices, e.g., the risks of voltage-control hunting and SSTI with local synchronous generators are higher.

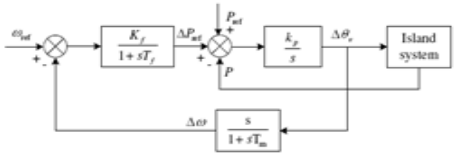

Fig.4.1 Frequency droop controller.

Controller design:

It is assumed that the VSC-HVDC link is connected to a strong system at the other converter station, which controls the direct voltage of the dc link constant disregarding the power variations of the converter connected to the island system. Thus, only the controllers of the converter station connected to the island system are discussed.

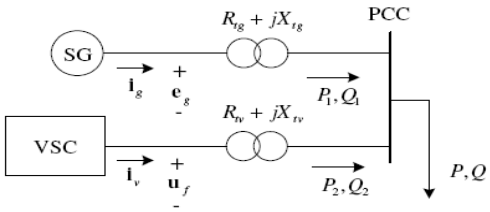

Fig. 4.2 Voltage droop control for parallel connected voltage-control units.

VSC-HVDC converter is using the so-called “load compensation”, which is a common solution for synchronous generators terminated at the same bus [32]. That is, instead of controlling the alternating voltage of the point-of-common-coupling (PCC) bus, the VSCHVDC converter and the synchronous generator both control voltages between their own terminal/filter-bus voltages and the voltage of the PCC to give droop characteristics to their alternating-voltage controls.

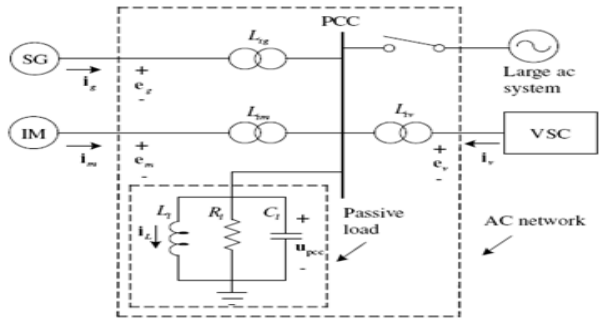

Fig. 4.3 A typical island system

.

Where the compensation ratios kg and kc are typically chosen between 50% and 80%. By adjusting the compensating ratios, the reactive-power sharing between the VSC-HVDC converter and the synchronous generator are re-distributed.

Dynamic D-Q Model

The following assumptions are made to derive the dynamic model:

(i) uniform air gap;

(ii) balanced rotor and stator windings, with sinusoidal distributed mmf; The dynamic performance of an ac machine is somewhat complex because the three-phase rotor windings move with respect to the three-phase stator windings as shown in Figure 3.2(a).

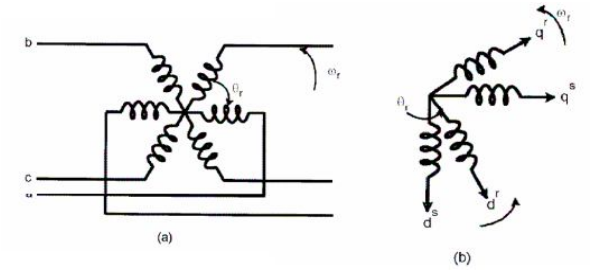

Fig .4.4 (a) Coupling effect in three-phase stator and rotor windings of motor,(b) Equivalent two-phase machine

Basically, it can be looked on as a transformer with a moving secondary, where the coupling coefficients between the stator and rotor phases change continuously with the change of rotor position θ_r correspond to rotor direct and quadrature axes. The machine model can be described by differential equations with time-varying mutual inductances, but such a model tends to be very complex. Note that a three-phase machine can be represented by an equivalent two-phase machine as shown in Figure 4.4(b), where $d^s \sim q^s$ correspond to stator direct and quadrature axes, and $d^r \sim q^r$ torque expressions can be derived easily as follows:

$$T_e = \frac{3}{2}\left(\frac{P}{2}\right)\psi_{dm} i_{qs} - \psi_{qm} I_{ds}$$

$$T_e = \frac{3}{2}\left(\frac{P}{2}\right)\psi_{ds} i_{qs} - \psi_{qs} I_{ds}$$

$$T_e = \frac{3}{2}\left(\frac{P}{2}\right)L_m (i_{qs} i_{dr} - i_{ds} i_{qr})$$

$$T_e = \frac{3}{2}\left(\frac{P}{2}\right)(\psi_{dr} i_{qr} - \psi_{qr} I_{dr})$$

The composite system is of the fifth order and nonlinearity of the model is evident. Figure 4.8 shows the block diagram of the machine model along with input voltage and output current transformation

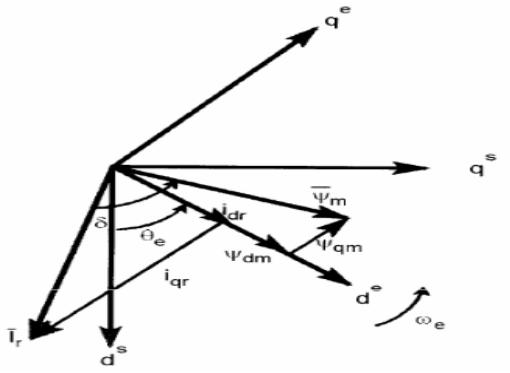

Fig 4.5 Flux and current vectors d^e - q^e frame

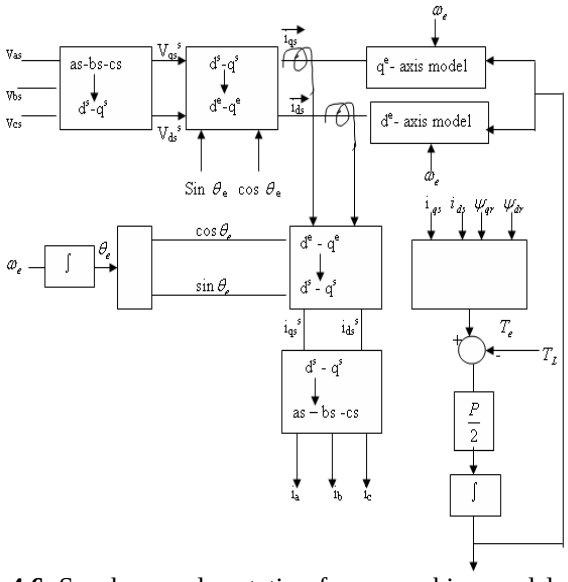

Fig 4.6. Synchronously rotating frame machine models with input voltage and output current transformations

Where $v_{qr} = v_{dr} = 0$. The variables appear as sine waves in steady state with sinusoidal inputs.

$$T_e = \frac{3}{2}\left(\frac{P}{2}\right)\psi^s_{dm} i^s_{qr} - \psi^s_{qm} i^s_{dr}$$

$$T_e = \frac{3}{2}\left(\frac{P}{2}\right)\psi^s_{dm} i^s_{qs} - \psi^s_{qm} i^s_{ds} \quad (4.48)$$

$$0 = R_r i^s_{qds} + \frac{d}{dt}\psi^s_{qdr} - j\omega_r \psi^s_{qdr} \quad (4.62)$$

$V^s_{qds} = V^s_{qs} - jV^s_{ds}$, $\psi^s_{qds} = \psi^s_{qs} - j\psi^s_{ds}$, $i^s_{qds} = i^s_{qs} - ji^s_{ds}$, $\psi^s_{qdr} = \psi^s_{qr} - j\psi^s_{dr}$ etc. The complex equivalent circuit in stationary frame is shown in Figure 4.10(a). Often, a per phase equivalent circuit with CEMF ($\omega_r \overline{\psi}_r$) and sinusoidal variables is described in the form of Figure 4.10(b) omitting the parameter L_m.

$$0 = R_r i_{qr} + \frac{1}{\omega_b}\frac{dF_{qr}}{dt} + \frac{(\omega_e - \omega_r)}{\omega_b}F_{dr} \quad (4.68)$$

$$0 = R_r i_{dr} + \frac{1}{\omega_b}\frac{dF_{dr}}{dt} + \frac{(\omega_e - \omega_r)}{\omega_b}F_{qr} \quad (4.69)$$

where it is assumed that vqr = vdr = 0.

Multiplying equations (4.32) - (4.37) by ω_b on both sides, the flux linkage expressions can be written as

$$v_{ds} = \frac{R_s}{X_{ls}}(F_{ds} - F_{dm}) + \frac{1}{\omega_b}\frac{dF_{ds}}{dt} - \frac{\omega_e}{\omega_b}F_{qs} \quad (4.93)$$

$$0 = \frac{R_r}{X_{lr}}(F_{qr} - F_{qm}) + \frac{1}{\omega_b}\frac{dF_{qr}}{dt} + \frac{(\omega_e - \omega_r)}{\omega_b}F_{dr} \quad (4.94)$$

$$0 = \frac{R_r}{X_{lr}}(F_{dr} - F_{dm}) + \frac{1}{\omega_b}\frac{dF_{dr}}{dt} + \frac{(\omega_e - \omega_r)}{\omega_b}F_{qr} \quad (4.95)$$

which can be expressed in state-space form as

$$\frac{dF_{qs}}{dt} = \omega_b\left[v_{qs} - \frac{\omega_e}{\omega_b}F_{ds} - \frac{R_s}{X_{ls}}(F_{qs} - F_{qm})\right] \quad (4.96)$$

$$\frac{dF_{ds}}{dt} = \omega_b\left[v_{ds} + \frac{\omega_e}{\omega_b}F_{qs} - \frac{R_s}{X_{ls}}(F_{ds} - F_{dm})\right] \quad (4.97)$$

$$\frac{dF_{qr}}{dt} = -\omega_b\left[\frac{(\omega_e - \omega_r)}{\omega_b}F_{dr} + \frac{R_r}{X_{lr}}(F_{qr} - F_{qm})\right]$$

$$\frac{dF_{dr}}{dt} = -\omega_b\left[-\frac{(\omega_e - \omega_r)}{\omega_b}F_{qr} + \frac{R_r}{X_{lr}}(F_{dr} - F_{dm})\right]$$

$$T_e = \frac{3}{2}\left(\frac{P}{2}\right)\frac{1}{\omega_b}(F_{ds}i_{qs} - F_{qs}i_{ds})$$

V. VOLTAGE SOURCE CONVERTER

VSC system connected to weak grid

When a VSC is connected to a weak grid, the voltage at the point of common connection (PCC) will vary and become a function of several variables: the grid voltage behind the impedance describing the grid, the grid current and the short-circuit parameters of the grid. The transformation angle q (*t*) is used to transform grid currents and grid voltages at the PCC to the *dq*-coordinate system needed in the vector current controller. The reference voltages from the current controller are transformed back to three-phase values.

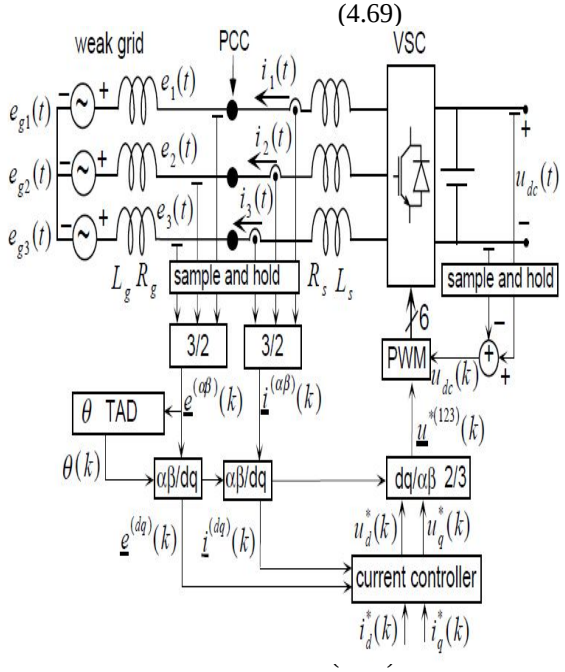

Fig 5.1: VSC system diagram consisting of the VSC, the grid filter, the weak grid and the vector current controller

Tad Based On Low-Pass Filtering Of Grid Voltage

A simple method is obtained by low-pass filtering (LP-filtering) the grid voltage vector and the method is denoted by LP-TAD. A first-order Butterworth filter is utilized. The cut-off frequency is tuned to between 0.1 and 25 Hz. The phase lag of a first-order filter depends on the grid frequency and the cut-off frequency. The desired phase lag of 90° occurs at an infinte frequency. The phase lag will, thus, be less than 90° due to the grid frequency of 50 or 60 Hz. The phase lag increases when the cut-off frequency decreases. By using a coordinate transformation, the LP-filtered grid voltage vector can be rotated by an angle Dq so that the phase lag becomes 90°. Fig.5.3 shows a diagram of the LP-TAD.

(4.96) finally, from equation (4.49)

(4.97) Equations (4.93) - (4.97), descri

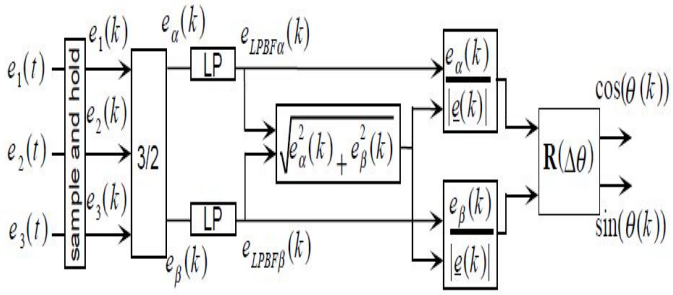

Fig5.3: Diagram of the LP-TAD.

Two calculated step responses to a 10° phase-shift in the grid voltage vector are presented in Figs.5.4 and 5.5. The grid frequency is 50 Hz and the cut-off frequency is 0.5 Hz or 5.0 Hz. Different steady state angle errors, due to different cut-off frequencies, can be observed in Figs. 5.4 and 5.5. The phase-shift errors are approximately 1° and 6° for cut-off frequencies 0.5 and 5 Hz, res-pectively. Unfortunately, the detector characteristics are undamped and oscillate. The damping is increased by a higher cut-off frequency. This behavior makes the detector unsuitable for applications where phase jumps can occur. In practice, every grid connected VSC is exposed to grid phase jumps due to short circuits in other nodes of the grid.

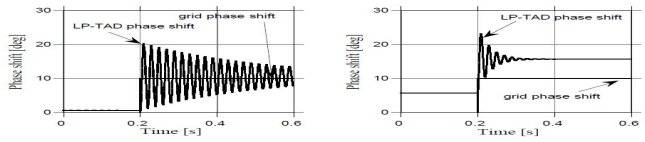

Fig 5.4: LP-TAD phase shift response to a grid phase shift step. The cut-off frequency is 0.5 Hz.

Fig 5.5: LP-TAD phase shift response to a grid phase shift step. The cut-off frequency is 5 Hz.

B) The Influence of Grid Voltage Harmonics

The gain of the SVF-TAD for grid voltage harmonics is determined by two simulations

Performed by injecting a 10 % voltage harmonic component of the 5th or 11th order. The grid frequency is 50 Hz and the sample time is 200 ms. The gain from the input to the out-put of the SVF for the harmonic voltage components is displayed in Fig.5.8. The forgetting factor varies between 0.9 and 0.999. The gain of the voltage harmonics decreases as the forgetting factor is reduced. The variance of the grid angle deviation displays how much voltage harmonics affect theSVF. Fig.5.9 shows this variance when the forgetting factor varies between 0.9 and 0.999. The variance of the SVF output angle deviation is lower than 0.01°2 when the forgetting factor is higher than 0.99. The SVF handles the distorted grid successfully. The 5th and 7th voltage harmonics have the same gain factor (and the same is valid for the 11th and 13th harmonics) due to the use of the rotating coordinate system.

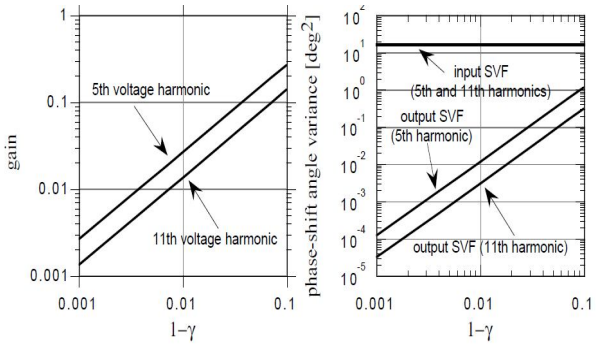

Fig 5.8: The gain from the harmonic grid voltage component to the harmonic voltage component after SVF.

Fig5.9: Variances of the grid phase shift and the SVF-TAD phase shift.

Tad Based On Space Vector Filtering For Varying Grid Frequency

The SVF-TAD can be adapted to a varying grid frequency and is then called extended SVF-TAD. A phase shift occurs when the grid frequency varies and the forgetting factor of the SVF is high. If the frequency of the SVF is higher than the grid frequency, The Q-vector is fed to a discrete PI-regulator, which is connected to the SVF, as shown in Fig.5.10. The PI regulator output is the estimated frequency deviation.

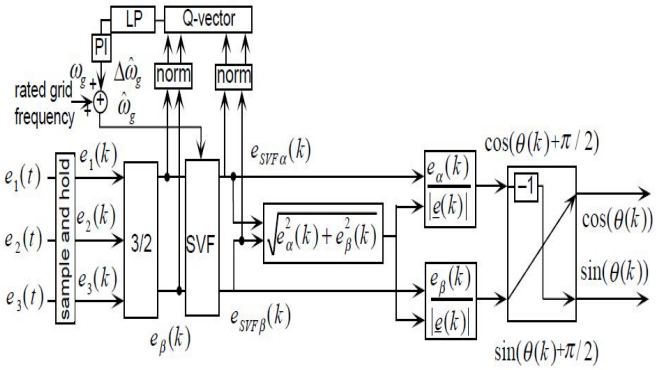

Fig 5.10: Diagram of the extended SVF-TAD.

Compared with the basic SVF-TAD, the proposed non-linear filter for fluctuating frequency is difficult to analyses. Several parameters must be determined to get a good filter performance. To minimize the influence of the voltage harmonics on the grid, a 150 Hz first-order LP-filter is placed between the Qvector block and the discrete PI-regulator. The problem of tuning the discrete PI-regulator is the conflict between frequency tracking

and sensitivity to voltage harmonics. The time constant of the PI-regulator is set to one grid period. The simulation parameters, which have been selected by an iterative process to decouple the SVF and the frequency regulator, are listed in Table 1.

TABLE 1

PARAMETERS OF EXTENDED SVF-TAD.

T_S = 200 µs	k_{PSVF} = –4.0
γ = 0.99	k_{ISVF} = –0.04

DC filter circuits

Harmonic voltage which occur on the DC side of a converter station cause AC currents which are superimposed on the direct current in the transmission line. These alternating currents of higher frequencies can create interference in neighboring telephone systems despite limitation by smoothing reactors. DC filter circuits, which are connected in parallel to the station poles, are an effective tool for combating these problems. The configuration of the DC filters very strongly resembles the filters on the AC side of the HVDC station.

VI. SIMULATION RESULTS

Simulation Diagram:

Below Diagram shows synchronization process with VSC which is used in HVDC system as mentioned in paper.

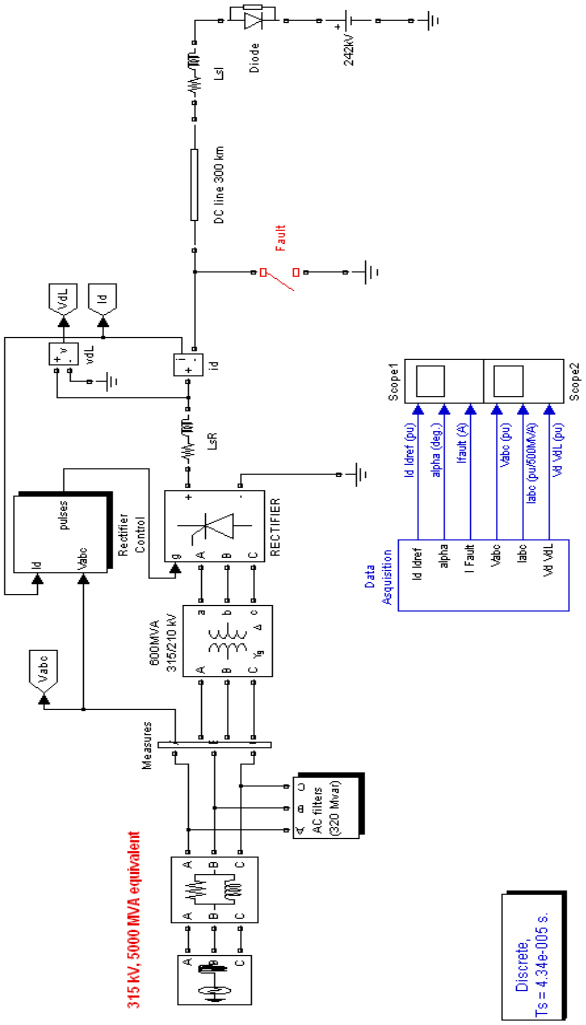

Fig: 6.1 synchronization in HVDC

Operation:

A 500 MW (250 kV, 2 kA) DC linter connection is used to transmit power from a 315 kV, 5000 MVA AC network. The network is simulated by a LLR damped equivalent (impedance angle of 80 degrees at 60 Hz and 3rd harmonic). The converter transformer and the rectifier are modeled respectively with the Universal Transformer and Universal Bridge blocks the converter is a 6-pulse rectifier. It is connected to a 300 km distributed parameter line through a 0.5 H smoothing reactor LsR. The inverter is simulated by a simple DC voltage source in series with a diode and smoothing reactor LsI. The reactive power required by the converter is provided by a set of filters (C bank plus 5th, 7th and high pass filters; total 320 Mvar). A circuit breaker allows applying a DC line fault on the rectifier side. The control system uses two main blocks: the Synchronized 6-pulse generator of the Extras/Control library and a PI Current Regulator. The whole control system is discretized (Sample time = 1/360/64 = 43.4 us).The DC line current at the output of the rectifier is compared with a reference. The PI regulator tries to keep the error at zero and outputs the alpha firing angle required by the synchronizing unit. Inputs 3 and 4 of the current regulator allow to bypass the regulator action and to impose the alpha firing angle.

Sub-System Circuits:

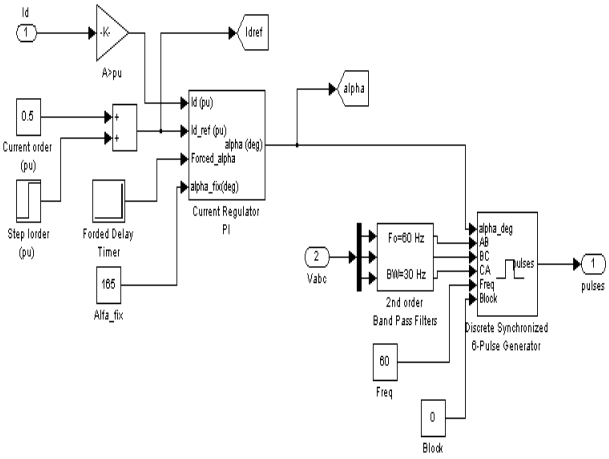

6.2. Measuring unit system

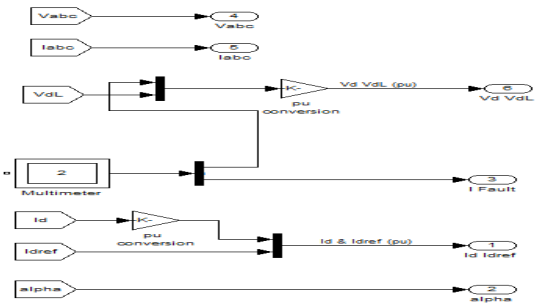

Fig: 6.3. Measuring units of system

Results:

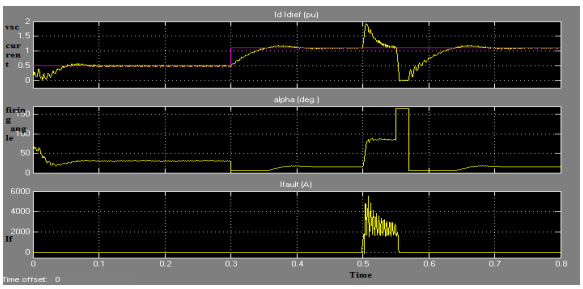

Fig: 6.4. Current waveforms

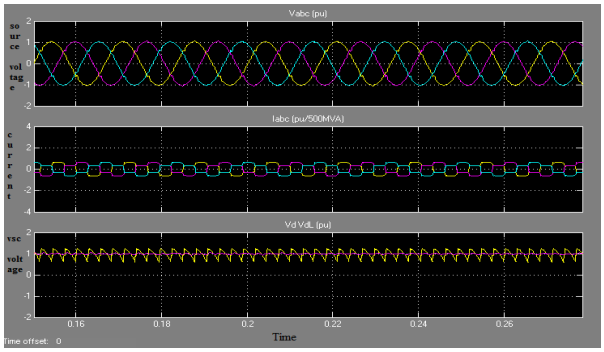

Fig: 6.5 Voltage related waveforms HVDC current wave form:

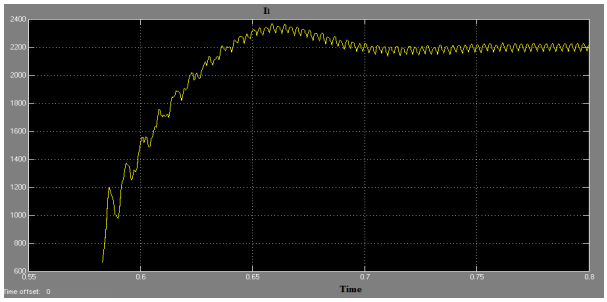

Fig: 6.6 HVDC Line current

The concept of power synchronization is proposed for control of grid-connected VSCs. The proposed control is general for grid-connected VSCs, but may be of most importance for VSC-HVDC connected to weak ac systems. By using the power-synchronization control method, VSC-HVDC operates almost in the same way as a synchronous machine. Therefore, in principle, it has no requirement on the short-circuit capacity of the ac system to be connected. On the other hand, VSC-HVDC gives the weak ac system strong voltage support, just like a normal synchronous machine does.

However, a weak ac system connection still represents a more challenging operating condition for VSC-HVDC than a strong ac system connection due to the relatively higher load angles. Thus, it is recommended that VSC-HVDC shall run with a control system having a lower bandwidth when connected to a very weak ac system in order to maintain a safe stability margin.

VII. CONCLUSION

PWM-based VSC-HVDC systems show many advantages compared to the thyristor based LCC-HVDC system. One prominent feature is that the VSC-HVDC system has the potential to be connected to very weak ac systems where the LCC-HVDC system has difficulties. In this thesis, the modeling and control issues for VSC-HVDC links connected to weak ac systems are investigated.

In order to fully utilize the potential of the VSC-HVDC system for weak-ac-system connections, a novel control method, i.e., power-synchronization control, for grid-connected VSCs is proposed. A grid-connected VSC using power-synchronization control basically resembles the dynamic behavior of a synchronous machine. However, due to the technical requirements for a VSC-HVDC link and various limitations of VSC valves, additional control functions are required to deal with various practical issues during operation. Such control functions include:

1. A high-pass current control function to damp various resonances in ac systems.
2. A current limitation function to ride through ac-system faults.
3. A bumpless-transfer scheme for switching the synchronization input of the VSC, and an anti-windup scheme for alternating-voltage control.
4. A negative-sequence current controller to mitigate unbalance valve currents in the steady state or during unbalanced ac-system faults.

By the comparison performed in the thesis, it is shown that power-synchronization control is superior to the traditional vector current control for VSC-HVDC links connected to weak ac systems.

FUTURE SCOPE

The following is a list of possible future work:

1. Power-synchronization control is a feasible control system for any grid-connected VSC. Another possible application is control of STATCOMs with energy storage. By using power-synchronization control, the STATCOM is able to operate with various challenging operating conditions
2. By using power-synchronization control, the SCR of the ac system is no longer a limiting factor for VSC-HVDC links connected to weak ac systems. However, the variation of SCRs, i.e., model uncertainty, is still a challenge. Besides the robust control methods proposed in the thesis, other possible solutions to deal with model uncertainties are

1. Adaptive control. 2. Online detection of the SCR of the ac system.

3. The losses of the VSC valves have been neglected in the linear models in the thesis. However, it was shown by frequency-scanning results that the representation of the valve losses in linear models has an importance if dc resonances are of concern The structure proposed for interconnecting two very weak ac systems has a possibility to be simplified. A possible simplification is to remove the power-synchronization control loop but to use the direct-voltage control to supply the synchronization input to the VSC instead. Such a modification has the potential to improve the response time of the VSC-HVDC link and reduce the dc-capacitance requirement.

4. The modeling concept of the ac Jacobian transfer matrix is useful for studying the interactions of high power-electronics devices located in the vicinity, e.g., multi in feed HVDC links, interactions between HVDC links and FACTS devices, etc.

APPENDIX

A. Parameters of the VSC-HVDC System table list the VSC-HVDC system parameters.

VSC-HVDC SYSTEM PARAMETERS

Rated apparent power S_{sys}	350.0 MVA	1.0 p.u.
Rated (base) voltage U_b	195.0 kV	1.0 p.u.
Maximum valve current I_{max}	1.12 kA	1.08 p.u.
Phase reactor inductance	0.052 H	0.15 p.u.
Phase reactor resistance	0.06 Ω	0.0055 p.u.
Converter transformer rating	380.0 MVA	
Converter transformer ratio	195 kV/400 kV	
Transformer leakage reactance	12%	0.11 p.u.
Direct voltage v_{dc}	±150.0 kV	1.0 p.u.
DC capacitor	114 μF	
System frequency f	50 Hz	
Switching frequency f_{sw}	1650 Hz	

REFERENCES

[1]. Fei Wang, Mohamed C. Benhabib, Jorge L. Duarte, and Marcel A. M. Hendrix ,"High Performance Stationary Frame Filters for Symmetrical Sequences or Harmonics Separation Under a Variety of Grid Conditions" IEEE ©2009.

[2]. L. Zhang, L. Harnefors, and P. Rey, "Power system reliability and transfer capability improvement by VSC-HVDC (HVDC light)," in *Cigr´e Regional Meeting*, Tallin, Estonia, 2007.

[3]. P. Fischer, "Modelling and control of a line-commutated HVDC transmission system interacting with a VSC STATCOM," Ph.D. dissertation,Royal Inst. Technol., Stockholm, Sweden, 2009.

[4]. S. J. Ahn, J. W. Park, I. Y. Chung, S. I. Moon, S. H. Kang, and S. R.Nam, "Power-Sharing Method of Multiple Distributed Generators Considering Control Modes and Configurations of a Microgrid," *IEEE Trans. Power Delivery*, vol. 25, pp. 2007-2016, 2010.

[5]. L.Harnefors, M. Bongiornos, and S. Lundberg, "Input-admittance calculation and shaping for controlled voltage-source converters," *IEEE Trans. Ind. Electron.*, vol. 54, no. 6, pp. 3323–3334, December 2007.

[6]. Nader Anani1, Omar Al-Kharji Al-Ali1, P. Ponnapalli1, S.R. Al-Araji2 and M. Al-Qutayri2, Synchronization of a single-phase wind energy generator with the low-voltage utility grid" Las Palmas de Gran Canaria (Spain), 13th to 15th April, 2010

[7]. D. N. Zmood, D. G. Holmes, and G. H. Bode, "Frequency-domain analysis of three phase linear current regulators," *IEEE Trans. Ind. Applicat.*, vol. 37, no. 2, pp. 601– 610, March/April 2001.

***Banothu Thavuworking as Asst. Professor department of EEE, Daripally Anantha Ramulu College of Engg & Tech, Kuravi Road, Khammam Dist, Andhra Pradesh, Pin.Code: 507003,* e-mail: tej.abhinaik@gmail.com**

Thuraka Rajendraworking as a Asst. Professor, department of EEE, Daripally Anantha Ramulu College of Engg & Tech, Kuravi Road, Khammam Dist, Andhra Pradesh, and Pin.Code: 507003 e-mail: : rajendraturaka@gmail.com

Ravi Bukya working as a Asst. Professor, , department of EEE, Daripally Anantha Ramulu College of Engg & Tech, Kuravi Road, Khammam Dist, Andhra Pradesh, Pin.Code: 507003, e-mail: naiks006@gmail.com

M. Maheswararao[4] , Asst. Professor, department of EEE, Swarna Bharathi Institute of Science and Technology, Khammam. (Dist) Andhra Pradesh. Pin: 507001, e-mail: mahi214@gmail.com

Design of Intelligent Solar Power System Using PSO Based MPPT with Automatic Switching between ON grid and OFF Grid Connections

K.GAYATHRI, S.GOMATHI and T.SUGANYA

Abstract *– Green energy generation is the most emerging research area in present scenario. Technologies like solar, wind, tidal are classified as renewable resources because of their sustained availability. PV systems are gaining much interest because of their increased efficiency. Solar energy fluctuates with the intensity of the radiated light. As a result the output power of the panel varies. This varying supply can neither be connected to grid nor used for load. Hence to obtain a maximum power, maximum power point technology (MPPT) is proposed. Existing algorithms like Perturb and Observe technique and Incremental Conductance proved to be less efficient in finding the optimal solution. Hence soft computing technique called Particle Swarm optimization algorithm (PSO) is proposed to find the maximum power. The proposed MPPT control algorithm is developed in MATLAB, which optimizes the panel voltage. Generated solar energy usually requires conversion to an alternating quantity, which is achieved using inverters. A three level inverter is implemented to obtain a harmonic less AC output. Simulation results show that the proposed algorithm is more efficient than the existing techniques.*

Keywords: Soft Computing technique, Particle Swarm optimization algorithm, Maximum power point tracking, three level inverter, Buck Boost DC-DC converter.

I. INTRODUCTION

The global energy consumption is increasing everyday due to increased population and advanced technologies. But due to unreliable electrical system, our country is facing severe power shortage problems. India and China are the two countries responsible for major consumption of energy. Due to Global warming concerns, there is a strong need to deploy clean energy sources and implement energy efficient solutions to meet future energy demand. Energy engineers all over the world are focusing on solar projects to increase the generation capacity. A solar system is made up of solar modules. Number of cells combines to form a module and these modules are in turn connected to form the PV system. The output DC voltage of the panel is then converted to desirable AC voltage for feeding excess power to the grid. Despite of advanced technologies, a grid connected PV system is always subjected to several complexities. Maximum Power Tracking algorithms were developed in past methodologies [1] to obtain continuous constant power. Comparison of various conventional MPPT algorithms is discussed in [2].

K.GAYATHRI, S.GOMATHI and T.SUGANYA are UG Scholar, Department of EEE, KPR Institute of Engineering and Technology, Coimbatore, India Email: gaynks@gmail.com, gomseee3@gmail.com, sugueee29@gmail.com.

Soft computing based algorithms were recently developed to obtain the global optimal solution under varying environmental conditions. The PSO [3] method is a simple and effective meta heuristic approach for obtaining optimal solution. It requires assignment of random weights and velocity vector. The proposed Particle Swarm Optimization algorithm (PSO) is a swarm behavior based technique and is relatively easier to develop.

The proposed work concentrates on designing DC-DC converter operated through the MPPT algorithm and a three level inverter to obtain AC supply. Section II explains PSO algorithm and its steps to find the optimal value. Section III explains the implementation of PSO technique to find the maximum power. Section IV the adopted converter and inverter topologies are discussed..

II. PARTICLE SWARM OPTIMIZATION ALGORITHM

Particle swarm optimization was first developed by Kenney and Eberhart [4].PSO is used to solve power system optimization problems. It provides optimal solution to problems like Economic load dispatch, Unit commitment, optimal reactive power dispatch etc., PSO is based on swarm intelligence to solve constrained optimization problems. The initial set of solution is called population and each member in the population is called as swarms [5]-[7].

PSO uses a initial solutions called swarms which are generated at random.

$$X=[X_1, X_2, X_3 \ldots Xn]$$

These particles move in the search space to find a good optimal solution. Particles find their search direction by using social and cognitive information. The best position that a particle has found is called pbest and the best position that any particle found is called gbest. The new position of a particle is found by the equation

$$X(t+1)=X(t)+V(t+1) \quad (2.1)$$

The formula to calculate the new velocity $V_i(t+1)$ as follows.

$$V_i(t+1) = w * V_i(t) + c_1 * rand(1) * (x_{pbesti} - x_i) + c_2 * rand(1) * (x_{gbesti} - x_i) \quad (2.2)$$

where w is the inertia weight, x_{pbesti} is the particle's pbest, x_{gbesti} is the position of the leader, c1 and c2 are the acceleration constants (user-defined) to control the influence of the cognitive and social elements respectively, rand() is a function that generates a uniform-distributed random real number between 0 and 1.

III. PSO BASED MPPT ALGORITHM

PSO based MPPT algorithm is developed to track the maximum power from the PV system. The output voltage and current from the panel varies according to insulation level. Since solar energy is time variant, a control algorithm

I_{ph}=photon current
I_{sat}=cell reverse saturation current
q = electron charge (1.6×10^{-19} C)
k = Boltzmann's constant (1.38×10^{-23} J/K)
A = ideality factor
I_{sh} = Short circuit current
V_{oc} = Open circuit voltage
T_{ref} = Reference temperature (K)
T = solar cell temperature (K)
S_{rad} = solar cell radiation
K = short circuit current temperature co efficient

Once value of current is computed, the corresponding voltage value that gives maximum power is computed from PSO. It finds the optimal voltage value to be produced by the The block diagram of the proposed model is shown in the Figure 1.

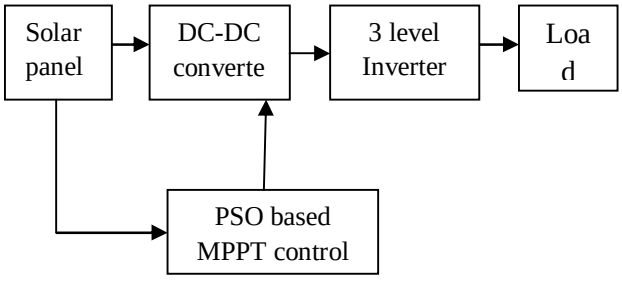

Figure 1: Block diagram for proposed model

Based on the steps discussed above, the algorithm finds the optimal V value that maximizes the objective function. The controller adjusts the duty ratio of Buck-Boost converter to get the required output voltage. Thus whole PV system's maximum power is tracked all the time and converted to desired AC value suitable for the load.

IV. POWER ELECTRONIC CIRCUITRY

The buck boost converter can either bucks or boosts the panel's DC voltage. The advantage of proposed inverter topology is that it produces AC quantity with reduced harmonic content and low switching losses. The converter is controlled through MPPT controller that is coded with PSO. The output voltage of a converter is adjusted as per the duty cycle. The output of the PV panel is connected to the inverter is developed to keep in track the value of power which is maximum irrespective of time [8]. The following expressions prove that the panel's output current is directly proportional to the incident radiation and temperature.

$$I = n_p I_{ph} - n_p I_{sat}[\exp\left(\frac{qV}{kATn_s}\right) - 1] \quad (3.1)$$

$$I_{ph} = [I_{sh} + \frac{K}{1000}(T - T_{ref})]S_{rad} \quad (3.2)$$

$$I_{sat} = I_{ph}/(\exp((V_{oc} * q)/kAT) - 1) \quad (3.3)$$

n_p =number of cells in parallel connection
n_s = number of cells in series connection

Buck-Boost converter based on power value. The population set containing voltage values is initially chosen.

$$V = \{V_1, V_2, V_3, \ldots \ldots \ldots \ldots V_{oc}\} \quad (3.4)$$

The fitness function is maximization function expressed as

$$f(x) = \max(P) \quad (3.5)$$

Where $P = (V * I)$
Thus

$$f(x) = \max(V * I) \quad (3.6)$$

via DC-DC buck boost converter. The buck boost converter's duty cycle is adjusted as per the MPPT algorithms optimal voltage value. Several converter topologies were used in the past decades [9]. Conventional boost or buck converters employ hard switching. This increases switching losses and thus reduces the overall efficiency [10]. Two stage systems consist of cascaded connections with increased number of switches. Power loss is high in such topologies.

The obtained DC voltage should be converted to a corresponding AC quantity. A general overview of different types of PV inverters is given in [11] and [12]. Here three level inverter configuration is employed for the conversion process. Switching losses are eliminated to a greater extent. Comparatively higher or lower output is obtained as per the load requirements. The proposed system is designed and implemented using three level inverter and it is simulated using MATLAB software

V. SIMULATION RESULTS

The algorithm and simulation circuits are developed in Mat lab environment. The efficiency is tested using different number of swarms and iterations. Convergence of the algorithm depends on velocity and random factors. Various optimal values for a module with 36 cells, open circuit voltage 21.75V and short circuit current 4.75A is tabulated below. PSO traps the global optimal value when radiation level is different due to environmental conditions. The various values of optimal voltage and power for each iteration are tabulated in the table 1, 2 and 3.

Table 1: Maximum power of the panel for radiation=300 W/m^2, I=1.0689Aand Table T: population=100 particles

Iterations	Optimal voltage (Volts)	Power (Watts)
30	16.7262	17.8786
60	16.7266	17.8787
100	16.7266	17.8786

Table 2: Maximum power of the panel for radiation=500 W/m^2,I=1.7849A and population=100 particles

Iterations	Optimal voltage (Volts)	Power (Watts)
30	17.2851	30.8515
60	17.2849	30.8514
100	17.2849	30.8514

Table 3: Maximum power of the panel for radiation=750 W/m^2 I=2.6812A and population=100 particles

Iterations	Optimal voltage (Volts)	Power(Watts)
30	17.7406	47.5655
60	17.7406	47.5655
100	17.7406	47.5655

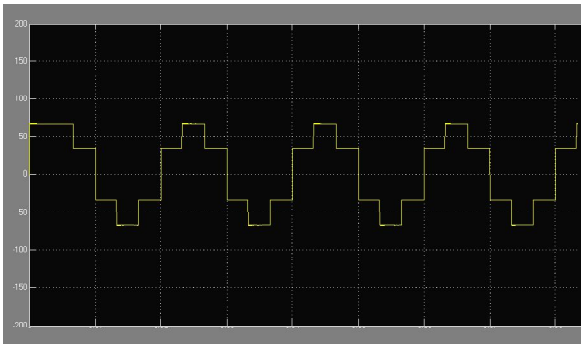

Fig 2: Current waveform of 3 level inverter

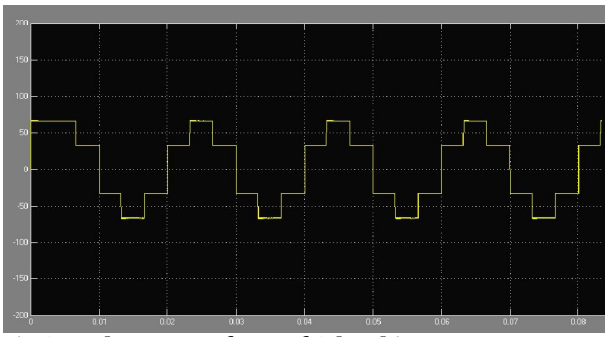

Fig 3: Voltage waveform of 3 level inverter

Current and voltage waveforms of the proposed inverter circuit are shown in Figure 2 and Figure 3. Circuit shows that less number of switching devices is used which reduces the switching losses. Thus the overall efficiency of the solar system is increased

VI. CONCLUSION

An optimization algorithm called Particle swarm Optimization Algorithm is proposed to obtain maximum power from the panel. The proposed algorithm effectively tracks the global optima of power value. Efficiency of the system is further increased by three level inverter configurations. The topology proves to be more efficient in both cost and gain. Losses are highly reduced with proposed inverter model. Existing MPPT algorithms like Perturb & Observe, Incremental Conductance fails to track the optimal value under partial shaded conditions. The proposed optimization technique overcomes this problem. Thus overall efficiency is improved with the proposed techniques.

REFERENCES

[1]. Nicola Femia, Giovanni Petrone, Giovanni Spagnuolo, "Optimization of Perturb and Observe Maximum Power Point Tracking Method" IEEE Transactions on Power Electronics, volume. 20, no. 4, July 2005.

[2]. Trishan Esram and Patrick L.Chapman, "Comparison of Photovoltaic Array Maximum Power Point Tracking Techniques" IEEE Transactions on Energy Conversion, volume. 22, no. 2, June 2007.

[3]. Masafumi Miyatake, Mummadi Veerachary, Hideyoshi Ko, "Maximum Power Point Tracking of Multiple Photovoltaic Arrays: A PSO Approach" IEEE Transactions on Aerospace and Electronic Systems, volume. 47, no. 1 January 2011.

[4]. J. Kennedy and R. Eberhart, "PSO optimization," in Proceedings, IEEE International Conference on Neural Networks, volume. IV, 1995, pp. 1941–1948.

[5]. M.Clerc and J.Kennedy:"The Particle Swarm Explosion, Stability, and Convergence in a Multi dimensional Complex Space", IEEE Transactions Evolutionary Computation,Volume .6,No.1, pp.58–73,2002.

[6]. I.C.Trelea:"The Particle Swarm Optimization Algorithm: Convergence Analysis and Parameter Selection",Information Processing Letters, Volume .85, No.6, pp.317–325,2003.

[7]. F.BerghandA.P.Engelbrecht:"A Study of Particle Swarm Optimization Particle Trajectories",Information Sciences, Volume.176, No.8, pp.937–971, 2006.

[8]. Liang Rui Chen, Chih Hui Tsai, Yuan Li Lin, and Yen Shin Lai "A Biological Swarm Chasing Algorithm for Tracking the PV Maximum Power Point" IEEE Transactions on Energy Conversion, volume. 25, no. 2, June 2010

[9]. B.G.Dobbs, P.L.Chapman, "A Multiple Input DC-DC Converter Topology," IEEE Power Electron. Lett., volume. 1, no. 1, pp. 6–9, Mar. 2003.

[10]. Billy M. T. Ho, Henry Shu Hung Chung, "An Integrated Inverter with Maximum Power Tracking for Grid Connected PV Systems" IEEE Transactions on Power Electronics, volume. 20, no. 4, July 2005.

[11].S.B.Kjaer, J.K.Pedersen, and F.Blaabjerg, "A review of single phase grid connected inverters for photovoltaic modules," IEEE Transactions on Industrial Applications., volume. 41, no. 5, pp. 1292–1306, Sep/Oct. 2005.

[12]. S.Daher, J.Schmid, and F.L.M.Antunes, "Multilevel inverter topologies for standalone PV systems," IEEE Transactions on Industrial Electronics, volume. 55, no. 7, pp. 2703–2712, July. 2008.

Analysis of Five Level Inverter

Mr. Ambadas. S. Mane and Mr. Vijay. B. Suryawanshi

ABSTRACT : The power electronics device which converts DC power to AC power at required output voltage and frequency level is known as inverter. Multilevel inverter as compared to single level inverters has advantages like minimum harmonic distortion, reduced Electromagnetic interference (EMI)/Radio frequency interference (RFI) generation and can operate on several voltage levels. A multi-stage inverter is being utilized for multipurpose applications, such as active power filters, static var compensators and machine drives for sinusoidal and trapezoidal current applications. The drawbacks are the isolated power supplies required for each one of the stages of the multi converter and it's also lot harder to build, more expensive, harder to control in software. Some industrial applications of inverters are for adjustable speed ac drives, induction heating, standby aircraft power supply, Uninterruptible Power Supply for computers, High Voltage DC transmission lines etc. The DC power input to the inverter is obtained from an existing power supply network or from a rotating alternator through a rectifier or a battery, fuel cell, photovoltaic cell etc.

Keywords- Electromagnetic interference (EMI), Multilevel inverter, Photovoltaic cell, Radio frequency interference, Uninterruptible Power Supply.

I. INTRODUCTION

The inverters which produce an output voltage or a current with levels either 0 or +V or -V are known as two level inverters. In high-power and high-voltage applications these two-level inverters however have some limitations in operating at high frequency mainly dueto switching losses and constraints of device rating. This is where multilevel inverters are advantageous. Increasing the number of voltage levels in the inverter without requiring higher rating on individual devices can increase power rating. The unique structure of multilevel voltage source inverters' allows them to reach high voltages with low harmonics without the use of transformers or series-connected synchronized-switching devices. The harmonic content of the output voltage waveform decreases significantly.

Mr. Ambadas. S. Mane and Mr. Vijay. B. Suryawanshi are with *Electrical Engineering Department, Government College of Engineering Karad, India*

The three level inverter offers several advantages over the more common two level inverter. As compared to two level inverters, three level inverters have smaller output voltage steps that mitigate motor issues due to long power cables between the inverter and the motor. These issues include surge voltages and rate of voltage rise at the motor terminals and motor shaft bearing currents. In addition, the cleaner output waveform provides an effective switching frequency twice that of the actual switching frequency. Should an output filter be required, the components will be smaller and less costly than for an equivalent rated two level inverter. Most often the NPC inverter is used for higher voltage inverters.

Advantages of this multilevel approach include good power quality, good electromagnetic compatibility (EMC), low switching losses, and high voltage capability. The main disadvantages of this technique are that a larger number of switching semiconductors are required for lower-voltage systems and the small voltage steps must be supplied on the dc side either by a capacitor bank or isolated voltage sources. The first topology introduced was the series H-bridge design.

II.INVERTERA

Dc-to-ac converter whose output is of desired output voltage and frequency is called an inverter.

Based on their operation the inverters can be broadly classified into

- Voltage Source Inverters (VSI)
- Current Source Inverters (CSI)

A voltage source inverter is one where the independently controlled ac output is a voltage waveform. Voltage source inverter or voltage fed inverter is one in which the dc source has small or negligible impedance. In other words the voltage source inverter has stiff dc voltage source at its input terminals. A current source inverter is one where the independently controlled ac output is a current waveform. A current fed inverter or current source inverter is fed with adjustable current from a DC source, DC source of high impedance.

On the basis of connections of semiconductor devices, inverters are classified as

- Bridge inverters
- Series inverters
- Parallel inverters

Some industrial applications of inverters are for adjustable- speed ac drives, induction heating, stand by air-craft power supplies, UPS (uninterruptible power supplies) for computers, hvdc transmission lines etc.

III.MULTILEVEL INVERTERS

Numerous industrial applications have begun to require higher power apparatus in recent years. Some medium voltage motor drives and utility applications require medium voltage and megawatt power level. For a medium voltage grid, it is troublesome to connect only one power semiconductor switch directly. As a result, a multilevel power converter structure has been introduced as an alternative in high power and medium voltage situations. A multilevel converter not only achieves high power ratings, but also enables the use of renewable energy sources. Renewable energy sources such as photovoltaic, wind, and fuel cells can be easily interfaced to a multilevel converter system for a high power application.

The concept of multilevel converters has been introduced since 1975. The term multilevel began with the three-level converter. Subsequently, several multilevel converter topologies have been developed. However, the elementary concept of a multilevel converter to achieve higher power is to use a series of power semiconductor switches with several lower voltage dc sources to perform the power conversion by synthesizing a staircase voltage waveform. Capacitors, batteries, and renewable energy voltage sources can be used as the multiple dc voltage sources. The commutation of the power switches aggregate these multiple dc sources in order to achieve high voltage at the output; however, the rated voltage of the power semiconductor switches depends only upon the rating of the dc voltage sources to which they are connected. A multilevel converter has several advantages over a conventional two-level converter that uses high switching frequency pulse width modulation (PWM). The attractive features of a multilevel converter can be briefly summarized as follows.

● Staircase waveform quality: Multilevel converters not only can generate the output voltages with very low distortion, but also can reduce the dv/dt stresses; therefore electromagnetic compatibility (EMC) problems can be reduced.

● Common-mode (CM) voltage: Multilevel converters produce smaller CM voltage; therefore, the stress in the bearings of a motor connected to a multilevel motor drive can be reduced. Furthermore, CM voltage can be eliminated by using advanced modulation strategies .

● Input current: Multilevel converters can draw input current with low distortion.

● Switching frequency: Multilevel converters can operate at both fundamental switching frequency and high switching frequency PWM. It should be noted that lower switching frequency usually means lower switching loss and higher efficiency.

Unfortunately, multilevel converters do have some disadvantages. One particular disadvantage is the greater number of power semiconductor switches needed. Although lower voltage rated switches can be utilized in a multilevel converter, each switch requires a related gate drive circuit. This may cause the overall system to be more expensive and complex. Plentiful multilevel converter topologies have been proposed during the last two decades. Contemporary research has engaged novel converter topologies and unique modulation schemes. Moreover, three different major multilevel converter structures have been reporter in the literature: cascaded H-bridges converter with separate dc sources, diode clamped (neutral-clamped), and flying capacitors (capacitor clamped). Moreover, abundant modulation techniques and control paradigms have been developed for multilevel converters such as sinusoidal pulse width modulation (SPWM), selective harmonic elimination (SHE-PWM), space vector modulation (SVM), and others. In addition, many multilevel converter applications focus on industrial medium-voltage motor drives, utility interface for renewable energy systems, flexible AC transmission system (FACTS), and traction drive systems.

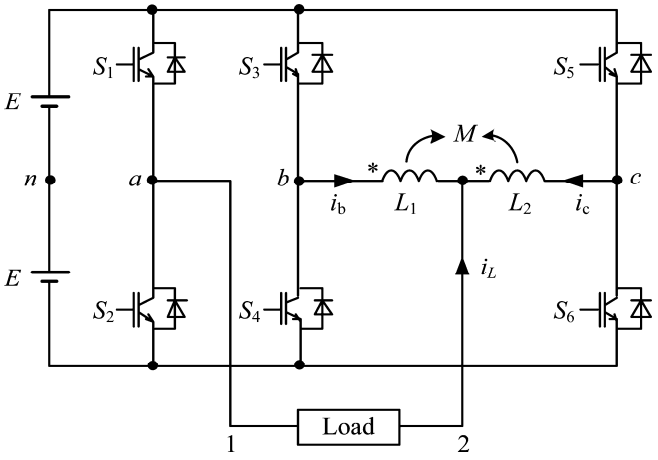

Fig 1: Single phase five level inverter

IV.SINGLEPHASE FIVE-LEVEL INVERTER

Fig. 1 shows the circuit of the proposed single-phase five level inverter. In Fig. 1, 2E is the dc-link voltage and L1 andL2 are the two coupled inductors. The mutual inductance of the two inductors is M and the output terminals of this inverter are1 (the same point as the output of arm a) and 2. Obviously, this topology is very simple and can be constructed simply by adding two coupled inductors to a conventional three-arm inverter bridge.

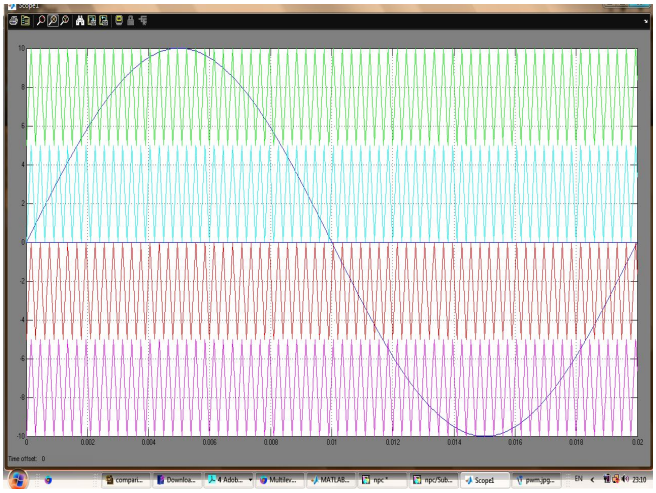

Fig 2:Modulation scheme for five level inverter

A) Switching States for Five-Level Output Voltage

From Fig. 1 and (5), the output voltage of the proposed inverter can be expressed as
u12 = u1n − u2n = u1n − (ubn+ ucn)/2

In the following discussion, the power switches in one arm areassumed to switch complementarily. For instance, S2 must beturned OFF if S1 is turned ON and vice versa. So the followingdiscussion will only focus on the switching states of S1 ,S3 , andS5 . For convenience of analysis, the number "1" will be usedto denote the ON state of one switch and "0" will be used todenote the OFF state.

In fact, u1n ,ubn, and ucnall can generate two-level voltage(+E and −E). According to equation the voltage levels of u12 can be summarized in Table no1.Obviously, the proposed inverter can generate five voltagelevels at its output terminals. From Table I, it should be pointedout that the switching state of S1 must be 1 if u12 ≥ 0 and theswitching state of S1 must be 0 if u12 ≤ 0. This means S1 andS2 will switch at the fundamental frequency of the referencesignal. So, the switching losses of S1 and S2 will be very lowin the proposed inverter.

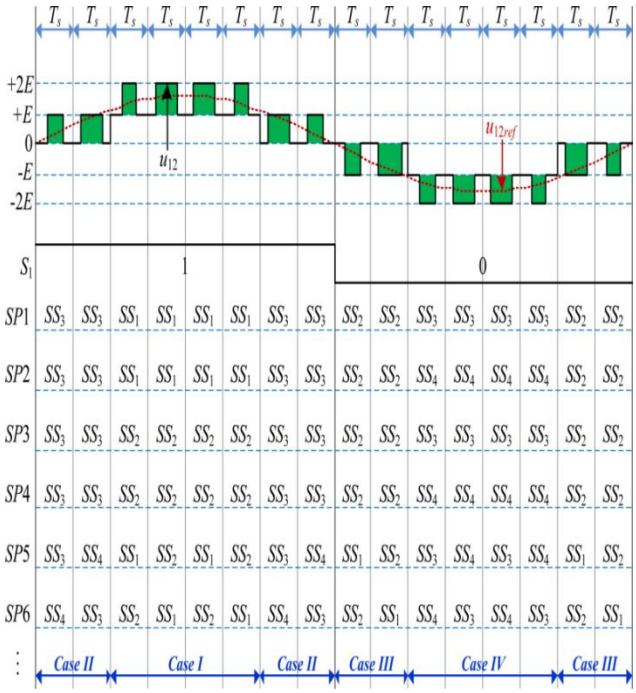

S_1	S_3	S_5	u_{12}
1	0	0	+2*E*
1	0	1	+*E*
1	1	0	+*E*
1	1	1	0
0	0	0	0
0	0	1	-*E*
0	1	0	-*E*
0	1	1	-2*E*

Table no.1: Switching states and output voltage of the inverter.

Fig 3.Dwelling time (green part) within every Ts and the some of the possible switching patterns for S3 and S5 (SP1–SP6).

Advantages:

- Simple construction and easy implementation,
- The switching losses is less compared with the excising system,
- The effective control of the switches is achieved.

Application:

- Motor Drives,
- Active Filters,
- Power conditioning.

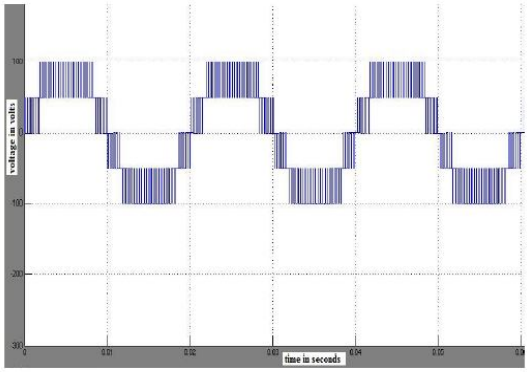

Fig 4.Simulation results of five level inverter

V..CONCLUSION

This paper proposed a novel single-phase five-level inverter based on coupled inductors. This inverter can output five-level voltage with only one dc source and no split of the dc voltage capacitor, totally avoiding the voltage balancing problem. The height of the staircase in the output voltage is only half of the dc-link voltage under any modulation index. Meanwhile, the voltage stresses on all the power switches are the same and only four switches are operated at high frequency. Operation mechanism of this inverter was analyzed and the optimized switching Patterns were also presented to minimize the passive component. Verification results show validity of the proposed topology together with the modulation method. The coupled inductors may be the flaw of this converter. However, the switches taking the high current have low-switching frequency while the switches taking the low current have high-switching frequency. Therefore, the presented topology is very suitable for low to medium power applications, especially for high-current cases.

REFERENCES:

[1].IEEE transactions on power electronics,vol.27, no.6,june 2012.
[2].J. Li, S. Bhattacharya, and A. Q. Huang, “A new nine-level active NPC (ANPC) converter for grid connection.
[3].J. Shi,W. Gou, H. Yuan, T. Zhao, and A. Q. Huang, “Research on voltage and power balance control for cascaded modular solid-state transformer,” IEEE Trans.
[4].J. Rodriguez, J.-S. Lai, and F. Z. Peng, “Multilevel inverters: A Survey of topologies, controls, and applications,” IEEE Trans.
[5].Book – Power electronics-Converter applications and design by Mohan,Undeland ,Riobbins.
[6].R.W. Erickson , Fundamental of power electronics, first edition, Chapman and Hall, ISBN 0-412-08541-0, 1997, New York

Series Resonant Converter

Mr. Ambadas S. Mane and Mr Vijay P. Mohale

ABSTRACT: **Increasing the frequency of operation of power converters is desirable, as it allows the size of circuit magnetic and capacitors to be reduced, leading to cheaper and more compact circuits. However, by increasing the frequency of operation switching losses are increased hence reducing the system's efficiency. One solution to this problem is to replace the "chopper" switch with a "Resonant" switch, which uses the resonances of circuit capacitances and inductances to shape the waveform of either the current or the voltage across the switching element, such that when switching takes place, there is no current through or voltage across it, and hence no power dissipation. A circuit employing this technique is called resonant converter. Resonant converter is recent technology which is used in X-ray machine, Electrical vehicle charger etc. Resonant converter reduces switching loss through mechanism known as zero current switching and zero voltage switching. When the series resonant converter are operated below resonance the zero current phenomenon can occur and circuit acts as capacitive circuit, leading power factor. When resonant converter operate above resonance the zero voltage phenomenon can occurs and acts as inductive circuit, lagging power factor. Electrical Vehicle Battery Charger is an important part in automobile.**

I. INTRODUCTION

Resonant converters operate at relatively high switching frequencies, and this enables the use of small inductive components which improve the dynamic behaviour and reduce the size of the converter. Despite the above-mentioned benefits of SMPS's, there are several parameters, which are not desired and have a strong influence on the converters behaviour being mainly:[1,2]

- Non-linear components in the converter structure,
- Line and load variations, and
- Electro-magnetic interferences (EMI).

The Resonant converter has non-linear components, the value of which changes non-linearly if the converter is disturbed or may change within time. These parameters force the converter to deviate from the desired operating condition. If the parameter deviation increases, this will cause the converter not to operate in steady state. Each control method has its own advantages and drawbacks due to which that particular control method appears to be the most suitable control method under specific conditions, compared to other control methods. It is always demanded to obtain a control Method that has the best performances under any conditions [4].

II. OPERATION OF SERIES RESONANT CONVERTER

In resonant converter chargers, drawbacks of switch mode chargers are overcome. Rectified AC input is turned into high-frequency AC using high frequency switching device (e.g. MOSFET).Voltage or zero current conditions are achieved using resonant tank circuit and a high-frequency transformer reduces the voltage to the exact level needed to charge the battery[6].

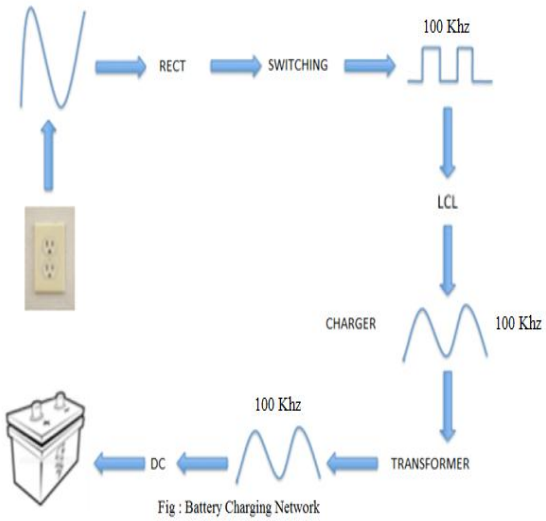

Fig.1 Block Diagram of Series Resonant Converter[5]

In the coming years, electric vehicles are predicted to dominate large segments of the automotive industry. Presently there are no widely accepted standards for electric vehicle charging techniques and many different methods are in use. The electric vehicle charger using a series L-C-L type resonant converter configuration will incorporate the benefits of maximized safety, efficiency, speed and ease of use. Fig.2 shown below represents battery charging circuit. In this circuit L-C-L type resonant converter configuration will be used and MOSFET will be used as a switch because it has low switching losses. It is proposed to design series resonant converter for charging of electric vehicle battery. The sequence of design is shown in figure below.[7].

Mr. Ambadas S. Mane, Mr Vijay P. Mohale **are with** *Electrical Engineering Department, Government College of Engineering Karad, India.*

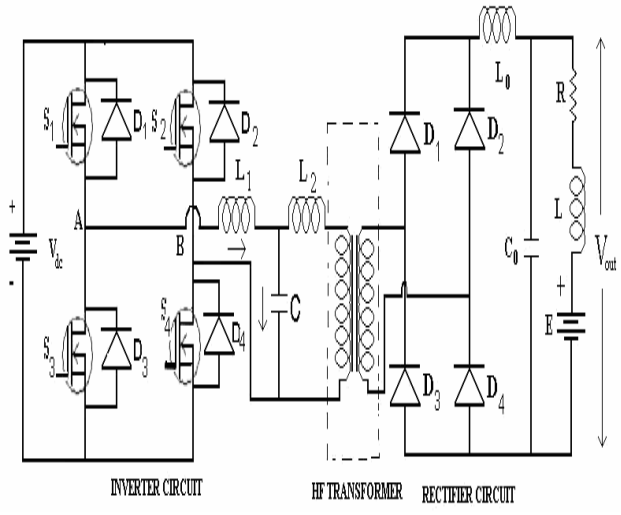

Fig.2 Circuit Diagram of Series Resonant Converter[7]

The aim of this project is to develop a fast and efficient method of electric vehicle battery charger using L-C-L type Resonant Converter topology. For ease of use, the entire system will be monitored by microcontroller which will control the power output of the charger and monitor the state of batteries to protect system from line born disturbances.

SI

1. Zero –voltage switching:

When the series resonant converter is operated above resonance, the zero voltage switching phenomenon's can occur, in which the circuit causes the transistor voltage to become zero before the controller turns the transistor on. With the minor circuit modification, the transistor turn-off transition can also be caused to occur at zero voltages. This process can lead the significant reductions in the switching losses of converters based on MOSFETs & Diodes.

For the full bridge circuit of fig13.theswitch output voltage Vs (t), &its fundamental component Vsl (t), as well as the approximately sinusoidal tank current waveform is (t), are plotted in fig18.

For the half cycle 0<t<Ts/2, the switch voltage Vs (t) is equal to +Vg. For 0<t<ta, the current Is (t) is negative & diodes D1 & D4 conduct. Transistor Q1& Q4 conduct when Is (t) is positive, over the interval ta<t<Ts/2.The waveform during Ts/2<t<Ts are symmetrical. Since the zero crossing of Vs (t) leads the zero crossing of Is (t), the transistor conduct after their respective anti parallel diode.

In general, zero voltage switching can occurs. When the resonant tank present an effective inductive load to the switches, & hence the switch voltage zero crossing occur before the switch current zero crossing.

The transistor turn-off transition in fig. is similar to that of PWM switch. In converters the employ IGBTs or other minority-carrier devices, significant switching loss may occur at the turn-off transition. The current tailing phenomenon causes Q1 to pass through a period of high instantaneous power dissipation & switching loss occurs. An additional advantage of zero-voltage switching is the reduction of EMI associated with device capacitance.

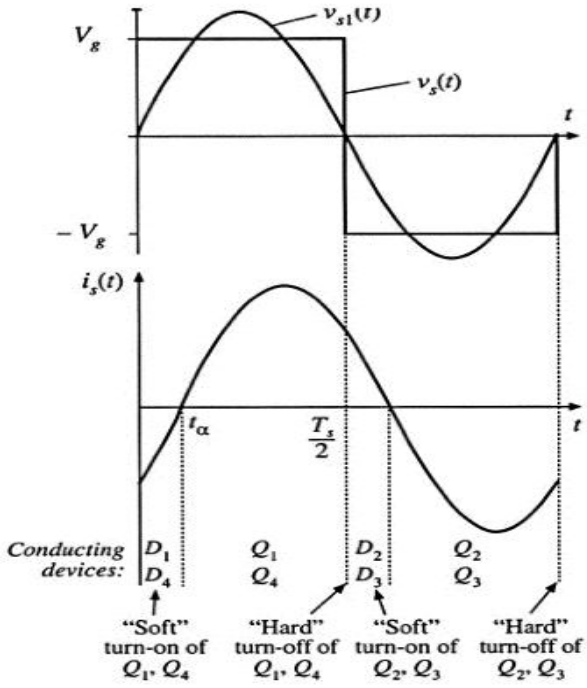

Fig.3 Switch Network Output Waveforms for Series Resonant Converter

III. SINUSOIDAL ANALYSIS OF RESONANT CONVERTERS

The class of resonant converters contains a controlled switch network (Ns) which drives a linear resonant tank network (Nr). In resonant inverter, the tank network drives a resistive load . The reactive component of the load impedances, if any, can be effectively incorporated into the tank network.

In the case of resonant DC-DC converter, the resonant tank network is connected to an uncontrolled rectifier network (Nr), filter network (Nf), load R. Many well known converters can be represented in this form, which includes the series, parallel, LCC topology.

In the most recommended modes of operation, the controlled switch network produces a square wave output voltage Vs (t) whose frequency (Fs) is close to tank network's resonant frequency (Fr). In the c as where the resonant tank responds primarily to the fundamental component Fs of switch waveform of frequencies Fs. In the case where the negligible response at the harmonic frequencies n(fs), Where n=3, 5, 7….then the tank waveform's are well approximated by their fundamental components.

As shown in the fig.9, this is indeed case where the tank network contains a high Q-resonance at or near the switching frequencies and a low pass characteristics at higher frequencies. Hence neglect harmonics and compute the relationship between the fundamental components of the tank terminal waveforms Vs (t), Is (t), Ir (t) and Vr(t).

1. Controlled switch network model:

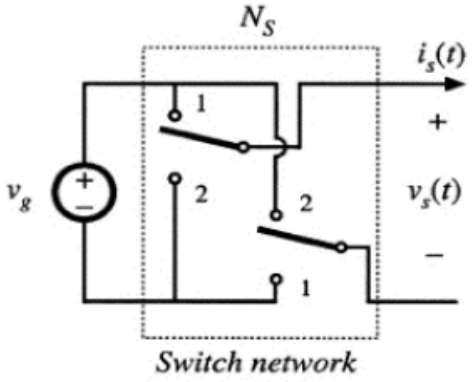

Fig.4 Ideal Switch Network

$$V_{s1} = -\frac{4V_g}{\pi}\sin(\omega_{st}) = V_{s1}\sin(\omega_{st})$$

$$V_s(t) = \frac{4\,V_g}{\pi}\sum_{n=1,3,5}\frac{1}{n}\sin(n\,\omega_s\,t)$$

$$i_{st}(t) \approx I_{s1}\sin(\omega_{st} - \phi)$$

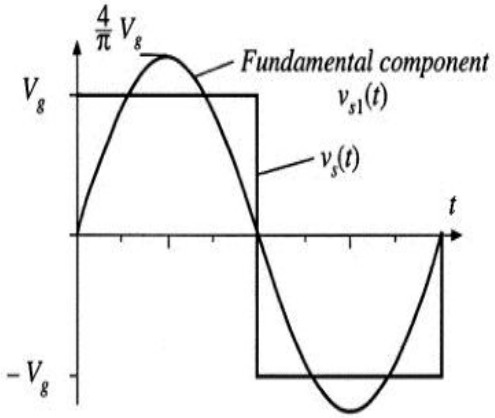

Fig.5 Switch Network Output Voltage Vs (t) and its Fundamental Component Vs1(t)

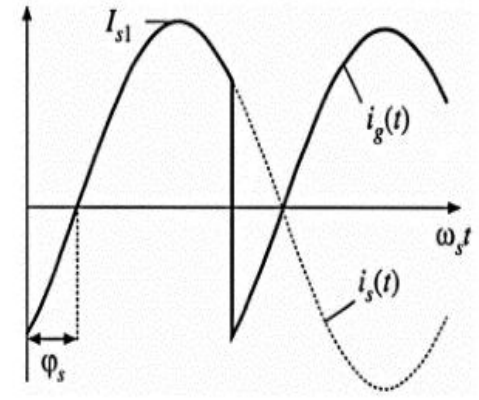

Fig.6 Switch Network Waveforms Is (t) and Ir (t).

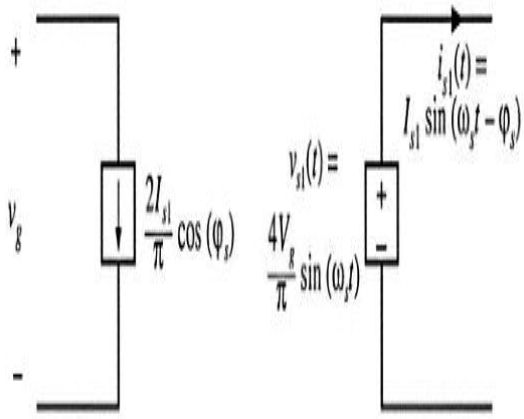

Fig.7 Equivalent Circuit For The Switch Network

$$\langle i_g(t)\rangle_{Ts} = \frac{2}{T_s}\int_0^{\frac{T_s}{2}} i_s(\tau)\,d\tau$$

$$= \frac{2}{T_s}\int_0^{\frac{T_s}{2}} I_{S1}\sin(\omega_s\tau - \varphi_s)\,d\tau$$

$$= \frac{2}{\pi} I_{S1}\cos(\varphi_s)$$

IV. CONCLUSION

In order to study and analyze the Switch Mode Control effect on the converter behavior and to compare it to another control method, a comparison will be done for the output voltage and the inductor current responses of the Series LCL

T- type Resonant converter controlled with the PID control and the SMC. Test results will be obtained in steady state and under dynamic conditions.

Resonant converters have advantages such as reduction in cost, size and weight of the power supply. Fast transient response, reduction in switching losses, di/dt and dv/dt stresses of power devices gives additional advantages of using resonant converters. It also reduces Electro-Magnetic Interference (EMI).

Resonant converter is recent technology which is used in X-ray machine, high HV pulsed load applications, Ozone generation using LCC RC, high-power industrial application of CO2 laser also needs HV power supply, Electrical vehicle charger etc.

ACKNOWLEDGEMENT

This paper proved to be quite interesting endeavour. There were many people who helped me while preparing paper and I am deeply thankful to our guide Prof. Mr. A.S.Mane who helped us a lot & played central role to co-operate with me. I would also like to thank our Head of the Department Prof. Mr. V.B.Waghmare for his firm support. And I am thankful to whole staff in our department for their help. Also I would like to mention here special thanks to my friends who helped & supported me

REFERENCES

BOOKS

[1] Mohan, N, Undeland, T, Robbins, W. 1989. Power Electronics: Converter, Applications, and Design. JOHN WILEY & SONS, ISBN 0-471-61342-8, 1989, USA.
[2] R.W. Erickson , Fundamental of power electronics, first edition, Chapman and Hall, ISBN 0-412-08541-0, 1997, New York
[3] Mohammad H. Rashid, Power Electronics-circuit devices & applications, Third Edition, PEARSON, ISBN 978-81-317-0246-8, 2009, INDIA

PAPERS

[4] G.S.N.Raju and Seshagirirao Doradla, “An LCL Resonant converter with PWM Control Analysis, simulation, and Implementation”, IEEE Transactions on Power Electronics, vol.10, No.2 March 1995.
[5] Xinke Wu and Zhaomimg Qian, New current driven synchronous rectifier for series parallel resonant(LLC DC-DC converter).
[6] A.K.S Bhatt. Senior member IEE Dept. of elect engg. “Analysis and design of LCL Type series resonant converter, Victoria (B.C.) V8W (2Y2) CANADA, 172-173.
[7] A.K.S Bhatt. Senior member IEE Dept. of elect engg. “Analysis and design of fixed frequency LCL Type series resonant converter, Victoria (B.C.) V8W(3P6) CANADA, 253-256.
[8] Implementation of a series resonant converter with, Bor-Ren, senior member , IEEE, and BO-Ren Hou, Department of electrical engineering National Yunlin University of science and technology, Yunlin 640,Taiwan